Department Biologie II
Anthropologie und Humangenetik
Ludwig-Maximilians-Universität München

Nuclear architecture explored by live-cell fluorescence microscopy using laser and ion microbeam irradiation

Hilmar Strickfaden

Dissertation der Fakultät für Biologie der Ludwig-Maximilians-Universität München
Eingereicht am 1. Juli 2010

Nuclear architecture explored by live-cell fluorescence microscopy using laser and ion microbeam irradiation

Dissertation der Fakultät für Biologie
Der Ludwig Maximilians Universität München (LMU)

vorgelegt von:
Dipl. Biol. Hilmar Strickfaden
aus Freiburg im Breisgau

Gutachter:
Prof. Dr. Thomas Cremer
Prof. Dr. Peter Becker

Tag der mündlichen Prüfung: 20.12.2010

Das Leben kommt auf alle Fälle
aus einer Zelle.
Doch manchmal endet's auch bei Strolchen
in einer solchen.
Heinz Erhardt (1909–1979)
(German Comedian)

Table of Contents

1 Summary

Nuclear architecture is a biological field of research that studies the spatio-temporal organization of the components within cell nuclei. Since nuclei are the organelles that harbor the genome and epigenome, they are the place where most of the genetic processes like replication, transcription, splicing, gene-regulation, DNA repair, recombination etc. are carried out.

In the presented doctoral thesis modern 4D live-cell microscopy in combination with laser or ion microbeam irradiation (to label or damage chromatin, respectively) was used to study nuclear architecture in living cells over extended periods of time at the single cell level.

The results presented in this thesis can be partitioned into three main parts: (a) chromatin dynamics in cycling cells, (b) adaptation of the ion micro beam facility SNAKE to the needs of live-cell observation (including first experiments) and (c) exploring spatio-temporal dynamics of DNA repair proteins after laser micro irradiation.

(A) Chromatin dynamics in cycling cells

Distribution of interphase chromosomes within cell nuclei has been found to be non-random with respect to gene density and chromosome size. Changes in nuclear organization have been reported in several disorders and diseases. To which extent relative chromosome positioning is conserved through mitosis in cycling cells and whether certain chromatin domains are able change their relative position dramatically in the interphase nucleus has been the subject of various mechanistic models and controversial discussions. In 1909 German biologist THEODOR BOVERI was the first one to comment on this topic in his publication: "Die Blastomerenkerne von *Ascaris megalocephala* und die Theorie der Chromosomenindividualität" (included as an appendix to this thesis). In order to test BOVERI's hypotheses, 4D live-cell observations were carried out on a modern spinning disc confocal microscope using a human cell line that possesses photoactivatable chromatin. In experiments that used photoactivation and photobleaching of chromatin, it could be demonstrated that – as stated by Boveri – chromatin proximity relationships are in general not conserved through mitosis but destroyed during early prometaphase by the mechanics of mitosis. Other experiments showed that nuclear rotations in a conveyer-belt-like manner are able to bring initially distant chromatin domains into close proximity in a matter of a few minutes.

(B) Adaptation of the SNAKE micro beam facility to the needs of live-cell microscopy (including first experiments)

Since ordinary irradiation sources lack the ability to perform targeted micro irradiation at the micrometer scale and laser micro irradiation produces an artificial mix of various DNA damages, the ion microbeam SNAKE represents an interesting tool to explore the dynamics of repair proteins in a spatio-temporal context. In the course of a collaboration project the ion microbeam was adapted to the needs of long-term live-cell microscopy. These adaptations and first live-cell experiments performed at the refurbished ion micro beam are described in this part of the results.

(C) Exploring spatio-temporal dynamics of DNA repair proteins after laser micro irradiation.

Mutation of genetic information can cause serious harm to a cell or even a whole organism. DNA repair serves to protect and clean the genome from undirected potentially hazardous changes. Compared to the wealth of information which is available about DNA repair at the molecular level only little attention has been payed to it in context of nuclear architecture. In the last part of the results cells stably expressing GFP tagged versions of the repair proteins MDC1, Rad52 and 53BP1 were damaged by laser micro irradiation and imaged over extended periods of time. It could be demonstrated that at the used damage induction conditions most of the cells show only minor changes with respect to localization of damage signals, kinetochores and nucleoli pattern over time. Furthermore, disappearance of spontaneous 53BP1-GFP foci in favor of protein recruitment to damaged chromatin and mutual exclusion between kinetochore signals and Rad52-GFP damage foci could be observed. In a few U2OS Rad52-GFP nuclei DNA damage foci disappeared simultaneously after a dramatic phase in which the total number of foci drastically increased – even adjacent to the laser damaged chromatin.

2 Introduction

"A picture tells more than a thousand words."

This quote which is accredited to an early emperor of the XIA dynasty in China about 4000 years ago emphasizes the power of a visual impression compared to a linear sequence of information (like this text). However although a picture of something is well-suited for displaying geometric or spatial properties, it is sometimes difficult to use it for expressing temporal information. Exploring dynamic processes in which geometric properties change within time, an ordered sequence of pictures representing each a different point in time-point might be an adequate solution. So one could say – analogous to the introductory quote – "A movie tells more than a thousand pictures".

You might wonder why a doctoral thesis with focus on nuclear architecture opens with rather general philosophical reflections about how reality can be described in the most efficient way? But since these introductory words easily demonstrate the advantage of "live-cell confocal microscopy" – the main method used in this thesis – over "conventional" approaches that provide information for only one point in time, it is rather useful to start making this point right from the beginning.

The past decades were accompanied by an enormous increase of knowledge in the life-sciences and during this development a lot of different methods emerged to answer specific questions. With respect to the field of nuclear architecture methods like immunofluorescence, 3D-FISH and the chromatin conformation capturing (to name only a few) have and had a big impact on our todays knowledge. But one property that all of the methods mentioned above have in common and which impairs them in their explanatory power is that the information they provide origins from fixed cells and represents only a snapshot of the moment when they were fixed.

Evaluating a population of fixed cells under the microscope is somehow like looking at an old painted picture showing a scene with many people. Although each person on the picture can be described and evaluated for every thinkable visible property it remains unclear what has led e.g. to a certain expression on some person's face or e.g. what will result from the situation shown in this picture. It is even worse when we look at methods often applied in molecular biology. Here the situation reminds less of a picture but more of a survey that is given to a large number of people. Although it is possible to access discrete information about several distinct properties – the experimental output however is somehow limited to only a small number of properties per experiment that is given with respect to a whole cell population.

One advantage of those methods over an observation of individual cells in space and time is that they give fast access to a plethora of information that often might not be accessible by imaging methods. Although the evaluated properties might vary to some extent within different cell populations, the use of high sample numbers and statistics can put the conclusions drawn from these onto a solid fundament.

In contrast to experiments that use fixed cells, the method of choice used in this

thesis is live-cell microscopy. This method allows to create 3 dimensional images obtained from serial light optical sections over time of individual, living cells. Although this method (at least in the set-up used here) is not appropriate for high-throughput approaches including the observation of thousands of cells, it has been well suited to successfully approach general questions in nuclear architecture that haven't properly solved yet and that have been a matter of controversial discussions for a long time.
In particular the main topics of this thesis are:

- the dynamics of chromosomes in cycling mammalian cells (testing the Boveri-Hypothesis)
- spatiotemporal changes in the nuclear architecture after induction of DNA damage using laser and ion-micro beam irradiation.

To motivate the field and for a better understanding of the techniques used in this thesis the next paragraphs will give the reader a small introduction into:

- the cell-nucleus and its components
- the different stages of mitosis
- Theodor Boveri's hypotheses and the controversy about them
- DNA damage repair
- the history of microscopy and its latest developments
- the benefits and problems of live-cell microscopy
- fluorophores that can be used in live cell microscopy

2.1 The Nucleus

The nucleus is a cellular compartment that is surrounded by a double-membrane structure called the **nuclear envelope**. The outer membrane (towards the cytoplasm) passes into the rough endoplasmic reticulum and is often coated with ribosomes. Inner and outer nuclear membranes meet at the **nuclear pores** that act as import and export gates for exchanging cellular materials between cytoplasm and the nucleus. Recent studies report that the nuclear pore complex functions as

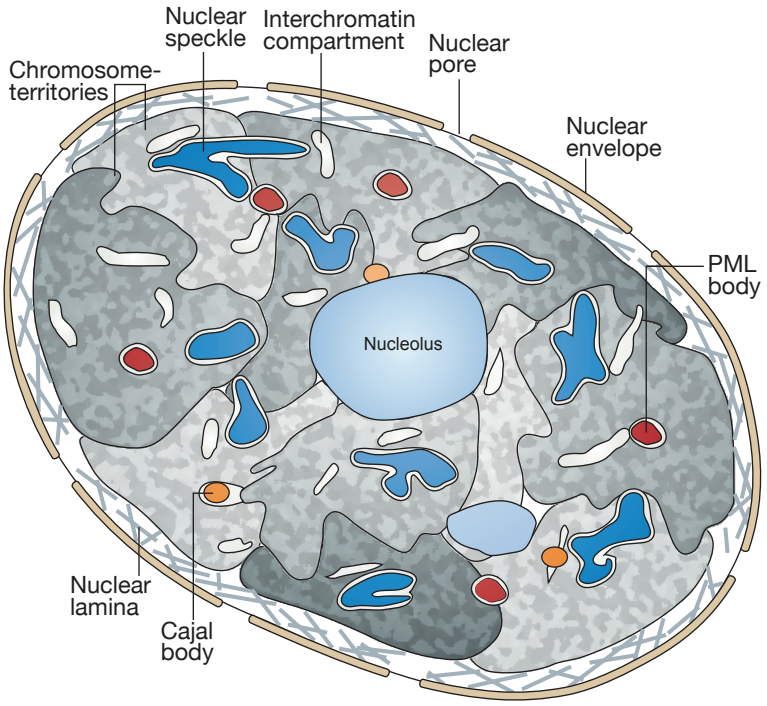

Fig. 2-1: Schematic drawing focussing on the components within an eukaryotic cell nucleus. Apart from the nucleolus other nuclear bodies like nuclear speckles (blue), cajal- (orange) and PML bodies (red) can be found in the interchromatin space between the chromosome territories. The nuclear envelope and the lamina represent the outer barriers that encompass the inner compontens of the nucleus (modified from Lanctôt et al., 2007)

a transcriptionally permissive nuclear neighborhood to facilitate expression (Akhtar and Gasser, 2007; Ruault et al., 2008). The peripheral **nuclear lamina** is located at the lumen side of the the nuclear envelope and consists to a big extent of lamins A/C and B (class V intermediate filaments) (Dechat et al., 2008). Other proteins that can be found in the lamina are the lamin-B-receptor (LBR) and proteins containing the SUN and the LEM domains (Heessen and Fornerod, 2007). The lamina is thought to play a role in regulating and maintaining nuclear envelope structure and anchoring/tethering interphase chromatin at the nuclear periphery. Although the inner nuclear matrix and the peripheral nuclear lamina are reported to define a transcriptionally repressive compartment (Reddy and Singh, 2008) (which is quite feasible since they harbor centromeres and other heterochromatic sequences that can easily be seen in a fluorescence microscope using a DNA counterstain) other studies report about transcriptionally permissive microdomains in this region (Kumaran and Spector, 2008).

The interphase chromosomes are organized into **chromosome territories** (CTs) which reside in the nuclear space, (Cremer and Cremer, 2010). Active genes are expected to be located all over the surface of the loosely packed subchromosomal domains which is referred to in some studies as **perichromatin region** (PR) (Cmarko et al., 1999; Cmarko et al., 2003; Solimando et al., 2009). According to the **CT–IC** (**c**hromosome **t**erritory-**i**nter**c**hromatin) model (Albiez et al., 2006), which in this thesis is the preferred model, the chromosome territories form a network of chromatin domains which is interspersed by a network of channels and lacunae that are virtually chromatin free (interchromatin compartment) and harbors the non-chromatin nuclear bodies. In this model it is assumed that chromatin domains consist of 1Mb domains (replicon clusters) and have a sponge-like surface with channels to the inside. At the surface of the territories many small loops of sizes between 30-200 kb are expected (perichromatin region) where the active genetic processes (e.g. replicaton

transtription and repair) may happen.

Genes looping out several microns of their CT in protrusions (so called "Giant Loops") can sometimes be observed in nuclei (Chambeyron et al., 2005; Küpper et al., 2007; Volpi et al., 2000). Whether these structures can transiently be established by a directed mechanism upon stimulation bringing co-regulated or co-transcribed genetic sequences spatially in close proximity or whether even whole chromosome territories can change their position significantly during interphase (Hu et al., 2008; Lin et al., 2009; Mehta et al., 2010) is a very controversially discussed topic since several years and one of the questions examined in this thesis.

It has been found that the spatial distribution of CTs within nuclei is not completely random. While in round cell nuclei of most cell types a preference of gene rich chromosomes and transcriptionally active chromatin domains could be found towards the interior, gene poor chromosomes and transcriptionally inactive chromatin were preferentially detected towards the nuclear periphery (Küpper et al., 2007). In flatly shaped nuclei, territories of large chromosomes were mostly found at the nuclear rim, while small chromosomes had a preference for the center of the nucleus (Bolzer et al., 2005). A recent study by Solovei et al., (2009) reported an exception to this rule. In rod cells of some nocturnal mammals transcriptionally inactive heterochromatin could be found in the interior of the nucleus whereas transcriptionally active euchromatin was located close to the lamina.

Chromosomes contain several functional elements. Every chromosome contains **centromeres** – which are covered with special proteins to form the **kinetochores** (the place where the microtubules attach to the chromosomes during mitosis and where the chromatids are torn apart in anaphase) and **telomeres** that are located at the ends of the linear chromosomes to stabilize them and prevent the ends from being detected as double strand breaks. Other functional sites are the **NOR**s (**N**ucleolar **O**rganizing **R**egions) which contain rRNA sequences that have the ability to form the nucleolus. Although not functional regions but whole highly condensed chromosomes the **Barr-bodies** (Lyon, 1962) represent inactivated X-chromosomes in female mammalian cells which are in the context of dosage compensation epigenetically silenced in favor of only one active X-chromosome.

The chromosomes are composed of DNA, proteins and RNA which is called **chromatin**. Although secondary structures of chromatin (10 nm fiber "beads on a string", 30 nm fiber (solenoid structure)) have been found in electron microscopic preparations, no bigger stable higher order chromatin structure could be doubtlessly characterized, yet.

During the past years **epigenetic modifications** of the chromatin – primarily DNA methylation, nucleosome positioning, histone variants and histone modifications (like acetylation, phosphorylation, methylation, ubiquitination, biotninylation, etc.) – have moved into focus of many studies because of their big impact on gene and genome regulation (Segal and Widom, 2009). Though not changing the sequence of the genomic DNA, these modifications/variants add information to the chromatin that can persist over many cell generations (Gluckman and Hanson, 2004).

Inside the nucleus several nuclear bodies were found which will be introduced briefly

here (Spector, 2006): The **nucleolus**, the most prominent nuclear body that is already visible in the light microscope, is the site of rRNA synthesis, rRNA processing, and assembly of ribosomal subunits. It disappears during the condensation of the chromosomes in mitosis and reappears again in telophase. Nucleoli contain the rDNA of different chromosomes possessing a NOR and thereby take a big influence on nuclear architecture (Schwarzacher and Wachtler, 1983). They belong to the most dense structures within living cells (1,35g/cm^3) (Kleinig and Sitte, 1999). In many cell types, **heterochromatin** (to a big extent genetically inactive, dense chromatin) is found associated with the nuclear lamina and the nucleoli. Apart from that, accumulation of heterochromatin can also be found in form of **PcG bodies** in more central nuclear regions (Bernardi and Pandolfi, 2007). **Nuclear speckles** which consist of pre-mRNA splicing factors are approx. 25–50 small nuclear bodies being diffusely distributed throughout the nucleoplasm (Lamond and Spector, 2003). Other nuclear bodies related to transcription and processing of nascent RNA are the **OPT domains** (appear in G_1-phase, where they are often located next to nucleoli, and disappear during S-phase) (Spector, 2006), the **Cajal bodies**, previously called coiled bodies, the **perinucleolar compartment** (Pollock and Huang, 2009) and the **PML-bodies** (Bernardi and Pandolfi, 2007). After introduction of DNA damage **repair-foci** consisting of many then thousands repair proteins appear around the damaged site. These foci will be discussed more in detail in a later section.

2.2 Mitosis

For rotatable 3D reconstructions of the respective mitotic stages please click on fig. 2-2 in the 3D-PDF version on the enclosed DVD.

2.2.1 Prophase

Chromatin condensation starts at the onset of prophase (Greek προ meaning before) and generates highly ordered structures, called the mitotic chromosomes. All of these structures consist of two sister chromatides which represent two identical copies of a chromosome that has been replicated during the preceding S-phase. These sister chromatids are held together at the centromeres until the end of metaphase.

Centrosomes are organizing centers for microtubules that dupicate in G_1-phase and consist of a pair of centrioles that are situated in close proximity of the nucleus. In early prophase, myosin dependent cortical movements (Rosenblatt et al., 2004) and molecular motor proteins (dynein) then push the centrosomes apart from each other. Together with the microtubules, the two centrosomes form the mitotic spindle. Microtubules grow from the centrosomes which form the spindle poles by polymerizing soluble tubulin. Centrosomes are not essential and can be subsituted by other microtubule organizing centers in many fungi and plants (which don't even have centrosomes) to form the mitotic and meiotic spindle (Lloyd and Chan, 2006; Varmark, 2004)

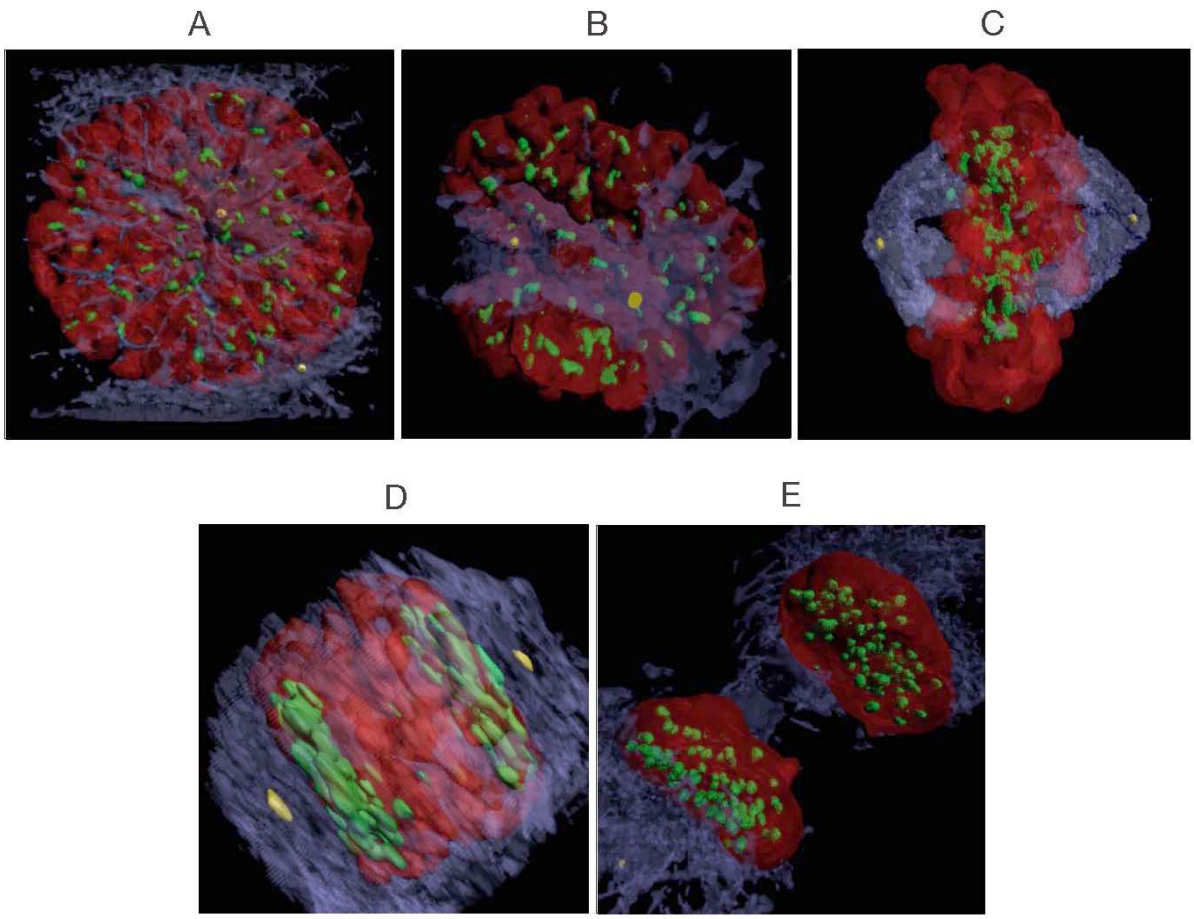

Fig. 2-2: Different phases of mitosis. **a**: prophase, **b**: prometaphase **c**: metaphase, **d**: anaphase and **e**: telophase. chromosomes / chromatin are shown in red (DAPI), kinetochores in green (α-CREST antibody), centrosomes in yellow (α-pericentrin antibody) and microtubules (α-tubulin antibody)

2.2.2 Prometaphase

In prometaphase the nuclear envelope breaks down. Microtubules can thus access the space containing the condensed chromosomes. At the centromeres of each chromatid a complex protein structure is formed which is called the (outer) kinetochore. Kinetochores are the structures that connect the chromosomes to the kinetochore microtubules. Non-kinetochore microtubules growing from different centrosomes and interacting with each other form the mitotic spindle. For further information see (Chaly and Brown, 1988) and (Alexander and Rieder, 1991).

2.2.3 Metaphase

During prometaphase the microtubules connect to kinetochores and the chromosomes line up to form the metaphase plate or equatorial plane, (in the middle between the two centrosomes and perpendicular to connection line they are forming). In this phase the chromosomes are arranged for optimal chromatid separation in anaphase. Meta (μετα) is the Greek word for „in-between“.

2.2.4 Anaphase

After all kinetochores are positioned perfectly within the metaphase plate for chromatid separation, the cell is ready to switch into anaphase (ανα Greek for "up"). For initiation of anaphase two major events have to take place: Cleavage of the proteins that connect the sister chromatids and separation of the sister chromatids. The latter is performed by decreasing the lenth of the kinetochore microtubules and moving the chromatids towards the respective centrosomes to which they are tethered. After that, the centrosomes are pushed further apart from each other by elongation of the non-kinetochore microtubules. In this phase the condensed chromosomes are showing the RABL orientation as a consequence of the mechanics that are involved – meaning that the centromeres are located proximal to the centrosomes on one side and the telomeres distal to the centrosomes on the other side.

2.2.5 Telophase

In telophase (τελος Greek meaning "end" or „destination") the events of prophase and prometaphase seem to occur in the opposite order. The nuclear envelope forms again around the nascent daughter nuclei by recycling fragments of the nuclear envelope that fromally belonged to the mother cell and nucleoli re-emerge. The chromosomes decondense again into interphase chromatin. Completion of telophase marks the end of mitosis.

2.2.6 Cytokinesis

Cytokinesis – although actually not a real phase of mitosis since it is absent in some syncytia – is necessary for completing cell division. A contractile ring emerges in animal cells in-between the nascent nuclei in order to physiologically separate them from each other. In plant cells separation of the two nuclei is accomplished by assembling a plate at the center of the former mother cell, which later turns into a cell wall.

After cytokinesis the genome of the mother cell has been partitioned to equal parts into two independent daughter cells.

2.3 Theodor Boveri's Hypotheses

Cytogenetics was established in the early 20th century with the BOVERI-SUTTON theory of chromosomal heredity. THEODOR BOVERI (1862-1915) (fig. 2-3) and WALTER S. SUTTON (1877-1916) explained the genetic segregation discovered by GREGOR MENDEL (1822-1884) with chromosomes as bearers of a hereditary molecular architecture. This theory explained not only Mendelian ratios but, as BOVERI proudly stated in his seminal publication from 1909, all the facts known about certain numbers, sizes, forms and arrangements of chromosomes in normal and abnormal cases, including the fact of the reduction of chromosome number in germ cells (BOVERI, 1909) (for review see CREMER AND CREMER, 2006). In his search for a link between Mendelian genetics and the behavior of chromosomes BOVERI studied embryos of the horse roundworm *Parascaris equorum* (or *Ascaris megalocephala* as the worm was called in BOVERI's days) (fig. 2-4) during the first two post-zygotic cell cycles. Cells of *Ascaris megalocephala univalens* contain two chromosomes, while *Ascaris megalocephala bivalens* contains four chromosomes during this early embryonal stage (fig. 2-4).

Fig. 2-3: Theodor Heinrich Boveri 12.10.1862 Bamberg – 15.10.1915 Würzburg

Although the cytologist CARL RABL (1853-1917) was the first who argued that chromosomes occupy defined nuclear subregions in nuclei of *Salamandra maculata* (RABL, 1885) (for review see (CREMER AND CREMER, 2006), it was THEODOR BOVERI who coined the term chromosome territory (CT) in his 1909 publication[1]. Boveri compared CTs to a sponge which is formed by a reticulum of interconnected chromatin bundles and separated by a chromatin free space and he envisioned the formation of a CT by comparison with the formation of pseudopodia by a rhizopode. When the interphase nucleus is formed, he speculated, chromatin appendages expand from all directions of each participating chromosome. Appendages from a given chromosome anastosome with each other but not with appendages from neighboring chromosomes forming the chromatin recticulum of a given CT.

The central tenet of BOVERI's model of nuclear architecture was the prediction that chromosomes – despite their substantial structural changes during M–G_1 and G_2–M transitions – maintain their individuality throughout cell generations. At his time this prediction stood in stark contrast to the then prevailing view that chromosomes dissolve into chromatin particles during interphase and reaggregate only at the begin-

1 Die Anschauung, daß im ruhenden Kern der höheren Tiere und Pflanzen eine Anzahl von Territorien bestehen, deren jedes aus einem bestimmten Chromosoma der vorhergehenden Mitose entstanden ist und bei der nächsten Mitose wieder zu einem bestimmten Chromosoma sich zusammenzieht, diese Anschauung hat, seit sie zuerst ausgesprochen worden ist, durch vielfältige und sehr verschiedenartige Studien im Tier- und Pflanzenreich immer neue und kräftigere Stützen gewonnen.

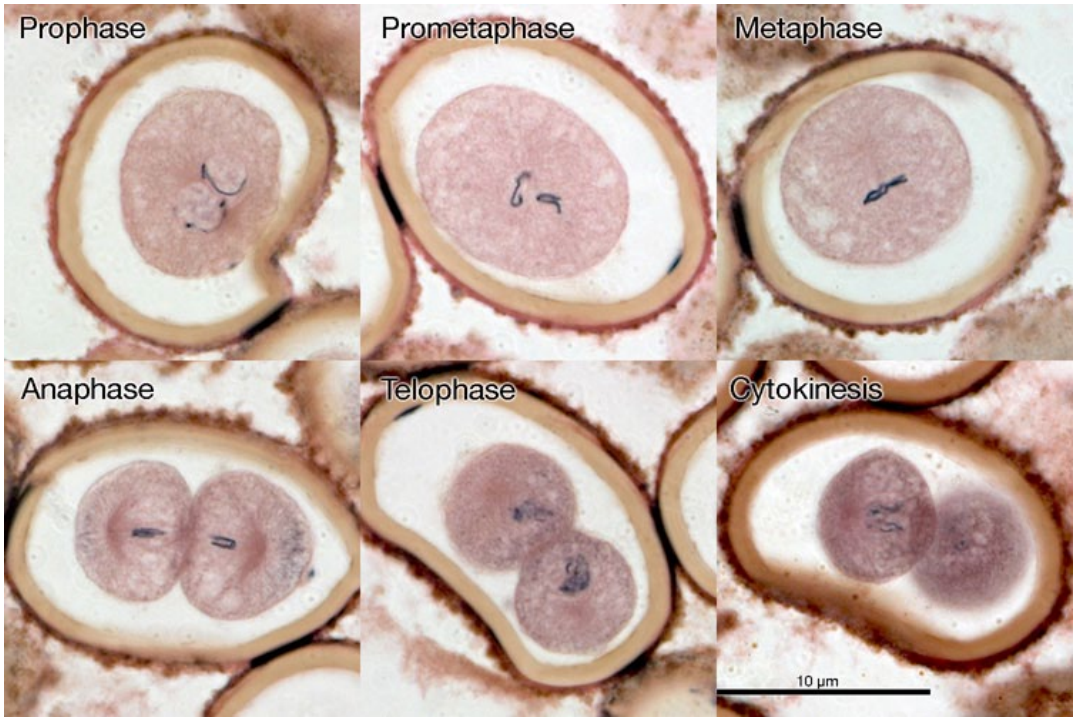

Fig. 2-4: Pictures of mitotic stages in early *Parascaris equorum* embryos taken from histological sections. The **upper panel** displays the stages of the first embryonic cleavage of *Parascaris equorum univalens* the **lower** the same for *Parascaris equorum bivalens.* Observations like these formed the base of Theodor Boveri's theory of chromosome individuality. Sections from the ovaries of *Parascaris equorum univalens* and *bivalens* were stained with iron hematoxylin. (Pictures were taken from old samples found in the zoological archive of the Biocenter (own work)).

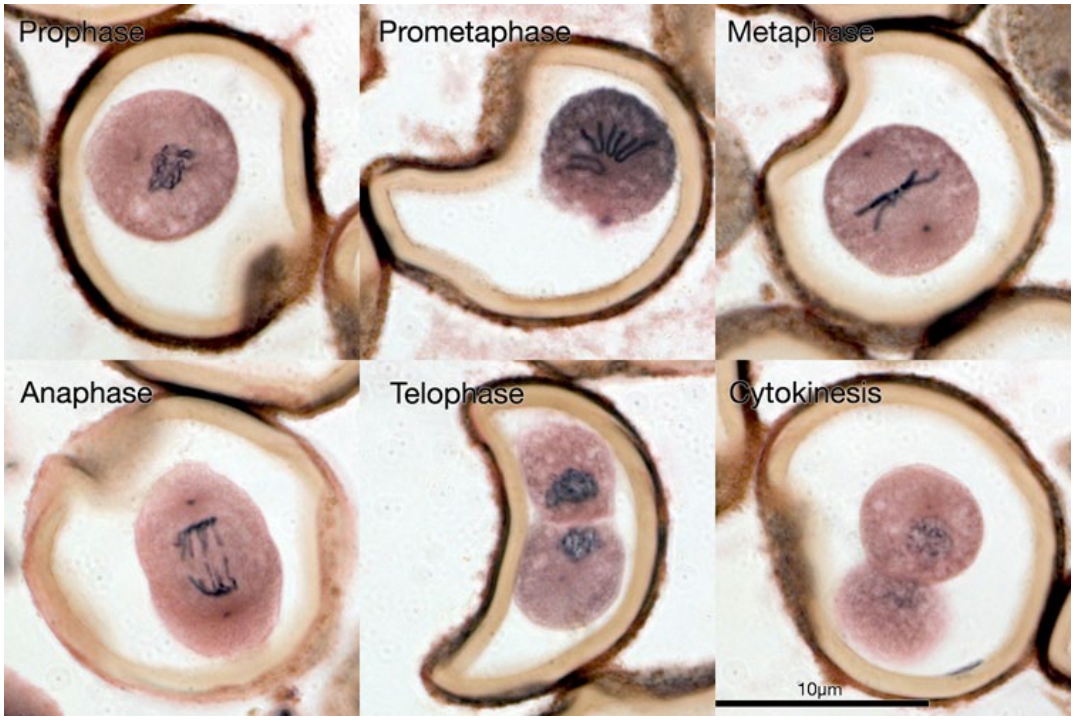

ning of the next mitosis. Since BOVERI was not able to prove the presence of CTs in *Parascaris* nuclei directly, his whole argument in favor of CTs as persistent structural counterparts of mitotic chromosomes was based on indirect evidence. In present terminology this argument runs as follows:

- As long as individual chromatids can be distinguished, they show strikingly similar positions in the two sets of chromatids at the very end of the first mitosis of the zygote (fig. 2-4).
- In the emerging daughter nuclei each chromatid is transformed into a CT at the nuclear region, where it was last observed at telophase.

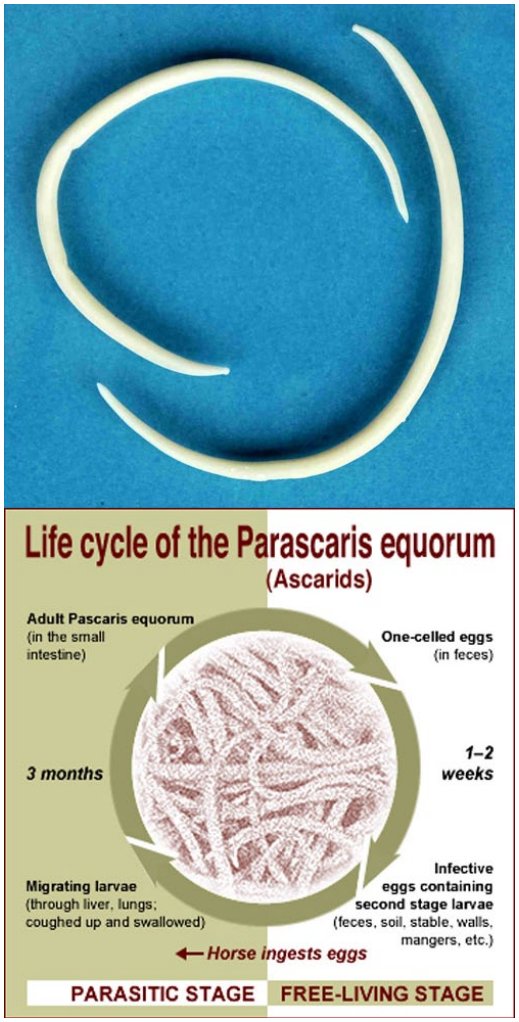

Fig. 2-5: (upper picture) adult stage of two *Parascaris equorum* worms that are 15–50 cm in size (© universidad de cordoba). **(lower picture)** life-cycle of Parascaris equorum.

BOVERI predicted that each individual chromosome, which enters the nucleus at the beginning of interphase, emerges at the next prophase as the same individual chromosome and at the same site despite the fact that it has duplicated in the meantime. This bold hypothesis was supported by studies of fixed two- and four-cell *Parascaris* embryos, where BOVERI compared the arrangements of chromosomes just before they became invisible in daughter cell nuclei at the end of the first mitosis with the arrangements of prophase chromosomes at the onset of the second mitotic division. These still mitotic chromosome arrangements were strikingly similar within studied pairs but showed much inter-pair variation.

BOVERI's studies of CT arrangements in interphase nuclei were hampered by the fact that he could not directly observe CTs. In an attempt to overcome this deficit to the best possible extent, BOVERI took advantage of a structural peculiarity of *Parascaris* nuclei. In these nuclei the ends of chromosomes stick out in protrusions of the nuclear envelope. Using the strikingly similar nuclear topography of these protrusions in pairs of daughter nuclei at all interphase stages as landmarks for the positions of CTs Boveri made two predictions:

I. Each mitotic chromosome reappears at the next prophase in exactly the same nuclear region, where it was transformed into a chromosome territory at the beginning of interphase.

II. The positions of CTs do not change during interphase.

III. Studies of embryos of *Ascaris megalocephala univalens*, however, yielded strong evidence that CT arrangements are stably maintained during interphase, but change from one cell cycle to the next. In four cell stage embryos BOVERI distinguished two pairs of nuclei. Each pair showed a similar topography of their nuclear protrusions, while they differed distinctly between the two pairs (fig 2-5). Boveri assumed that:

IV. movements of chromosomes involved in the formation of the metaphase plate often result in a change of chromosome neighborhood arrangements, whereas

V. The similar arrangements of chromosomes at the end of mitosis result from mirror-like chromatid movements during anaphase and telophase.

Contemporary opponents of BOVERI's theory argued that the observed stability of the positions of chromosome ends sticking in the protrusions of the nuclear envelope did not rule out the possibility that other parts of the chromosomes disintegrated into pieces during interphase and were randomly rearranged into complete chromosomes only at the onset of the next mitosis. In their imagination mitotic chromosomes were just random chromatin aggregations which allowed movements by the spindle apparatus. Boveri, in contrast, considered chromosomes in his own words as "individuals, I would like to say, as the most elementary organisms" (BOVERI, 1909; CREMER AND CREMER, 2006). Yet for him individuality did not mean immutability in every aspect. He insisted that his theory of chromosome individuality was consistent with dramatic changes of size, shape, structure and function of chromosomes during cell cycle and development. Despite these liberal views with respect to genetic persistence of individual chromosomes (as we may phrase the problem of chromatin persistence and change in present days scientific language) and all the concession he made to his contemporary scientific critics, BOVERI stuck categorically to his tenet of chromosome individuality. The reason for his stubborn defense of chromosome individuality was his realization that the Boveri-Sutton theory of heredity stood or fell with the validity of this central tenet. A dissolution and mixture of chromosomes at the beginning of interphase was compatible with Mendelian segregation ratios only under the assumption that all particles belonging to a given chromosome entering the nucleus possess an affinity towards each other of such a kind that they come together again in one chromosome at the end of interphase. If his opponents were correct with their claim that chromosomes dissolve during interphase, an additional 'ad hoc' hypothesis was necessary to explain why the disintegrated chromatin pieces do not assemble into different chromosomes with strikingly different arrangements in the subsequent prophase.

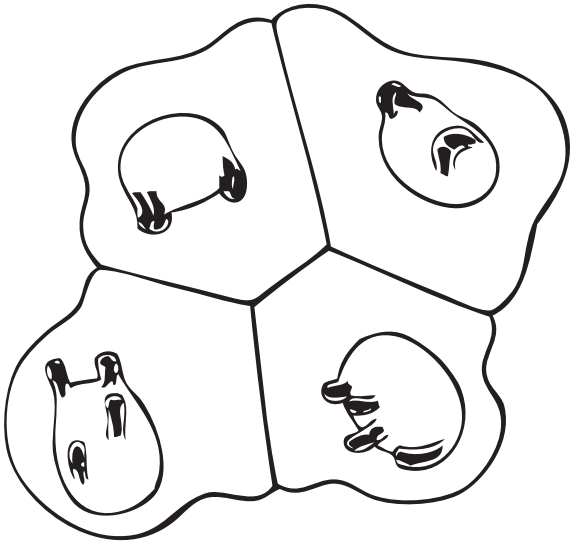

Fig. 2-6: Four cell stage embryo of *Parascaris equorum univalens*. Analysing the configuration of the protruding chromosome ends allows to determine which two cells are daughters and which cells are cousins (BOVERI 1909).

A territorial organization of interphase chromosomes is now generally accepted (for reviews see CREMER AND CREMER, 2010; MISTELI, 2007; PEDERSON, 2004; TADDEI ET AL., 2004; ZHAO ET AL., 2009). In this thesis a new and compelling experimental evidence in favor of the three other major predictions of Boveri's theory of nuclear architecture will be presented. CTs maintain stable neighborhood arrangements during interphase.

GERLICH et al. studied the positioning of chromosomes during the cell cycle in live rat kidney (NRK) carrying chromatin labeled in vivo with H2B-CFP and H2B-YFP (CFP, cyan fluorescent protein; YFP, yellow fluorescent protein) (GERLICH ET AL.,

2003). Laser-microirradiation (λ=514 nm) was used to bleach YFP fluorescence in half of the nuclear volume or single spots during early prophase, while CFP fluorescence of the microirradiated chromatin remained unchanged. Differentially labeled chromatin was followed through mitosis to G_1 using a confocal microscope specifically designed for 4D (space and time) imaging. In addition, computer simulations based on stochastic movements of individual chromosomes were performed. These simulations predicted randomization of chromosome order in mitosis. In contrast to this expectation the experimental data argued for the maintenance of a striking order of chromosomes throughout mitosis.

Independently, a study was designed and carried out at the same time with a HeLa cell line expressing GFP-tagged H2B by (Walter et al., 2003). This study confirmed the stability of CT arrangements during interphase, but in agreement with boveri's model and contrary to the claim of (Gerlich et al., 2003) argued that mitosis results in major changes of CT neighborhood arrangements between a mother nucleus and its two daughters. Nuclei were photobleached in G_2 maintaining a contiguous zone of unbleached chromatin at one nuclear pole. This zone was stably preserved until the onset of prophase, whereas the contiguity of unbleached chromosome segments was lost to a variable extent, when the metaphase plate was formed. Accordingly, chromatin patterns observed in daughter nuclei differed significantly from the mother cell nucleus. A pronounced variability of CT neighborhoods during clonal growth was further confirmed by chromosome painting experiments. The stability of large-scale CT arrangements during interphase was tested by two experimental approaches. In nuclear stripe photobleaching experiments cross stripes or mesh-like geometrical patterns were bleached into HeLa cell nuclei with GFP-tagged H2B at different stages of the cell cycle. These patterns disappeared after some hours due to the replacement of H2B with bleached GFP by new fluorescent H2B-GFP molecules but as long as the bleached chromatin could be followed the patterns did not change but were faithfully maintained.

walter et al. also used a second, fully independent experimental approach to study movements of individual CTs in nuclei of living cells (Walter et al., 2003). Cells were labeled during S-phase with fluorescent nucleotides, such as Cy3-dUTP or Cy5-dUTP. Replication foci, which replicated during the labeling period, were used as live cell markers of ~1-Mb chromatin domains.

Both approaches were not able to confirm the findings of (Gerlich et al., 2003). As a fall-out of the publications from (Gerlich et al., 2003) and (Walter et al., 2003) several reviews (Williams and Fisher, 2003) and additional experimental studies were published both in favor (Essers et al., 2005) and against (Cvacková et al., 2009) the faithful inheritance of chromosome order. In the study presented in this thesis the advances in live-cell microscopy, the usage of photoactivatable chromatin, the comparison between different cell types (including the line that gerlich et al. used) could explain and reproduce the different results observed in (Gerlich et al., 2003, Gerlich et al., 2003) and (Walter et al., 2003) by understanding the mechanics of mitosis.

2.4 DNA Repair

Since "*omnis cellula e cellula*" (every cell is generated by another cell Virchow, 1858), the integrity and the maintenance of its genetic information is of crucial importance. Because deregulations of the cell cycle caused by mutations can result in aging or severe diseases like cancer, surveillance of the DNA is vital for the whole organism. DNA damages can be caused by a variety of different influences like ionizing radiation, UV-Light, radicals and alkylating substances to name only a few. Unfortunately all these different mutagens can cause different kinds of damages to the DNA. For instance UV-light can cause pyrimidin-dimers, organic substances like Mitomycin C can lead to DNA inter-strand cross-links and ionizing radiation leads to the formation of single- and double-strand breaks (Sancar et al., 2004).

To counteract these various DNA damages the cell has developed numerous strategies to detect and revert unforeseen changes in the DNA. Fig. 2-7 shows an illustration which displays some of the information that is already known about the molecular pathways involved and associated with DNA repair. Already from this simplified and incomplete scheme, which shows so many protein-species participating in the defense of the cell's genetic information, one can guess the complexity of this vital task.

The pathways involved in DNA-repair usually comprise proteins that detect and label the damages, others that recruit repair proteins to damaged sites, and proteins that communicate with important cellular regulatory pathways (Misteli and Soutoglou, 2009; Shiloh, 2003). These pathways are e.g. cell cycle control, which can cease cell cycle progression until repair is completed, chromatin remodeling that can open, repair and finally restore the epigenetic information of the damaged chromatin, and finally pathways that decide whether the cell will be repaired or if apoptosis has to be initiated.

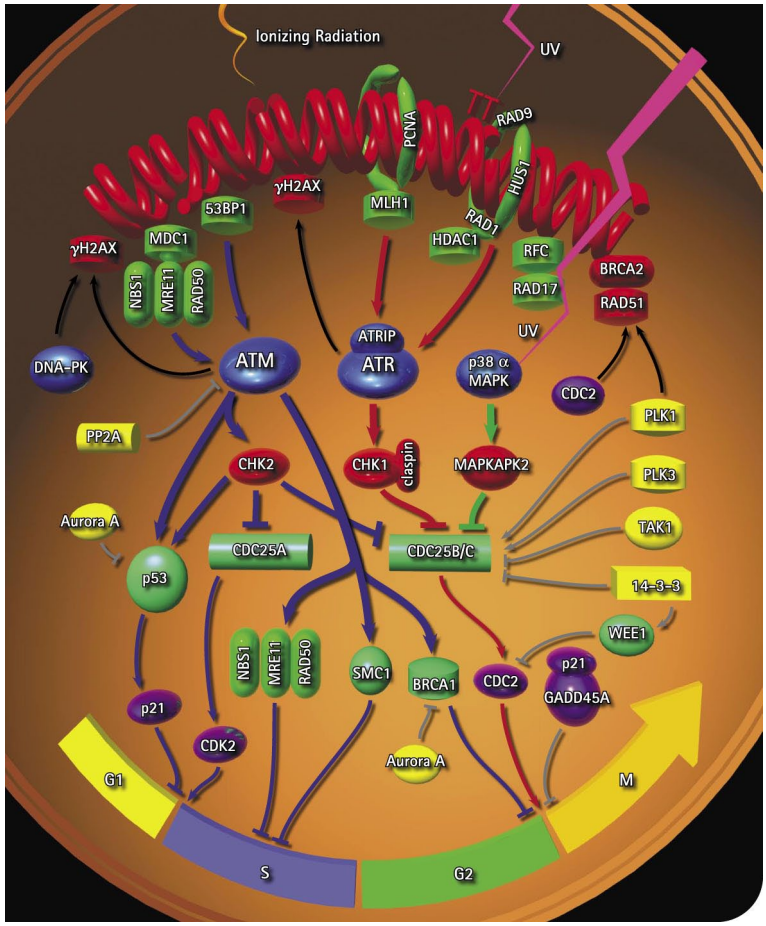

Fig. 2-7: Schematic illustration showing some of the components involved in DNA repair and their relationship to each other forming a complex network. (borrowed from Calbiochem).

In general most of the DNA damages can be repaired very efficiently. The most dangerous DNA damages for the cell are DNA double-strand breaks (DSBs). Due to the linear nature of eukaryotic chromosomes unrepaired

DSBs can lead to partial aneuploidy (by losing big parts of chromosomes) which often results in cell death. Misrejoined DSBs can lead to potentially carcinogenic chromosome rearrangements (Wyman and Kanaar, 2006).

Already a lot about the molecular level of double-strand break repair is known.

DSB repair is mostly carried out by two main pathways: non-homologous end joining (NHEJ) and homologous recombination repair (HRR).

NHEJ (fig. 2-8 (left)) is the major pathway for repairing non-replication-associated breaks and occurs predominantly in G_1-phase of the cell cycle. It is assumed to be error-prone since overlapping single stranded DNA is removed at the ends of the breaks and the resulting blunt DNA ends are just fused together. At sites of multiple DSBs this can lead to misrejoined DSBs and thus to chromosome translocations. By contrast, HRR (fig. 2-8 (right)) occurs mainly during late S–G_2-phase. And, whereas DSB ends are simply joined in NHEJ, HRR uses a sister homologue as a template for repair. This way of repairing DSBs is assumed to be error-free.

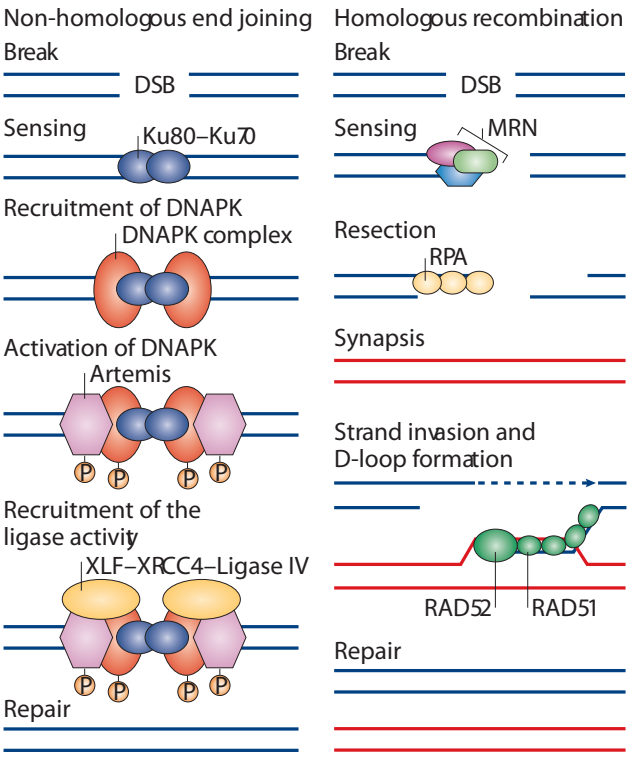

Fig. 2-8: Comparison between alternative ways to repair DNA double strand breaks. **Left:** Non Homologous End Joining (NHEJ) which just fuses broken DNA ends together without verifying them for homology. **Right:** Homologous Recombination (HR) that restores the initial sequence at the (DSBs) by using a homologous chromosomes as a template. Picture taken from (Misteli 2009)

DSB repair starts with the activation of a complex cellular DNA-damage response (DDR) cascade, which includes sensing the DNA damage, subsequent amplification and transmission of a damage signal in order to generate a multitude of cellular responses. DDR pathways are universal and the majority of the involved proteins are highly conserved from yeast to humans. (Misteli and Soutoglou, 2009)

Sites of double strand breaks are detected by the MRN complex. MRN stands for the involved three proteins MRE11 (a DNA binding protein that possesses 3',5' -exonuclease activity, as well as an endonuclease activity that cleaves DNA hairpins), Rad50 (forms homodimers that associate with two MRE11 molecules allowing this structure to form bridges between free DNA ends or between sister chromatids) and NBS1 (NBS1 expression is required for optimal phosphorylation of ATM substrates in damaged cells) (Abraham and Tibbetts, 2005). Like many nuclear proteins, DNA-repair proteins diffuse rapidly within the nucleus and are then recruited to DNA lesions where they bind and thus have an increased residence time (Misteli and Soutoglou, 2009). The MRN complex is crucial for the recruitment and for activation of the kinase ATM, an important player in DSB repair that phosphorylates the histone H2A variant H2AX at the Serin 137 of its C-terminus (γ-H2AX) (Ismail and Hendzel, 2008). This phosphorylation which usually spreads ca.2 Mb around the region of the dam-

aged chromatin is an epigenetic marker that is responsible for the recruitment of many other proteins like MDC1, 53BP1 and proteins that decondense the chromatin around the break. Interestingly many proteins of the DDR and some members of the homologous pathway (if this pathway is chosen) aggregate in such high copy numbers around the damaged DNA (repair-foci), that they can even be visualized by microscopic methods (Lukas et al., 2005). This suggests that the repair of DSBs takes place in a special chromatin microenvironment.

While a lot of information about DNA-repair could already obtained using molecular biology techniques, some of its topological aspects require spatio-temporal imaging methods. Since live-cell 4D microscopy allows the recording of selected cells expressing GFP-tagged proteins in space and time, some still open questions about the spatial properties of DNA-repair are addressed in this thesis.

One of these questions is how the dynamics of different repair-proteins contribute to the formation of DNA repair foci. The dynamics of accumulation at the DNA damage might indicate an order of how the foci are assembled. Since some of the repair-proteins reside within "spontaneous" or "cryptic" nuclear foci before damage is induced it is interesting to investigate whether these foci have some kind of a storage function and whether repair proteins have a different affinity to these structures than towards DNA breaks. Comparison between the dynamics of DDR proteins in different cell types can test wether the dynamics of DDR are the "universal" in all cell types or not.

Another interesting point to address is the spatial correlation between repair foci and other nuclear structures like e.g. nucleoli or centromeres.

A third interesting question that will be examined in this thesis is whether machineries for DNA repair and possibly also for restoration of epigenetic information are built up directly at nuclear sites, where the damages are located. Alternatively, it seems possible that repair machineries are first assembled at other places and then brought the sites of damage – or that damaged DNA/chromatin needs to be moved to a nuclear compartment favorable for the execution of repair, respectively. Recent evidence has supported the hypothesis that the perichromatin region (PR) – in addition to its roles in DNA replication and transcription – serves as the preferential nuclear compartment for DNA repair (Solimando et al., 2009). These new discoveries emphasize the importance to study the topography and kinetics of DNA repair in space and time (4D) at the ultrastructural level.

In the course of this thesis four expression plasmids coding for GFP-tagged repair-proteins involved in double strand repair were available. The constructs were kind gifts of jeroen essers from the roeland kanaar-Lab (Erasmus MC Rotterdam) and of guido drexler from anna friedl's Group (institute for radio biology, LMU). In the following paragraphs these DNA-repair proteins will be briefly introduced.

2.4.1 MDC1

MDC1 (Mediator of DNA-damage checkpoint 1) is a nuclear, 2089 amino acids long protein, participating in the DDR. It possesses two BRCA1 C-terminal (BRCT) motifs (that bind to γ-H2AX), an N-terminal forkhead domain, and a central domain

with 13 repeats of an approx. 41-amino acid sequence (Goldberg et al., 2003). It binds and accumulates to γ-H2AX in repair-foci (Stucki et al., 2005). and amplifies recruitment of the ATM–MRN complex. It is required for activation of the intra-S-phase and G_2/M-phase cell cycle checkpoints in response to DNA damage (Goldberg et al., 2003).

The GFP expression construct used in this thesis was sequenced and a deletion of one of the above mentioned 41 bp repeats was found (see Appendix F).

2.4.2 53BP1

P53 binding protein 1 (53BP1) shows a multitude of structural motives on a 1972 amino acid long polypeptide chain. It contains two Breast Cancer Gene 1 (BRCA1), C-terminal (BRCT) repeats, multiple PIK kinases and cyclin dependent (CDK) phosphorylation sites, two dynein light chain (LC8) binding sites, a GAR methylation stretch and tandem Tudor domains (Adams and Carpenter, 2006). It binds the famous p53 protein which is sometimes referred to be the "guardian of the genome" via the C-terminal BRCT region. In ≥50% of all human cancers P53 is inactivated or defective. In undamaged cells Mdm2, an E3 ubiquitin ligase, interacts with the N-terminus of p53 and ubiquitinates it, thus marking the protein for degradation by the proteasome. ATM phosphorylates p53 in response to DSBs, an event that prevents its Mdm2-mediated degradation and results in the stabilization and accumulation of the protein (Ditullio et al., 2002; Zgheib et al., 2005)(Adams and Carpenter, 2006). Since 53BP1 binds to histone acetyltransferase (HAT) (which is even required for 53BP1 IRIF-formation) (Murr et al., 2006) and histone deacytelase complexes (HDACs)(Kao et al., 2003) (both co-localize in IRIFs with 53BP1) it is a strong candidate for participation in both DSB repair and chromatin remodeling close to the damage. 53BP1 is also involved in the amplification of the DNA damage response signal by participation in a positive feedback loop (Mochan et al., 2003) and accumulates in IRIFs (Bekker-Jensen, 2005). Both γ-H2AX and MDC1 are required for the accumulation of 53BP1 to IRIFs. 53BP1 binds to the MDC1 using its BRCT domain.

2.4.3 Rad51

Rad51 is a small 339 amino acid comprising recombinase involved in the homologous repair of double strand breaks and homologous recombination. It is a highly conserved essential protein and recombination homolog to REC. Rad51 expression is cell cycle dependent in mammals (Yuan et al., 2003) with a maximum in G_2-phase and is involved in detection of homology and for strand pairing stages. Proteins of the RecA/Rad51 family form helical nucleoprotein filaments (Galkin et al., 2006) on DNA and can interact with the ssDNA-binding protein RPA, p53 and Rad52 (Tashiro et al., 2000).

2.4.4 Rad52

Rad52 consists of 418 residues and binds to single stranded DNA in order to anneal complementary strands during homologous recombination repair and meiosis. Furthermore it binds to the replication protein A (RPA) and Rad51 (Gasior et al., 1998; Jackson et al., 2002). In vertebrates its functions can be complemented by Rad51

paralogs like XRCC3. Rad52 can be phosphorylated during DNA repair (Fujimori et al., 2001; Liu and Maizels, 2000).

Electron microscopy (EM) has revealed formation of ring-shaped Rad52 structures (Ø 9–13 nm), and higher-order aggregates. Furthermore Rad52 binds to DNA ends as an aggregated complex that ranges in size from approximately (Ø 15–60 nm) (Ranatunga et Al., 2001). This binding promotes end-to-end association between DNA molecules and stimulates the ligation of both cohesive and blunt DNA ends (Ranatunga et Al., 2001, Shinohara et al., 1998).

2.5 Microscopy – past, present and future

Compared to the relatively young discipline of molecular biology, cytology looks back on a much longer history. It can be traced back to the days of renaissance and since then it is inseparably connected to the enhancement and development of new microscopes. Giving visual access to the formally invisible structures of the microcosmos and describing the components of life paved the way for a better understanding of how life is organized at its common basic level – the cell.

As shown in fig. 2-9(a & b) the discoveries in cell biology and the successful implementation of cutting edge technology into microscopes went seamlessly hand in hand. Some milestones to mention in microscopy development were the invention of achromatic lenses, photographic acquisition of pictures, oil-immersion, contrasting methods like phase contrast and DIC and of course electron microscopy. During the last 30 years fluorescence microscopy has become a more and more important tool of cell biology allowing to specifically stain certain structures of interest within cells. The constantly enhanced techniques of labeling proteins and nucleic acids demanded the construction of more and more powerful microscopes. The development of confocal laser scanning microscopes which can reduce the off-focus light from other parts of the observed sample using two pin-holes in the beam-path (Cremer and Cremer,

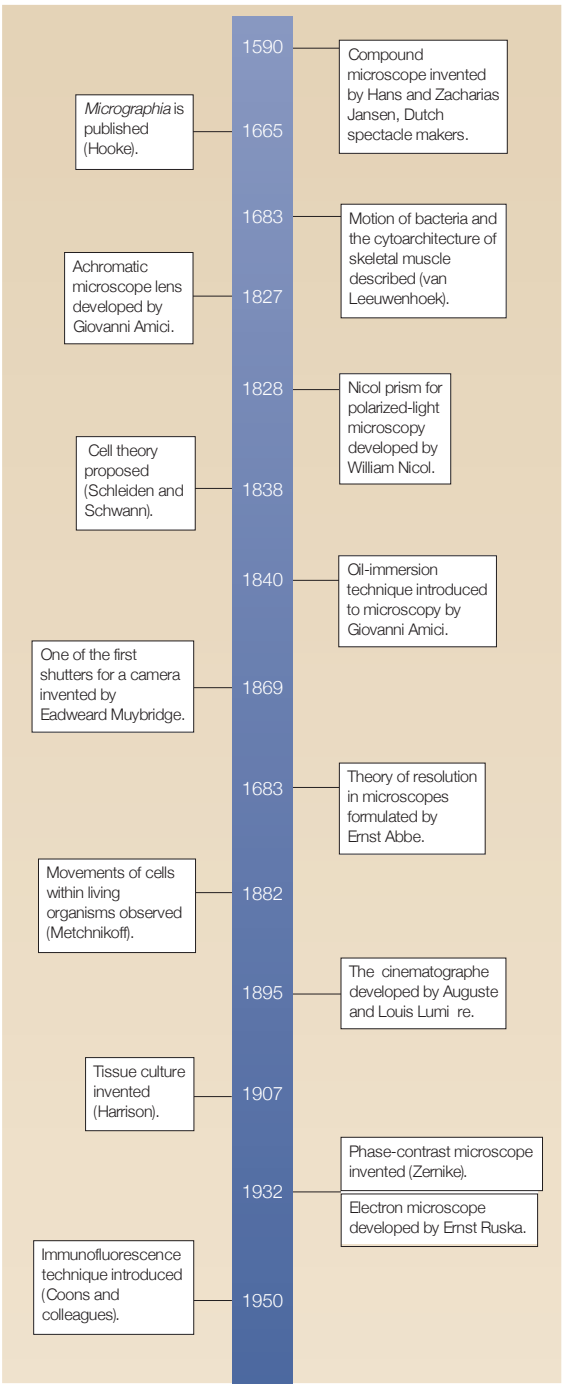

Fig. 2-9a: Timeline on the developments in microscopy (inspired by Dunn et al. 2004).

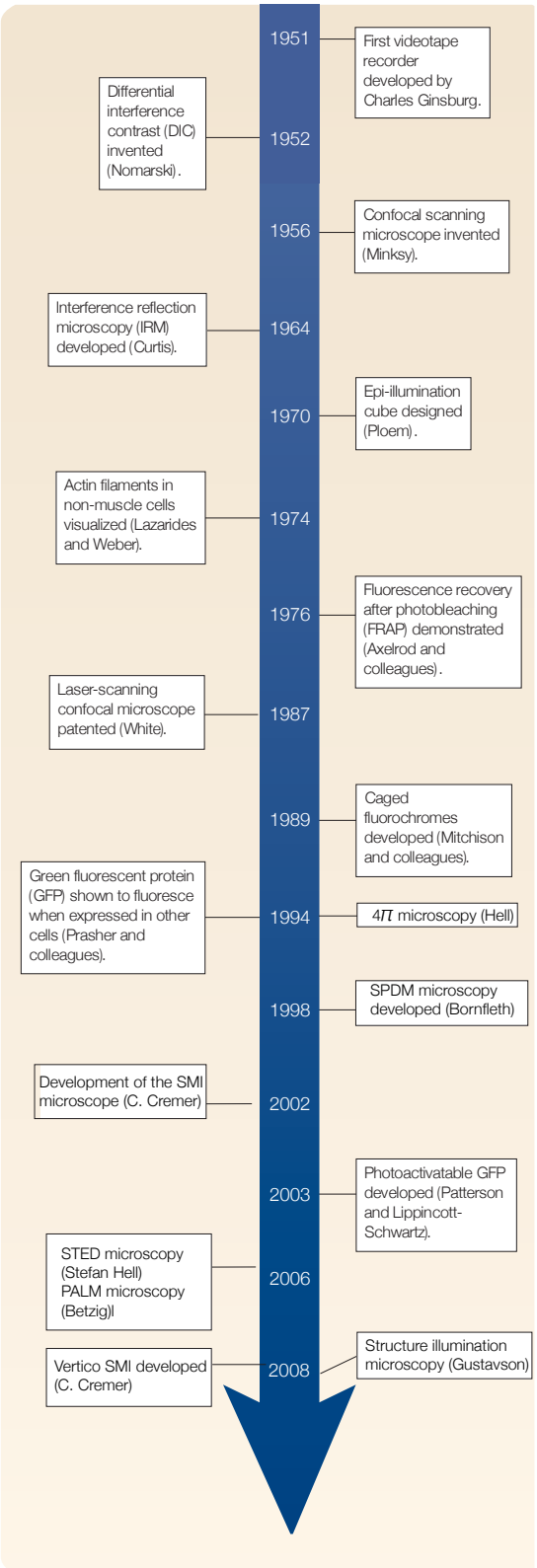

Fig. 2-9b: Timeline on the developments in microscopy part II (inspired by DUNN ET AL., 2004)

1978) currently define the state of the art equipment of every modern cell biological institute (for review see DUNN AND JONES, 2004). These instruments are able to image microscopic samples in 3D and allow to explore the kinetics within a living cell or a cell nucleus. At present, the calls for higher spatial resolution are getting louder and louder.

While electron microscopes have a much higher resolution than light microscopes they are limited in other properties making them sometimes difficult to use in cell biology. Since electron beams can only be used in a vacuum, biological specimens have to be prepared in very thin fixed dehydrated serial sections to look e.g. inside of cells. In contrast to light microscopy that can use colors to discriminate different structures, electron microscopic samples in general have to be treated with electron dense stains or antibody-bound metal (gold) nano-particles in order to label specific structures or to increase the otherwise weak contrasts.

Recent developments in electron microscopy allow 3D reconstruction at an ultrastructural level by progressive ablation of the sample using a diamond knife or a particle beam (ROUQUETTE ET AL., 2009; SCHROEDER-REITER ET AL., 2009).

Until now light microscopes were limited to a resolution down to 200 µm. Although electron microscopes are able to show much smaller structures than that, it is much harder to obtain 3D data with differently labeled structures using this kind of microscopy and live cell imaging cannot be performed with this method at all. Recently new revolutionary methods were developed to circumvent the Abbe limit in light microscopy. The ABBE limit:

$$d_{\min} = \frac{\lambda}{2 \cdot NA}$$

is a physical equation formulated by ERNST ABBE in 1873 describing how light-optical resolution (d_{min}) is limited by the dependencies between wavelength λ, and the numerical aperture of the object lens (NA). These new approaches will be briefly mentioned in the next paragraphs.

2.5.1 4Pi Microscopy

The 4Pi microscope is a confocal laser scanning microscope that uses two objective lenses to illuminate a point on the sample. By superposition of the excitation light axial (z)-resolution is increased (up to 7 fold) (Hell, 2007) whereas the resolution in x and y does not differ from a conventional confocal microscope. The microscope was built 1994 by stephan hell but the principles were developed in the early seventieth by thomas cremer and christoph cremer.

2.5.2 PALM (Photoactivation Localization Microscopy)

This method uses the fact that fluorophores, even if their distance is below the optical resolution limit, can be separated if they emit light at different times. The fluorophores are first excited into a state of blinking and then the their stochastic light emission is recorded over time. After computation of the intensity centers of the recorded fluorescence events these are then compiled into an image. Like other superresolution approaches (e.g. STED) the improvement in resolution is only achieved in the (x,y)-plane but not on the z-axis (Betzig et al., 2006).

2.5.3 Vertico SMI

The Vertico SMI is an instrument combining the PALM technique with a technique called Spatially Modulated Illumination (SMI) that allows the excitement of fluorochromes only at locally constraint planes in z – which are located in the maxima of a standing light wave (the Vertico SMI has two opposing objectives that encompass the sample). Combining the PALM and the SMI technique can lower the resolution to approx. 10 nm in (x,y) and ca. 30 nm in z (Gunkel et al., 2009).

2.5.4 SIM (Structured Illumination)

This approach increasing the resolution below the Abbe limit uses a normal fluorescence widefield microscopic set-up. The illumination here is carried out by lasers projecting different geometric patterns onto the sample. The pictures of the recorded illumination pattern are then combined by a complex mathematical computation into a picture that has a resolution of down to 100 nm in x and y (2 fold better then a conventional widefield) fluorescence microscope. Axial resolution is reduced as well down to 100 nm when recording image stacks (even 5 fold better) (Gustafsson et al., 2008; Schermelleh et al., 2008).

2.5.5 STED (Stimulated Emission Depletion)

This approach uses the illumination of an area on the sample by a laser beam (like in normal confocal microscope) followed by a second beam with the wave-length of the fluorescent emission line resulting in destructive interference that anihilates all light except the light in a very small central area. Using the fluorescent light emitted by this small area in (x,y) combined with the knowledge of its position allows to generate pictures with a resolution increasement in (x,y) up to 12 fold (< 20 nm) better compared to a normal confocal microscope (Donnert et al., 2006). However this approach doesn't enhance resolution in z.

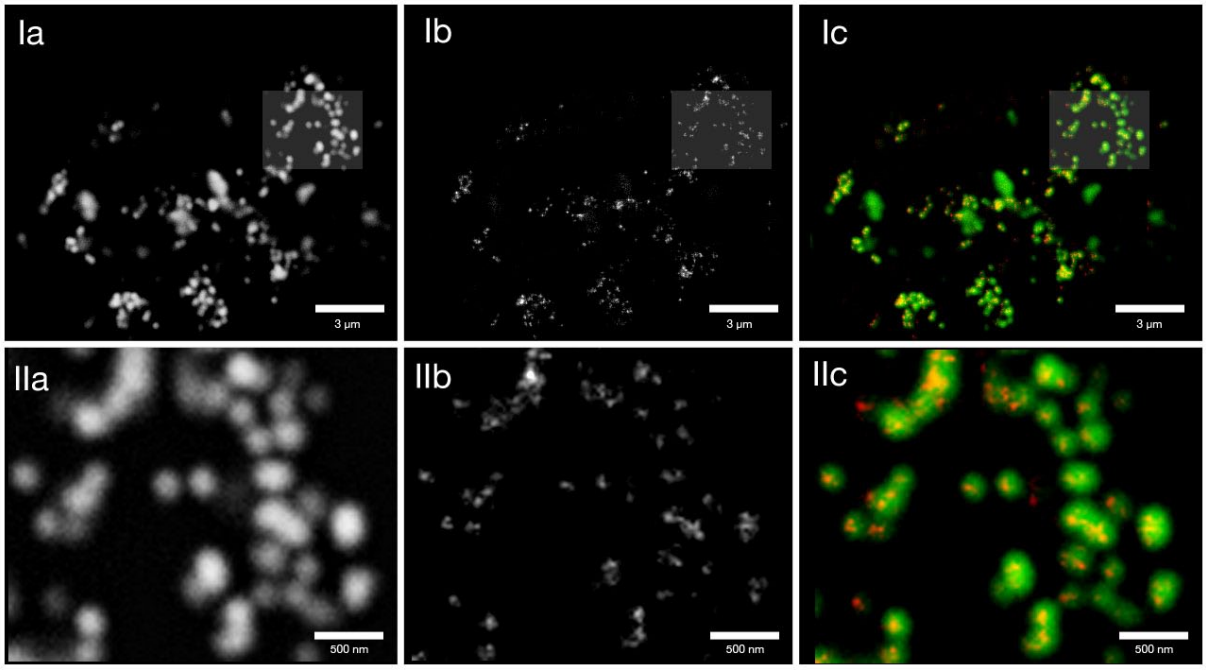

Fig. 2-10: Confocal and STED-Images (single section) of replication labeled U2OS cells (own work). The cells were labeled by scratch labeling (see 3.3.4) using dUTP-Atto 647N and then incubated for several replication and division cycles. It is clearly visible that the replication foci recorded by a conventional confocal set-up (Ia and IIa) are about 200 nm in size as predicted by the Abbe limit. STED imaging of the same object demonstrates the enhancement in resolution showing even distinct foci in cases where the signals recorded by the conventional confocal mode can't be separated from another. Further Ib and IIb also show signals that are not spherical as they appear in the confocal images.

2.6 Live-cell fluorescence microscopy

2.6.1 Advantages and disadvantages of live-cell microscopy

Whereas the advantages in microscopy of fixed samples, which somehow represent a snapshot in time of a cell population, lie within the relative simple experimental requirements, preparations and long-term stability of the samples, live-cell microscopy is able to provide information about the temporal development and the order of processes e.g. morphological changes in the nucleus of individual cells. These benefits unfortunately go hand in hand with much higher demands with respect to experimental conditions, instrumentation, required data space and planning.

The following paragraphs will give an overview of the many requirements which have to be met when successful live-cell microscopy is desired.

When it comes to the observations of living cells the **first** and most important point of all is the choice of the right cells. While since the development of cell-culture in 1907 (Harrison, 1907) a lot of different cultured cell lines are available from many different species, tissues and tumors, the right choice of cell type can be crucial for the success of an experiment. Since many experiments in biochemistry or molecular biology address to metabolic or general genetic questions, established tumor cell lines may be an adequate choice as they grow fast, are easy to handle and only have little demands with respect to culture conditions. Although these cell lines – like the cancer line HeLa – may be optimal e.g. for metabolic research they might be inappropriate for many other experiments since tey are derived from tumors and so do not reflect the properties of original tissue in a living, healthy organism. The HeLa cell

line serves as a good example for a cell line that has been taken into culture since a long time and that has meanwhile diversified into different sub-strains and has opted for the growth in incubators.

Secondly, working with adherent cells that are growing on an optical glass slide implies the choice of an inverse microscope (that watches the cells from below). When looking at cells that contain fluorescence tags or when looking at small-scale structures it is recommended to use immersion objectives (e.g. oil, glycerol or water), since – given a high numerical aperture – they provide the highest possible optical resolution and allow to collect the most of the emitted light. The microscope should also be equipped with a flawlessly working auto-focus system which compensates for small, thermally caused, axial movements of the substrate at which the cells are growing and an acquisition software that at least runs stable within the observation period. If no adequate auto-focus system is available, then thermal fluctuations in the system should be minimized in order to guarantee observation of the same focal plane in z over time.

Despite the benefits of high optical resolution provided by the use of high numerical aperture oil immersion objectives, they should only be taken to observe structures that are not too far away from the optical substrate they are mounted on (like e.g. adherent mono-layer cell-cultures growing on a cover slip). If tissues or cell types that can grow in hight (e.g. embryonal stem-cells) have to be imaged, other objectives like glycerol immersion objectives might considered since the depth at which oil immersion objectives can provide still acceptable image quality is limited to 20 µm away from the cover slip (or other optical substrates).

Third – illumination and signal detection are other big issues that mustn't be neglected. The choice of the illumination source is an extremely critical point in terms of cell viability, when using fluorescence-live-cell microscopy. Since in this case the objective lens serves as objective and condenser at the same time – the illumination intensity at the observed cells increases with the magnification power of the used objective lens and its numerical aperture. Since illumination sources like mercury lamps (that have their highest emission peak within the ultra violet spectrum at around 360 nm) are very frequently used in fluorescence microscopes it is very important to rule out that any DNA-damaging ultraviolet light is getting into contact with living cells. To avoid this scenario which can add enormous bias to your experimental observation (Chuang et al., 2006) it is strongly recommended to use an alternative light source e.g. a laser, a monochromator or simply a 12 V 100 W Halogen lamp in combination with a 450 nm longpass (LP) filter (since ordinary fluorescence filters don't cover the whole visible and UV-spectrum as one might assume). Using light emitting diodes (LEDs) for excitation of the fluorophores is a relatively new but very promising and inexpensive technical development which recently appeared on the market.

However since radicals emerge during the illumination of the sample even with intensive visible light, the time intervals between image acquisitions are still critical to the cells, even when using the least toxic illumination sources and filter sets. To decrease photo toxicity caused by long exposure times a very sensitive camera or photomultiplier can be helpful.

Fourth – it is necessary to generate adequate culture conditions for the observed cells at the microscopic stand which are at least similar to those existing in the a normal incubator (although these are far from being optimal compared to the conditions that exist in the original organism). This requires the use of a suitable cell-chamber which is controlled by a heating-unit and a temperature-controller. Usually mammalian cells are cultivated at a physiological pH level (pH 7.2). In an ordinary cell incubator this is achieved by an amount of 5% CO_2 in a saturated humid atmosphere and the presence of a $NaCO_3$ buffer system in the medium. Stable pH conditions can be generated at the microscope either by controlled influx of CO_2 into the observation chamber (using an extra device) – or by adding a HEPES-buffer to the medium that keeps the pH constant independently of the carbonate-buffer-system (mind correcting for the osmolarity!).

During live-cell observations (especially when using fluorescence) it is recommended to use phenol-red free medium since phenol-red might produce radicals that are cytotoxic during the observation. Reducing the damaging effects of radicals can be optimized by the use of scavengers, like Trolox (vitamin E derivative), that integrate into the cell's membrane-system and should be added approximately 12 h prior to observation.

When observing cells for longer time periods, evaporation of the medium can change the concentrations of the medium's ingredients and osmolarity. This can strongly change the experimental conditions and bias the results. To prevent that, make sure that evaporation of the medium is minimized by sealing the live-cell-chamber with a piece of para-film or the use of a humidifier.

Fifth – long-term observations of living cells (especially if you are recording 4D data sets of multiple positions) require a lot of data storage space and powerful computers and computer programs to analyze them.

Last but not least and different from the microscopy of fixed specimen the available en-bloc observation time should be sufficient long to record the things you want to observe.

Although it is not extraordinarily difficult to handle each of this points separately, the main difficulty lies in fulfilling all these requirements all at once. The scenario gets even more complicated when working with transgenic cells where the expression-level of the transgene (e.g. a GFP-tagged fusion protein) is important for the observation or when looking at quite rare events like e.g. mitotic divisions.

This thesis strongly benefited from the circumstance that nearly unlimited access to one of the latest generation spinning-disc confocal microscopes was possible. Unlike a normal point scanning confocal light microscope which illuminates and scans the sample line by line, this instrument applies a technique which is illustrated in fig. 2-11, where the illumination and confocal imaging of many points on the sample is achieved simultaneously using a rotating (spinning) disc that contains numerous pinholes. This reduces the cytotoxicity and allows quick acquisition of images. Another advantage of this microscope is that it is equipped with a very sensitive 14-bit EM-CCD camera.

With the set-up as it was used for this thesis it is also possible to perform FRAP

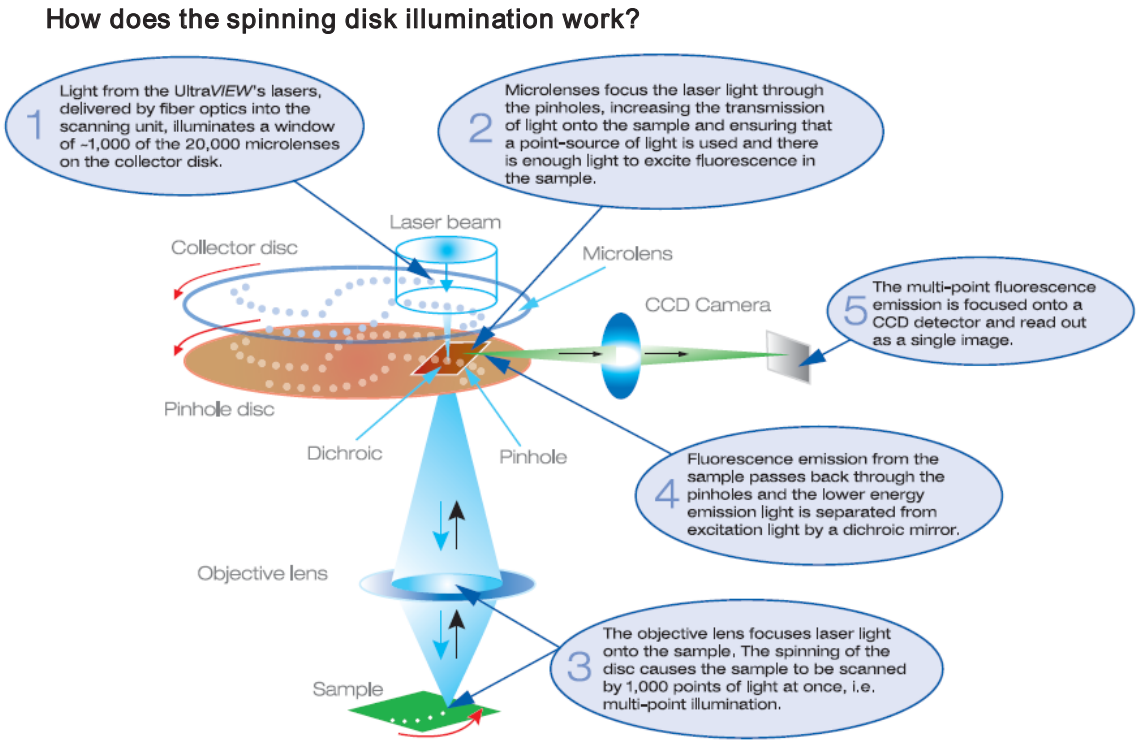

Fig. 2-11: Draft of the spinning disc confocal principle (taken from the Volocity 5 user guide (Improvision/PerkinElmer)). In contrast to point scanning confocal microscopes this microscopical technique uses a rotating NIPKOW disc containing many pinholes allowing illumination and detection of multiple areas on the sample simultaneously. A CCD camera serves as light detector.

(Fluorescence Recovery after Photobleaching) Experiments. This feature was especially helpful to explore the kinetics of repair proteins and "abused" to photoactivate patterns into chromatin.

2.6.2 Live-cell fluorophores

While in fluorescence light microscopy of fixed samples the usage of chemical fluorophores attached to antibodies or DNA probes is well established, the labeling of specific structures in living cells is much more delicate. Since for immunostaining of fixed samples the cell membranes have to be permeabilized, antibodies and probes have direct access to their specific targets inside of the cells. In contrast to that the plasma membrane of living cells is vital for their survival and represents a problematic barrier for the most of the staining methods and dyes. Although in principle fluorochrome labeled antibodies could be brought into the cell via microinjection, the tediousness of this method is not suitable for the observation of a large numbers of cells.

Nevertheless since a couple of years some great methods were established which allow fluorescence microscopic visualization of specific structures in living cells.

These methods will be introduced in the following paragraphs:

Labeling the DNA within the nucleus of a living cell can be performed using Hoechst, a chemical dye very similar to DAPI which is used as standard counterstain in most of the immunofluorescence or FISH preparations. Due to its small molecular weight it can pass the membranes of the cells and bind (putatively) to the minor groove of the DNA. However Hoechst alters the structure of the chromatin and has been found to be mutagenic.

Another way to label DNA directly for live-cell observations is to provide the cells with fluorochome labeled nucleotides during S-phase. Because of their disability to pass the cell's membranes, they have to be brought into the cytosol actively. This can be performed by scratch-labeling (see 3.3.4), electroporation (see 3.3.5) or microinjecton (see 3.3.6). During DNA replication the nucleotides are incorporated into the newly synthesized DNA. While theoretically half of the DNA and full chromosomes are labeled, when incorporation of the fluorescent nucleotides takes place directly before S-phase, only a couple of late replicating replicons are stained, when the nucleotides enter the cell just before the end of S-phase. If replication labeled cells are cultured for a couple of cell cycles the amount of fluorescent DNA decreases due to the segregation of the labeled chromosomes during mitosis. Interestingly cells and their DNA-polymerases seem to tolerate the labeled nucleotides despite their bulky fluorophores.

A very elegant an non-invasive way to label in vivo structures (e.g. the whole nucleus) was introduced by the use of GFP-fusion proteins (e.g. H2B-GFP). Fluorescent protein fusion proteins represent an universal tool to labeling specific protein species and will be introduced in the next section.

2.6.2.1 GFP (Green Fluorescent Protein) and other fluorescent proteins

The 1990th brought an abundance of technical advances that allowed the combined use of high quality optical microscopy and molecular cloning techniques. One major step in this context was the adapation of GFP (and other fluorescent proteins) to serve as an efficient fluorescent live-cell marker.

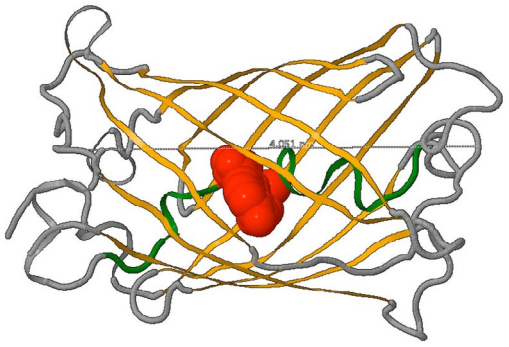

Fig. 2-12: 3D Model of the wild-type green fluorescent protein (GFP) (238 amino acids, 26,9 kDa). The amino acid backbone is shown in a "cartoon" representation. Orange colored areas show the antiparallel β-sheets that form the barrel structure. The green colored part shows amino acid sequence that crosses the inner part of the barrel. The three amino acids that form the fluorophore are shown in red (space-filled representation). (Own work). Structure-Data taken from 1GFL.pdb. Rendered with JMol.

The history of GFP can be traced back to the early 1960th, when the bioluminescent properties of the jellyfish *Aequorea victoria* were studied. Beneath a Ca^{++} dependent bioluminescent protein (*Aequorin*) (Shimomura et al., 1962) another protein was found which was not itself luminescent but which fluoresced green under UV light. This 26,9 kd protein was named green fluorescent protein (GFP). GFP was cloned in 1992 (Prasher et al., 1992) and first used for tracking gene expression in 1994 (Chalfie et al., 1994). Since then GFP was broadly used and optimized in molecular biology for a variety of different purposes ranging from being a simple indicator for gene expression to the visualization of chromatin domains or specific proteins when expressed as a fusion protein tagging a certain protein species with its ability to fluoresce.

Like for the majority of proteins, the 3-dimensional structure of the GFP protein is

essential for its function. The protein consists of 11 antiparallel β-strands (Ormö et al., 1996) which are forming the remarkably stable barrel structure surrounding the actual fluorochrome that is formed by a cyclisation reaction (called maturation) of three consecutive amino acids in the inner part of the protein (see fig. 2-12 and fig. 2-13). The spatial arrangement of these three interconnected amino acids (Ser65, Tyr66, and Gly67) (4-(p-hydroxybenzylidene)-5-imidazolinone) is responsible for its fluorescent properties.

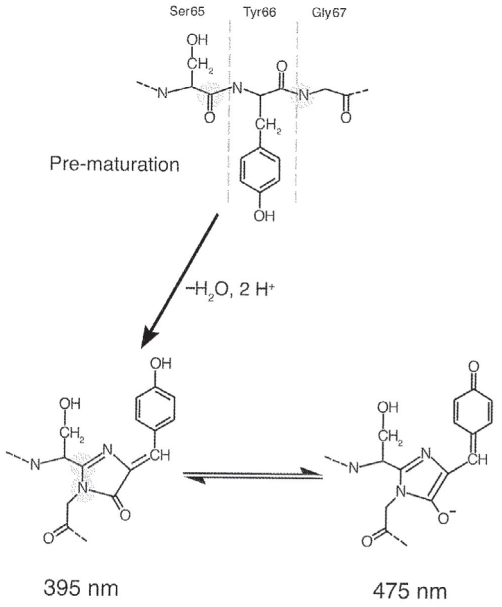

Fig. 2-13: Maturation of the GFP fluorophore. Reaction of the carboxyl carbon of Ser65 and the amino nitrogen of Gly67 (highlighted) leads to formation of the fluorophore. Two absorptive states are known to exist; a predominant, protonated form that absorbs at 395 nm and a less prevalent, unprotonated form that absorbs at approximately 475 nm. (Live-Cell Imaging: a laboratory manual (Book))

Biochemical engineering of the wild-type GFP by mutagenesis has made this protein an extremely useful marker of gene expression and protein trafficking in living cells. For these applications, the genetic sequences of GFP and a protein of interest are concatenated to obtain a functional fusion protein with a fluorescent tag. Novel hues, including blue, cyan and yellow GFP variants, were created by protein engineering, thus allowing multicolor applications, e.g. Förster resonance energy transfer (FRET)-based studies on protein–protein interaction.

During the last years, the GFP family of proteins was profoundly augmented by the discovery of GFP-like proteins in non-bioluminescent *Anthozoa*. Besides cyan, green and yellow emitters, red fluorescent variants that were sought-after for a long time were finally identified among these novel homologs. Fluoro proteins with emission in the red part of the spectrum were highly wanted for live-cell imaging applications because background generating cellular autofluorescence is reduced in the red spectral range, excitation with light of longer wavelength is less phototoxic and because red emitting fluorophores can be used for multicolor labeling or FRET experiments. Finally non-fluorescent, but strong absorbing GFP-like chromoproteins (CPs) found in sea anemones and other cnidarians were engineered into far-red-emitting fluoro proteins and an encoded photosensitizer (Bulina et al., 2005) (Wiedenmann and Nienhaus, 2006).

One of the problems of the wild-type forms of fluoro proteins are, that they often polymerize and form cytotoxic aggregates.

Beyond the modification of coelenterate proteins phytochromes fluorescing in infra red of bacterial origin were found to be an interesting alternative to label cellular structures in tissue since infrared light can be used to look deep into tissues (Shu et al., 2009).

In 2008 the contributions of osamu shimomura, martin chalfie and roger tsien in discovering GFP, enhancing it and to developing it into a widely used tool in the biosciences were awarded with the nobel prize for chemistry (Service, 2008).

2.6.2.2 Photoactivatable GFP and photoswitchable FPs

Stable conversion to the anionic state due to decarboxylation of Glu222 can be caused by intense irradiation of the neutral GFP chromophore. This causes a threefold increase in fluorescence when exciting the protein bulk at approximately 488 nm (van Thor et al., 2002; van Thor et al., 1998; Yokoe and Meyer, 1996). This effect was further enhanced in the photoactivatable GFP variant (PA-GFP) by a single mutation (Thr203His). Intense exposure to approximately 400 nm light causes irreversible photoconversion, with excitation and emission maxima at 504 and 517 nm, respectively. This can generate an emission increase (for excitation at 488 nm) by a factor of approximately 100 in live cells (Lukyanov et al., 2005; Patterson and Lippincott-Schwartz, 2002, 2004) (Wiedenmann and Nienhaus, 2006). Recently it was reported by the lab of jennifer lippincott-schwarz, that a photoactivatable RFP has been developed (Subach et al., 2009).

Beside photoactivatable fluorescent proteins there are also photoconvertable fluorescent proteins like EOS-FP, or Dendra2 which change their color from green to red after exposing them to blue light (Lukyanov et al., 2005; Wiedenmann and Nienhaus, 2006).

2.6.2.3 Chromobodies

A very interesting and promising new approach to specifically stain structures within the cell was recently made by ulrich rothbauer and heinrich leonhardt. They created a hybrid between an epitope-recognizing fragment of a monovalent *Alpaca* antibody and a chromoprotein that is expressed as one fusion protein. Due to the small size of the used fragment from the *Alpaca* antibody the genetic information for these „Chromobody“ named fusion proteins fit into an ordinary expression plasmid (Rothbauer et al., 2006).

One benefit of this system is that non-protein structures or post translational modifications can be visualized in living cells. In contrast to FP-fusion proteins, which represent an additional protein species to the endogenous protein pool, chromobodies can visualize the endogenous protein population at unbiased expression levels.

3 Materials and Methods

3.1 Amplification, preparation, and storage of expression plasmids

Plasmids are extra chromosomal, self replicating DNA of prokaryotes. Within this thesis plasmid constructs were used to express certain transgenes in mammalian cells. This section describes some of the used methods to amplify, isolate and to store plasmid based gene expression vectors.

3.1.1 Transformation of bacteria with plasmids

In order to amplify expression plasmids within the bacteria species *Escherichia coli*, the plasmids have to be transferred into the bacteria. The following protocol uses heat shock induced transformation of chemical competent cells.

Materials:

- Chemical competent bacteria (e.g. DH5α)
- Control plasmid pUC 19
- Microcentrifuge for 600 µl tubes
- Micropipette and tips
- Ice/ ice-water bath
- PCR machine and 600 µl tubes
- Parafilm®
- Plasmid DNA
- Shaker at 37°C

Method:

- Dilute the plasmid DNA (to a concentration of about 10 ng/µl of DNA) and place it on ice.
- Dilute pUC 19 (control vector) to a concentration of 1 ng/µl (place on ice).
- Thaw competent bacteria on ice.
- Transfer 100µl bacteria into pre-chilled to 1.5 ml Eppendorf tubes.
- Add 1 µl of each diluted plasmid construct and the diluted control vector (pUC) to the bacteria on ice.
- Mix gently and incubate on ice for 30 minutes.

- Heat the tubes to 42°C for 20-30 seconds in the PCR machine.
- Place on ice for 2 minutes.
- Transfer bacteria into 15 ml Falcon tubes.
- Add 3 ml of LB medium.
- Shake at about 150 rpm for 45 minutes at 37°C.
- Plate 100 µl of the bacteria onto one agar plate without antibiotic.
- Plate 100 µl of the bacteria onto one agar plate with antibiotic.
- Plate 200 µl of the bacteria onto another agar plate with antibiotic.
- Invert the plates and place them at 37°C overnight.
- Seal the plates with parafilm and store at 4°C or
- pick colonies to inoculate LB medium (e.g. for producing glycerol stocks or a preculture)

3.1.2 Glycerol stocks

Materials:

- Glycerol
- dd H_2O
- Overnight liquid bacteria culture
- Screw-cap tubes

Method:

- Pipet 0.5ml of 50% glycerol into each screw-cap tube
- Add 0.5ml of overnight liquid bacteria culture into each tube
- Pipet up and down to gently mix
- Store in -80°C freezer

3.1.3 Preparation of plasmid DNA

Materials:

- 5 ml pipettes
- 50 ml Falcon tubes
- 70% ethanol

- Antibiotics
- Centrifuges
- Glycerol stocks for the respective plasmid
- Isopropanol
- LB Medium
- QIAprep® Midiprep Kit

Method:

Plasmid DNA was purified with the QIAprep® Midiprep Kit according to the manufacturer's instructions.

- Inoculate 5 ml LB medium (containing the respective antibiotic) with a tip that was used to scratch the surface of an *E. coli* glycerol stock and incubate on a shaker (60 rpm) at 37°C for 5 h
- from this pre-culture use 50 µl to inoculate a new flask containing 50 ml LB medium (with antibiotics)
- after incubation of ca. 15 h on a shaker (60 RPM) at 37°C, transfer into a 50 ml Falcon tube and centrifuge at 5000 RPM for 5 minutes
- discard supernatant and resuspended the pellet in 4 ml P1 buffer from the extraction kit
- for lysis add 4 ml P2 buffer invert the tubes 6x and incubate at RT for 5 minutes
- stop lysis reaction using 4ml P3 buffer and pour the suspension into a filter syringe; wait for 5 minutes
- equilibrate the DNA affinity column with 4 ml of QBT buffer
- Add a plunger and squeeze the suspension through the filter into the DNA affinity column
- Wash the column with 20 ml QC buffer
- Elute the plasmid DNA using 5 ml of QF
- Add 3.5 ml isopropanol to and centrifuge at 15,000 x g for 10 min
- Wash the pellet with 2 ml of 70% ethanol
- Air dry the DNA until it is visible as a small translucent pellet.
- Solve this pellet in water
- Measure concentration in a DNA photometer (a 260/280 nm ratio of >1.7 is required for transfection of eukaryotic cells)
- Dilute the isolated DNA in H_2O dd down to a concentration of 1 µg/ml
- Store at -20°C until usage

3.2 Cell cultivation

Cells were cultured in a humidified incubator at 37°C in a 5% CO_2 atmosphere. Growth media were supplemented with 10% FCS, 100 U Penicillin, 100 µg/ml Streptomycin. For live-cell observations phenol-red free medium supplemented with 25 mM HEPES and 10 µM Trolox was used. The growth media were used dependent on the chosen cell line.

- HeLa cells were cultured in RPMI-1640 (Roswell Park Memorial Institute).
- U2OS cells were cultured in D-MEM (Dulbecco's Modified Eagle Medium),
- RPE1 cells were cultured in HAMs F-12/D-MEM 1:1

Cell culture work was carried out under sterile conditions using a sterile work bench.

3.2.1 Thawing cells

Materials:

- Bunsen burner
- Centrifuge
- Cryo-tubes with deep-frozen cell suspension stored in liquid nitrogen at -196°C
- Falcon tubes (15 ml)
- Growth medium at 37°C
- Incubator (37°C, 5% CO_2 humidified atmosphere)
- Pipettes 5 & 10 ml
- Tissue culture flask or dish (25 cm^2 75 cm^2)
- Water bath at 37°C
- Waste bottle

Method:

- Remove cryo-tube from liquid nitrogen tank and transfer it to the water bath (37°C) only for so long until its content gets liquid!
- Transfer the thawed cell suspension quickly into a culture flask or dish, once it is defrosted
- add ~10 ml pre-warmed growth medium
- Incubate cells for ca. 30 min until they have adhered to the flask/dish
- Change medium in order to remove DMSO that was used to prevent ice

crystal formation during storage at low temperatures

- Transfer culture flask (or dish) with cells back into the incubator
- Alternatively, especially if you have to handle cells growing in suspension resuspend molten content of the cryo-tubes in 10 ml of the respective cell culture medium (to dilute the DMSO) and then centrifuge the suspension for 5 min at (1000 RPM) 156 g
- Discard the supernatant and resuspend the cells in 10 ml of fresh medium
- transfer the cell suspension to a cell culture flask

3.2.2 Sub-culturing

Materials:

- 1x PBS (azide-free) at 37°C
- Centrifuge
- Growth medium at 37°C
- Incubator (37°C, 5% CO_2 humidified atmosphere)
- Tissue culture flasks or dish (25 cm^2, 75 cm^2)
- Trypsin/EDTA solution (in 1xPBS), at 37°C

Method:

- Grow cells in culture flasks or dishes
- Remove growth medium using a pipette (adherent cells) or a centrifuge (suspension cells) at 1000 rpm (in 156 g) for 10 min
- Wash cells with 1x PBS to remove bivalent ions that inactivate trypsin by dilution.
- Incubate cells in Trypsin/EDTA solution for some minutes in the incubator to detach them from the surface (adherent cells)
- Dilute cells as required in adequate amounts of culure medium
- Transfer cells back into a dish/flask and place them into an incubator

3.2.3 Seeding cells on coverslips

Materials:

- Bunsen burner
- Coverslips in 100% ethanol
- Dishes (35 mm, 60 mm) or 6-well plates, respectively
- Growth medium at 37°C
- Incubator (37°C, 5% CO_2 humidified atmosphere)
- Poly-L-Lysine solution (1 mg/ml)
- Sterile water
- Sterile forcepts
- Water bath at 37°C

Method:

- Take coverslips out of the ethanol with sterile forcepts and “dry” them using a bunsen burner
- To adhere cells growing in suspension: coat coverslips with Poly-L-Lysine by incubating them for 30 min with a drop of Poly-L-Lysine solution on top. Rinse coverslips in sterile distilled water to wash away excessive Poly-L-Lysine
- Transfer coverslips in Petri-dishes or 6-well plates
- Generate a cell suspension of adequate concentration in growth medium
- Seed the cell suspension onto dishes/wells with coverslips
- Transfer cells into incubator for proper adherence

3.2.4 Deep-freezing cells

Materials:

- Cryo-medium: FCS (or growth medium) supplemented with 5-10% DMSO
- Cryo-tubes
- Freezer (-80°C)
- Growth medium at 37°C
- Liquid nitrogen tank
- Styrofoam box or isopropanol freezing container

Method:

- Bring cells into suspension by Trypsine/EDTA treatment (like described for sub-culturing)
- Add cryo-medium (don't dilute cell suspension too much!)
- Fill 1.5 ml of the "cryo"-suspension into cryotubes
- Transfer cryo-tubes into styrofoam box or into the isopropanol freezing container
- Put these containes in a -80°C freezer for ca. 24 h
- Transfer cryo-tubes into cryo-boxes of a liquid nitrogen tank for long-term storage
- Update cell-inventory records

3.3 Manipulation of living cells

3.3.1 Transfection of cells by lipofection

Materials:

- 1,5 ml Eppendorf tubes
- FuGene HD transfection reagent
- Growing cells (approx. 60% confluent) in 24- or 6-well plates
- Incubator (37°C, 5% CO_2 humidified atmosphere)
- Plasmid Expression construct (DNA stored in H_2O_{bidest} at -20°C)
- Serum-free OptiMEM medium

Method:

The given concentrations and volumes in this description are appropriate for the transfection of cells in four wells of a 24 well plate.

- Remove FuGene HD reagent from the fridge and wait until it has reached RT
- Preparation of the transfection mix:
  - Place 100 µl serum free medium into an 1.5 ml Eppendorf tube
  - Pipette 7 µl of FuGene HD reagent directly in the serum-free medium without touching the tube's wall
  - Add ~2 µg DNA (260/280 nm ≥1.8) plasmid DNA to the mix

- Blend transfection mix by gently tapping the tube with the index finger and incubate for approx. 20 min at RT
- Use approx. 25 µl of the transfection solution for cells growing (at ~ 50% confluency) in a well of a 24 well plate.
- Reasonable expression of the transfected DNA is obtained (depending on the used cell type) 24h -72h after adding the transfection mix to the cells.

3.3.2 Generation of stable transgenic cell lines

Materials:

- 1x PBS
- Cell culture dishes
- Fluorescence microscope with the adequate filters
- G418 (Geneticin)
- Medium
- Pipettes
- Water resistant pen

Method:

- Transfect cells (see paragraph above)
- Seed transfected cells onto several cell culture dishes at different dilutions
- Add selection medium (containing an antibiotic – here G418) to kill all cells that don't possess the expression plasmid.
- Observe growing cell colonies under the fluorescence microscope and label colonies that express the transfected, transgenic, fluorescent protein at a reasonable level
- Pick the labeled colonies from the culture dish by softly treating it with Trypsin/EDTA and use a pipet tip to transfer the colonies into a 24 well plate.
- If necessary re-pick colonies from the 24 well plates – or if available sort the cells by FACS
- Grow the best clone in a T75 flask and freeze it down in cryo-tubes.

3.3.3 How to determine the right selection conditions?

Materials:

- 6 well plates
- Cell culture medium
- Selective antibiotic like e.g. G418 or Hygromycin B
- Sterile filter (0.22 µm pores)
- Trypsine/EDTA

Method:

- Dissolve the selective antibiotic (e.g. G418 or Hygromycin B) in fully supplemented growth medium to a concentration of 5 mg/ml using a 0.22 µm filter.
- Prepare 6-well cell culture plates by adding the selective antibiotic to the growth medium at different concentrations. A range from 100-1,200 µg/ml in 100 µg increments is recommended.
- Dilute a cell suspension down to a concentration of 4000 cells/ml.
- Add 100 µl of cell suspension to each well and incubate plates within a humidified CO_2 atmosphere at 37°C
- After 10 to 14 days all cells that were exposed to an antibiotic concentration above the lethal level are dead.
- Note the highest concentration of the respective antibiotic that untransfected cells can tolerate and take the concentration up one step for selection of stably transfected cells.

3.3.4 Fluorescence labeling of replication foci and / or chromosomes in living cells

Background:

By incorporation of fluorochrome-tagged nucleotides (e.g. TexasRed-dUTP) into S-phase cells, replication foci can be visualized within living cells. Nucleotides carry a triphosphate group and a bulky fluorophore that prevents them from simple diffusion through the cytoplasma membrane. In order to bring them into cells the cytoplasma membrane has to be transiently disrupted. This can be achieved either by microinjection, or – less tediously – by electroporation or scratch-labeling (Schermelleh et al., 2001). Especially the electroporation treatment but also the scratch label method lead to a high number of replication labeled cells, even in unsynchronized cell cultures. After several replication cycles, segre-

gation patterns appear in nuclei consisting of fluorescently labeled chromosome domains (sometimes even big parts of a whole chromosome). These patterns are generated during mitosis by random segregation of labeled and non-labeled chromatides to the daughter cells. Thus the average amout of labeled chromosomes per cell generation decreases by the power of 2.

Materials:

- Cells growing (semi-confluent) on coverslips in Petri-dishes or 6-well plates
- Fluorochrome labeled dUTP nucleotide stock solutions (~1 mM) (Cy3-dUTP, TAMRA-dUTP, TexasRed-dUTP)
- Growth medium at 37°C
- Hypodermic needle
- Incubator (37°C, 5% CO_2 humidified atmosphere)
- Petri-dishes (60 mm) or 6-well plates
- Paper wipes

Method:

- Prepare working solution of the fluorochrome-labeled nucleotides by diluting the stock solution down to a final concentration of ~50 µM in growth medium.
- Remove cells growing on a cover slip from the petri-dish or 6-well plate, dry the bottom side with a paper wipe and place the coverslip in the middle of a 60 mm petri-dish
- Pipette ~10 µl of labeling solution onto of the coverslip
- Use the hypodermic needle to draw parallel lines on the cell layer as if hatching a paper area. Put the coverslip back into medium, soon to avoid drying of the cells
- Incubate scratched cells in the incubator to facilitate incorporation of labeled nucleotides into the DNA of S-phase cells

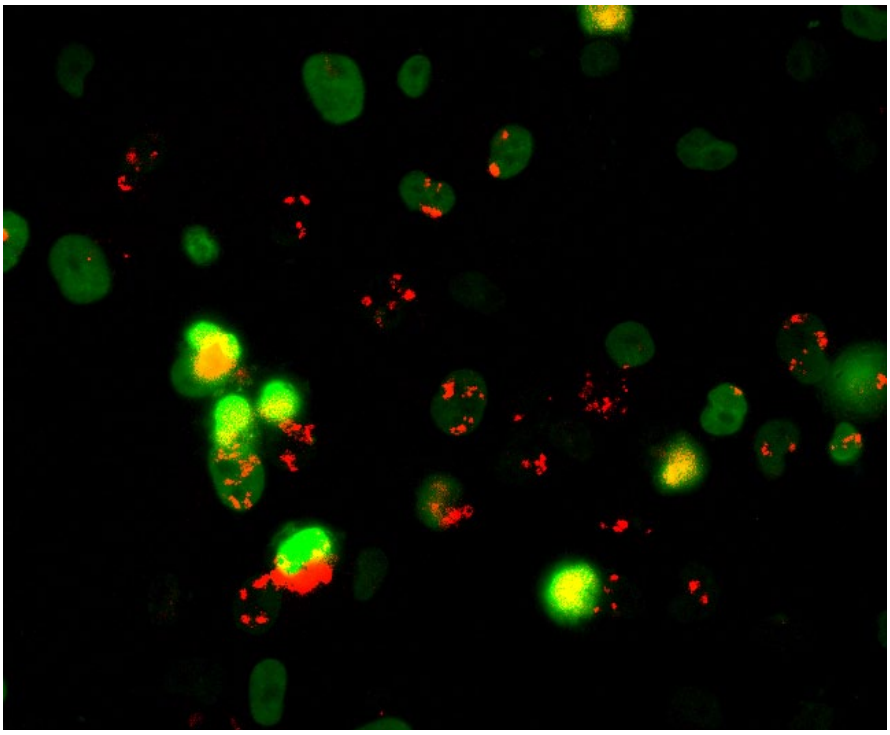

Fig. 3-1: Living HeLa H2B-GFP cells that were replication labeled by electroporation. This method has a much higher yield than replication labeling by the scratch method. Dependent on the amount of cells in S-Phase more than half of the electroporated cells contain labeled chromatin domains. (the picture contains 79 unlabeled cells in comparison to 95 labeled cells) (Own work).

3.3.5 Electrolabeling

Fluorochrome labeled nucleotides can also be incorporated when the cells' plasma membrane is transiently permeabilized by electricity. To do so a Multiporator from Eppendorf was used. This self invented method was specially designed for the targeted cell irradiation at the ion microbeam (see 4.2.2.1) in order to generate a much higher yield of replication labeled nuclei than obtained by the scratch label protocol.

Materials

- (see above) plus
- Cell counting chamber
- Eppendorf Multiporator
- Hypotonic KCl solution (provided Eppendorf for use with the Multiporator)
- Plastic cell culture dishes

Method

- Get (adherent) cells into suspension by trypsin EDTA treatment (see subculturing)
- Count cells and calculate the approximate total cell number

- Centrifuge the suspension and remove the supernatant.
- Resuspend the cells in hypotonic medium in portions of 100 µl each containing around 1.5 x 10^6 cells/ml
- Add 5-10 µl of fluorochrome labeled dUTP stock solution to the suspension and transfer 100 µl into a cuvette with an electrode spacing of 1 mm. (make sure that you expose the cells as short as possible to the nucleotide-mix, since it contains DMSO which cells (especially electroporated cells in suspension don't like too much!)
- Transfer the filled and assembled cuvette into the multiporator which is adjusted to the respective electroporation setting. These settings differ from cell line to cell line (e.g. 800V and 100 µs is appropriate for HeLa cells). Start the electroporation.
- Incubate the cells for about 5 minutes in the cuvette and then seed them onto cover slips, live-cell chambers or to a plastic dishes.
- Put the cells back into the incubator.
- As soon as the cells have adhered, carefully change the medium and leave them in the incubator until usage.

3.3.6 Microinjection

Background:

Sometimes neither transfection via electroporation nor lipofection works to bring a reasonable amount of an expression plasmids, fluorochrome labeled dUTPs or other bigger molecules into cells. In these cases microinjection serves as good alternative to transfer substances into cells or nuclei. During this thesis microinjection was performed at an Eppendorf microinjection device ("FemtoJet" (compressor) combined with an "InjectMan" (micro manipulator)). When starting microinjection, a fluorescent visual positive control (fluorescent additive to the injection mix) is beneficial. In this thesis dextran-conjugates (e.g. FITC dextran and TRITC dextran) served as such a positive control. Although the fluorescent dextrans seem to be inert to the cells' physiology, they might affect the cells by molecular crowding effects which is thought to be involved in regulation of higher order chromatin control (Richter et al., 2008). Since microinjection is a tedious technique, it can be applied (depending on the skill of the experimenter) to only a limited number of cells. (<200)

Materials:

- Cells growing on a round (Ø42 mm) coverslip for the POC chamber, or in another live-cell chamber system (e.g. POC, LAB-Tek or Ibidi)
- Centrifuge

- Eppendorf *Microloader* tips (keep box closed to prevent contamination with dust that might block the injection capillaries!)
- Growth medium at 37°C containing HEPES buffer (to stabilize pH)
- Injection mix: centrifuged 2 times for 20 min at 13,000 RPM
- Live-cell microscope equipped with a temperature conrol system
- Microinjection device (microcontroller *InjectMan* and compressor *FemtoJet*)
- Microinjection capillaries (self pulled or Eppendorf *FemtoTips II*)

Method:

- Spin down injection mix for about 20 min at 13,000 RPM to pellet aggregates within the mix which might block the capillary. Transfer the injection mix to a new eppendorf tube and centrifuge again for about 20 min.
- Mount POC, Ibidi or Lab-Tek chamber at the microscopic stage
- Make sure that the temperature controller is switched on and set to (37°C).
- Pipette 4 µl of the injection mix with a microloader tip (make sure that during storage the microloader tips are not exposed to dust that could contaminate and/or clog the capillaries) into the injection capilarry carefully without creating air bubbles
- Attach the injection capillary to the InjectMan and bring the injection mix to the tip of the capilarry by applying pressure (push “clean”). Switch the compressor from standby to on in order to apply compensation pressure (make sure that injection mix flows out of the capilarry and no medium into it).
- Move the capillary carefully down inside the live-cell chamber towards the cell-layer. Always look at the descending needle using long distance air objectives (10x, 20x and 40x), since immersion objectives (although better in collecting light) cannot look very far in depth due to their high numerical aperture (approx. 20 µm for oil objectives). Descend more slowly (switch from the course to the fine mode) when approaching the cell-layer.
- Begin microinjection with the standard parameters for injection pressure [P_i], compensation pressure [P_c] and injection time [t] (for adherent cells and FemtoTips II e.g. : P_i 120-150 hPa; P_c: 30 hPa; t=0.3 sec)
- Find out the best suited parametes [Pi , [P_c] and [t] empirically for the used combination of cell line and capillary so that cells don’t burst but still take-up sufficient amounts of injection mix and survive.

3.3.7 Sensitizing DNA with BrdU

Materials:

- Adherent cells growing in live-cell chambers. (POC, LabTeK or Ibidi).
- BrdU stock solution (50 mM)
- Growth medium at 37°C
- Incubator (37°C, 5% CO_2 humidified atmosphere)

Method:

- Add BrdU solution to Petri-dishes to achive a final concentration of 33 µM (10 mg/ml)
- Incubate cells in the incubator until usage.
- Avoid direct exposure to light.

3.3.8 DNA Damage induction via NCS

In order to create DNA damages in cells, Neocarzinostatin can be used in culture medium at a concentration of 200 nM. The macromolecular chromoprotein Neocarzinostatin contains a highly DNA damaging prosthetic group. The apoprotein in NCS stabilizes, the chromophore, protects it and guides it to the DNA.

3.3.9 Induction of reversibly hypercondensed chromatin (HCC)

Background:

Treatment of cells with solutions of high osmolarity leads to the reversible formation of hypercondensed chromatin (HCC). The osmolarity of a physiological standard growth medium is about 290 mOsm. Concentrations of >500 mOsm generate hypercondensation of chromatin. The condensation medium used in this protocol was measured to be ~750 mOsm (Albiez et al., 2006). Using higher concentrations does not generate further condensation if not longer incubation periods are applied (Albiez et al., 2006).

Materials:

- 20x PBS
- Cells growing in live-cell chamber
- Growth medium at 37°C

Method:

- Condensation medium (~750 mOsm) is produced by adding 9 ml of growth medium (~290 mOsm) to1 ml of 20x PBS
- Incubate cells in condensation medium (full condensation reached after 5 min)
- Incubation of the cells in medium or buffer with 290 mOsm reverses the effect of hypercondensation within 5 minutes.

3.4 Immunofluorescence protocol

3.4.1 Fixation and permeabilization

Materials:

- 1x PBS
- Cells growing on coverslips in live-cell or in irradiation chambers
- Ice bath
- Paraformaldehyde (PFA) (powder)
- PBST (0.01% Tween / in 1x PBS)
- Triton X-100

Method:

- Prepare PFA fixative (4 mass % PFA in 1 x PBS buffer). Heat the mixture-up until PFA has dissolved entirely, then cool down on ice.
- Prepare 0.4% Triton solution (in 1x PBS)
- Wash coverslip, live-cell chamber or irradiation chamber with adherent cells in 1x PBS
- Fix the cells for 10 min at RT in the PFA fixative (see above)
- Wash fixed cells approx 3 times with 1x PBS
- Treat fixed cells for 15 min with 0.4% Triton solution (see above)
- Wash fixed cells with 1x PBS and store them until using them for immuno-labeling.

3.4.2 Immuno-cytochemistry and DNA counterstaining

Materials:

- Anti-fade embedding medium (Vectashield)
- Bovine serum albumin (BSA)
- Counterstain solution
- Fixed and permeabilized cells in PBST
- Humidified chamber
- Microscope slide
- Nail polish
- Parafilm
- PBST (0.01% Tween / 1x PBS)
- Primary antibody stock solution
- Secondary antibody stock solution
- Water bath at 37°C

Method:

- Dissolve 4 g BSA in 100 ml PBST to prepare (4% BSA) blocking buffer
- Prepare working solutions for primary and secondary antibody by dilution in blocking buffer
- Incubate the fixed and permeabilized cells for >10 min in blocking buffer to reduce background from unspecific antibody binding.
- Wash cells 3x5 min in PBST
- Pipette ~50µl of the primary antibody solution onto a piece of parafilm and place the coverslip carrying the cells upside-down onto the spotted antibody solution. When using Lab-Tek slides use 100 µl antibody solution and carefully move it over the cells. Let antibodies bind for >45 min in a humidified chamber at 37°C (or o/n at 4°C)
- Wash cells 3 x 5 min in PBST
- Use secondary antibody solution like described for the primary antibody and let the antibody bind for ~30 min in a humidified chamber at 37°C
- Wash the cells 3 x 5 min in PBST
- Use the counterstain solution (~50µl) like described for the antibodies above and incubate it on the samples for 2–5 min
- Wash coverslip in 1x in PBST
- Embed the cells in anti-fade medium (Vectashield) on a microscope slide or in the live-cell chamber.
- Seal specimen (if possible) with nail polish for longer storage life.

3.5 Microscopy

3.5.1 Confocal microscopy of fixed samples

In this thesis a Leica TCS SP5 scanning confocal microscope and a Perkin Elmer Vox Ultra *View* spinning-disc confocal unit attached to a Zeiss Axio Observer D1 microscopic stand were used. These systems differ to some extent with respect to handling and configuration. In general confocal microscopy of fixed specimen was carried out as follows:

Method:

- Laser excitation power was adjusted in order to generate a good compromise between best signal to noise ratio and least photobleaching of the sample.
- "Gain" and "offset" (the spinning disc unit) were set to values that allowed to use the maximal dynamic range of the used photo sensors.
- Photomultiplier sensitivity or "enhanced sensitivity" at the EM-CCD camera were adjusted in order to get the best compromise between long exposure time and "noisy" images.
- Electronic noise in images acquired at the Leica SP5 was reduced further by averaging the images of 4 scans per image slice.
- The filters (PE Ultra*VIEW* Vox) and the filter ranges at the Leica SP5, respectively were chosen or set in in order to minimize bleed through artefacts coming from other fluorescence channels.
- At the Leica SP5 a pixel size of 50x50 nm was consequently used.
- The z-step size was set according to the needs of the experiment. In live-cell experiments the z-step size was often used quite corse to reduce phototoxic damage. When scanning fixed samples the z-intervals were set sometimes down to 200 µm
- At the SP5 a pinhole size of 1 Airy unit was used, the sizes of the pinholes at the spinning disc microscope can't be changed. They have a fixed diameter of each 50 µm.
- Chromatic shifts were measured and corrected as described see Appendix C.

3.5.2 Live-cell microscopy

Background:

Microscopic live-cell observations require some special care e.g. with respect to pH value temperature and phototoxicity (see also *Introduction* 2.6.1)

Materials:

- Cells growing at the bottom of live-cell chambers like POC, LabTek chamber, Ibidi µ-slide, etc.
- Growth medium at 37°C, containing HEPES buffer
- Live-cell microscopes equipped with temperature control systems (Zeiss Axiovert 200M, Perkin Elmer Ultra *View* Vox, or Leica SP5)
- Trolox stock soluiton (100 mM)

Method:

- If necessary assemble the live-cell chamber (e.g. POC). Make sure that the chamber is airtight and that the the surface getting into contact with the immersion oil objective is dry and clean.
- Put the live-cell chamber onto the stage of the microscope.
- If possible use an oil immersion objective, and a microscope which is equipped with a controller for temperature, CO_2 and humidity to generate an enviromment like in an ordinary incubator for mammalian cells.
- Use HEPES buffered medium and ad Trolox to in (final concentration 10 µM) in order to prevent toxic changes in pH and to neutralize harmful free radicals.
- Laser excitation power has to be set to the lowest possible level that still leads to a sufficient excitation of the fluorochromes.
- Exposure time (or scan frequency) should be set to a value which still allows an acceptable image quality (for fast processes like anaphase acquisition times shouldn't be too long).
- Depending of the task to fulfill, the pinhole (if working at a point scanner) can be be adjusted. If confocality isn't critical for evaluation, opening the pinhole leads to brighter images or shorter (and less cytotoxic) acquisition times.
- The zoom at a point scanner should be adapted to the needs of the planned experiment, too. Although technically possible, voxel sizes smaller than 80x80x250 nm don't lead to increased optical resolution.
- Since axial resolution is 500-800 nm, z-step size can be increased in some cases to further minimize total light exposure.

3.5.2.1 Fluorescence-Recovery-after-Photobleaching (FRAP):

Method:

- Put a cell chamber onto the stage of the spinning disc microscope.
- Make sure that the temperature of the cells is kept at (37°C)
- Select the 'FRAP' module of the Volocity software
- Use the laser line best suited for bleaching the expressed fluorophore
- Select an adequate optical mid-section within a selected nucleus, and define a region-of-interest (ROI) to be bleached.
- Enter the recording settings for the pre- and post-bleach confocal image acquisition. For evaluation of the recovery kinetics, fluorescence intensities the photobleached region has to be corrected for background, photobleaching over time and normalized to to the mean of the pre-bleach values.
- Use maximal laser power to bleach the ROI to background levels and use as little "bleach frames" as possible
- Use small time intervals to record fluorescence recovery directly after photobleaching. Depending on the FRAPped protein, fluorescence recovery can be very fast!
- Increase the time intervals between the image acquisitions as the fluorescence revovery slowly saturates to minimize phototoxicity.
- Multiple nuclei have to be averaged for a solid quantitative evaluation of photobleaching experiments. Data of the mean curve as well as the standard error of the mean curve has to be computed and displayed. The graphs in this study were created using the software MS Excel and Mathematica. (Mortusewicz et al., 2007).

3.5.2.2 Photoactivation of H4-PA-GFP

Method:

- Put a cell chamber onto the stage of the spinning disc microscope.
- Use the 'FRAP' module of the Volocity software
- Use the 440 nm laser at low intensity (for this study 4% was used)
- Select a nucleus of interest and define a region of interest (ROI) to be photoactivated
- Photoactivate ROI with as little iterations over the selected area as necessary (usually 10)
- Start time series
- Proceed with image analysis.

3.5.2.3 Laser microirradiation with light from a 405 nm continuous diode laser

Method:

- Mount cells that have previously been sensitized with BrdU onto the spinning disc microscope and proceed like described above for FRAP.
- Make sure that the temperature of the cells is kept at (37°C)
- In contrast to the relative mild conditions that are used for photoactivation and photobleaching set the 405nm diode laser to 100% of its power and use 400 iterations to scan over the selected region of interest.
- Proceed with imaging and image analysis as described above for FRAP. Like in FRAP, laser microirradiation data of individual cells has to be corrected for background and photobleaching over time and must be normalized to to the mean of the pre-irradiation values.
- For quantitative evaluation of laser microirradiation experiments, data of multiple nuclei has to be averaged and the mean curve as well as the standard error of the mean curve have to be calculated and displayed. The graphs in this study were created using the software MS Excel and Mathematica (Mortusewicz et al., 2007)

3.6 Rotatable 3D reconstructions

The rotatable 3D reconstructions of mitotic or interphase cells presented in this thesis were generated from light optical confocal serial sections. The surfaces of these 3D models were generated using the program Amira®. To embed the surfaces into PDF documents they were exported from Amira® choosing the "VRML" format and assembled/post-processed using the Adobe Acrobat 3D Reviewer. The complete models were imported as "u3d" files into the respective PDF-Document with Adobe Acrobat 9. The whole procedure can be reviewed in more detail in (Ruthensteiner and Hess, 2008). Rotatable 3D reconstructions that are embedded into figures can be found in fig. 2-2, fig. 4-77 in the main text and in the "Supplemental Figures" folder on the enclosed DVD.

3.7 Cell lines and constructs

3.7.1 Used cell lines

Within this thesis the following cell lines were used

- HeLa (Kyoto) (cultured in RPMI-medium)
- HeLa H2B-GFP (cultured in RPMI-medium)
- U2OS (cultured in DMEM)
- RPE1 hTERT (cultured in DMEM :F-12 medium 1:1)

All culture media were supplemented with fetal calf serum (10%) and antibiotics (penicillin/streptomycin 1%)

For further details see the entries from the ATCC in Appendix E.

3.7.2 Used expression plasmids:

- H4-PA-GFP (kind gift from Roeland Dirks (University of Leiden) and Jeroen Essers (Kanaar Lab, Dr. Molewaterplein 50, 3015 GE Rotterdam, The Netherlands)
- H2B-mRFP (kind gift from Horst Wolf (Brack-Werner Lab, Helmholtz Zentrum München,Institute of Virology, Ingolstädter Landstraße 1, D-85764 Neuherberg))
- CENP-B-mRFP (kind gift from Horst Wolf (Brack-Werner Lab, Helmholtz Zentrum München,Institute of Virology, Ingolstädter Landstraße 1, D-85764 Neuherberg))
- mRFP-PCNA (kind gift from Heinrich Leonhardt, BioCenter Department of Biology II, Großhaderner Str. 2, 82152, Planegg-Martinsried)
- eGFP-PCNA (kind gift from Heinrich Leonhardt, BioCenter Department of Biology II, Großhaderner Str. 2, 82152, Planegg-Martinsried))
- MDC1-GFP (kind gift from Jeroen Essers (Kanaar Lab, Dr. Molewaterplein 50, 3015 GE Rotterdam, The Netherlands))
- 53BP1-GFP(kind gift form Guido Drexler (Friedl Lab, Institute of Radiobiology, Schillerstraße 42, 80336 Munich))
- Rad51-GFP (kind gift from Jeroen Essers (Kanaar Lab, Dr. Molewaterplein 50, 3015 GE Rotterdam, The Netherlands))
- Rad52-GFP (kind gift from Jeroen Essers (Kanaar Lab, Dr. Molewaterplein 50, 3015 GE Rotterdam, The Netherlands))

For plasmid maps of the constructs see Appendix F.

3.7.3 Stable cell lines created in the course of this thesis:

- RPE1 H4-PA-GFP H2B-mRFP
- RPE1 Rad52-GFP
- RPE1 Rad52-GFP CENP-B-mRFP
- RPE1 53BP1 GFP
- RPE1 MDC1-GFP
- U2OS Rad52-GFP
- U2OS MDC1-GFP
- U2OS 53BP1-GFP
- V79 Rad51-GFP H2B-mRFP

3.8 Consumables and technical equipment

3.8.1 Chemicals and Reagents

Chemicals	Company
10x Buffer	Amersham Pharmacia Biotech, Braunschweig
Acetic Acid (Glacial) 100%	Merck, Darmstadt
Agarose SeaKem ME	Cambrex Bio Science Rockland, Rockland, ME, USA
Bovine Serum Albumin (BSA) for PBS-Solutions	Sigma-Aldrich, Deisenhofen
Bovine Serum Albumin (BSA) for SSC-Solutions	MP Biomedicals, Solon, OH, USA
Certipur (Calibration Solution for pH-Meter)	Merck, Darmstadt
Colcemid 10 µg/ml	Biochrom AG, Berlin
DAPI	Sigma-Aldrich, Deisenhofen
Dextran Sulfate	Amersham Pharmacia Biotech, Braunschweig
Dextran TRITC (79 kDa)	Sigma-Aldrich, Deisenhofen
Dimethylsulfoxid (DMSO)	Sigma-Aldrich, Deisenhofen
DH5α chemical competent bacteria	Invitrogen, Carlsbad, CA, USA
Dulbecco's MEM Medium (DMEM)	Biochrom AG, Berlin
Dulbecco's MEM Medium (DMEM) w/o Phenolred	Gibco, Karlsruhe
EDTA (Titriplex III)	Merck, Darmstadt
Ethanol p. a.	Merck, Darmstadt
Ethanol technical	VWR, Darmstadt
Ethidium Bromide	Sigma-Aldrich, Deisenhofen
Fetal Calf Serum (FCS) (FBS Superior)	Biochrom AG, Berlin
Formamide	Merck, Darmstadt
G418 Geneticin	Roche
Glutamine 200 mM	Biochrom AG, Berlin
Glycerin	Merck, Darmstadt
Ham's F10 Medium	Biochrom AG, Berlin
Ham's F10 Medium w/o Phenolred	Biochrom AG, Berlin
HCl smoking (12,5 N)	Merck, Darmstadt
Immersionoil (Immersol 518)	Zeiss, Jena
Loading Dye 6x	Fermentas, St. Leon-Rot
Methanol	Merck, Darmstadt
NaOH	Merck, Darmstadt
Neocarzinostatin (NCS) 500 µM	Sigma-Aldrich, Deisenhofen
Nitrogen (liquid)	Messer Griesheim, Krefeld
OptiMEM	Invitrogen, Carlsbad, CA, USA
Paraformaldehyde	Merck, Darmstadt
Penicillin/Streptomycin (10000 U / 10000 µg/ml)	Biochrom AG, Berlin

Chemicals	Company
Poly-Lysin-Hydrobromide	Sigma-Aldrich, Deisenhofen
Potassium Chloride (KCl)	Merck, Darmstadt
RPMI 1640 Medium	Biochrom AG, Berlin
Sodium-Azide (NaN_3)	Merck, Darmstadt
Sodium Chloride (NaCl)	Merck, Darmstadt
Sodium Dodecyl Sulfate (SDS)	Sigma-Aldrich, Deisenhofen
Sodium Hydrogen Phosphate (Na_2HPO_4)	Merck, Darmstadt
Tris	Roth, Karlsruhe
Tris-HCl 1 M, pH 7.8	Sigma-Aldrich, Deisenhofen
Tris-HCl 1 M, pH 8.0	Sigma-Aldrich, Deisenhofen
Triton-X-100	Sigma-Aldrich, Deisenhofen
Trolox	Sigma-Aldrich, Deisenhofen
Trypsin-EDTA-Solution 10x	Biochrom AG, Berlin
Tween 20	Calbiochem, San Diego, CA, USA
Vectashield Antifade Medium	Vector Laboratories, Burlingame, CA, USA

Antibodies, Fluorochromes	Dilutions	Company
Avidin-Alexa488	1:200	Molecular Probes, Eugene, OR, USA
Donkey α Goat-Alexa488	1:400	Molecular Probes, Eugene, OR, USA
Donkey α Mouse-Cy3	1:200	Jackson Immuno Research, Newmarket
Donkey α Rabbit-Cy3	1:200	Jackson Immuno Research, Newmarket
Goat α Avidin-FITC	1:200	Vector Laboratories, Burlingame, CA, USA
Goat α Human-FITC	1:200	Jackson Immuno Research
Goat α Mouse-Cy5	1:100	Dianova, Hamburg
Goat α Mouse-F(ab)-Cy3	1:200	Jackson Immuno Research, Newmarket
Goat α Mouse-TexasRed	1:200	Jackson Immuno Research, Newmarket
Goat α Rabbit-Alexa633	1:200	Molecular Probes, Eugene, OR, USA
Goat α Rabbit-F(ab)-Cy3	1:200	Jackson Immuno Research, Newmarket
Goat α Rabbit-F(ab)-TexasRed	1:50 / 1:100	Jackson Immuno Research, Newmarket
Human antiserum CREST	1:200	Euroimmun
Mouse α Tubulin (DM-1A)	1:500	Sigma-Aldrich, Deisenhofen
Mouse α γH2AX	1:350	Upstate Biotechnology Inc, Lake Placid, NY, USA

Antibodies, Fluorochromes	Dilutions	Company
Mouse α PAR	1:200	Trevigen, Gaithersburg, MD, USA
Rabbit α Pericentin	1:1000	Abcam, Cambridge
Sheep α Mouse-Cy3	1:500	Dianova, Hamburg
Streptavidin-Cy3	1:500	Jackson Immuno Research, Newmarket

3.8.2 Media and Solutions

Medium / Solution	Compounds	Notes
Agarose-Gel	1% Agarose in TAE-Buffer	Boil 2 g Agarose in 200 ml TAE-Buffer in the mikrowave oven respct. Boil on a hotplate while stiring until the solution is clear
Blocking Solutions	4% BSA in 1x PBS/0.01% Tween 2% BSA in 1x PBS/0.01% Tween	4 g BSA → ad 100 ml mit 1x PBS/0.01% Tween 20 ml 4% BSA in 1x PBS/0.01% Tween + 20 ml 1x PBS/0.01% Tween
Complete Medium with 200 nM NCS	Dependent on the celltype respective Complete Medium, NCS 500 µM	10 ml Complete Medium + 4 µl NCS
DAPI-Working Solution 0.2 µg/ ml	DAPI-Solution 10 µg/ml 1x PBS oder 2x SSC	Correspends to a dilution of 1:50 → e.g. 5 µl DAPI-Soluton + 245 µl 1x PBS; use 2x SSC instead of 1x PBS for FISH
DAPI-Solution 10 µg/ml	DAPI-Stock Solution 500 µg/ml 1x PBS	20 µl DAPI-Stock Solution + 980 µl 1x PBS
DAPI-Stock Solution 500 µg/ml	DAPI $H_2O_{bidest.}$	10 mg DAPI + 20 ml $H_2O_{bidest.}$
DNA-Buffer	100 mM EDTA 200 mM Tris	2 ml 0.5 M EDTA + 2 ml 1 M Tris/HCl pH 7.8 or 8.0 + 6 ml $H_2O_{bidest.}$
Dulbecco's MEM complete medium	Dulbecco's MEM Medium, FCS, Penicillin/Streptomycin	450 ml Dulbecco's MEM Medium + 50 ml FCS + 5 ml Penicillin/Streptomycin
EDTA 0.5 M, pH 8.0	EDTA, $H_2O_{bidest.}$	1.86 g EDTA → ad 8 ml $H_2O_{bidest.}$; adjust with 1 N NaOH to pH 8.0
Ethanol 70%	Ethanol technical, H_2O_{dest}	75 ml Ethanol + 175 ml $H_2O_{dest.}$
Ethanol 90%	Ethanol technical, $H_2O_{dest.}$	25 ml Ethanol + 225 ml $H_2O_{dest.}$
Ethidium Bromide 1 mg/ml	Ethidium-Bromide, $H_2O_{bidest.}$	10 mg Ethidium-Bromide + 10 ml $H_2O_{bidest.}$
Ethidium Bromide Bath	1x TAE, 1 mg/ml Ethidium-Bromide	600 ml 1x TAE + 6 drops 1 mg/ml Ethidium-Bromide
Freezing medium	10% DMSO in FCS	9 ml FCS + 1 ml DMSO
Glycerin-Solution 20%	Glycerin, 1x PBS	50 ml Glycerin + 200 ml 1x PBS
HEPES / NaOH 1 M, pH 7.0	HEPES, $H_2O_{bidest.}$	119.1 g HEPES → ad 500 ml $H_2O_{bidest.}$; adjust with NaOH to pH 7.0

Medium / Solution	Compounds	Notes
HEPES / NaOH pH 7.4 100 mM	1 M HEPES / NaOH pH 7.0, $H_2O_{dest.}$	5 ml 1 M HEPES / NaOH pH 7.0 + 45 ml $H_2O_{dest.}$; adjust with 1 N NaOH to pH 7.4
"Holland"-Medium	Dulbecco's MEM Medium, Ham's F10 Medium, FCS, Penicillin/Streptomycin	22.5 ml Dulbecco's MEM Medium + 22.5 ml Ham's F10 Medium + 5 ml FCS (= 10%) + 500 µl Penicillin/Streptomycin
"Holland"-Medium w/o Phenolred	Dulbecco's MEM Medium w/o Phenolred, Ham's F-10 Medium w/o Phenolred, FCS, Penicillin/Streptomycin, Glutamine 200 mM	22.5 ml Dulbecco's MEM Medium w/o Phenolrot + 22 ml Ham's F10 Medium w/o Phenolred + 400 µl Glutamine + 5 ml FCS + 500 µl Penicillin/Streptomycin
"Holland"-Medium w/o Phenolred with 100 nM Trolox	Holland-Medium w/o Phenolred, 100 mM Trolox	10 ml Holland-Medium w/o Phenolred + 10 µl 100 mM Trolox
Hypotonic-Solution (0.56% KCl)	KCl, $H_2O_{dest.}$	1.4 g KCl → ad 250 ml $H_2O_{dest.}$
Hypotonic Solution		for Multiporator by Eppendorf
λ HindIII-Marker	λ HindIII, Loading Dye 6x, $H_2O_{bidest.}$	100 µl λ HindIII + 100 µl 6x Loading Dye + 50 µl H_2O_{bidest}
Methanol/Acetic Acid	Methanol/Acetic Acid 3:1 (V:V)	150 ml Methanol + 50 ml Acetic Acid
NaOH 1 N	NaOH, $H_2O_{bidest.}$	20 g NaOH → ad 500 ml $H_2O_{bidest.}$
Paraformaldehyde	4% respct. 1% PFA in 1x PBS	Solve 4 g respct. 1 g PFA in 100 ml 1x PBS completely while stiring and heating. Cool down before use.
PBS-Buffer 1x	For Cell-Culture usage: 20x PBS (→ 140 mM NaCl, 2.7 mM KCl, 6.5 mM Na_2HPO_4, 1.5 mM KH_2PO_4), H_2O_{bidest} for Lab usage: contains 0.04% Sodium Azide	25 ml 20x PBS + 475 ml $H_2O_{bidest.}$; → autoclave 1 l 1x PBS + 1 small spatula-tip Sodium Azide
PBS-Buffer 1x / 0.01% Tween	1x PBS, Tween 20	50 µl Tween 20 + 500 ml 1x PBS
PBS-Buffer 20x, pH 7.4	2.8 M NaCl, 54 mM KCl, 130 mM Na_2HPO_4, 30 mM KH_2PO_4	320 g NaCl + 8 g KCl + 57.6 g Na_2HPO_4 + 9.6 g KH_2PO_4 → ad 2 l $H_2O_{bidest.}$, adjust pH to 7.4 with HCl
Pepsin Stock Solution	Pepsin, $H_2O_{bidest.}$	1 g Pepsin + 10 ml $H_2O_{bidest.}$
Poly-L-Lysin Working Solution 1.25 mg/ml	10 mg/ml Poly-L-Lysin-Stock Solution, $H_2O_{bidest.}$	1 ml 10 mg/ml Poly-L-Lysin-Stock Solution + 7 ml $H_2O_{bidest.}$
Poly-L-Lysin Stock Solution 10 mg/ml	Poly-L-Lysin-Hydrobromide, $H_2O_{bidest.}$	100 mg Poly-L-Lysin-Hydrobromide + 10 ml $H_2O_{bidest.}$
RPMI (Rosswell Park Memorial Institute)1640 Complete Medium	RPMI 1640 Medium, FCS, Penicillin/Streptomycin	450 ml RPMI Medium + 50 ml FCS + 5 ml Penicillin/Streptomycin
TAE-Buffer 1x	50x TAE (→ 40 mM Tris-Acetate, 1 mM EDTA), $H_2O_{bidest.}$	40 ml 50x TAE + 1960 ml $H_2O_{bidest.}$

Medium / Solution	Compounds	Notes
TAE-Buffer 50x, pH 8,0	2 M Tris-Acetate, 0.05 M EDTA	242 g Tris +18.6 g EDTA + 57.1 ml glacial acetic acid → ad 1 l $H_2O_{bidest.}$
TE-Buffer	10 mM Tris, 1 mM EDTA	20 µl 1 M Tris/HCl pH 7.8 or 8.0 + 4 µl 0,5 M EDTA + 1978 µl $H_2O_{bidest.}$
TE-Buffer ohne EDTA	10 mM Tris	20 µl 1 M Tris/HCl pH 7.8 or 8.0 + 1980 µl $H_2O_{bidest.}$
Tris-HCl 1 M, pH 7.5	Tris, $H_2O_{bidest.}$	60.6 g Tris → ad 500 ml $H_2O_{bidest.}$; adjust with HCl at pH 7.5
Triton-X-100 0,05%	1x PBS, Triton-X-100	50 ml 0.5% Triton-X-100 + 450 ml 1x PBS
Triton-X-100 0.5%	1x PBS, Triton-X-100	2.5 ml Triton-X-100 + 500 ml 1x PBS
Trolox 100 mM	Trolox, 1 N NaOH, 1 N HCl, $H_2O_{bidest.}$	0.25 g Trolox → ad 9.8 ml $H_2O_{bidest.}$ + 100 µl 1 N NaOH, vortex, until all of the Trolox is dissolved (clear, yellow); neutralize with 100 µl 1 N HCl
Trypsin/EDTA 1x	Trypsin/EDTA 10x, $H_2O_{bidest.}$	50 ml 10x Trypsin/EDTA + 450 ml $H_2O_{bidest.}$

3.8.3 Equipment and other Hardware

Device	Type	Company
(60°C) oven	Heraeus	Heraeus, Hanau
Bunsenburner with foot switch	GasProfi 1SCS	WLD-Tec GmbH, Göttingen
Centrifuge	C3i	Jouan Industries, Château-Goutier
Centrifuge	Biofuge pico	Heraeus, Hanau
Centrifuge	Rotana/S	Hettich, Tuttlingen
CO_2-Incubator	BB6220	Heraeus, Hanau
controller for thermo-printer	Gel Print 2000i	BioPhotonics, Ann Arbor, MI, USA
camera for taking gel pictures		MWG-Biotech, Ebersberg
Electroporator	Multiporator	Eppendorf
FemtoJet	Compressor for microinjection	Eppendorf
Femtotips II	Sterile microinjection capillary	Eppendorf
Freezer -20°C	different Types	Privileg / Quelle, Fürth AEG, Frankfurt a. M. Liebherr, Ochsenhausen
Freezer -80°C	VX 380 E	Jouan Industries, Château-Goutier
Fridge +4°C		Bosch, Gerlingen-Schillerhöhe
Gel-Chambers	Easy Cast B1A	OWL Separation Systems, Portsmouth, NH, USA

Device	Type	Company
Hot block	DB 2-D	Techne, Cambridge
Heating insert for live cell microscopy	Heating Insert P	Pecon
Heat-Controller	Tempcontrol 37-2 digital	Pecon
Heating unit for live cell microscopy	Heating Unit	Pecon
Ice machine	AF-10	Scotsman, Bettolino di Pogliano
Incubator	Ceromat HK	B. Braun Biotech International, Melsungen
InjectMan	Micromanipulator for microinjection	Eppendorf
Magnetic Stirrer	REO	IKA Werk, Staufen
Magnetic Stirrer	RH basic2	IKA Werk, Staufen
Magnetic Stirrer	RCT basic	IKA Werk, Staufen
Microloader	Micro injection capillary loader	Eppendorf
Mikrowave oven	Selection	Samsung, Schwalbach
Multiporator	Electroporation device	Eppendorf
Nitrogen-tank including (racks)		Messer Griesheim, Krefeld
pH-Meter	pH538	WTW, Weilheim
Photometer	GeneQuantII	Pharmacia Biotech, Cambridge
Precision balance	2254	Sartorius, Göttingen
Precision balance	KernEW	Kern&Sohn GmbH, Balingen
Rotator	Thermomixer 5436	Eppendorf, Hamburg
Shaker	KL-2	Edmund Bühler, Hechingen
Shaker	swip KL-2	Edmund Bühler, Hechingen
Shaker	Unimax 2010	Heidolph, Schwabach
Steam autoclave	Varioklav	H+P Labortechnik GmbH, Oberschleißheim
Sterile Workbench	Herasafe	Heraeus, Hanau
Tablecentrifuge	Minizentrifuge GMC-060	neolab, Heidelberg
Thermocycler	Techne Progene	Techne, Cambridge
Thermo printer for Gel pictures	UP-D860E	Sony, Tokyo, Japan
UV-Lamp for Sterile Workbench		Kendro, Langenselbold
Vacuumcentrifuge	Vaccuumconcentrator	Bachhofer, Reutlingen
Voltage-Controller	E835	Consort, Turnout, Belgien
Vortexer		neolab, Heidelberg
Waterbath	1004	GFL, Burgwedel
Waterbath	1003	GFL, Burgwedel
Waterbath	5	Julabo, Seelbach
Waterbath	M12	Lauda, Lauda-Königshofen
Waterbath	Thermocycler 60	Bio-med, Theres

Utilities	Specifications	Company
6-well-Plates		Greiner bio-one, Frickenhausen
8-well-ibidi-Chamber		Ibidi, Martinsried
Autoclave Boxes with Lid	Different sizes	Schubert Medizinprodukte GmbH, Wackersdorf
Autoclave Tape		VP GmbH, Feuchtwangen
Automatic Pipette		Gilson Inc., Middleton
Automatic Pipette	Swiftpet	Abimed, Langenfeld
Bunsen Burner-equipment: pressure reducer, Gas cartridge (C 206 super)		CampingGAZ, Hungen-Inheiden
Cell-culture Bottles	25 cm^2, 75 cm^2	Greiner bio-one, Frickenhausen
Clockmaker Tweezer		Dumont, Montiguez
Cover Slips	Ø 42 mm	PeCon GmbH, Erbach
Cover Slips	76x26 mm, 12x12 mm	Hecht, Sondheim
Cover Slips	8x8 mm, 15x15 mm, 24x60 mm	Menzel-Gläser, Braunschweig
Cover Slips	18x18 mm, 20x20 mm, 24x24 mm	Superior Marienfeld, Lauda-Königshofen
Cryo Tubes	1.8 ml	Greiner bio-one, Frickenhausen
Cuvettes		Schubert & Weiß, München
Diamond Pen	to cut the cover slips	Kraus & Winter, Hamburg
Falcon Tube	15 ml, 50 ml	Falcon / Becton Dickinson, S. Jose
Filter Paper, folded	Ø 125 mm	Schleicher & Schnell, Dassel
Fixogum		Marabuwerke, Tamm
Glas Bottles	25 ml, 50 ml, 100 ml, 250 ml, 500 ml	Schott, Stafford, UK
Injection Needles	Sterican 0,90x40 mm	Rose GmbH, Trier
Injection Needles	Sterican 0,45x25 mm	Braun Melsungen, Melsungen
Kim Wipes		Kimberly-Clark, Surrey, UK
Lab Gloves Latex		neolab, Heidelberg
Lab Gloves Nitril		neolab, Heidelberg
LabTek Chamber Slide	2 wells	Nunc (Thermo Fisher Scientific)
Leucosep	30 ml	Greiner bio-one, Frickenhausen
Microscope Slides		R. Langenbrink, Emmendingen
Micro Pipettes	10 µl, 20 µl, 200 µl, 1000 µl	Gilson Inc., Middleton
Nail Polish		Rival de Loop, Berlin
Parafilm TM		Pechiney Plastic Packaging Inc, Menasha, WI, USA
Pasteur Pipettes Glass	230 mm	Poulten & Graf GmbH, Wertheim
Pasteur Pipettes Plastic	3 ml	Falcon / Becton Dickinson, S. Jose

Utilities	Specifications	Company
Pasteur Pipettes Plastic Sterile	3 ml	Greiner bio-one, Frickenhausen
Petri Dishes	Ø 60 mm, 120x120 mm	Greiner bio-one, Frickenhausen
Pipettes (serologic)	5 ml, 10 ml, 25 ml	Sarstedt, Nümbrecht
Pipettes (serologic)	2 ml	Costar, Corning, NY, USA
Pipette Tips	white	Molecular Bio Products, San Diego, CA, USA
Pipette Tips	yellow and blue	Greiner bio-one, Frickenhausen
Pipette Tips for PCR		Molecular Bio Products, San Diego, CA, USA
POC-Chamber		Helmut Saur Laborbedarf, Reutlingen
POC-R-Chamber		Pecon
QuadriPerms		Greiner bio-one, Frickenhausen
Quarz Cuvette		Hellma GmbH, Müllheim
Reaction Tubes	1.5 ml	Eppendorf, Hamburg
Reaction Tubes	0.5 ml	Brand, Wertheim
Reaction Tubes	2 ml	Eppendorf, Hamburg
Reaction Tubes with Screw-Top	1.5 ml	neolab, Heidelberg
Sterile Filter	∅ 0.2 µm, ∅ 0.45 µm	Sartorius, Göttingen
Syringes, Sterile	1 ml, 5 ml, 50 ml	Henke Sass Wolf GmbH, Tuttlingen
Tungsten Pen	to draw the grid	Bel-Art Products, Pequannock, NJ, USA
Waste Bottle		Biochrom AG, Berlin
Wet Incubation Chamber	Petri dish (120x120 mm) painted black with plasic spacer and wet paper tissues	

Various		
Flue	Graduated cylinder	Silicagel balls
Boxes for reaction tubes	Pipetus	Wash bottle
Heat protection gloves	Storage boxes for microscope slides	Rack for falcon tubes
Dewar	Storage maps for microscope slides	Rack for reaction tubes
Sticky tape	Stirring fishes	Styrofoam container
Kitchen roll	Protective goggles	Styrofoam swimmer

3.8.4 Used Microscopes

Axiovert 40C	**Objectives:** A Plan 5x / 0.12 Ph0 A Plan 10x / 0.25 Ph1 LD A Plan 20x / 0.3 Ph1 Var1	Zeiss, Jena
Axiovert 25 C	**Objectives:** CP Achromat 5x / 0.12 CP Achromat 10x / 0.25 Ph1 LD Achrostigmat 20x / 0.3 Ph1 Achrostigmat 40x / 0.55 Ph2	Zeiss, Jena
Axiphot 2	**Objectives:** Plan NEOFLUAR 40x oil / 1.3 Plan Apochromat 63x oil / 1.4 Plan NEOFLUAR 100x oil / 1.3 Plan Apochromat 63x oil / 1.4 Ph3 FLUAR 40x oil / 1.3 Ph3 **Fluorescence filter set:** DAPI (BP 365, FT 395, LP 450-490nm) FITC (BP 450-490, FT 510, LP 515-565nm) Cy3 (BP 546, FT 580, LP 590nm) Cy5 (BP 575-625, FT 645, BP 660-710nm) Triple-Filter (TBP 400/495/570, FT 410/505/585, TBP460/530/610) **Camera:** Coolview CCD Camera System	Zeiss, Jena
Leica SP5 **DMI 6000 CS**	**Objective:** Plan-Achromat 63x oil / 1.4 **Laser:** Ar 100 mW 485, 476, 488, 496, 512 nm HeNe 2 mW 594 nm HeNe 10 mW 633 nm DPSS 10 mW 561 nm Diode 50 mW 405 nm **Beam Splitter:** Acousto Optical Beam Splitter (AOBS)	Leica, Heidelberg

Axiovert 200 M	**Objectives:** Plan NEOFLUAR 16x oil / 0.5 Ph2 A-Plan 10x / 0.25 Ph1 LD-Plan NEOFLUAR 40x / 0.6 Ph2 Plan Apochromat 63x oil / 1.4 Plan Apochromat 100x oil / 1.4 Plan NEOFLUAR 40x oil / 1.3 Ph3 **Fluorescence filter set:** DAPI (D360/40, D470/40, 400dclp) FITC (HQ470/40, HQ522/40, Q497lp) YellowGFP (HQ500/20; HQ535/30; Q515lp) Cy3v1 (HQ546/11; HQ567/15; Q557lp Cy3.5v1 HQ581/10, HQ617/40, Q593lp) Cy5 (HQ622/36; HQ667/30; Q647lp) UV-Filter for life-cell observations with the halogen lamp 3RD Millennium Longpass filter LC-3RD/450LP-25 Laser Components GmbH Olching **Camera:** Spot RT Diagnostic instruments inc; Sterling Heigths, MI, USA **Condensor (automatic, with Phase contrast):** 424242 (NA 0,55; WD 26 mm) **Halogen-Lamp:** Hal 100 **Bulbs:** HLX 64625 100W 12V; Osram, Augsburg	Zeiss, Jena
Axio Observer D1	**Objectives:** A-Plan 10x / 0.25 Ph1 LD-Plan NEOFLUAR 20x / 0.6 Ph2 Plan NEOFLUAR 40x oil / 1.3 Ph3 Plan Apochromat 63x oil / 1.4 Plan Apochromat 100x oil / 1.4 **Fluorescence filter set:** DAPI (G265, FT395, BP445/50, Filter set 49) FITC (BP470/40, FT495, BP525/50, Filter set 38) Cy3.5v1(BP565/30 FT585, BP620/60, Filter set 31) UV-Filter for life-cell observations with the halogen lamp 3RD Millennium Longpass filter LC-3RD/450LP-25 Laser Components GmbH Olching **Spinning Disc Confocal Unit:** Ultra *View* VoX Perkin Elmer, Waltham, MA, USA	Zeiss, Jena
Axiovert 200 M (Garching)	**Objectives:** LCI “Plan-Neofluar” 63x/1.3 NA **Diode fluorescence Illumination:** Colibri (Zeiss) **Camera:** Axiocam MR (Zeiss)	Zeiss, Jena

3.8.5 Image Processing Software

Adobe CS 4	Adobe Systems, Inc.
Amira 5.2.2	Visage imaging
Blender 2.49	Blender Foundation
Huygens Professional	Scientific Volume Imaging
ImageJ 1.42	Public Domain by Wayne Rasband
Leica Application Suite 1.7.0.	Leica Microsystems
Mathematica 7.0	Wolfram Inc.
MetaVue 6.2r2	Universal Imaging Group
MetaMorph 6.2r6	Universal Imaging Group
ROOT 5.28.00	CERN
Volocity 5.3	Improvision Inc.

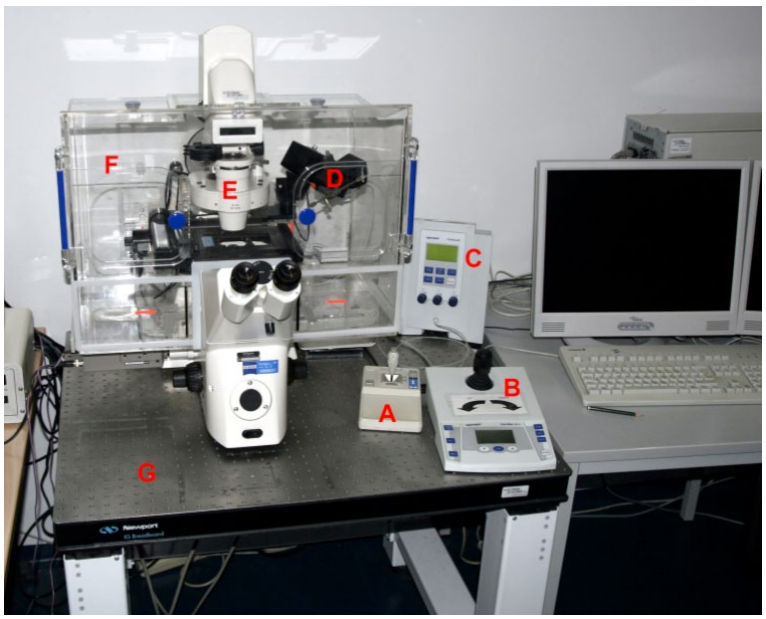

Fig.: 3-2: Set-up of the micro injection facility. (A) control of the microscopic stage, (B) control of the micro manipulator (Inject Man NI2), (C) compressor (Femto Jet) with control panel for the injection parameters (D) micromanipulator, (E) inverted epifluorescence microscope (Zeiss Axiovert 200M), (F) heatable incubator box, (G) vibration absorbing table.

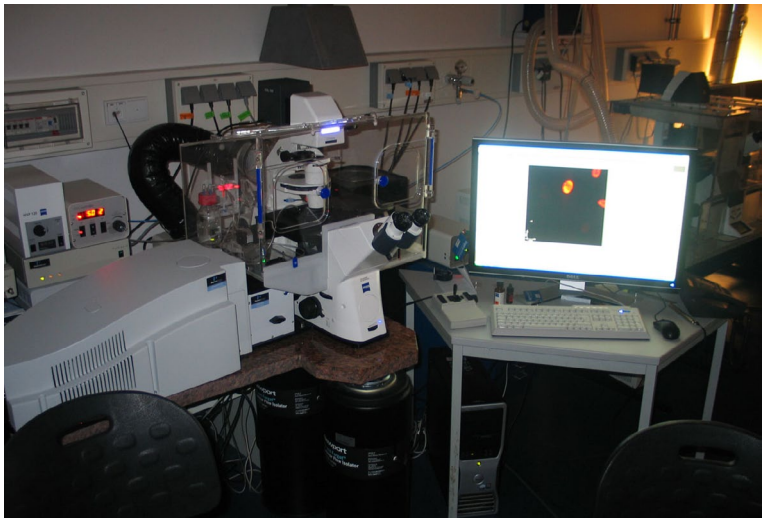

Fig. 3-3: Set-up of the spinning disc microscope. A VOX Perkin-Elmer spinning disc module is attached to the side port of a Zeiss Axio Observer D1 equipped with a motorized stage, a piezo z-drive, a temperature controlled Pecon incubator box and a CO_2 controller attached to a humidifier. The acquisition is controlled by a PC running Volocity 5 on Windows XP.

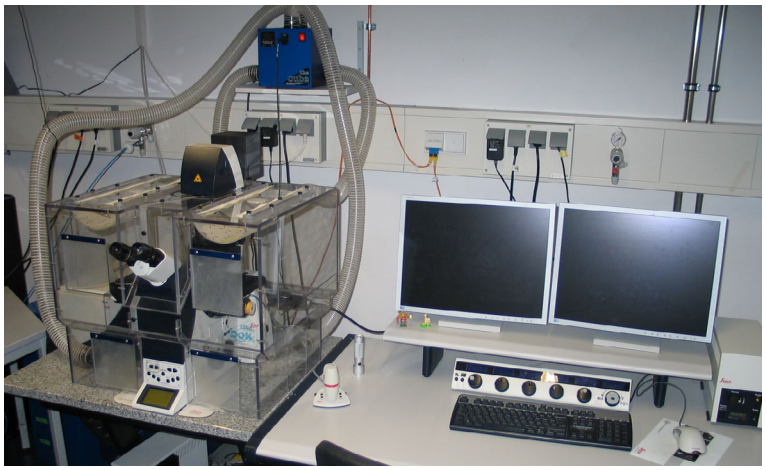

Fig. 3-4: Leica TCS SP5 point scanning microscope. For live-cell imaging an incubator box and a temperature controller are built around the microscope. Control of the set-up and image acquisition is performed via a specialized computer software.

4 Results

4.1 Revisiting Theodor Boveri‘s Hypotesis

4.1.1 Generation and characterization of the RPE1 H4-PA-GFP H2B-mRFP cell line

4.1.1.1 Generation of a stable cell line expressing two types of fluorescent histones

In order to generate a non-tumor derived cell line, which allows to trace photoactivated chromatin domains in cycling cells, the h-TERT immortalized, female cell line RPE1 (derived from the human retina pigment epithelium, see fig. 4-1 and Appendix E) was transfected with plasmid constructs coding for H4 photoactivatable GFP and H2B-mRFP. According to the instructions described in 3.3.2 a stable cell line was generated by lipofection and G418 selection. Since in G418 resistant, stable cell lines the integrated, transgenic constructs are sometimes spontaneously silenced (e.g. by epigenetic mechanisms), selection for cells expressing both transgenes was carried out repeatedly by FACS and/or by manual picking of appropriate cell clones. In the end the most promising cell clones were frozen down in liquid nitrogen where they were stored until usage.

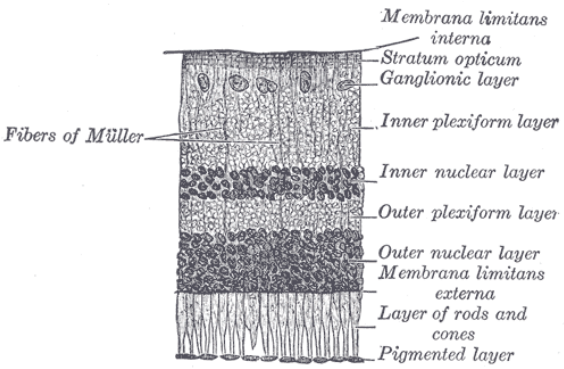

Fig. 4-1: Cross-section through a human retina. The retina pigment epithelium forms the outer layer of the retina that nourishes the retinal visual cells. Due to the pigments in the cells this layer is brown in humans and black in many animals (from GREY'S ANATOMY).

4.1.1.2 Description of the phenotype

Visual inspection of the RPE1 H4-PA-GFP H2B-mRFP cell line (shown in fig. 4-2) by fluorescence microscopy shows a considerable variability in the expression of the transgenes. While the fluorescence intensity levels of the transgenic expression products slightly vary in strength between different nuclei, some nuclei showed expression of one transgene only or did not show any (neither red nor green) fluorescence at all. This phenomenon is most likely caused by epigenetic promotor silencing (e.g. via histone and/or DNA methylation) at the viral promotors of the integrated transgenic expression constructs. Another reason for low or missing transgene expression might be the lack of selection pressure in the absence of G418. For the sake of minimizing cell toxicity during cell culture and live-cell fluorescence microscopy, the use of this selection reagent was waived. In principle it is possible to revert the silenced state of transgenes by adding agents like 5-Aza-2‘deoxycytidine, TSA (Trichostatin

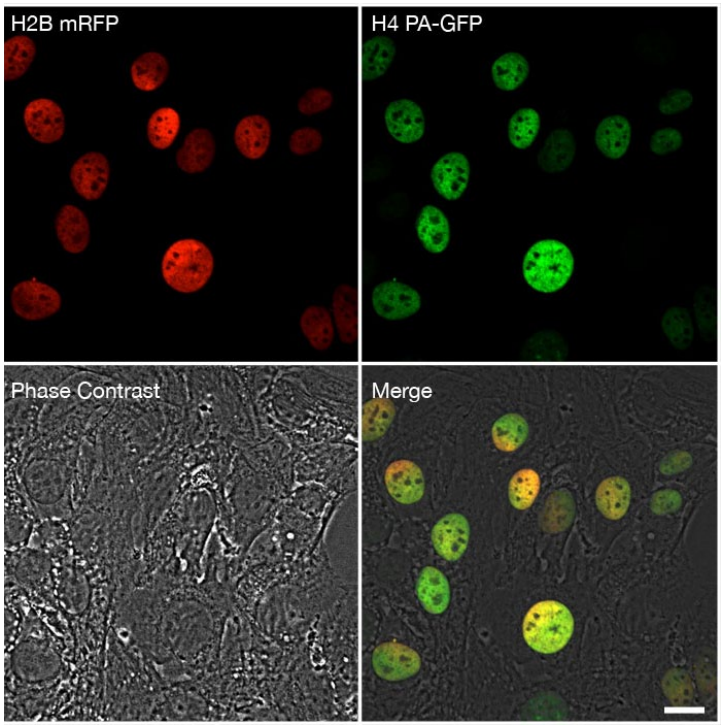

Fig. 4-2: RPE1 H4-PA-GFP H2B-mRFP cell line shown in phase contrast, PA-GFP- and mRFP fluorescence. Not all of the cells express both of the fluorescent transgenes equally strong and some of them do not express any of the transgenes at all. This circumstance most probably is caused by epigenetic silencing at the viral promotors of the used expression plasmids. Fluorescence of non activated H4-PA-GFP was visualized by longer exposure times (compared to the H2B mRFP).

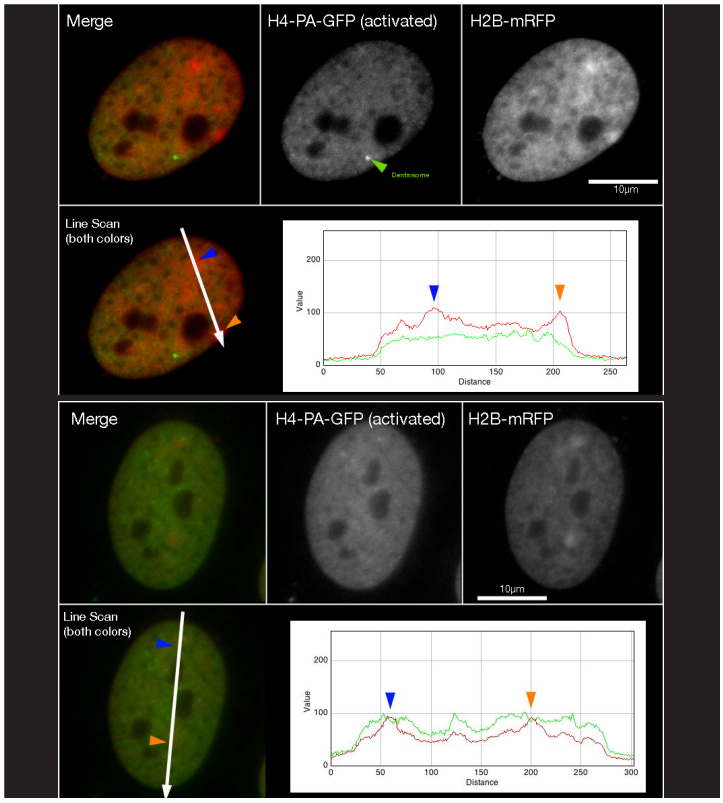

Fig. 4-4: RPE1 H4-PA-GFP H2B-mRFP nuclei (taken from a sample that was in addition transiently transfected with FOP-GFP, see 4.1.2.8) show differences in the distribution of the H4 PA-GFP and the H2B mRFP transgenic proteins within the nuclear volume. H4 is almost absent at the Barr bodies (see arrows in the images and in the line scan diagrams).

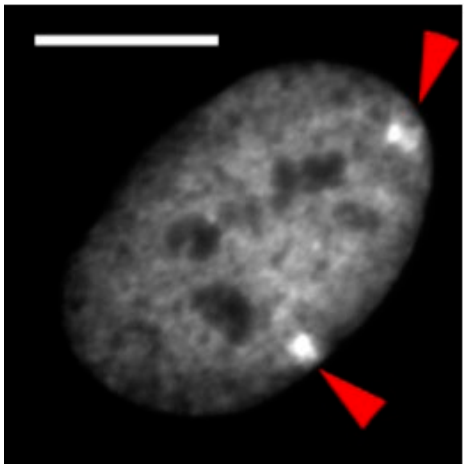

Fig. 4-3: RPE1 cell nucleus showing two Barr bodies (arrows). Expression of H2B mRFP was used for visualization of the whole chromatin in the nucleus.

A), or sodium butyrate (Choi et al., 2005) to the medium, which inhibit DNA methylation – or histone deacetlytion respectively. Nevertheless this option was not considered here because of the unpredictable side effects that a dramatic change in the epigenetic information of the cells might have on the subjects studied in this thesis.

In contrast to most cancer cell lines, the barr bodies (representing the inactive X-chromosomes in female cells) are clearly visible in the nuclei of the transgenic RPE1 cell line (see fig. 4-3). However although distribution of the fluorescently labeled histones H2B and H4 is similar over most of the nuclear volume, the fluorescence ratio between them interestingly differs at the sites of the barr bodies for still unknown reasons (fig. 4-4). While barr bodies in this cell line can easily be detected in images showing the H2B-mRFP fluorescence, they cannot be found in the images showing the H4-PA-GFP fluorescence alone.

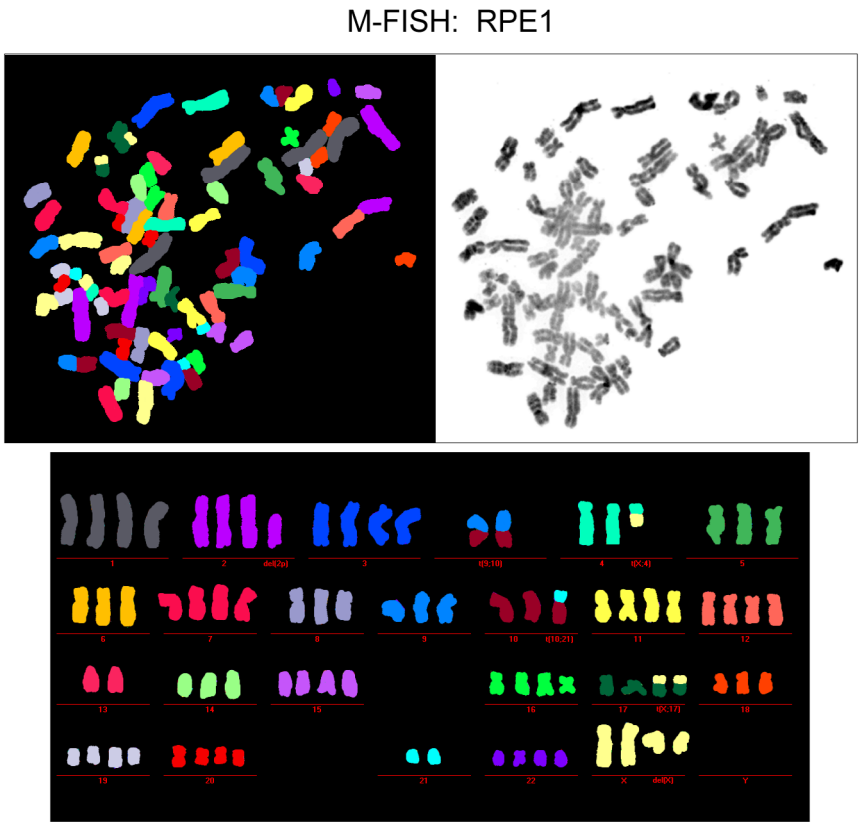

Fig. 4-5: M-FISH of the RPE1 H4 PA-GFP H2B-mRFP cell-line. The karyotype of this formally diploid, female cell line contains 72 chromosomes and appears to have become hypo-tetraploid during multiple passages, transfection and selection. The remaining chromosomes appear to be intact except for 3 chromosomes carrying translocations and one with a deletion (Picture kindly provided by Prof. Anna Jauch, Univ. of Heidelberg).

4.1.1.3 Analysis of the karyotype

The karyotype of the RPE1 H4-PA-GFP H2B-mRFP cell line was determined by M-FISH and described as hypo-tetraploid with few chromosomal rearrangements (fig. 4-5). The observed chromosomal changes in this female karyotype are caused most likely by transfection, selection and growing in cell culture over many generations. Cell culture conditions represent – compared to the original tissue from which the cell line was derived – an artificial environment with different selection pressures to which mutated cells might be better adapted than the the original wild-type cells (for further information see *Discussion*).

4.1.1.4 Growth and cell cycle length

Determination of the average cell cycle length in the RPE1 H4-PA-GFP H2B-mRFP cell line was carried out by two different methods independently.

In one method cells were seeded onto a petri dish, containing a marked area, photographed every day and then counted within the makred area. The resulting plot (cell number vs. time) and the assumption of an exponential cell growth model was then used to fing the mathematical term describing the experimental data best (fig. 4-6). The time interval in which the cells were counted comprised 4 days and the observation was stopped when logarithmic growth of the cells was affected by contact inhibition (making the cell cycle length more difficult to calculate). The average time for one cell cycle determined by this method was 30,2 h.

The other approach used to measure cell cycle length (and to validate the data ob-

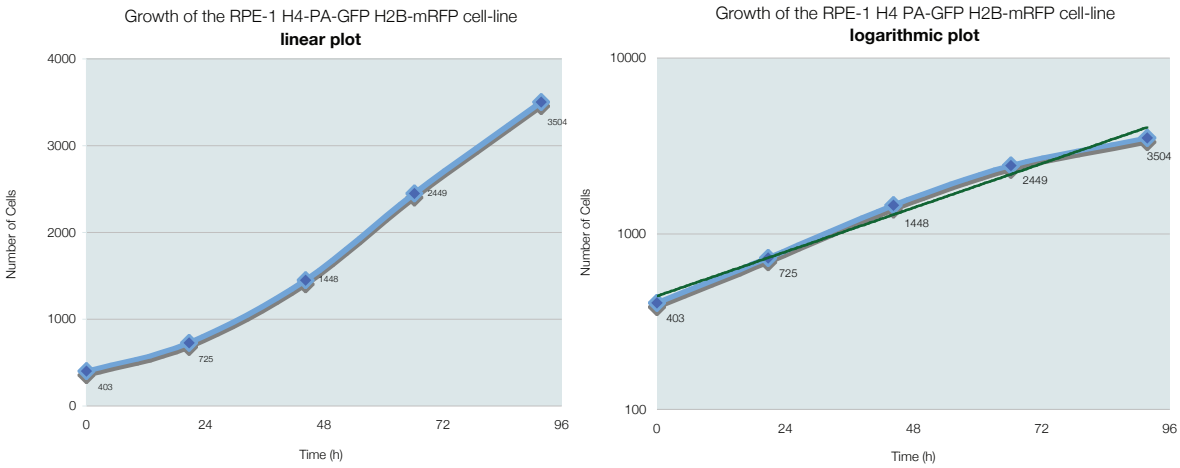

Fig. 4-6: Growth curves of the RPE1 H4 PA-GFP H2B-mRFP line generated by cell counting within a given area at different time points. The cells show logarithmic growth that can be best fit by the function $N(t) = N_0 e^{0,55\ t}$ (t stands for time measured in days). The length of an average cell cycle determined by this formula is approximately 30,2 h. Cell counting was stopped when a cell density was reached at which contact inhibition could start to affect cell proliferation.

tained by the method explained above), measured the time from one mitosis to the next in live-cell time-lapse movies. This data was generated under the same cell culture conditions as used for the other live-cell experiments in this thesis. Using this approach (only 13 cells could be observed and traced) an average cell cycle length of 33,63 h with a quite big standard deviation of 9,58 h was measured (see Appendix G).

4.1.1.5 Photoactivation of H4-PA-GFP

Good photoactivation results were obtained by (ab)using the FRAP unit of the spinning disc microscope (and the respective Volocity® software module) (described in 3.5.2.1, fig. 3-3). To photoactivate the fluorescence of the H4-PA-GFP fusion protein, a region of interest within a midsection of the nucleus was chosen by the selection tools of Volocity® (see 3.5.2.2). Although photoactivation is most efficient using light of a wavelength around 405 nm (Patterson and Lippincott-Schwartz, 2004) the 440 nm diode laser (set at only 10% of its full power) was preferred here in order to reduce the probability for simultaneous creation of DNA damages. The number of iterations for the 440 nm laser to scan over the chosen area with these parameters was set to ten.

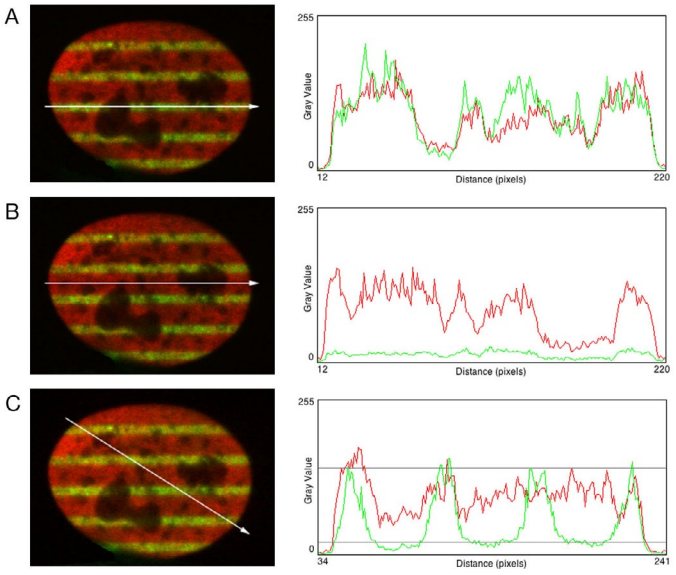

Fig. 4-7: Line-scans along and across the photoactivated line pattern of a fixed RPE H4 PA-GFP H2B-mRFP nucleus (midsection). A: Comparison between the intensity distributions of both FP tagged histone proteins along a line show rather similar intensity profiles. B: Fluorescence of not photoactivated H4-PA-GFP was significantly weaker than H2B-mRFP fluorescence C: Differences in fluorescence between photoactivated and not photoactivated PA-GFP range approx. around factor 5.

Applying this relatively mild conditions for photoactivation allowed to create fluorescence patterns that penetrated the flat RPE1 nuclei per-

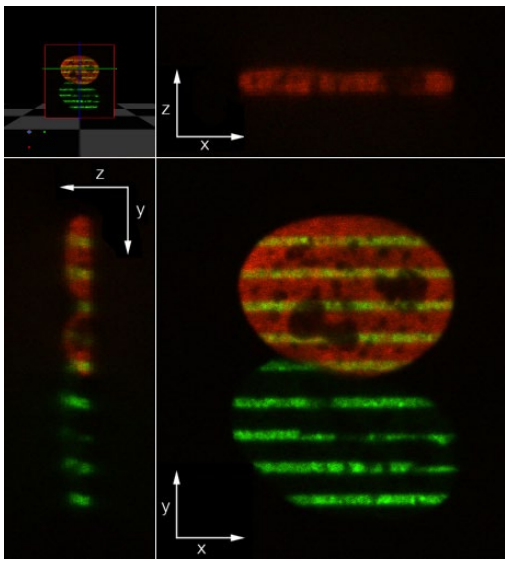

Fig. 4-8: Photoactivation patterns in RPE1 H4-PA-GFP H2B-mRFP nuclei shown in top and side views. Photoactivation at the used spinning disc microscope results in fluorescence patterns that perpendicularly traverse through the nuclear volume. (The figure shows the same nuclei like fig. 4-7)

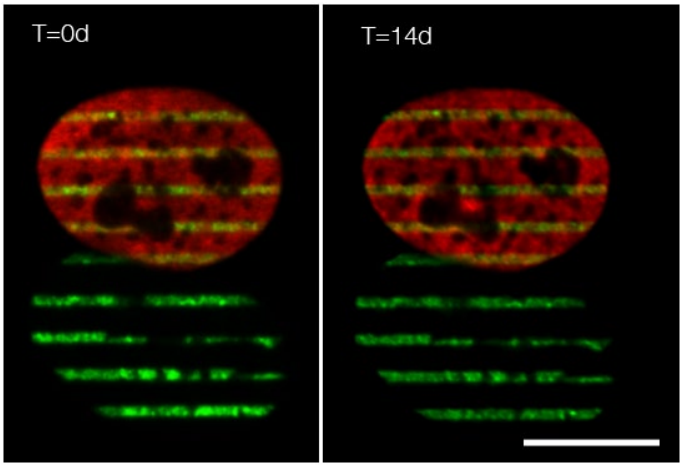

Fig. 4-9: Photoactivation can be performed in fixed cells, too. The photoactivated fluorescent pattern persist unchanged in fixed cells. (same nuclei as shown in fig. 4-7)

pendicular to the x,y-plane (fig. 4-8) and could be easily distinguished from not photoactivated and much less fluorescent chromatin parts. Comparing the fluorescence of the photoactivated to not photoactivated chromatin (fig. 4-7) yielded a ratio of 5 which is however sufficient for the purposes of this thesis but much smaller than the ratio reported by other publications (which is up to 100 fold!) (Lukyanov et al., 2005). Depending on the expression levels, the photoactivatable GFP fluorescence can vary to some extent between different cell nuclei. Interestingly photoactivatable GFP can still be activated in fixed cells and demonstrates the precision of PFA fixation drastically (fig. 4-9).

4.1.1.6 Checking photoactivated chromatin for DNA damages

To check whether photoactivation of chromatin – as described in 4.1.1.5 – can lead to DNA-damages (single or double strand breaks), cell nuclei were photoactivated 1 h prior to fixation and then immunostained with antibodies specifically binding to sites of damage. To check for double strand breaks a monoclonal antibody binding against γ-H2AX (Ismail and Hendzel, 2008; Takahashi and Ohnishi, 2005) was used. To test for single strand breaks an antibody binding against polyadenylated ribose (PAR) was chosen (fig. 4-10). Co-lo-

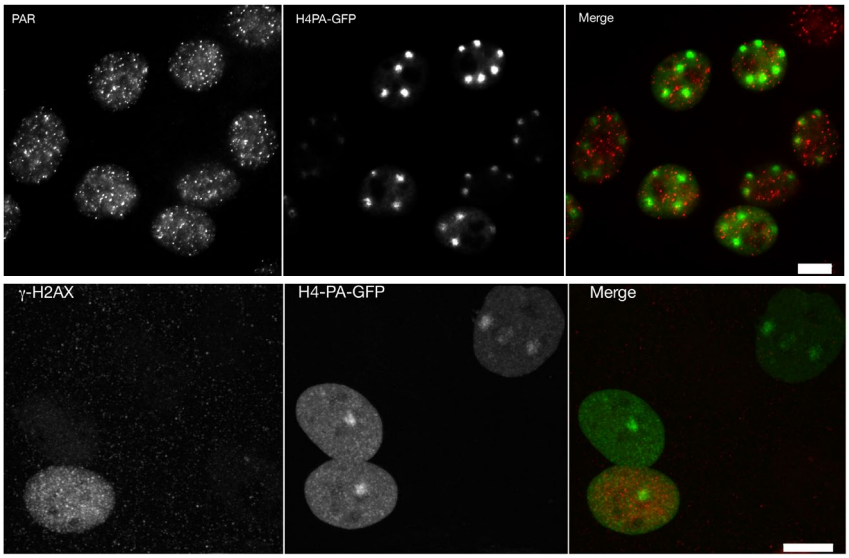

Fig. 4-10: Immunofluorescence stains of partially photoactivated RPE1-PA-GFP H2B-mRFP nuclei using γ-H2AX and PAR antibodies as indicators for DSBs SSBs. No co-localization between the antibody signals and the photoactivated chromatin could be observed, suggesting that the process of photoactivation with the settings used in this work doesn't induce significant DNA damages.

calization of DNA damage and photoactivated chromatin could not be detected in the observed samples. Although this result clearly argues against the generation of severe DNA damages caused by photoactivation as carried out in this thesis, it cannot completely rule out photoactivation related DNA damages. This is e.g due to limited optical resolution and thus detection sensitivity of this microscopic approach and the variety of damages that are not detected by the use of the antibodies mentioned above.

4.1.1.7 To which extent is photoactivatable GFP activated by normal image acquisition in long-term observations?

Since photoactivation of H4-PA-GFP is possible within a broad interval of wavelengths (although at different efficiencies – see 4.1.1.5) it was of major interest to find out whether the imaging conditions used for the long term live-cell observations could lead to unspecific photoactivation over time. An experiment in which a nucleus showing a photoactivated pattern was heavily imaged at its mid-section showed that apart from bleaching of both – photoactivated and not photoactivated chromatin – no detectable unspecific photoactivation was caused by the process of imaging (fig. 4-11). This is most likely due to the fast and mild imaging conditions used at the spinning disc microscope since another study (Müller et al., 2010) reported a considerable increase of unspecific photoactivation using a point scanning confocal microscope. In this study the photoactivated patterns vanished after observation periods longer than 6 hours.

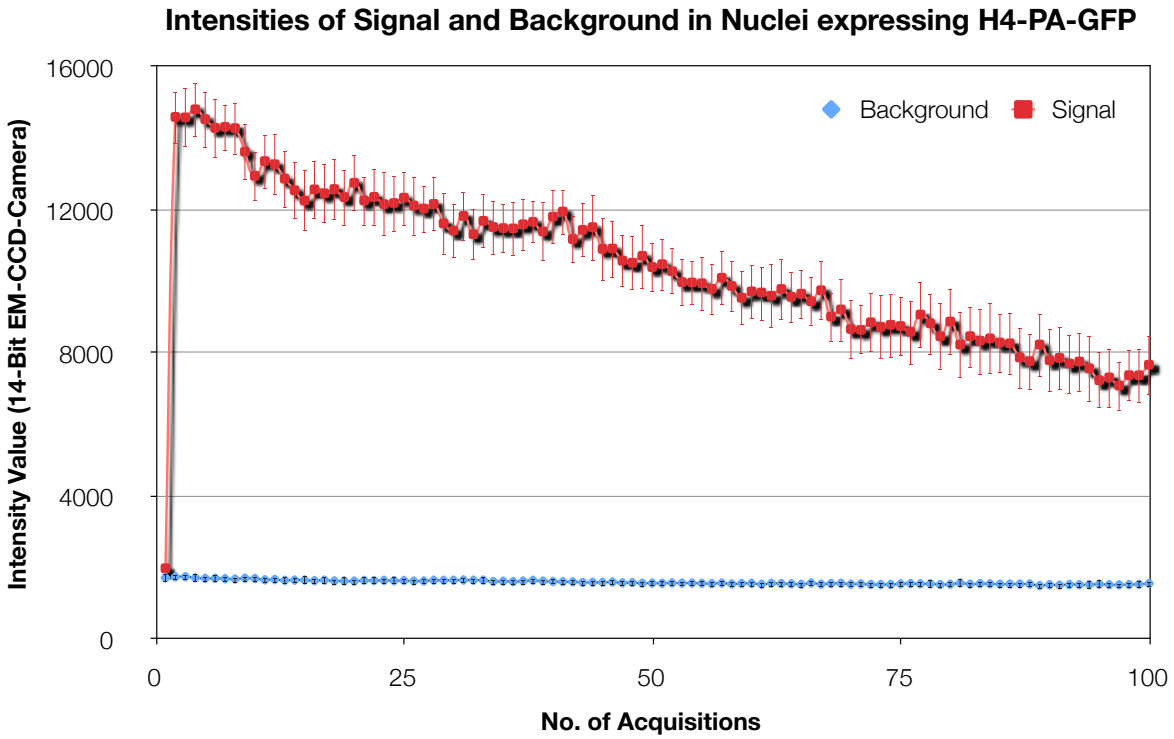

Fig. 4-11: Photobleaching versus photoactivation. Using the 488 nm laser of the spinning disc confocal at 4% of its power for image acquisition leads to photobleaching over time but not to photoactivation. The **red** data points show the average intensity of a photoactivated area over the numbers of images acquired from the sample. The error bars show the standard deviation of intensity within the measured area. Compared to the weak fluorescent not-activated photoactivatable chromatin (**blue**) which only bleaches insignificantly, the photoactivated GFP gets remarkably weaker with increasing numbers of image acquisitions.

4.1.1.8 Hypercondensed Chromatin Condensation (HCC) in interphase nuclei doesn't change nuclear architecture

Reversible hypercondensation of chromatin is caused by treating cells with hypertonic medium and results in visible changes with respect to the appearance of the whole nucleus. Within the nuclei chromatin- and interchromatin compartment become separated forming two interacting networks (Albiez et al., 2006). Experiments using HCC in the past in order to explore the consequences of this phenomenon on nuclear architecture were performed by photobleaching of GFP labeled chromatin. These experiments did not demonstrate major changes caused by the hypertonic treatment. Using a cell line expressing photoactivatable chromatin was accompanied with hopes to have a better tool for the identification of changes in nuclear architecture before, during and after hypercondensation. Fig. 4-12 shows that – maybe due to the limited optical resolution of the used microscope – hypercondensation-related changes to the nuclear architecture of the nucleus could not be observed. The only changes that were visible consisted in higher fluorescence intensity levels during HCC.

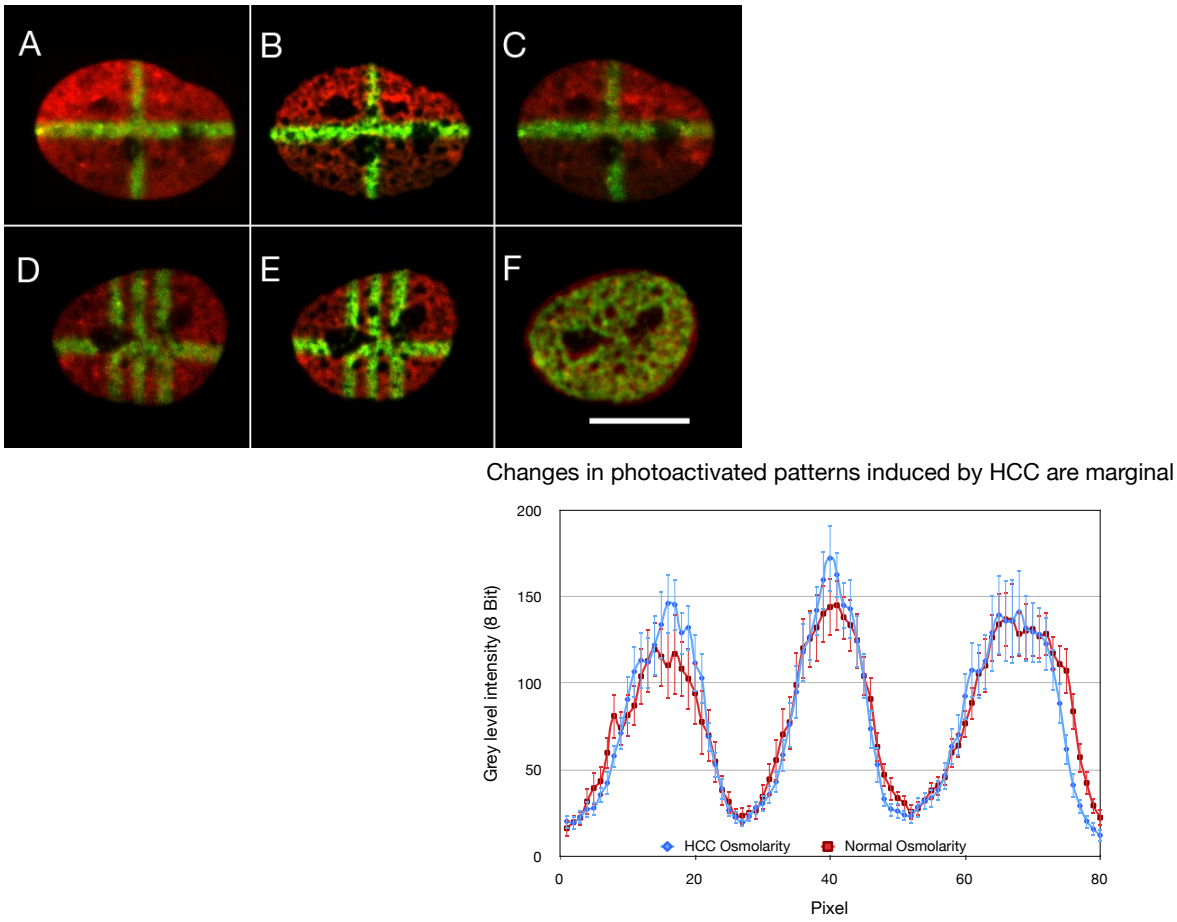

Fig. 4-12: Hypercondensation of chromatin only leads to minor changes in nuclear architecture and appears to be completely reversible. **Upper panel:** (A-C) Nucleus containing a photoactivated cross before (A), during (B) and after (C) hypercondensation induced by a 750 mOsm PBS solution. Pictures (D) and (E) show a nucleus before and during hypercondensation. Picture (F) shows the overlay of the H2B-mRFP channels of (D) and (E). Despite the different visual appearance the geometrical differences between both states appear to be rather small. **Lower Panel:** the graph shows the average fluorescence of the photoactivated chromatin in the stripes of the lower half of (D) and (E). Differences between both curves affect mainly the intensity of fluorescence between hypercondensed and normal chromatin.

4.1.2 Testing Boveri's hypotheses and exploring the mechanics of mitosis

In order to test the hypotheses stated by THEODOR BOVERI in his seminal work from 1909 the next section describes 4D live-cell studies including photobleaching and photoactivation experiments that were mostly performed with the RPE1 H4-PA-GFP H2B-mRFP cell line described before.

4.1.2.1 Chromosomes occupy distinct territories within the interphase cell nucleus

A chromosome protruding out of a horizontal prometaphase rosette was photoactivated (fig. 4-13). Revisiting the same position a few hours later shows that a distinct area is highlighted in each of the daughter nuclei – demonstrating the territorial organization of interphase chromosomes in the nucleus.

Although the result of this simple experiment brings no new insight into the field of nuclear architecture, it impressively demonstrates the elegance and power of the cell line created in this thesis to study nuclear architecture and the mechanics of mitosis. Due to the slow turnover of the H4-PA-GFP in nucleosomes this experiment also demonstrates the traceability of photoactivated chromatin domains over time.

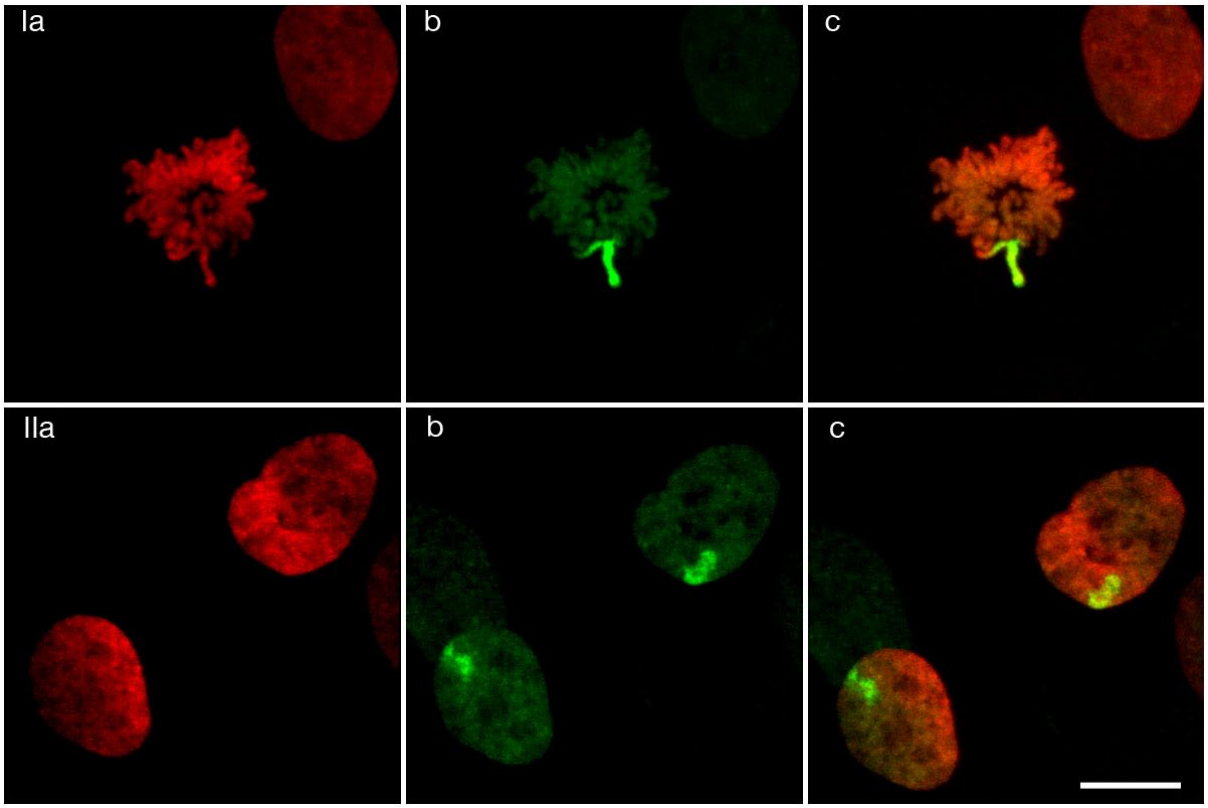

Fig. 4-13: The **upper panel** (Ia-Ic) shows a horizontally oriented prometaphase rosette of a RPE1 H4-PA-GFP H2B-mRFP cell. One in particular protruding chromosome was photoactivated. The **lower panel** (IIa-c) shows the same region several hours later showing two daughter nuclei each-one containing a distinct photoactivated area demonstrating the the territorial organization of chromosomes in the interphase nucleus.

4.1.2.2 Arrangements of chromosome territories are stably maintained during interphase in most of the observed cells

To assess the long-term stability of chromatin arrangements within distinct regions of an interphase nucleus, geometric patterns were generated in nuclei by photoactivation and observed over longer time intervals up to an entire interphase. The idea behind this procedure was, that large-scale movements of distinct CTs in interphase (if there were any) would lead to a significant distortion or even to a complete breakdown of the geometric fluorescence, patterns.

4.1.2.2.1 During S-phase large scale movements of chromosomes are not mandatory

During S-phase the whole genome inside a cell nucleus is replicated. Therefore it was of particular interest to test for large-scale movements during this phase of the cell cycle. RPE1 cells were transiently transfected with constructs coding for H4-PA-GFP and PCNA-mRFP. PCNA acts as loading clamp for the DNA-polymerase during DNA-replication and forms replication foci which exhibit a specific temporal pattern depending on the respective stage of S-phase (Chagin et al., 2010). Fig. 4-14 shows an example of a RPE1 nucleus which was labeled with a double-cross (by photoactivation) before entering S-phase (compare movie S1). One can easily see from the PCNA-mRFP patterns that the cell passed through the typical stages of S-phase whereas the photoactivated double cross-like pattern persisted more or less unchanged (except for some minor changes that can be explained by confined chromatin diffusion). All 15 cells that were observed through S-phase this way showed conservation of the photoacitvated fluorescence patterns. These findings clearly argue against large-scale changes in CT arrangements caused by the dynamics of DNA-replication.

4.1.2.2.2 During interphase CT arrangements persist in the vast majority of nuclei

Long-term observation of RPE1 cells (in total about 150) ranging from 2 h up to 36 h showed that the initial photoactivation patterns remained stable through interphase with only few exceptions (4 cases ≈ 3%) which will be discussed in detail later. The time series in fig. 4-15 shows a nucleus that was observed from early G_1-phase throughout the complete interphase until prophase of the next mitosis. Although the shape of this nucleus varies slightly, the photoactivated cross remains stable during the entire interphase (see also movie S2(a) and movie S2(b) on the enclosed DVD).

Since Chuang et al., (2006) have reported that directed chromatin movements might be suppressed by photo-toxic effects, long-term stability of chromatin was checked by acquiring 3D image stacks of photo-labeled nuclei only twice: once at the beginning (directly after photoactivation) – and once at the end of the experiment (ca.15-18 h later) (see fig. 4-16). Although cells that were treated this way were exposed to much less photo-toxic stress, the initial irradiation patterns were still entirely conserved and recognizable. Visual inspection of these nuclei did not allow to detect pronounced differences in the degree of confined chromatin diffusion compared to nuclei that were imaged continuously.

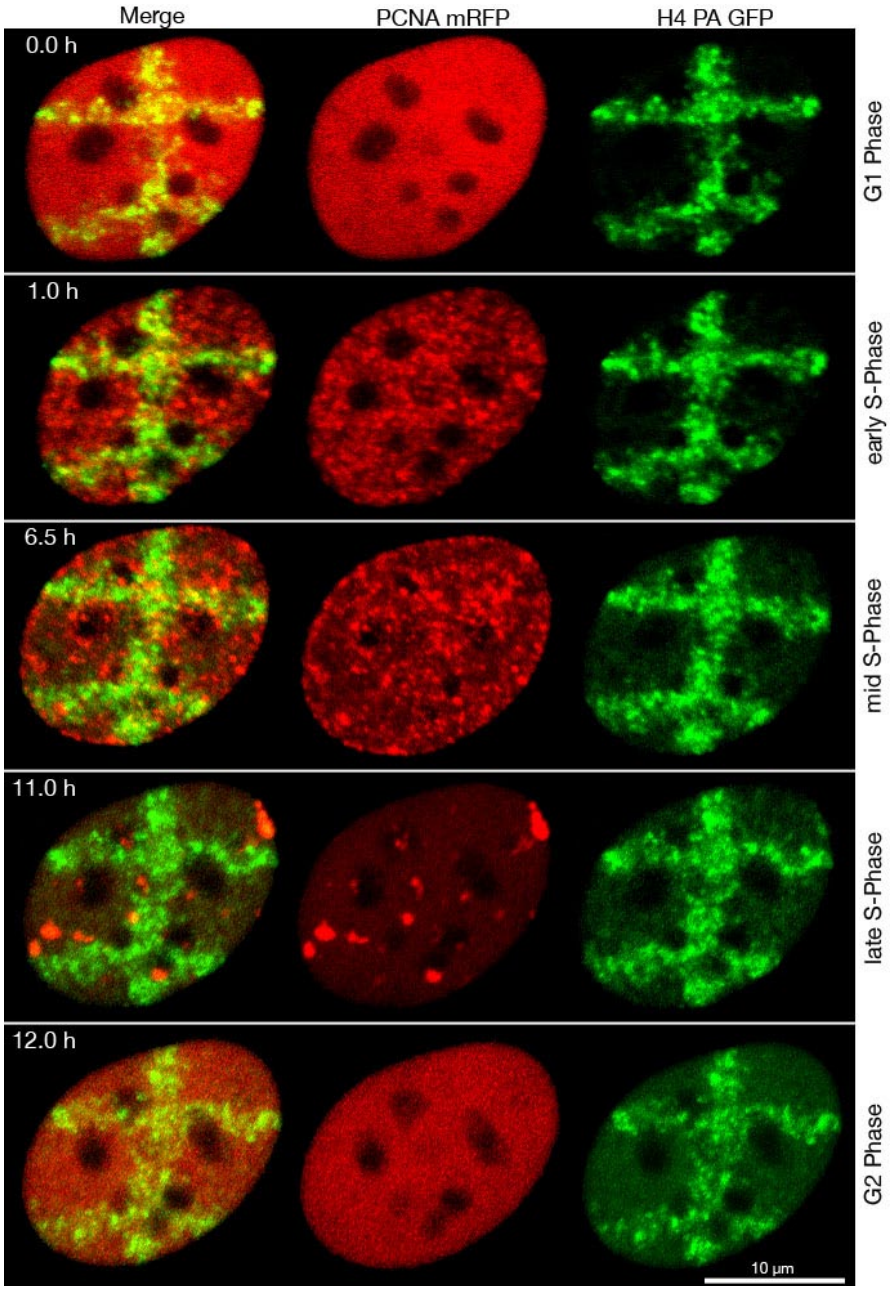

Fig. 4-14: RPE1 cells that were transiently transfected with H4-PA-GFP and PCNA-mRFP were photoactivated with a cross pattern prior to S-phase and then observed through S-phase. The nuclei that moved to G_2-Phase show that the initial pattern – although blurred – was conserved. Note that the shown nucleus was corrected for rotation and that some bleaching occurred which decreased the signal to noise ratio.

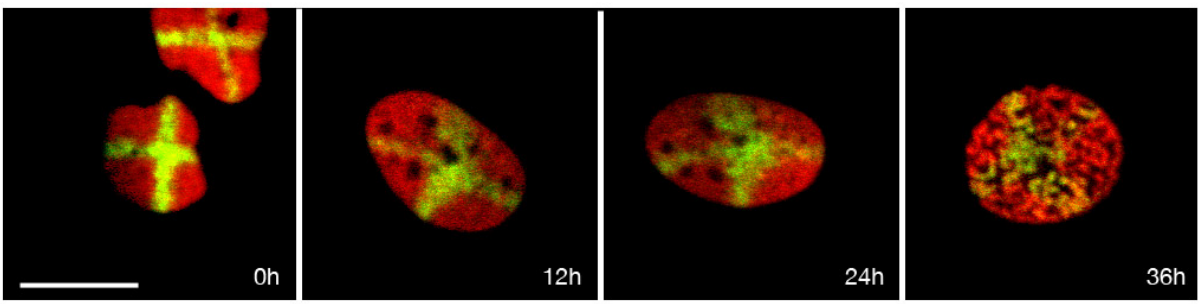

Fig. 4-15: Interphase stability of chromatin. A cell nucleus in late telophase was photoactivated with a cross pattern and guided through the whole cell cycle. The photoactivated pattern persists through the entire cell cycle. The distorion visible after the first shown time point is most likely caused by the circumstance that at the time of photoactivation the nucleus hasn't been completely parallel to the substratum.

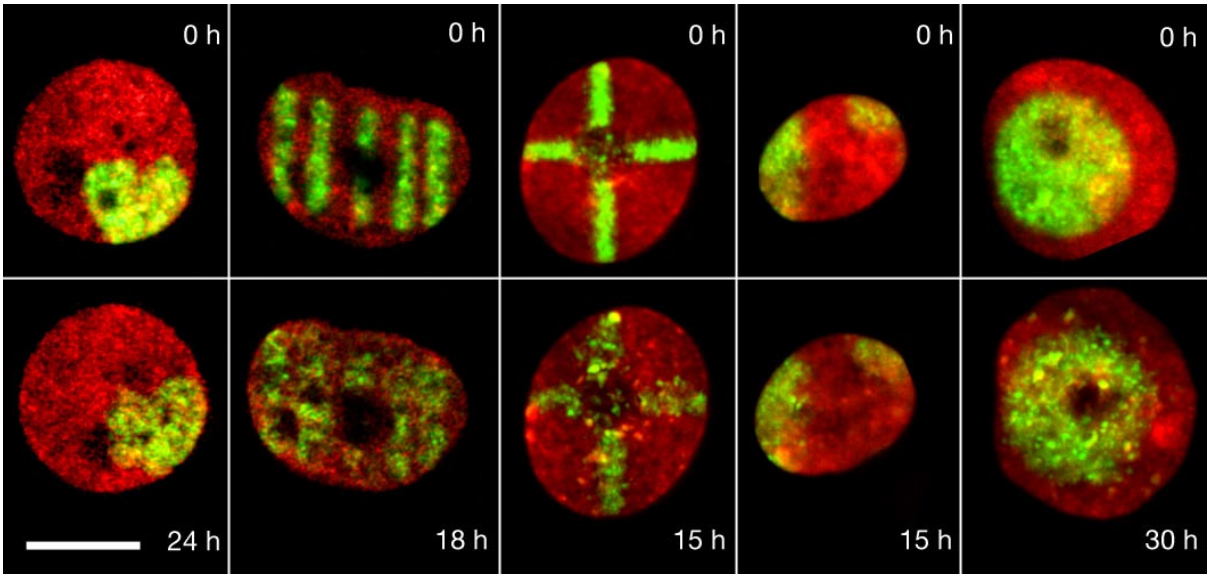

Fig.4-16: Nuclei that have been imaged directly after photoactivation and then revisited several hours later show that photoactivated patterns remain stable over long periods of time and that the conservation of patterns is most likely not an artifact produced by photo-toxicity.

In all observations performed for this thesis, the photoactivated irradiation pattern were not distorted fundamentally neither during S-phase nor during a whole cell cycle. In some cases distortions of the photoactivated patterns were caused by geometric deformations of the whole nucleus. In other cases distortion of the photoactivated patterns occurred in nuclei that were photoactivated directly after mitosis, when the nuclei still haven't taken their final position parallel to the substratum. Except for four examples (in which the photoactivated patterns transiently collapsed) nothing except confined chromatin diffusion was observed during interphase.

4.1.2.3 Quantification of confined chromatin diffusion using photoactivatable chromatin

As cell nuclei have to be flexible to adopt to their environment, the genome has to be a plastic structure. The dynamics described in this section are of small scale-nature and caused by the confined diffusion of chromatin. As observed in the previous figures, these chromatin movements only lead to a blur in once sharply defined photoactivated patterns and happen within a range smaller than 2 µm.

In order to examine the properties of confined chromatin diffusion the thinnest possible lines were photoactivated onto cell nuclei and nested time lapse series of different interval length (Δt=6 sec for 10 min, Δt=30 sec for 50 min and Δt= 30 min for 9 h) were acquired from the same focal plane to trace the temporal changes in width of the photoactivated chromatin line (see movie S3(a)). To asses the increase in line-width over time, the images of all time points were rotated and moved using an ImageJ registration plugin (StackReg, → Rigid Body Registration) to correct for changes in the orientation of the nucleus. Next, the intensity profile along the y-axis was fitted by a gaussian function for each x-position using the program "doline" which was developed in the the data analysis framework "Root" by the DOLLINGER group. Mean and standard deviation of these gaussian curves were used as estimators to describe the progression and the width of the photoactivated line. Overlaying these statistical estimators over a false color image displaying the photoactivated part of the

nucleus (see fig. 4-17) shows how well these parameters are suited to describe the line. It should be mentioned that this method is completely threshold independent. For this reason the method is especially qualified for evaluation of this kind of data since with increasing numbers of pictures, photobleaching effects become more and more pronounced (see fig. 4-11). However, the program "doline" allows a manual decision whether to accept or reject a suggested gaussian fit. This is important to prevent unreasonable fits within noisy areas (e.g. left and right of the line or in areas which exhibit a poor signal to noise ratio). Taking an intensity value of 1000 (in a 14-bit image) as a start value to search for a signal to be fit seemed to be a good choice and was used for all evaluations presented below.

In fig. 4-17 the stroked line represents the best line fit through the mean values of the photoactivated line and its width – characterized by its FWHM (Full Width Half Maximum) (dashed lines) – respectively (see movie S3(b)).

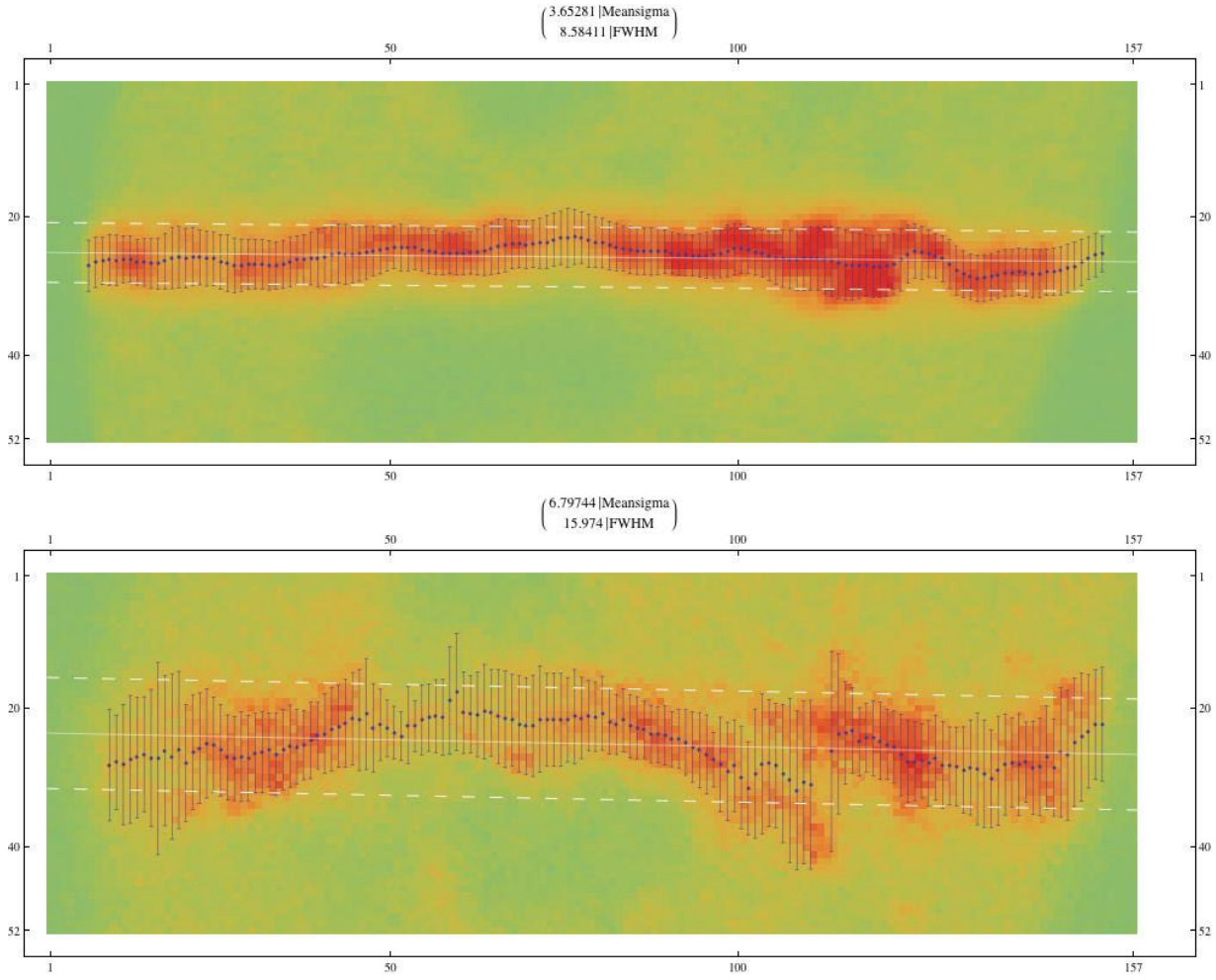

Fig.4-17: Width of a line photoactivated across the chromatin of a nucleus at the begin (**upper**, 0 h after photoactivation) and near the end of the observation (**lower:** 9 h after photoactivation). The mathematically fitted parameters "Mean" and "sigma" (single gaussian fits shown in blue) seem to match the photoactivated line pretty well. The white line in the middle of each picture represents the best fit through the means. The dashed lines parallel to it show the mean FWHM (width) of the photoactivated line. It is clearly visible that the photoactivated signal broadens through time. One pixel in the pictures is equal 0.109 µm, i.e. the distance between 1 and 100 at the x-axis represent 10.9 µm. The intensity of the photoactivated chromatin seems to decrease due to photobleaching and confined diffusion of the chromatin (fig. 4-18).

Plotting the mean widths (standard deviations) of each acquired time point (representing the width of the photoactivated line) in combination with their own variations

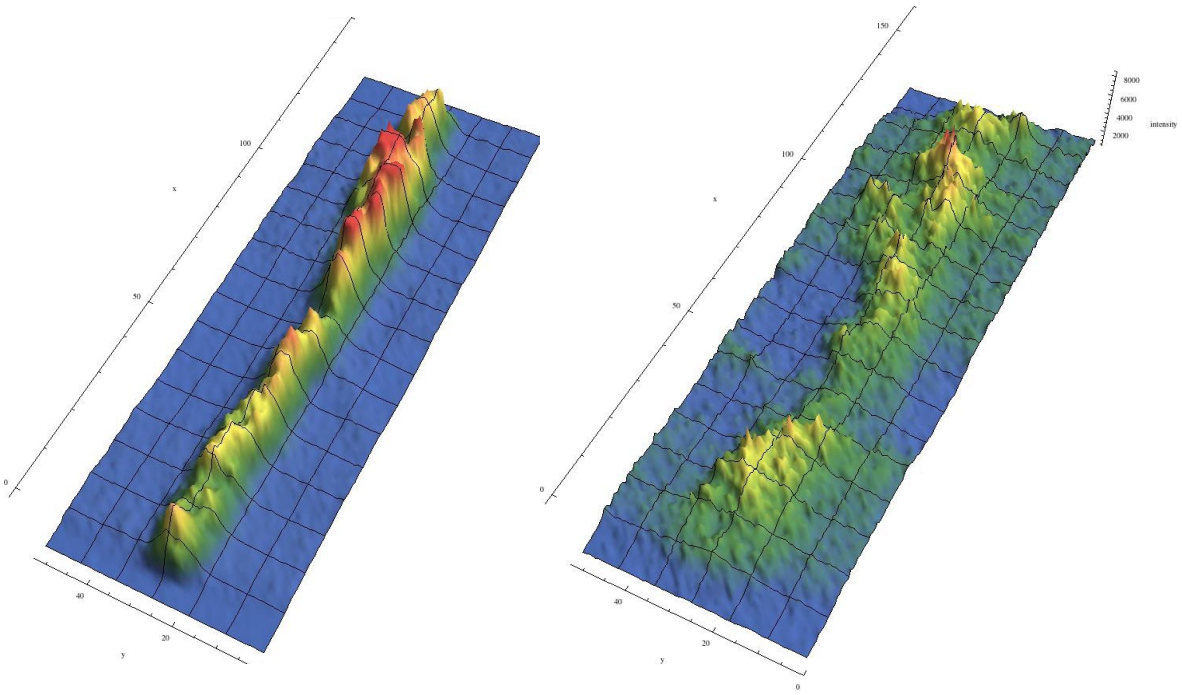

Fig.4-18: The intensity of the photoactivated chromatin (intensity is shown as hight) decreases with time from the beginning (**left**) to the end (**right**) of the observation period due to photobleaching and diffusion of the fluorescent chromatin. At the beginning of the observation (0 h) the signal to background ratio is much more pronounced compared to the image from the end of the observation period (ca. 9 h) One square in the figures has the dimensions of 1 µm ^{2}.

(standard deviations) as error bars against time (see fig. 4-19) makes it easy to recognize that changes in the line-width (initially ≈ 400 nm) are quite small over the course of time compared to the optical resolution limit of a light microscope which is about 186 nm for the used emission wavelength of GFP (λ ≈ 520 nm) and the numerical aperture of the objective (NA = 1,4) . The resolution limit of light microscopes is also represented by the rather huge error bars compared to the changes of the line width which makes it not always possible to confirm a "significant" increase of the signal by just looking at the graph.

The shape of the curve reminds of a square root function. Actually taking the physical formula:

$$c(\vec{r}, t) \propto e^{-\frac{r^2}{4Dt}}$$

as a model for diffusion suggests an expansion behavior that follows a square root function:

$$\sigma = \sqrt{2Dt}$$

in which D represents the diffusion constant.

Fitting the measured points with a curve of the form:

$$\sigma = \sqrt{2Dt} + c$$

(c takes the starting width into account)
leads to following expression:

$$\sigma = \sqrt{2 * 5574.6 \frac{\text{nm}^2}{h} * t} + 451.8\,\text{nm}$$

Transforming D into SI Units results in:

$$D = 1,55\ 10^{-18}\ \frac{m^2}{s}$$

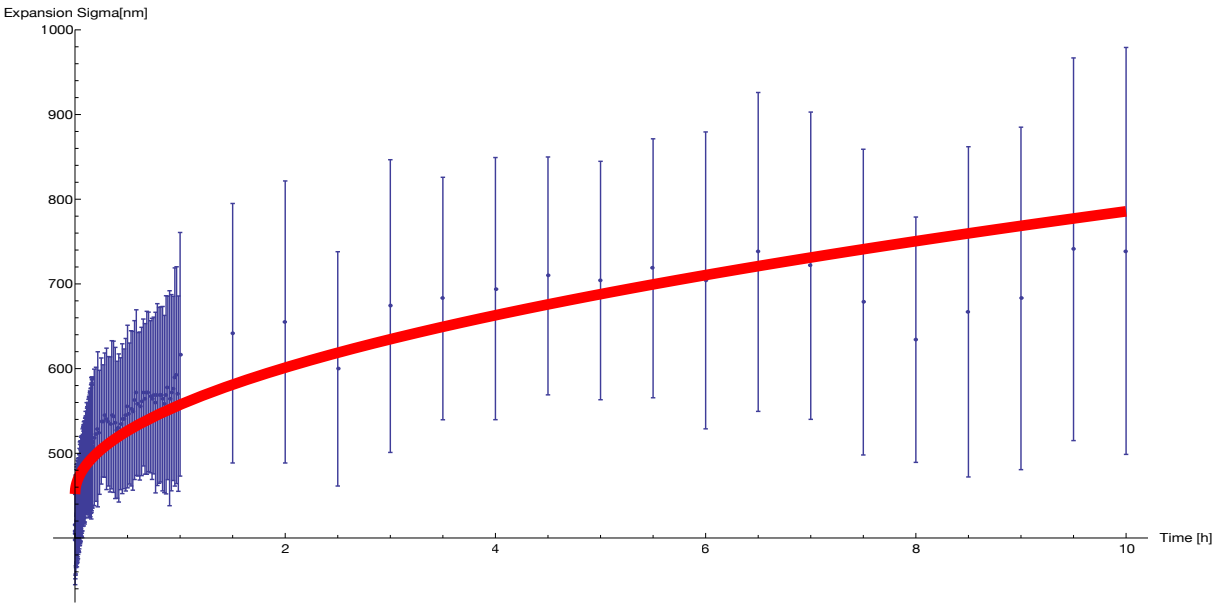

Fig.4-19: Increase in average line-width of a photoactivated line across a nucleus plotted over time. Measurements obtained using the microscopic pictures are shown in violet. Fitted curve according to a physical model for diffusion is shown in red.

With respect to the orders of magnitude this result fits well to previous studies focussing on diffusion of damaged chromatin generated at the ion microbeam (Hable, 2004). The difference of one order of magnitude might be explained by the fact that in contrast to (Hable, 2004) intact chromatin was monitored in the couse of this observation. It also has to be taken into account, that the diffusion measured here originates from a line of photoactivated chromatin that was arbitrarily drawn across the cell nucleus and thus comprises a mixture between the diffusion properties of heterochromatin and euchromatin. The big error bars in the plot might also contribute to a considerable error of the computed diffusion constant.

The differences between the values obtained in this study and the values obtained from the damaged chromatin at the ion microbeam could also result from the use of a different cell line (RPE1 vs. HeLa (derived from a malignant tumor)) and from the different experimental approach (live-cell imaging vs. evaluation of fixed cells). Cells that were used for this study were grown to a confluent layer and didn't appear to be still cycling in contrast to the always cycling HeLa cells. A cell cycle dependence of the diffusion parameter D would result at most in an average diffusion constant measured applying the used method, since the long observation intervals cover more than one cell cycle stage.

Recording fixed cells (as a control) under the same imaging conditions and recording 45 frames of 6 sec time intervals shows – as expected – no diffusion of the chromatin. The mean and the standard deviation of the fixed cells over the recorded frames was 413 ± 6.9 nm in contrast to 437 nm ±28.3 nm obtained from living cells after the same time interval. Again – even if these data have a clear tendency, they have to be handled with a lot of caution, since the measured differences lie far below the resolution limit of conventional light microscopes! It also should be noted here, that the number presented as diffustion constant of the chromatin above strongly depends on the physical model that was assumed to describe the process of diffusion.

4.1.2.4 In a few cells 4D observation led to the discovery of nuclear rotations around an axis parallel to the plane of the substratum while mostly keeping their flat cell shape

A very interesting but also very rare observation could be made in 4 nuclei (out of ca. 150 observations) that showed nuclear rotations along an axis parallel to the plane of the substratum while mostly maintaining their flat structure. In contrast to the very often occurring rotations around an axis perpendicular to plane the substratum, these four cases are special because the maintenance of their flat nuclear shape (characteristic for this cell type) implies pronounced dynamic changes in nuclear organization during the rotational movement.

As shown in fig. 4-20 (left panel) (see also fig. S1 and movie S4(a)) a ring-like structure was photoactivated at the x,y boundary of a nucleus. Within 10 minutes the pattern completely changed its configuration into a band spanning across the middle of the nucleus. Sections taken from a chosen (x,y)-z plane and color-coded by a false color lookup table show that the intensity distribution of the photoactivated chromatin looks like a peripheral ring-like configuration around the rim of the nucleus. It should be pointed out that the axial resolution of light microscopes is much poorer than its lateral resolution. This should be carefully considered while judging the z-sections. Subsequent images of this time lapse series show that this deformation is reversible and can change between the extremes described above and intermediate states within relatively short time intervals of about 10 minutes.

Fig. 4-20 (right panel) (see also fig. S1 and movie S4(b)) shows a second example of rotational movements along the nuclear periphery. Here a small spot at the lateral nuclear boundary was photoactivated. While in this case rotational movements around the perpendicular axis are pronounced, too, one can see in selected (x,y)-z sections that the photoactivated chromatin changes its relative position with respect to the total shape of the nucleus in such a way that the highly fluorescent chromatin moves towards the geometric center of the nucleus – while sticking to the nuclear periphery.

The third example shown in fig. 4-21 is shows mid-sections of a cell nucleus with rectangular photoactivated patterns. In this experiment the cell culture was stimulated by addition of serum to the medium after beginning the observation. Although most of the observed nuclei (ca. 50) didn't exhibit remarkable changes, the shown nucleus showed strong distortions in its pattern that were almost completely restored again during the observation period of 5 h and then remained in this configuration until the end of the experiment.

The big importance of these observations is that relative distances between distant CTs can change dramatically caused by these rotational conveyer belt-like movements without completely changing the neighborhoods of the chromosome arrangements.

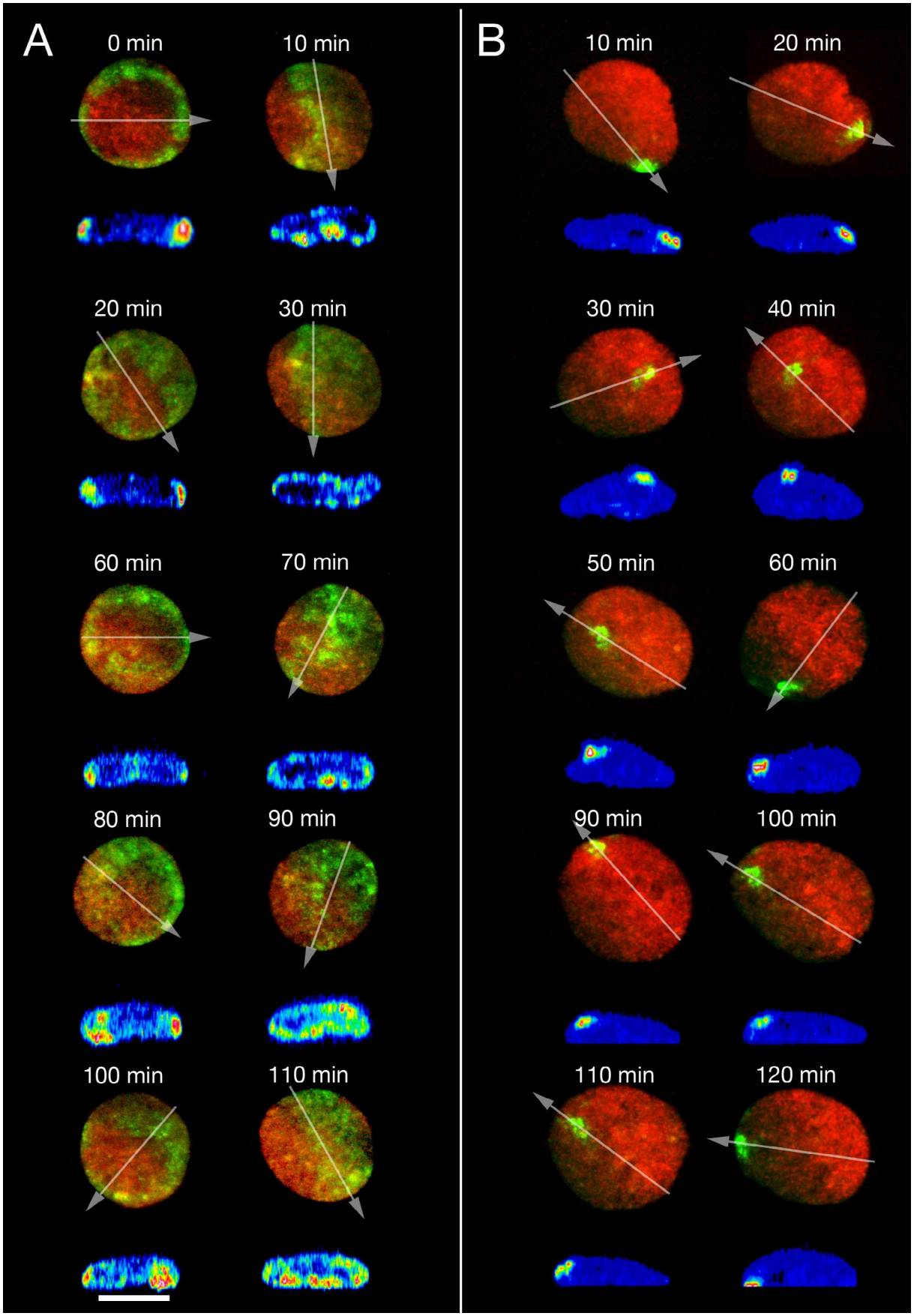

Fig.4-20: Changes in relative distances between CTs can be accomplished by conveyer belt-like motions of flat shaped nuclei. While in (A) the distortion and restoration of a ring-like structure can be followed multiple times, the example in (B) shows photoactivated chromatin located at the nuclear periphery that significantly changes its relative position towards the geometric center of the nucleus.

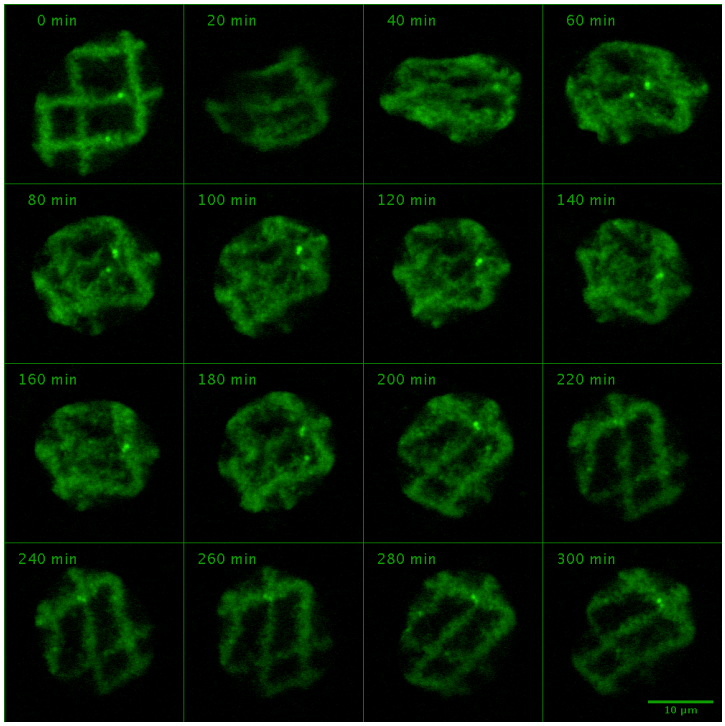

Fig. 4-21: 2D series of a RPE1 cell in which the photoactivated pattern gets strongly distorted after adding bovine fetal serum to the growth medium. The initial pattern gets almost completely restored at the end of the long-term observation.

4.1.2.5 Nuclear rotation can occur directly before the transition into mitosis but stops immediately at the onset of chromatin condensation

In order to explore whether nuclear rotation can influence nuclear architecture just right before the transition from interphase into mitosis, 4D datasets containing nuclei within this phase of transition were carefully reviewed. Although most of these observations didn't show nuclear rotation before entering mitosis at all (see fig. 4-15) – and thus nuclear rotation doesn't seem to have a vital function in this context – one very interesting example (fig. 4-22) was found. The nucleus shown here rotates (identified by the relative positional change of the BARR bodies) quite heavily during the first observed time points. Nuclear rotation could be confirmed by photoactivation of chromatin at the nuclear rim perpendicular to the assumed rotational direction and then finding these markers in the next 3D data set at the top and bottom of the nucleus respectively. Interestingly this nuclear rotation seemed to be independent from the movement of the centrosomes that were visualized in this experiment by the transgenic expression of the FOP-protein – a component of the centrosomes (FOP stands for FGFR1 oncogene partner). At the moment when the condensation of the chromatin became visible the nuclear rotation stopped immediately.

Fig. 4-23 shows a nucleus of a HeLa H2B-GFP cell line that was recorded on its way into mitosis. Although no nuclear rotation could be observed here it was still interesting to see internal movements that were caused by the condensation of chromosomes. Chromatin condensation tears loosely organized euchromatin to sites that are already occupied by the denser heterochromatin. This shows to some extent parallels to the reversible hyper chromatin condensation induced by medium of high osmolarity that was mentioned in an earlier section.

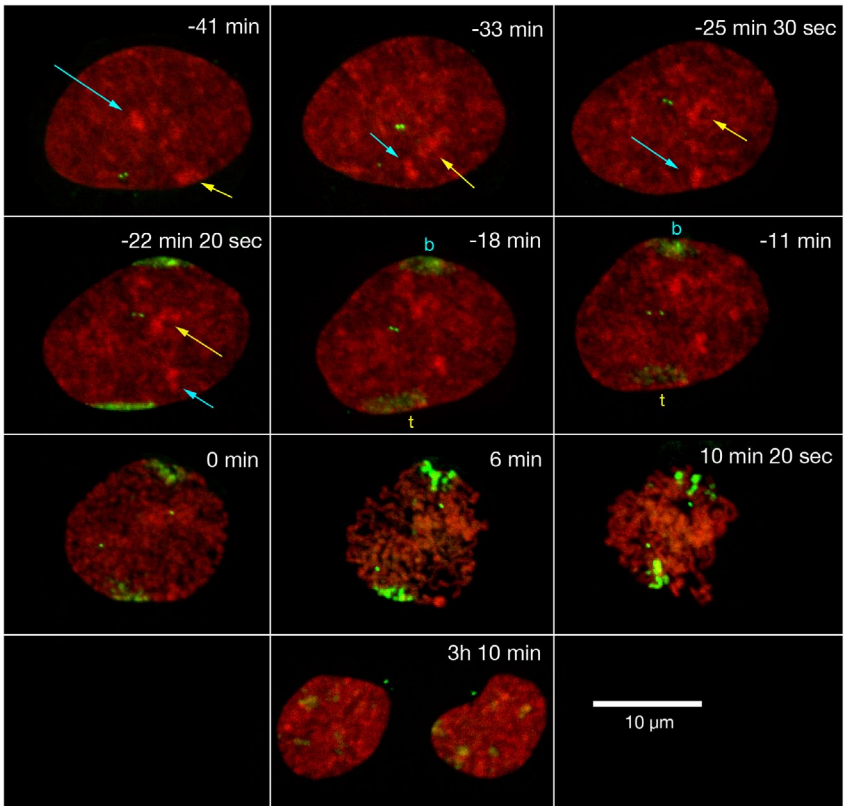

Fig. 4-22: Maximum z-projections of a RPE1 nucleus observed prior and during mitosis. An RPE1 H4-PA-GFP H2B mRFP cell transiently transfected with FOP-GFP was monitored during the last part of interphase and through mitosis. The changing positions of the BARR bodies (arrows) indicate a nuclear rotation in the opposite direction compared to the movements that are performed by the centrosomes under the nucleus (small green dots). While the BARR body at the tip of the yellow arrow moves at the top of the nucleus, the BARR body marked by the cyan arrow changes its orientation from the top layer to the bottom layer. These observations were confirmed by photoactivation of areas at opposite sides of the nuclear rim perpendicular to the assumed direction of rotation. As expected the movement leads to a rolling of the photoactivated chromatin to the top (t) or to the bottom (b) of the nucleus respectively as nuclear rotation proceeds. Once prophase leads to the condensation of the chromosomes, the rotation stopps. Note that nuclear rotation prior to mitosis (although observed here) doesn't seem to be mandatory for this cell line. (see fig. 4-15).

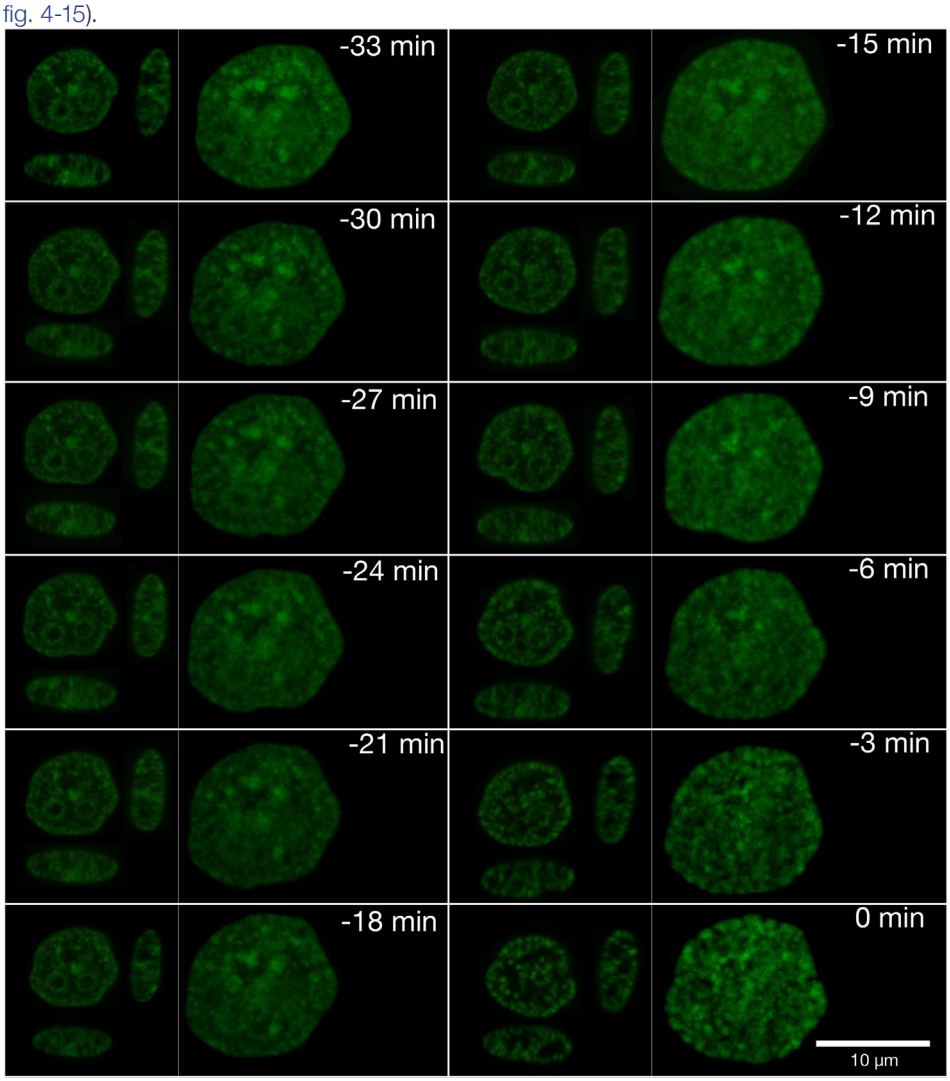

Fig. 4-23: HeLa H2B-GFP nucleus observed during the transition between interphase and mitosis. In this HeLa H2B-GFP nucleus no dramatic changes can be observed prior to mitosis. Nuclear rotation seems not to be mandatory for successful entry into mitosis. Note that the less dense chromatin (presumably euchromatin) is torn towards the constitutive heterochromatin during condensation of the chromosomes (see the the heterochromatin at the nuclear rim and at the nucleoli that still can be recognized at the end of prophase).

4.1.2.6 Chromosomal neighborhoods are not transmitted from one cell cycle to the next in RPE1, HeLa and Rat NRK cells

One of the most important tenets formulated in BOVERI's hypothesis is that changes in chromosomal neighborhoods appear during mitosis. This claim has often been subject to controversial debates from the past until today. To verify this statement in a set of first, simple experiments chromatin in nuclei of different cell lines was labeled with geometric patterns by photoactivation and photobleaching and then recorded before and after mitosis.

The first experiments shown in fig. 4-24 were performed with the RPE1 H4 PA-GFP H2B mRFP cell line (see 4.1.1). Small regions in the center or the periphery of the cell nucleus as well as geometric patters were photoactivated in late G_2-phase or in early prophase into the chromatin. The resulting daughter nuclei clearly showed photoactivated chromatin domains scattered all over the nuclear volume – interspersed by not highlighted chromatin. Further all initial patterns photoactivated into the mother nuclei were unrecognizably scrambled in the respective daughter nuclei – arguing against an active mechanism that conserves chromosomal neighborhoods in this cell line.

In order to test whether the observations made with the RPE1 cell line can be transferred to a bigger set of cell lines, similar experiments like the ones mentioned above were performed with two other cell lines that were claimed to possess an "anaphase mechanism" which "globally"conserves spatial chromosomal arrangements – at least to some extent (GERLICH ET AL., 2003). A HeLa cell line was transiently transfected with H4-PA-GFP and H2B-mRFP and nucli were photoactivated as shown in fig. 4-25. In this example the photoactivated chromatin domains were scattered all over the nuclear volume of the daughter nuclei after mitosis, too, repeating the results generated with the RPE1 line (see above).

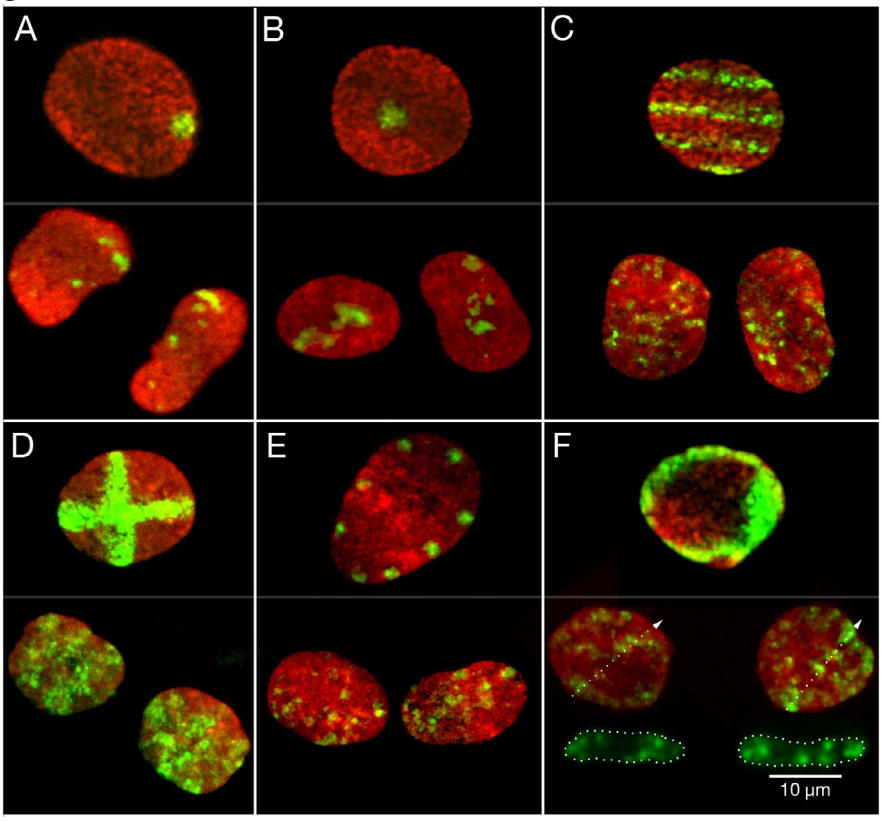

Fig. 4-24: Chromosomal neighborhoods are **not** transmitted through mitosis. Photoactivation of geometric patterns during early prophase (**upper panel** of each case) results in daughter nuclei in which the photoactivated chromatin domains are distributed over big parts of their nuclear volumes (**lower panel** of each case). Interspersed not photoactivated chromatin between the highlighted areas support the assumption that there is no global mechanism to conserve positional relationships between chromosomes through mitosis.

Next, photobleaching experiments like the ones performed with a HeLa H2B-GFP line in (WALTER ET

al., 2003) were carried out in a Rat NRK H2B-CFP line. Gerlich et al. claimed that in this cell line global chromosome positions are transmitted through mitosis. As shown in fig. 4-26 our observations are in clear contradiction to these findings. This confirmins once more the results obtained with the RPE1 and HeLa cell-lines. Moreover summarizing these results arguees in favor for Boveri's hypothesis that shuffling chromosome positions from one generation to the next seems to be – beyond the borders of species – the prevalent if not even the general case.

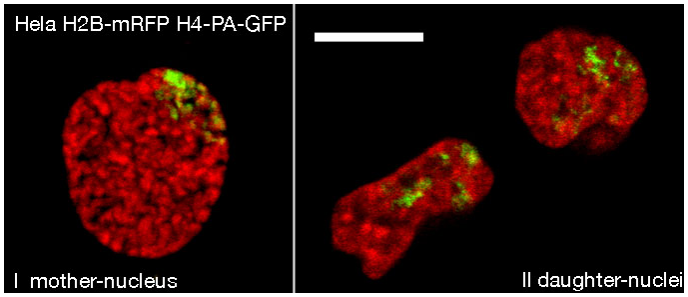

Fig. 4-25: HeLa cells transiently transfected with H2B-mRFP and H4-PA-GFP constructs show a dispersed pattern of photoactivated chromatin domains in daughter cells after photoactivation of a coherent area in the mother nucleus.

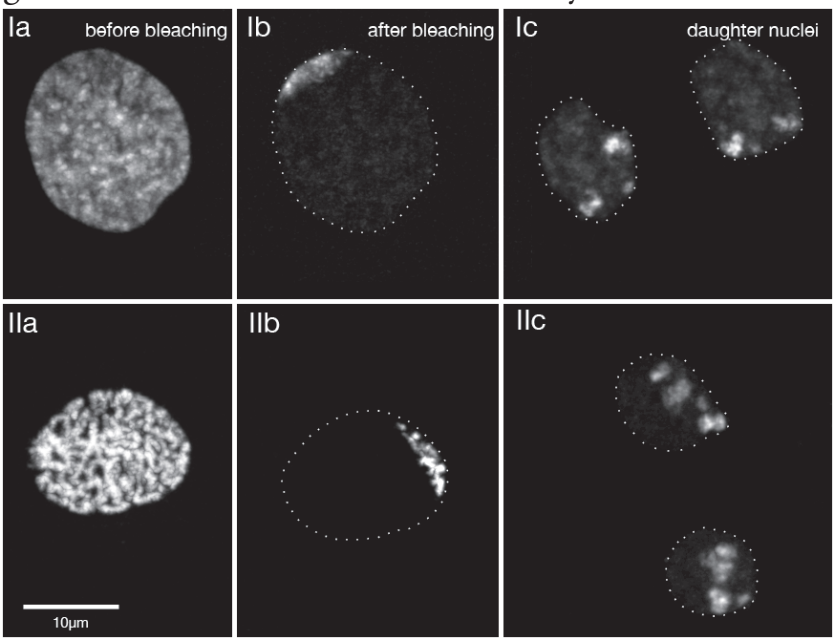

Fig. 4-26: Photobleaching experiments performed with Rat NRK cells (stably expressing H2B-CFP) leaving only a small peripheral portion of the chromatin unbleached show no different behavior with respect to chromatin distribution after mitosis compared to HeLa and RPE1 cells. Fluorescent chromatin is spread over large parts of the daughter nuclei. The left images (a) show the mother nucleus before bleaching. The middle images (b) the mother nucleus after photobleaching and the left pictures (c) show the daughter nuclei.

4.1.2.7 Chromosome proximity pattern change especially in prometaphase when chromosomes attach to the spindle and move towards the metaphase plate

To study the timing of chromosomes starting to change their relative positions during mitosis in detail, 3D time-lapse series with short time intervals were acquired. False coloring of single photoactivated chromatin domains in 3D reconstructions (see fig. 4-27 (a-c) and fig. S2) allowed to trace these through mitosis. It is very impressive to see the structural integrity of a coherent photoactivated spot being already destroyed within the first 10 minutes of the observation during the transition from prophase to early prometaphase (see movie S5).

These dramatic changes occur as soon as the nuclear envelope is broken down and microtubules attach to the kinetochores of the condensed chromosomes by a presumably stochastic process. Very interesting, too – but discussed in a later paragraph – is that changes in the relative position of the highlighted chromatin domains are minor after the onset of anaphase and seem to be mostly affected by the position that the nascent nuclei take during decondensation and nuclear flattening.

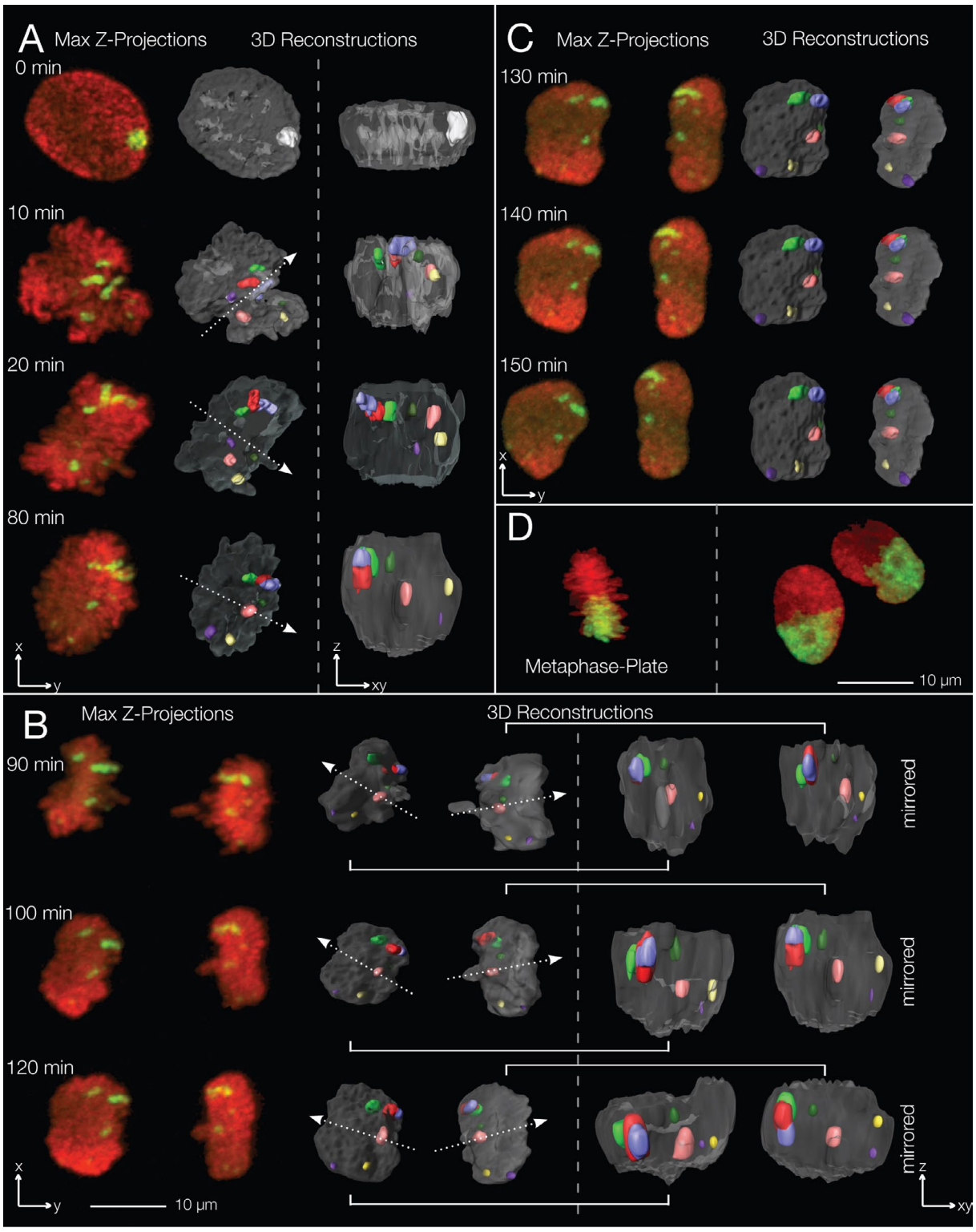

Fig. 4-27: RPE1 H4-PA-GFP H2B-mRFP cell nucleus photoactivated in early prophase and followed in 3D through mitosis. **Left column (A-C)** Maximum projections of the original 3D data. **Middle column (A-C)** 3D reconstructions of the projections shown in the left column. For the sake of better comparison the single photoactivated chromatin domains were color-coded. **Right column (A-C)** side views of the 3D reconstructions. It is clearly visible that the biggest changes with respect to relative positions between the photoactivated chromatin domains occur at early prometaphase after the breakdown of the nuclear envelope. (A) covers the mitosis from prophase until metaphase. (B) covers ana- and telophase. (C) shows the early daughter nuclei in G_1 phase. (D) shows a metaphase plate that was photoactivated in the lower half and the resulting daughter nuclei in which the photoactivated chromatin still resides iin one half of the nucleus - perpendicular to the former orientation of the spindle axis.

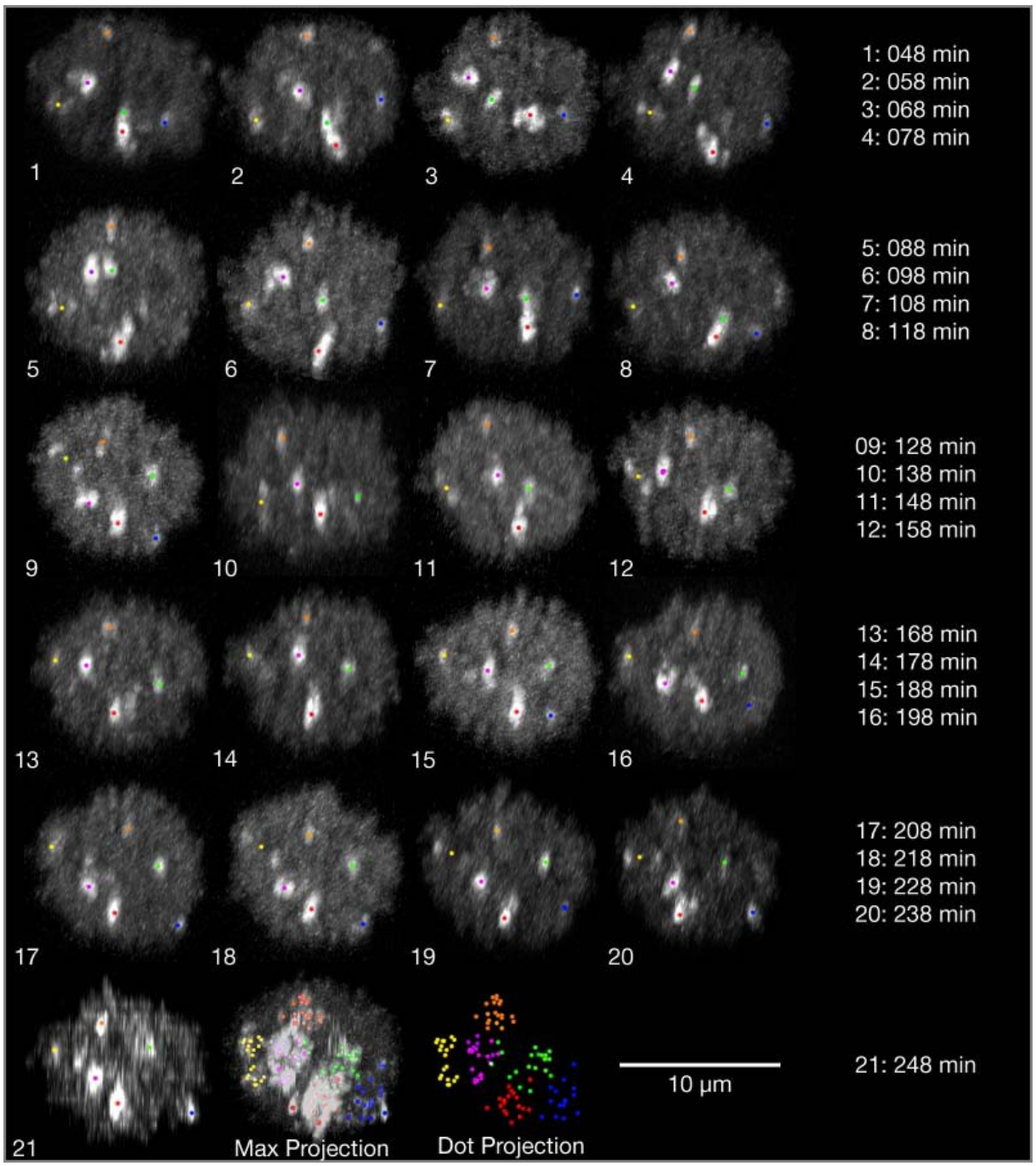

Fig.4-28: Traced photoactivated chromatin domains during an over 3 h lasting metaphase. Mobility of the photoactivated chromatin domains is rather confined compared to the profound changes occuring during prometaphase. In principle changes with respect to chromosome neighborhood relationships are possible but can neither be confirmed nor excluded by the method applied here.

In order to check whether the mobility of chromosomes is more pronounced in mitotic events of extended durations (mitoses with a long lasting metaphase stage that can sometimes be observed in cell culture) compared to mitotic events with a shorter metaphase (as shown in fig. 4-28) a 4D series of a mitosis with photoactivated chromatin domains that stayed in metaphase for more than 3 h was analyzed. This mitoses generated two inconspicious looking daughter cells. Time-points containing the metaphase plate were extracted from the 4D movie, resliced in a way that allows a frontal view onto the metaphase plate and projected (maximal z-projection). Color coding the individual photoactivated chromatin domains, tracking them over time and superposition of all these positional marks into one picture created a diagram

(fig. 4-28 middle of last row) that showed the motility of the labeled chromatin during the extended metaphase. Despite of some minor movements the motility of the labeled chromatin domains was restricted to areas of each having a diameter around 2 – 4 µm. These areas were rather separated from each other only showing overlaps in two cases.
Comparing this prolonged mitosis to the side-views obtained from the 3D models of the faster mitosis shown in fig. 4-27 supports the view that changes in the positioning of the labeled chromatin domains are only minor after prometaphase. These observations argue for only small changes in relative chromosome positions in metaphase – even then when metaphase is extended over a long time. Although differences in the positions of each traced chromatin domain might be sufficient to change the order between chromosomes in the metaphase plate, these changes don't seem to be that dramatic compared to the changes in prometaphase.

4.1.2.8 Unmasking the phenomenon "transmission of global chromosome positions through mitosis"

In contrast to the results presented in the previous sections, some groups claim that chromosome positions can be conserved through mitosis to some extent. These claims are based on observations showing areas of coherently photobleached chromatin covering half the nuclear volume in daughter cells after photobleaching half of a mother nucleus. To test these observation for reproducibility similar experiments were carried out with the photoactivatable RPE1 cell line. In some cases after photoactivating half of the chromatin in the mother nucleus coherent photoactivated areas were indeed found in daughter cells (shown in fig. 4-29(a)). In other cases (shown in fig. 4-29(b)) the photoactivated chromatin was scattered in patches all over the nuclear volume of the daughter cells. These oppositional results could be due to different reasons:
It could be that the cell line used here consists of two or more sub-populations of which at least one subset of cells has retained the ability to pass certain chromosomal positions from one generation to the next by some still unknown mechanism (assuming there is such a mechanism and it is a general feature of mammalian cells).

Another, easier way to explain the phenomenon is

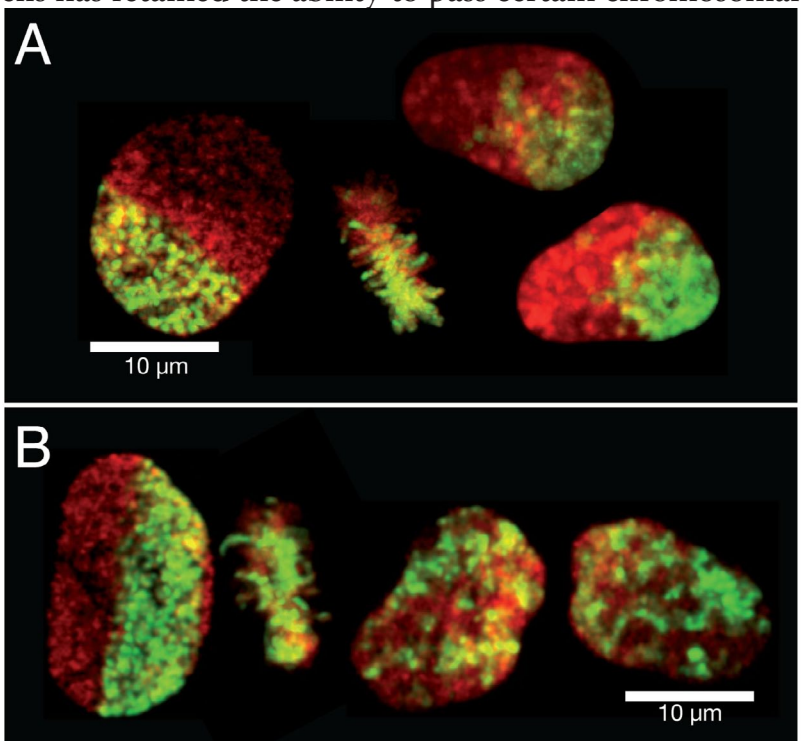

Fig. 4-29: Photoactivation of half the chromatin in cell nuclei parallel (A) and perpendicular (B) to the assumed spindle axis turns into daughter nuclei in which the activated chromatin is distributed coherently in one half (A) or scattered all over the nuclear volume (B). Z-projections of the metaphase plates (shown in the middle) often serve as a good indicator to reconstruct the orientation of the spindle-axis.

that the different outcomes of the photo labeling experiments reflect the mechanics on how chromosomes are passed through mitosis.

In a key experiment it could be shown that photoactivated chromosomes located at one side of a metaphase plate (perpendicular to the spindle axis) resulted in daughter nuclei carrying coherent photoactivated chromatin across one half of thir nuclear volume (fig. 4-27(d)). This observation gave the crucial hint leading to the discovery of two facts. First, the orientation of the mitotic spindle axis is decisive for the distribution of chromosomes in daughter cells and secondly – this will be discussed in detail in following paragraphs – the mobility of individual chromosomes within the nascent nuclei is strongly confined after metaphase.

As demonstrated in fig. 4-29 daughter nuclei exhibiting coherent photoactivated chromatin origin from a mother nucleus in which photoactivation was performed parallel to the assumed later spindle axis. In RPE1 cells that possess a fusiform cell shape, the spindle axis in most of the cases emerges along the short axis of the ellipsoidal nucleus. In contrast daughter nuclei with scattered patches of photoactivated chromatin mostly origin from mother cells that were photoactivated perpendicular to the assumed spindle axis. These findings imply that the chromosomes are – once they are attached to the spindle – just squeezed together along the spindle axis into a plane that will later turn into the metaphase plate.

This point of view is substantiated by looking at the respective metaphase plates in fig. 4-29. While in the first case (A) the photoactivated chromosomes are situated rather on one side, they appear to be mixed all over the plate in the second example (B). Further support for this model can be obtained from the data shown in fig. 4-32, fig. 4-33 and fig. 4-35 (next section).

Assuming the correctness of this model in a way that simple mitotic mechanics – and not a complex mechanism or a heterogeneous population of cells with different behavior – are responsible for the different outcomes in distribution of the photoactivated chromatin domains, both phenomena (scattered and coherent patterns of chromosome domains in daughter nuclei) should occur in one and the same nucleus simultaneously.

To prove this assumtion two experiments were carried out:

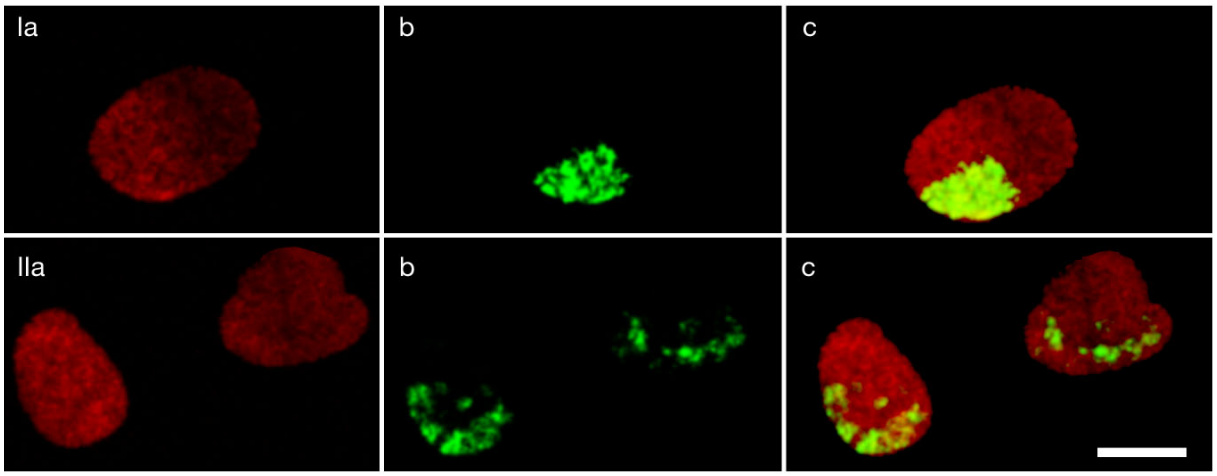

Fig. 4-30: Photoactivation of only one quarter of a cell nucleus along the geometric axes frequently results in daughter nuclei in which the activated chromatin is scattered only all over one half of the nuclear space. This experiment indicates that although photoactivated chromatin domains are found in only one half of the daughter nuclei, neighborhood relationships are not conserved.

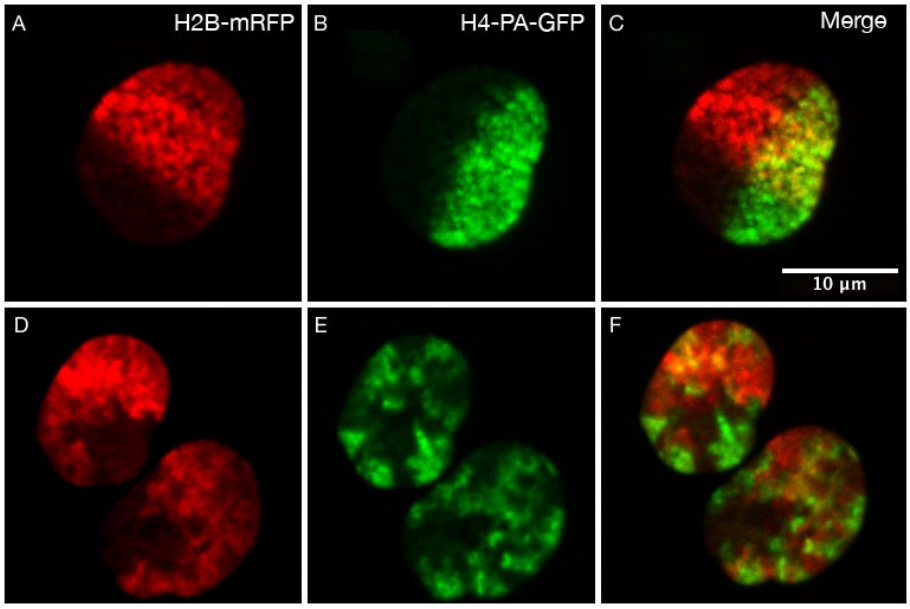

Fig. 4-31: Photoactivation and photobleaching simultaneously along the geometric axes within in the same prophase nucleus. „Coherent" and „Scattered" patterns in daugher nuclei reflect the mechanics of mitosis and can occur within one and the same nucleus. The photoactivated half (along the long axis) of the mother nucleus results in chromatin domains scattered all over the nuclear volume of the daughter nuclei. The parts that were bleached (along the short axis of the mother nucleus) remain coherent in daughters nuclei.

In the first experiment only a quarter of the nuclear volume (along half of both of the geometric nuclear axes) was photoactivated prior to mitosis and the resulting daughter nuclei were revisited several hours later (fig. 4-30). Interestingly the photoactivated chromatin in the daughter nuclei was scattered only over one half of the nuclear volume. This experiment shows that although photoactivation of chromatin along the short axis might results in coherently photoactivated areas in daughter cells, the relative positions between these chromosomes are not conserved at all!

The second experiment which confirmed this finding in an even more elegant way used a combination of simultaneous chromatin photobleaching and photoactivation. In one half of an early prophase nucleus, chromatin was photoactivated along its long axis (fig. 4-31), while in another half of the same nucleus along its short axis (and assumed later spindle axis) the H2B-mRFP was photobleached. The resulting daughter nuclei showed the expected pattern simultaneously in one and the same cell nucleus. Photoactivated chromatin was scattered throughout the nucleus whereas the photobleached parts formed a coherent area. This can be seen as a proof, that both kinds of oppositional patterns result from the mechanics taking place during mitosis and occur simultaneously in one and the same cell. The orientation of labeled chromatin relative to the mitotic spindle seems to be crucial for the observed patterns in the daughter cells. Until now it was only assumed that the mitotic spindle runs along the short axis of ellipsoidal shaped nucleus. Since the conclusions made in this paragraph strongly rely on the assumed orientation of the spindle axis and the theory of chromatin distribution through mitosis established here needed to be generalized and tested, it was necessary to visualize this axis, too.

Transient transfection with a plasmid expression construct encoding for FOP-GFP (a protein which colocalizes with the centrosomes) allowed to visualize the poles of the spindle axis. Although the FOP proteins label the centrosomes with the same GFP fluorescence, which is also used for visualizing of the photoactivated chromatin, their extrachromosomal localization and their relatively bright signals allowed a proper identification of the spindle poles.

Repeating the chromatin photoactivation experiments parallel and perpendicular

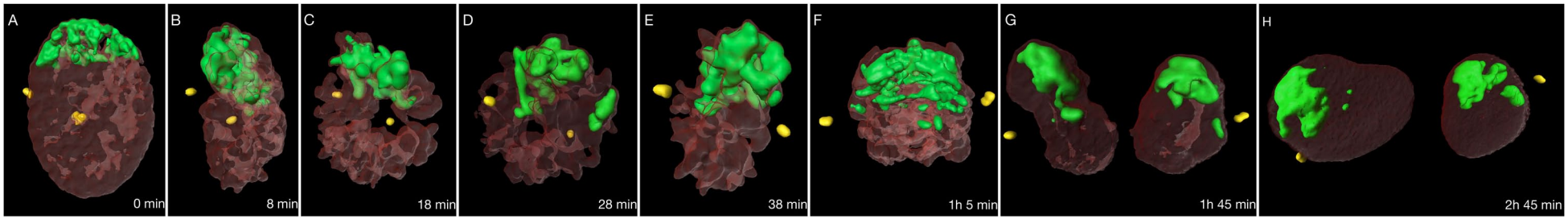

Fig. 4-32: 4D reconstruction of a cell nucleus photoactivated parallel to the spindle axis in prophase (shown by the centrosomes that are visualized by FOP-GFP displayed in yellow). Since the photoactivated chromatin is positioned parallel to the spindle axis it collides into a half labeled metaphase plate. The areas of coherently photolabeled chromatin in the daughter cells were misinterpreted as some sort of “global transmission” of chromatin domains from mother to the daughter cells by earlier studies.

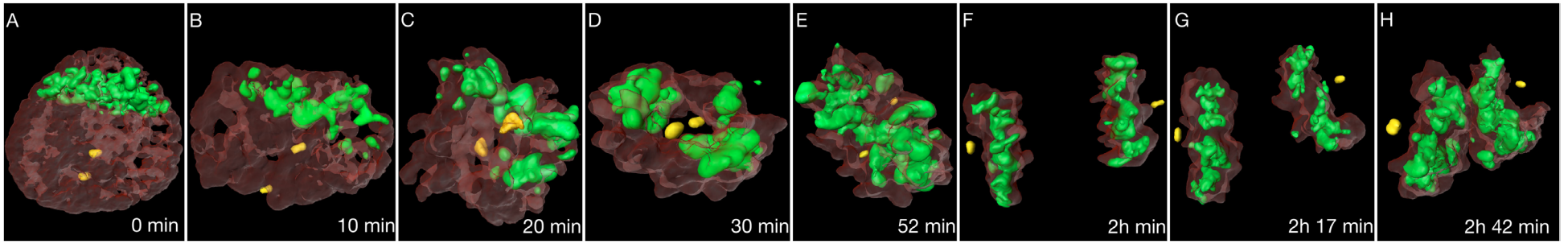

Fig. 4-33: 4D reconstruction of a cell nucleus photoactivated perpendicular to the spindle axis in prophase (shown by the centrosomes visualized by FOP-GFP and displayed here in yellow). Although following the same geometric transformations in prometapase as in the previous figure the photoactivated chromatin is getting mixed during metaphase plate formation with non-photoactivated chromatin from the side of the other spindle pole. Apart from that this example shows that the orientation of the spindle axis doesn’t always emerge along the small axis of the ellipsoid-shaped nucleus.

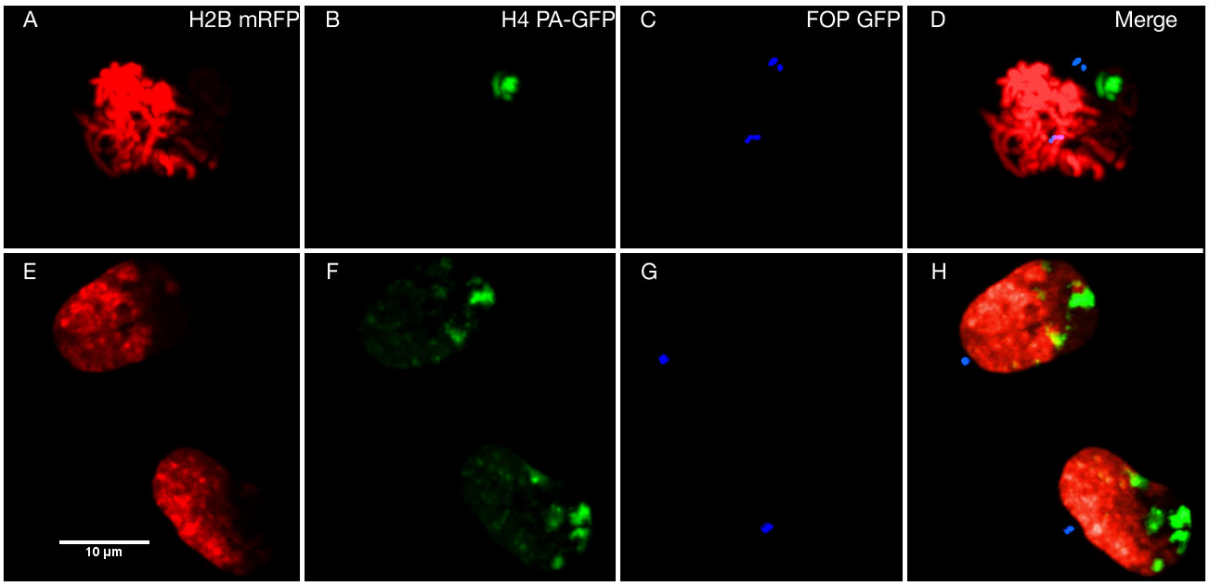

Fig. 4-34: Combined photobleaching of chromosomes in a prometaphase cell parallel to the spindle axis (visualized by FOP-GFP) and photoactivation of a smaller area within the bleached region. In the daughter nuclei of this mitosis show a coherently bleached area that is interspersed by chunks of photoactivated chromatin.

to the now visualized spindle axis (fig. 4-32, fig. 4-33 and fig. S3) and observing the progressing through mitosis in 3D at high resolution, revealed deep insights into the different steps of the mitotic mechanics.

After photoactivation of an early prophase nucleus (fig. 4-32(a)) at the nuclear border and parallel to the axis defined by the line that runs through both centrosomes, the condensed chromosomes seem to bend around the spindle axis at the transition between pro- and prometaphase (b). This process goes on in prometaphase (c) when the mitotic chromosomes attach to the microtubules until the mitotic axis is surrounded by a tube of chromosomes that is later squeezed into a rosette (d). Squeezing the chromosomes even closer together into a position that allows good access to all kinetochores from both sides of the spindle apparatus and filling up the hole in the middle, a metaphase (e) is formed that stands perpendicular to the substratum and shows the photoactivated chromatin – as previously predicted and also seen in fig. 4-27(d), fig. 4-29(a) (middle) and fig. 4-35 (right) – exclusively at one side of the spindle axis. Due to the relatively small amount of photoactivated chromatin (which was in this experiment less than a half the nuclear volume of the mother nucleus) the photoactivated chromatin doesn't cover one enire lateral half of the metaphase plate. In later stages of mitosis (f–h) the chromatids are separated but only minor changes in the relative positions of the highlighted chromatin domains occur. Although the labelled chromatin is not completely coherent in the daughter nuclei, one can easily see that the photoactivated chromatin domains are located in only one half of their nuclear volume.

Photoactivation perpendicular to the mitotic axis visualized by FOP-GFP in an early prophase nucleus (fig. 4-33) shows the same sequence of mitotic chromatin transformations as described above but with the exception that the photoactivated chromatin domains (now coming from only one spindle pole) are intermixed by collision with the unlabeled chromatin domains (coming from the other spindle pole) during formation of the metaphase plate (c–e) (see also fig. 4-29(b) and fig. 4-35 (left)).

Performing a double label experiment in a prometaphase nucleus with a visible

spindle axis (FOP-GFP) (fig. 4-34) confirms the observations obtained by previous experiments (without visible spindle axis) in the following points:

a) Photobleaching of chromatin parallel to the spindle axis results in daughter cells with coherent photobleached parts
b) Photoactivation of chromatin within a small part of the photobleached area described in *a)* leads to chunks of photoactivated chromatin being scattered all over the photobleached area of the daughter cells.

The biggest changes in chromosome neighborhoods during mitosis occur during prometaphase.

4.1.2.9 Neighborhood arrangements established in the metaphase plate are conserved throughout anaphase and telophase resulting in rather symmetrical daughter nuclei

Observing now the "second half" of mitosis – from metaphase until interphase of the daughter-nuclei – turned out to be fully consistent with THEODOR BOVERI's hypotheses, too. Cells that were photoactivated in prophase and traced at high resolution in 3D from late metaphase to the next interphase were resliced to allow a frontal view onto the metaphase plate and onto the falling ana- and telophase rosettes fig. 4-35. Although minor changes occurred, prominent chromatin domains could easily be recognized and traced through subsequent mitotic stages by their relative position to each other. Changes observed between chromatid separation and telophase nuclei were most likely caused by the ongoing decondensation of the chromosomes (and the difficulty to find a suitable plane for generating the projections) which clearly speaks against an active reorganization of chromatin domains after chromatid separation by a so-called "anaphase-mechanism". Looking back at fig. 4-27 also shows that the color coded chromatin domains do not undergo big spatial dynamics after metaphase. Although both daughter nuclei in this figure don't show perfect geometrical symmetry, the order of the highlighted chromatin domains remains symmetrical.

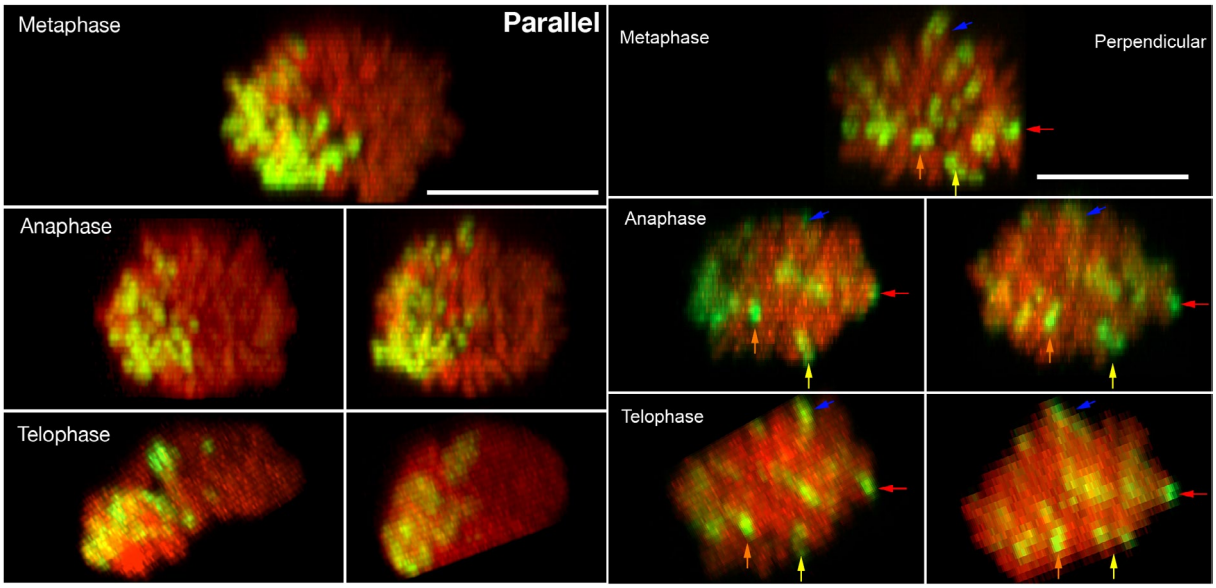

Fig. 4-35: Patterns established in late metaphase are only sightly changed in ana- and telophase. Resliced projections of metaphase plates, anaphase- and telophase rosettes (same mitoses like shown in fig. 4-32&33). In the left panel the early prophase was photoactivated perpendicularly to the mitotic axis whereas in the right panel the early prophase nucleus was photoactivated parallel to the mitotic axis (the telophase images are tilted for better visibility of the symmetry).

The mitosis in fig. 4-27 shows another interesting phenomenon. While the similarity and the sequence of the color coded chromatin domains argue for a symmetric orientation of the chromosomes in the daughter cells – the shapes of the daughter nuclei differ significantly from each other. This can be explained by following this mitosis in 3D after metaphase. While the left nascent daughter nucleus just falls to the side like a frisbee, the right nascent nucleus remains in a rather perpendicular position similar to its position at the onset of anaphase. Although this nucleus is flattening, too – this process takes longer and seems to have a remarkable impact on nuclear architecture and nuclear shape. While flattening this way it seems that CTs can be shuffled similar to the way a doe is dispersed. Data obtained from 3D-FISH experiments in which the genealogy of cell-clones was monitored and the arrangements of different chromosomes were compared (Köhler et al., 2011) (in preparation) also showed that the spatial arrangement of chromosomes in daughter nuclei can vary to some extent with respect to symmetry.

To directly test for a puative "anaphase mechanism" that should be responsible for restoring the initial chromosomal neighborhoods of a mother nucleus in the both daughter nuclei (Gerlich et al., 2003) the both anaphase rosettes of a mitotic cell were photoactivated – one at the "smooth" side (proximal to the respective centrosome) and the other (distal to the respective chromosome) at the "rough" side represented by the protruding chromosome ends. Revisiting the daughter nuclei of this cell division in G_1-phase shows photoactivated chromatin located at the top of the left and at the bottom of the right nucleus fig. 4-36. The easiest and most promising way to interpret this result is that the anaphase rosettes of the nascent daughter cells have just fallen down to opposite sides and decondensed – although it cannot be ruled out that photoactivation has biased the experimental system. Interestingly the photoactivated chromatin domains in the daughter cells are interspersed by unlabeled chromatin suggesting that flattening of the nucleus during decondensation of the chromosomes has a distinct influence on chromosomal neighborhoods in daughter nuclei.

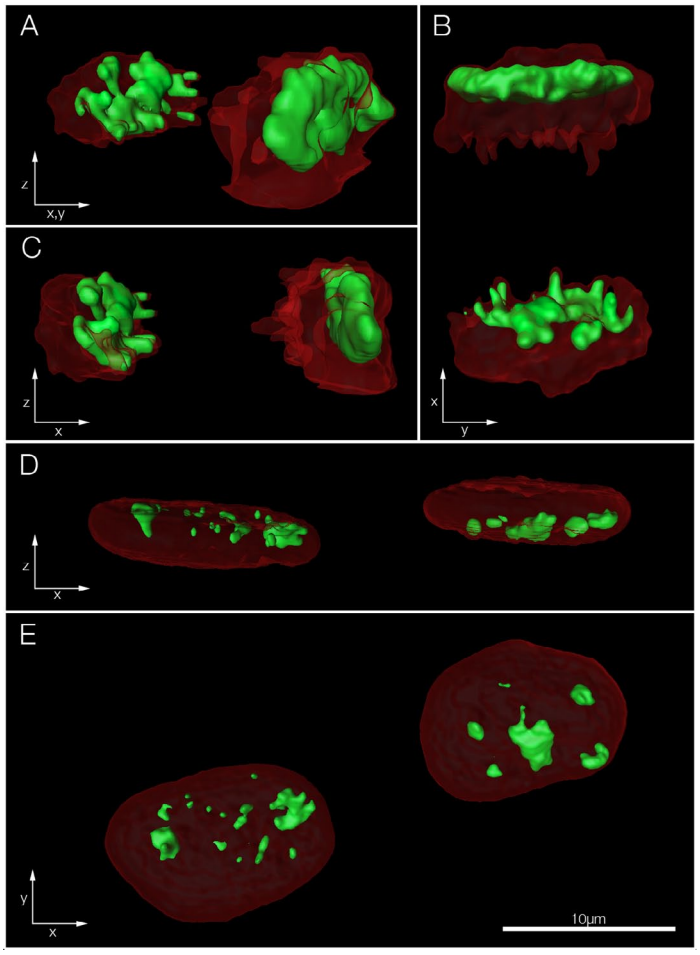

Fig. 4-36: During anaphase both anaphase rosettes were photoactivated either distal or proximal to the corresponding centrosome (not shown). After completing mitosis the daughter cells show the activated chromatin in one case (distal) at the top and in the other case (proximal) at the bottom of the nucleus interspersed by not photoactivated chromatin.

4.1.2.10 Photoactivation around the nuclear rim generates daughter nuclei with a croissant-like distribution of photoactivated chromatin

To test whether predictions about the distribution of chromatin through mitosis are possible (at least to some extent), a virtually circular mother nucleus being in late prophase was photoactivated around its nuclear rim (fig. 4-37). Taking a look at the resulting daughter nuclei shows that the highlighted chromatin mostly resides in an area distal to the nuclear center (compare folder „3D Ring“ on the enclosed DVD). The distribution of the photoactivated chromatin around the nuclear rim of the daughter cells however is less uniform compared to the mother nucleus.

Given a circular nucleus and that the mitotic spindle forms directly in the middle below this nucleus (which can be assumed in the example shown in fig. 4-37; note the small invagination at the bottom of the mother nucleus) then the chromosomes will be wrapped around the nuclear spindle as soon as the nuclear envelope disintegrates. Considering the circular photoactivation at the rim, the situation can be assumed to be like presented in fig. 4-38. When the so formed tube is then compressed into the prometaphase rosette (and subsequently into the metaphase plate), an entity of photoactivated chromatin emerges which is shaped like a croissant. As we have learned in the previous sections spatial patterns established during metaphase are mostly maintained if anaphase rosettes can fall entirely to the substratum before decondensation. Hence daughter nuclei can be expected that show a croissant-like distribution of the photoactivated chromatin domains. This is exactly what could be observed experimentally.

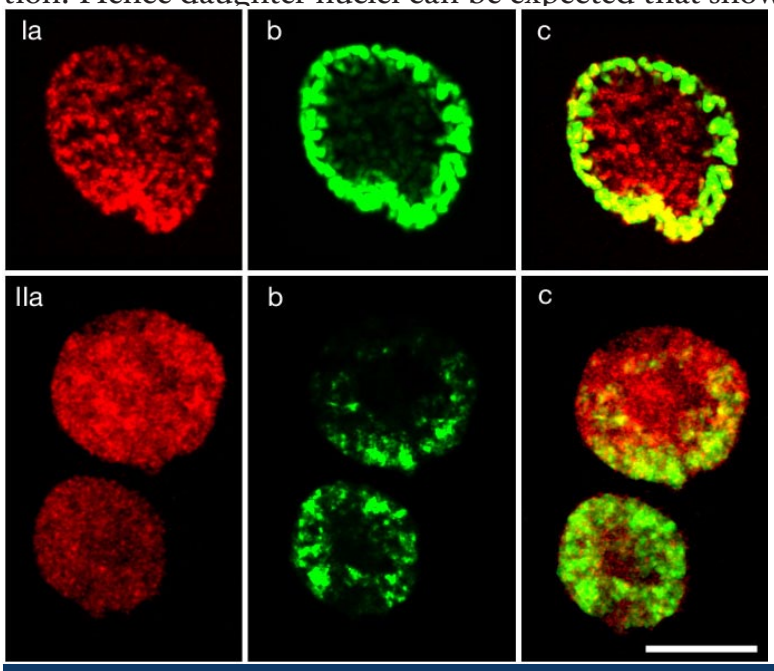

Fig. 4-37: Photoactivating the nuclear rim (in x,y) of a circular shaped prophase mother nucleus results in daughter nuclei that show a croissant shaped distribution of photoactivated chromatin in the daughter nuclei. This is caused by the mechanics of mitosis (see text and fig. 4-38).

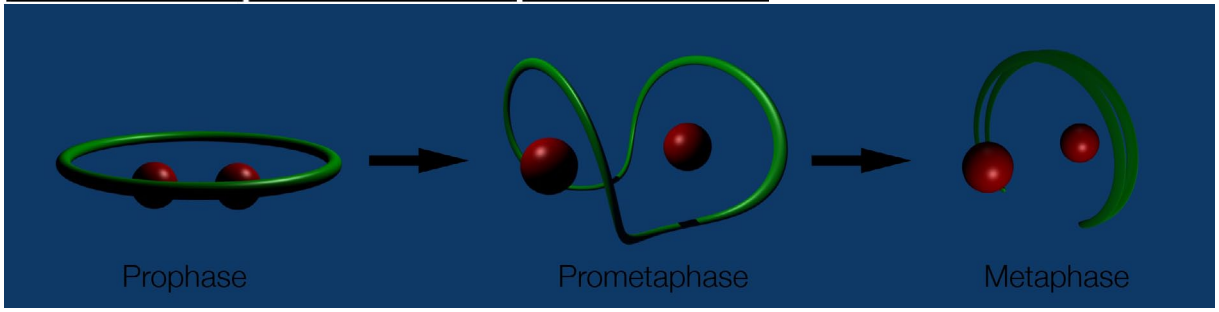

Fig. 4-38: Modelling of the processes that happen after photoactivation of the nuclear rim until metaphase if the spindle axis forms under the nucleus. After chromatid separation a croissant-like distribution of photoactivated chromatin can be observed in daughter cells (given that anaphase rosettes can fall entirely to the substratum) (see fig. 4-37).

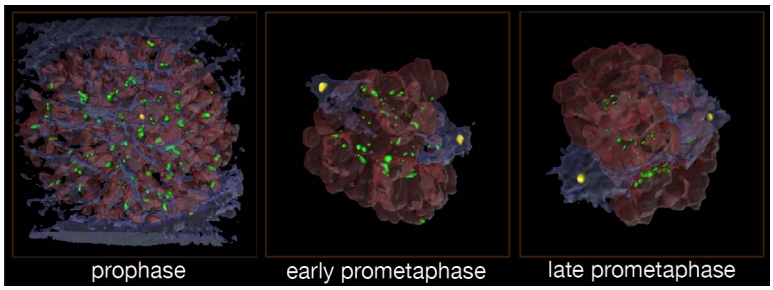

Fig.4-39: The mitotic stages from prometaphase to metaphase the way it was most often observed in RPE1 cells. After breakdown of the nuclear envelope the chromosomes attach stochastically to the spindle apparatus forming a „tunnel" in which the centrosomes are located at the inside. This tunnel gets squeezed to a prometaphase rosette which is then filled up to a metaphase plate (STRICKFADEN ET AL., 2010).

4.1.2.11 The different faces of mitosis are caused by different orientations of the mitotic spindle with respect to the nucleus at the onset of prometaphase

In fig. 4-27, fig. 4-32 and fig. 4-33 photoactivated chromatin was traced stepwise through the different stages of mitosis. In all of the cases presented yet, the mitotic spindle has formed below the prophase nucleus after disintegration of the nuclear envelope and wrapped the mitotic chromosomes in a stochastic manner (first come first served) around the spindle-axis. These events resulted in the formation of a prometaphase that adopted the form of a tunnel that transformed into a tube which then was compressed to a rosette ending in the formation of a metaphase plate (fig. 4-39 and fig. S4). Although this sequence of events was by far the most frequent case that was observed during the experiments that were performed in the course of this thesis, it should be noted that depending on the position of the mitotic spindle during early prometaphase the visual appearance of prometaphase can profoundly differ from what is discribed above.

Fig. 4-40 shows such a case. In this example the spindle forms lateral to the nucleus. After breakdown of the nuclear envelope the condensed chromosomes wrap around the spindle axis in a croissant-like manner forming the prometaphase rosette and the metaphase plate. Although in this case the proximity patterns can change dramatically during prometaphase, too the whole prometaphase looks completely different from what was shown in the previous figures. This demonstrates the importance of the spindle axis position in relation to the nucleus and makrs it as an additional randomizer for chromosome neighborhoods the latter global distribution of individual chromosomes in the metaphase plate (and thus in the daughter nuclei).

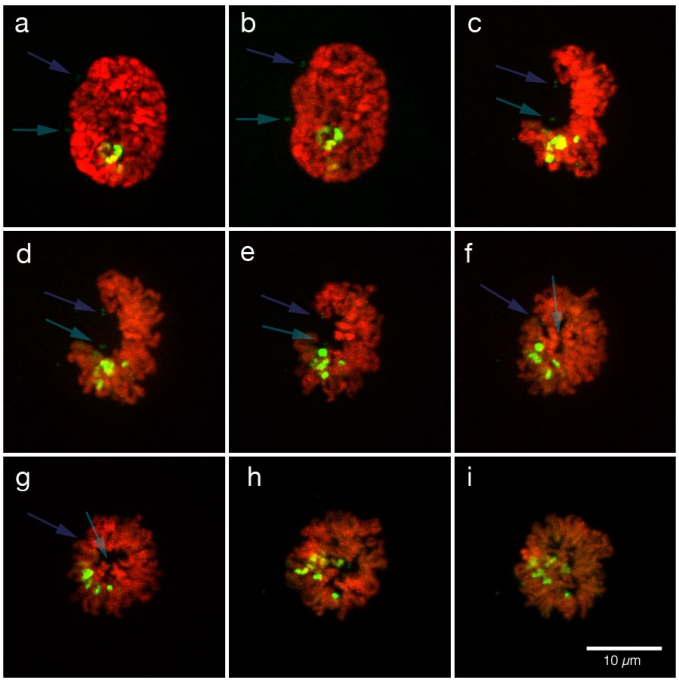

Fig. 4-40: Prophase – early metaphase of a cell nucleus that shows the rare case that the spindle axis (visualized by FOP-GFP) forms lateral to the cell nucleus. This leads to a prometaphase in which the chromosomes wrap around the spindle axis in a way that looks like a croissant. This „croissant" then puts its ends together and forms the prometaphase rosette that then is filled up to form the metaphase plate.

In another case (fig. 4-41, fig. S4C and movie S6) the spindle forms horizontally over and under the geometrical center of the prophase-nucleus. Connecting the mi-

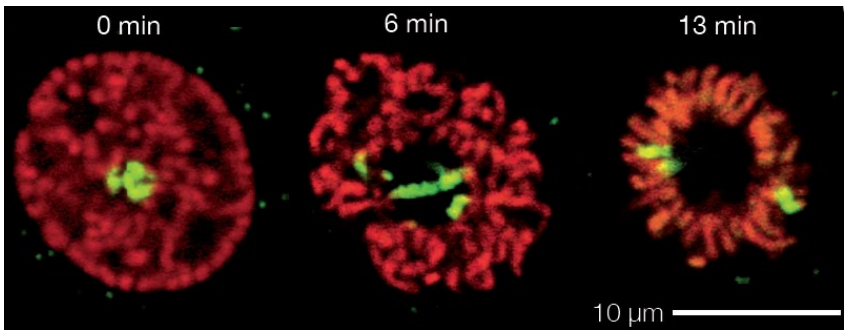

Fig. 4-41: Generation of a prometaphase rosette by a spindle axis that forms through the middle of the nucleus. While distal chromosomes (with respect to the spindle axis as "center") retain their orientation, their neighborhoods can be interspersed by proximal chromosomes. In extreme cases chromosomes in the center can be drawn apart to opposite sides of the rosette.

crotubules to the kinetochores in this orientation leads to the formation of a central hole and thus to the generation of a horizontal rosette. It is impressing to see how the neighborhood relations between the photoactivated chromatin domains can be drastically changed (chromosomes in the middle that get torn to opposite parts of the rosette) or partially conserved (chromosome neighbors at the rim remain in proximity to each other) at the same time.

Fig. 4-42 categorized the prometaphase figures that were observed during the work for this study, in three categories. While type A was by far prevalent, type B and C were much less frequent in RPE1 cells.

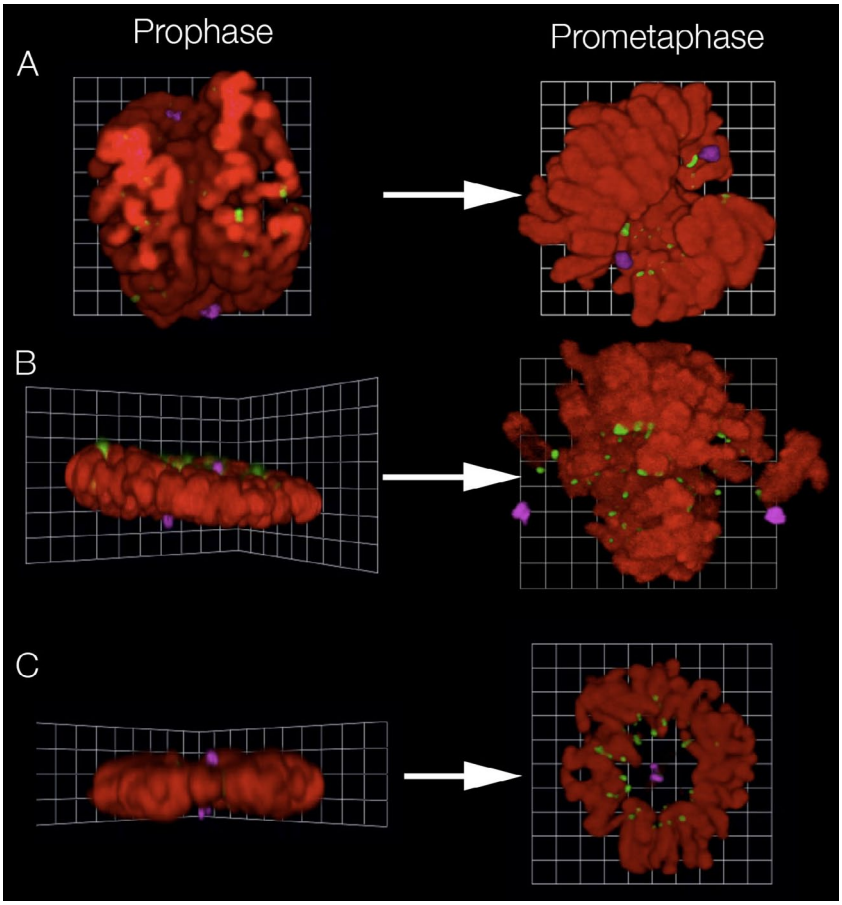

Fig. 4-42: Variations of a common theme. The three most common motifs in mitotic RPE1 cells that occur during the transition from prophase to metaphase. A: In prophase the spindle forms a tunnel under the nucleus in which the centromeres (green) are aligned before the tunnel turns into a tube which then is compressed into a prometaphase rosette. The hole of the prometaphase rosette is then filled up with chromosomes and turns into a metaphase plate. B: The spindle poles are positioned at different sides of the flat cell nucleus. After attaching to the microtubules the chromosomes are drawn to the metaphase plate without the formation of a rosette like intermediate state. C: The spindle poles are on top of each other at opposite sides of the flat nucleus. They form a common tunnel. In this rosette-like configuration the chromosomes are oriented around this axis with the centromeres facing to the inside perpendicular to the spindle axis.

4.1.2.12 Mitosis seems to be a robust, flexible and autonomous process that takes over control once it is initiated

During experiments in which the centrosome metabolism was influenced by knokking down one of its components, multipolar mitotic cell divisions occurred in high

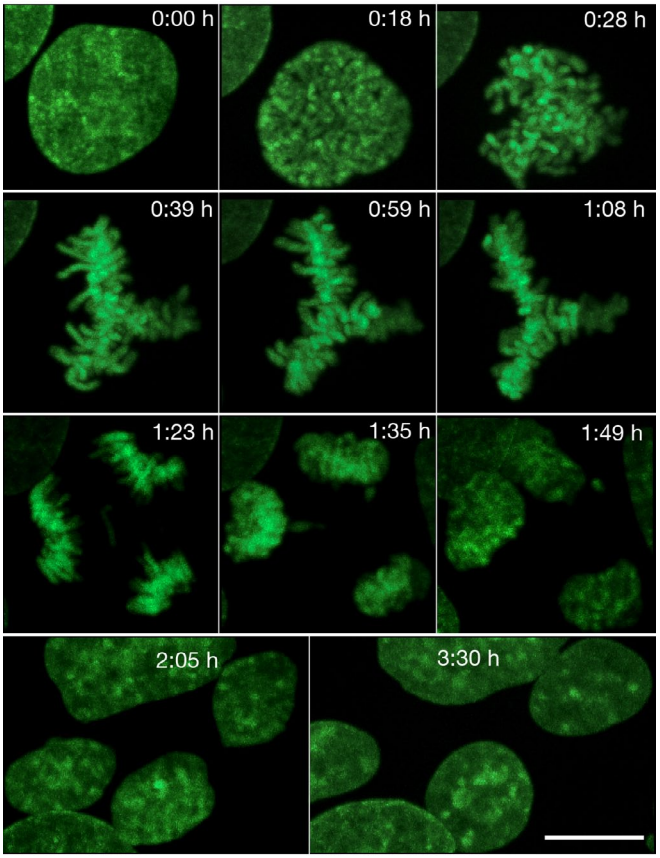

Fig. 4-43: Abnormal mitotic division of a HeLa H2B-GFP nucleus into 3 daughter cells. Despite of the abnormality of this mitosis the sequence of morphological events seems to be exactly the same as in normal mitoses. Abnormal cell divisions like this can be caused by the presence of multiple centrosomes.

numbers (Heisel et al., submitted). Abnormal mitotic events emerged due to a deregulation in the number of centrosomes which in wild-type mammalian cells is always two. Since cells with multipolar spindles partition sister chromatids into more than two daughter cells (fig. 4-43 and fig. S5) the products of such cell divisions are absolute lethal in other than tumor cells and nonsense seen from a biological perspective. However despite their biological irrelevance these abnormal mitotic events allow deep insights into the nature of mitosis and underscore the importance of the centrosomes as cellular organelles. The exact recapitulation of all mitotic stages and figures in these abnormal cells (that are despite their geometric peculiarities equivalent to those of ordinary cell divisions) tempt to assume, that mitosis is a highly conserved sequence of simple, mostly mechanic steps that, once mitosis is initiated, are executed autonomously until in G_1 gene expression takes over control again. The steps that are executed during this probably universal program could be formulated like this:

- Separation of the centrosomes and condensation of the chromatin: After the point of no return for mitosis has overcome, the condensation of the chromatin is initiated simultaneously as centrosomes move apart.
- Attachment of the chromosomes to the spindle: Regardless of the orientation of the spindle the chromosomes get tethered to the next best microtubules of the spindle apparatus.
- Formation of a metaphase plane: Attached to the spindle the chromosomes are pushed away from the spindle poles into the metaphase plane.
- Separation of the chromatids and drawing the chromatids to the poles. The chromatids are drawn in direction of the centrosomes and form the daughter nuclei.

Multipolar cell divisions with surviving daughter nuclei (see fig. 4-43) were also observed spontaneously – without extra treatment that influences the centrosome metabolism. This circumstance demonstrates how careful one must be when using fixed tumor cells for studies on nuclear architecture!

4.2 Experiments at the ion microbeam facility SNAKE

In the course of this thesis ion microirradiation of cells with subsequent live-cell observation was performed at the SNAKE (*Supraleitendes Nanoskop für Angewandte Kernphysikalische Experimente*). Initially SNAKE served as an irradiation device for cells that were subsequently fixed and immunostained for microscopic evaluation. In a collaboration project together with physicists around Prof. Dr. GÜNTHER DOLLINGER's and radiation biologists of PD. Dr. ANNA FRIEDL's group the SNAKE-set-up was adapted to the needs of live-cell microscopy and now allows time-lapse fluorescence microscopy immediately after ion microbeam irradiation.

While the DOLLINGER group contributed by installing a Zeiss Axiovert 200M fluorescence microscope at the existing experimental set-up, the biologists contributed by generating stable cell-lines expressing GFP-tagged repair proteins and with their expertise in live-cell fluorescence microscopy. The information presented in this section is result of collaborative research to which the author of this thesis contributed as part of a team.

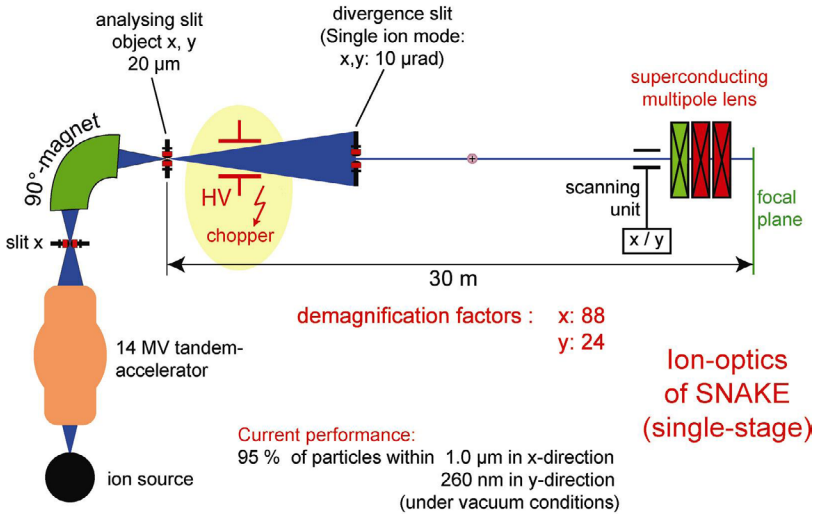

Fig. 4-44: Schematic diagram on how the ion micro beam is attached to an accelerator. Taken from (HAUPTNER ET AL, 2004).

4.2.1 The experimental set-up of SNAKE

4.2.1.1 A tandem accelerator serves as ion source for SNAKE

The microirradiation facility SNAKE is attached to a 14 MV linear VAN DE GRAFF particle accelerator (fig. 4-44) which produces highly energetic particles ranging from 4 MeV (protons) up to 200 MeV (gold ions) (HABLE ET AL., 2009A) (fig.4-45). Negatively charged ions that are sputtered out of an ion source by an electron beam are accelerated in a strong electric field (using up to 14 MV) inside the accelerator. In the middle of the accelerator the ions impact into a stripper foil that removes electrons from the outer electron shells and changes thei charge from negative to positive. Being located positively charged at a site with a very high positive, electric potential leads to a repulsion of the ions and accelerates the particles a second time. Using a strong electric magnet and aperture slits allows to turn the beam 90° and to chose for ions with the desired charge and speed properties.

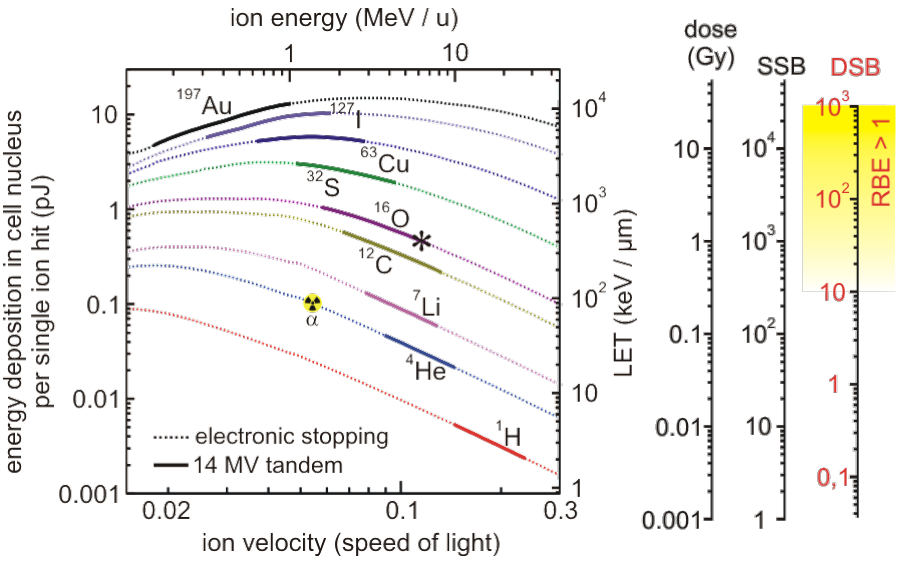

Fig. 4-45: Ions and energies available at the 14 MV tandem accelerator in the MLL-Lab. One of the advantages of this device is that different ion-species and energies can be used for irradiation experiments.(Hauptner et Al, 2004)

4.2.1.2 The ion microbeam SNAKE

The SNAKE set-up consists of superconducting electric lenses that can focus the beam down to a diameter of 500 nm (fig. 4-46) (Hable et al., 2009a) and a scanning unit that allows to move the ion beam within a microscopic range (fig. 4-47). A "chopper", located upstream of the SNAKE, can interrupt the beam and is used to deliver single ions to SNAKE via a feedback mechanism. This feedback is triggered by a photomultiplyer tube that detects scintillation light which is emitted by ions that have passes the sample. Behind the focal plane of the beam, a state of the art epifluorescence microscope is positioned tilted 90° to the side, sharing the same focal plane as the ion beam.

Irradiation and observation of cells perpendicular to the ground causes a lot of problems for time-lapse live-cell microscopy. First, the cells have to be grown in special containers that can be heated up to 37°C and closed tightly to prevent leakage and evaporation of the medium during long-term observations. Secondly, for single ion irradiation it is necessary to use a scintillator that allows the usage of the light triggered feedback mechanism which controls the chopper. Third, this material needs to have good optical qualities in order to to allow immersion fluorescence microscopy and must not be toxic.

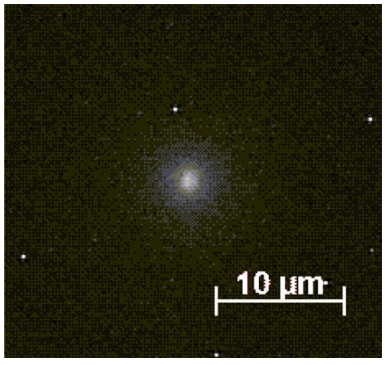

Fig. 4-46: Beam spot on the plastic scintillator which is used in the live-cell chambers at a particle rate of about 1 kHz visualized by a video camera This can be used for chekking the beam's position and focus before irradiation. The singular white spots are hot pixels on the CCD chip. Taken from (Hable et al., 2009).

Fig. 4-48 shows the live-cell chamber as it was constructed by the Dollinger group. As a scintillator, a scintillating plastic material that was cut into small discs with the same height as it is used for optical glasses in immersion microscopy (0,170 mm) was chosen.

The process of irradiation is illustrated in fig. 4-49&50. During irradiation the ions exit the vacuum of the accelerator through an ultra-thin Kapton® foil that is in contact which another ultra thin Mylar® foil belonging to the irradiation chamber. The particle beam then passes 60–20 µm through cell culture medium before it hits the cells. Due to the short range of corpuscular irradiation outside the vacuum (like α-irradiation) and for the sake of a good scanning resolution, the distance between the

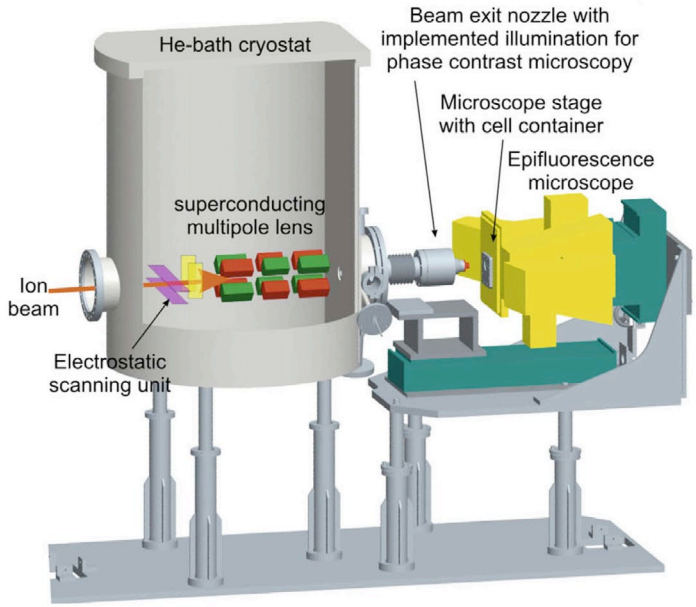

Fig. 4-47: The micoirradiation facillity SNAKE. (**Top**) CAD drawing of the SNAKE irradiation site with fluorescence microscope capable of live-cell imaging. (HABLE ET AL., 2009). (**Bottom**) Photograph of the experimental stet-up at the beam exit between microbeam and microscope.

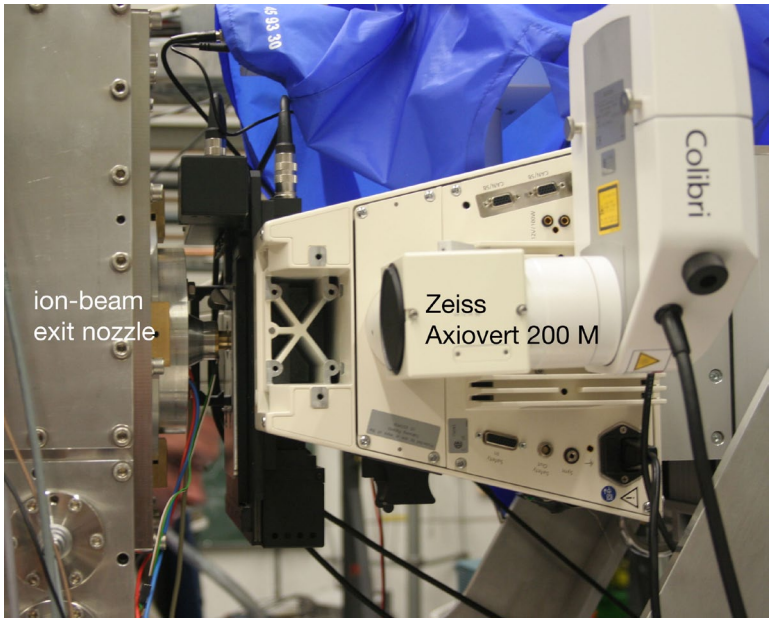

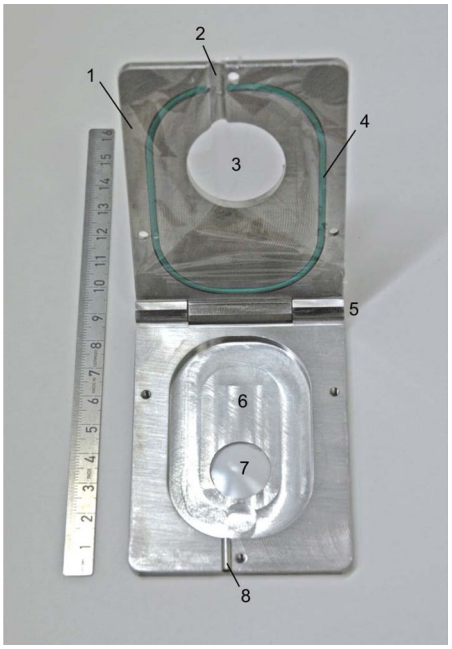

Fig. 4-48: Photograph of the live cell imaging cell containers used at SKAKE: (1) lid covered by Mylar foil, (2) pressure compensating groove, (3) entrance window, (4) o-ring, (5) hinge, (6) cavity to be filled with culture medium, (7) 170 µm thick BC418 plastic scintillator, (8) pressure compensation pipe. Taken from (HABLE ET AL., 2009).

ion beam exit nozzle and the cells is kept as low as possible. After the ions have passed the cell layer they impact into the plastic scintillator, generating a small flash of light (λ = 391 nm) which is detected by a photomultiplier. The photomultiplier forwards the signal to a controller that triggers the chopper to interrupt the ion beam. Repositioning of the beam is performed using a defined voltage in the electrostatic scanning unit. After pointing to the next postition to be irradiated on the sample, the machine is ready to deliver another ion.

After irradiation has finished the beam path is changed from irradiation to observation mode. Thus the fluorescent proteins within the cells on the sample can be excited through the used objective while a sensitive 12-bit CCD camera collects its emitted light. The illumination settings at the microscopic stand can be changed according to the fluorophores that are used in the observed cells lines. For better image quality and less reflections the irradiation nozzle will be gently moved away from the cells. A diode light source produced by Zeiss (*Colibri*) which avoids exposure of the cells to ultraviolet light was used for excitation of the fluorophores.

The ion microbeam is a very useful device that differs considerably from other irradiation facilities e.g. γ- or α- sources (GERARDI, 2006). Its main advantages over other

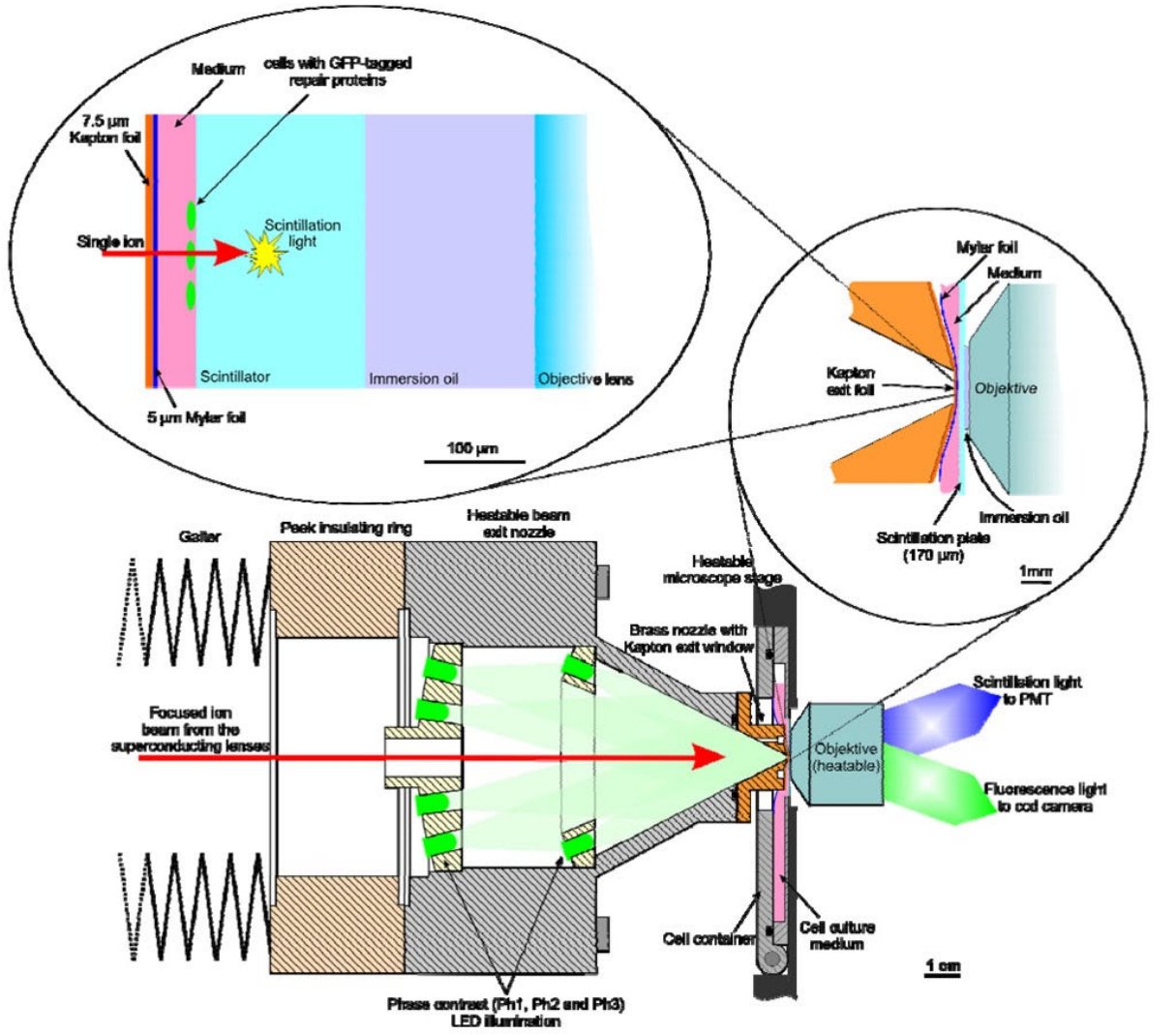

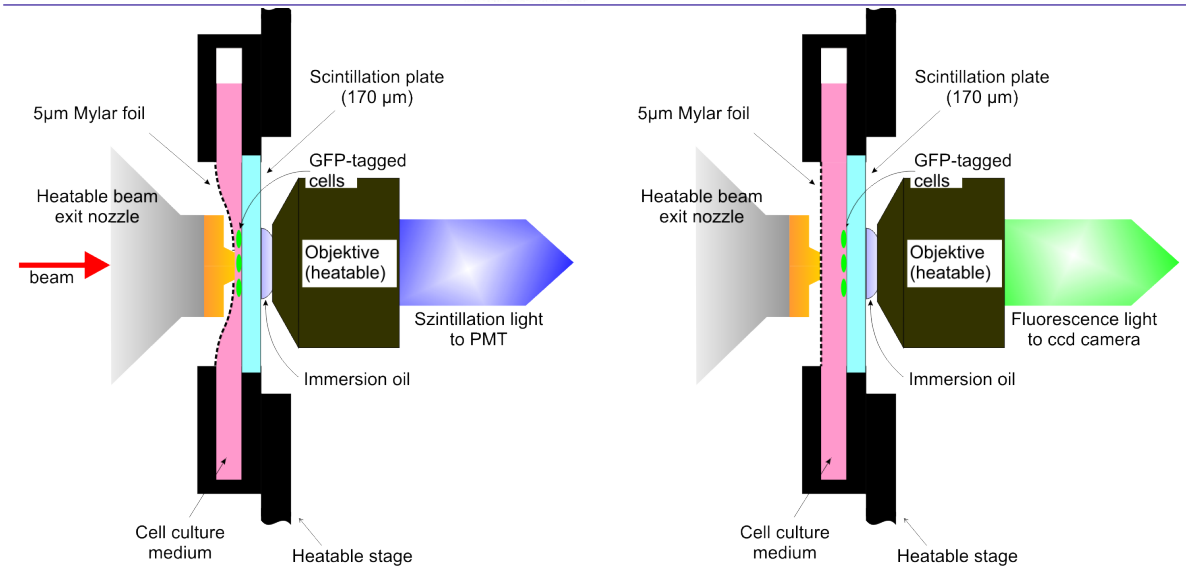

Fig. 4-49 (upper) **& Fig. 4-50** (lower)**:** Schemes showing the situation at the interface between beam exit nozzle, live-cell chamber and microscope and how ion beam irradiation is carried out at the SNAKE setup. In order to irradiate the cells that are growing on a plastic scintillator with a high positional accuracy, the irradiation nozzle has to be brought in close vincinity to its target. To avoid reflection artefacts the nozzle is moved away from the cells before starting fluorescence microscopy (see lower panel (fig. 4-50) left and right) (HABLE ET. AL 2009).

irradiation sources are its ability to control the irradiation position on a micrometer-scale as well as its property to deliver particles of an exactly defined energy to the cell nuclei (by choosing different voltages at the accelerator and/or by choosing another

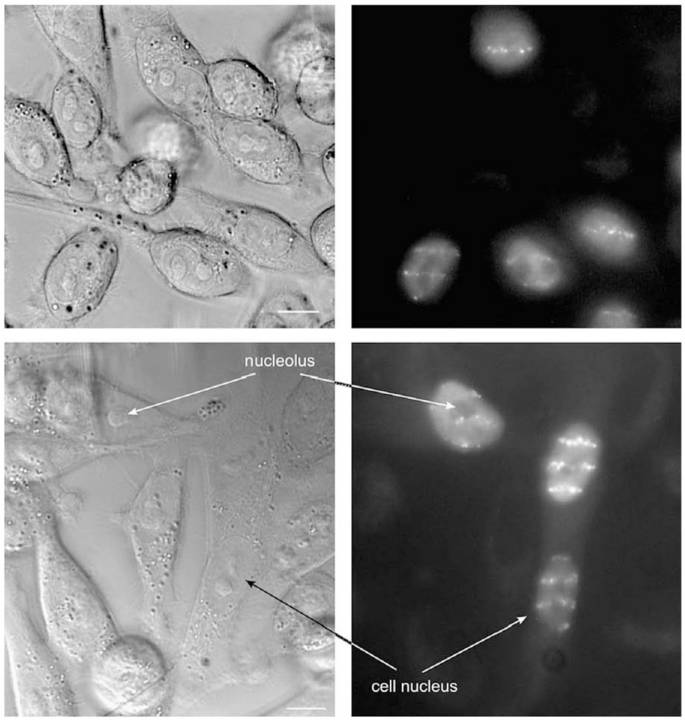

Fig. 4-51: Images of HeLa cells taken at the SNAKE irradiation set-up. Scale bars each 10 µm. **Left:** "Phase contrast" (Ph3) images of a cell sample grown on a 170 µm plastic scintillator using LED illumination built into the beam exit nozzle. A water/glycerin immersion objective Zeiss LCI Plan Neofluar 63 x was used. **Right:** Fluorescence image of the same sample as imaged on the left by phase contrast. Some, but not all nuclei express GFP tagged repair protein 53BP1 and show some of the proteins attached at foci around sites of DNA double strand breaks due to linewise irradiation with 55 MeV carbon ions. Both microscopy techniques also reveal nucleoli, which are areas in the cell nucleus with lower DNA density. Taken from (Hable et al., 2009).

ion-species that differs in atomic weight (see fig. 4-45)). Creation of DSBs in a quantitatively predictable way is the huge main advantage of ion- over UV-microirradiation devices which often depend on photo sensitizers like BrdU (Limoli and Ward, 1993) and that bleach big amounts of the fluorophores around the target during irradiation. In combination with live-cell imaging SNAKE is able to provide valuable information on damage dynamics at the single cell level.

However unfortunately there are some disadvantages, too. SNAKE is only one of many experimental set-ups that are attached to the particle accelerator, so that the time of usage for radiobiological experiments during the course of this thesis was strictly limited to a few time slots. This circumstance cuts down the time for radiobiological experiments to a few weeks per year. Due to the effort that is necessary for the preparation of the ion microbeam (to manually guide it from the ion source through the accelerator and the vacuum-tubing to the experimental set-up (e.g. SNAKE)) it is not possible to quickly change between different irradiation modes or ion species, what means that the allotted times for each experiment have to be taken *en bloc*. This leads to very tight time schedules all around the clock which are hard to fulfill and change in case of problems. As already pointed out in the *Introduction* successful live-cell experiments depend on a chain of events that partially depend on each other and have to succeed in order to work. The time pressure to to stay on schedule for the planned individual experiments (regardless of whether it is night or day), lets very little place for improvisation and affords much higher amounts of self-discipline and attention than it is already necessary for live-cell experiments in general, performed at ordinary microscopes. Another disadvantage lies within the reduced motility of the sample once the irradiation nozzle is brought into position. Because bringing the nozzle close to the cells is a tedious procedure, repositioning is difficult and time demanding. So the number of cells that can be observed during one time-lapse experiment is limited and restricted to that area that can be covered by the used objective. With regard to the limited time for the experiments in total and the limited cells that can be observed during one single observation, it is recommended to use transgenic (if possible stable) cell lines containing a high percentage of fluorescent cells. Unfotunately in praxis this is often hard to accomplish.

4.2.2 First experiments at the SNAKE using live-cell microscopy

4.2.2.1 Targeted cell irradiation

The current accuracy of the microbeam irradiation is demonstrated in fig. 4-52. In this experiment replication foci of stably MDC1-GFP expressing cells, were used as targets for irradiation. Replication labeling was carried out according to the methods in described in 3.3.4 and 3.3.5

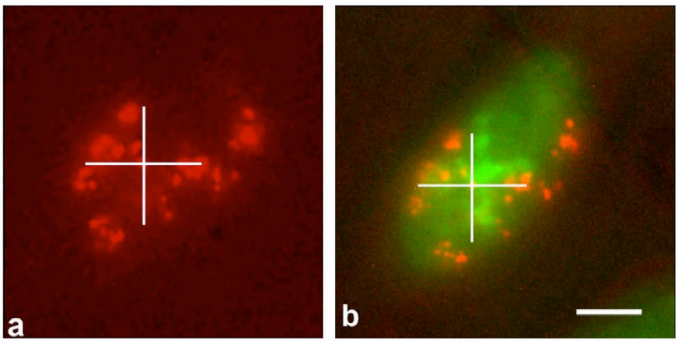

Fig. 4-52: Targeted cell irradiation at SNAKE. (a) Red fluorescence (λ = 615 nm) shows chromatin labeled with nucleotides that were labeled with the dye TexasRed. One of the smaller red spots was chosen as a target for ion microirradiation with a cross pattern (white cross), (b) superposition of green (GFP) and red (TexasRed) fluorescence images of the same nucleus as in (a) after irradiation. The GFP-tagged Mdc1 protein shows the intended irradiation pattern but is shifted to the right and upwards by about 1.5 µm. Scale bar: 5 µm. Taken from (Hable et al., 2009).

After irradiating a cross-like patten through the cells with the ion micobeam, MDC1-GFP proteins were recruited to sites of damaged chromatin (indicated by increased fluorescence. Comparison between the expected position of the cross and the position of the actual fluorescent cross yielded an accuracy of about 1.5 µm.

4.2.2.2 After ion microbeam irradiation patterns of damage foci remain stable over several hours in U2OS cells

Between 5 to 6 minutes after irradiation of a stable U2OS Rad52-GFP cell-line with C^{5+} ions (55 MeV) with a line pattern (1 µm x 5 µm), small point-like foci with a diameter below the optical resolution limit simultanously emerge (fig. 4-53). In the course of observation the irradiated line patterns persisted over several hours without major changes. Depending on the position of the cells, photobleaching faded the signals until they were hardly visible any more. Irradiated cells migrating from other areas into the field of observation (still showing good fluorescence), exhibiting the the initial irradiation patterns, argue against bigger rearrangements of chromatin after DNA damage induction (in contrast to several publications that claim pairing of homologous chromosomes induced by DNA damage (Abdel-Halim et al., 2004; Abdel-Halim et al., 2006; Abdel-Halim et al., 2005; Monajembashi et al., 2005)). Successful mitotic events in the recorded data argue for good long-term observation conditions (using a cell-friendly LED light fluorescence excitation (*Colibri*) and a 450 nm longpass filter) and against phototoxicity that is suspected to hamper

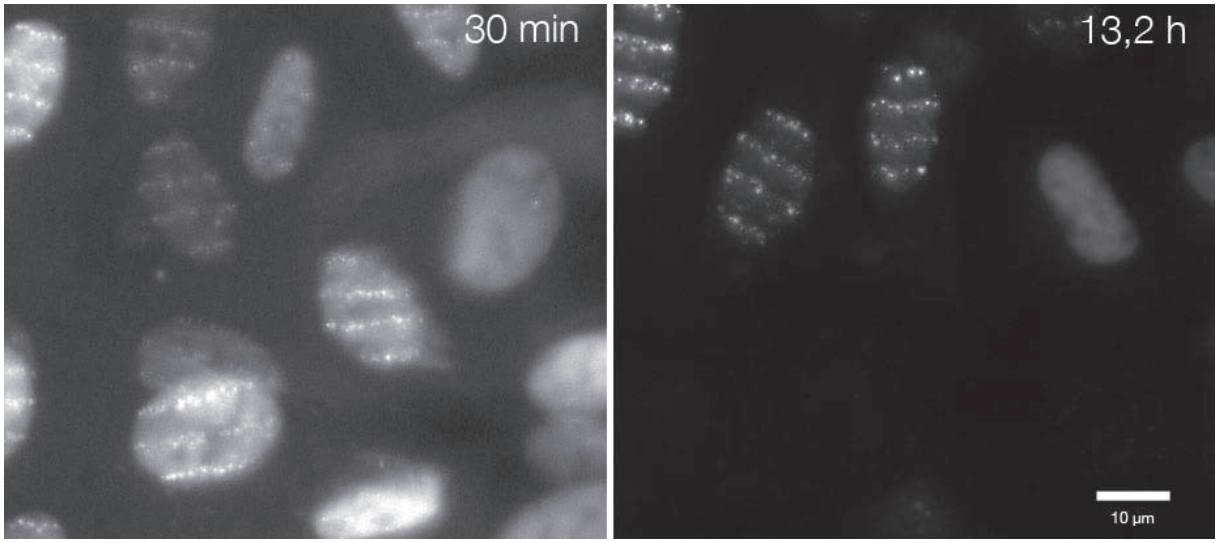

Fig. 4-53: Long-term observation of U2OS Rad52 GFP cells irradiated at the microbeam facility SNAKE. After irradiation, the cells were imaged over night for more than 13h. Although the cells initially imaged in the left pictures were mostly bleached due to at least 195 image acquisitions between irradiation and the end of the experiment, the observation conditions allowed cell divisions (not shown). Remarkably the distance between the irradiated nuclear line patterns remains constant between the begin and the end of the of the observation which argues against major changes in the nuclear architecture.

chromatin mobility. The conservation of the irradiation patterns over bigger time intervals support the results obtained from earlier immunofluorescence experiments.

4.2.2.3 MDC1-GFP binds to damaged chromatin ca. 20 seconds after DNA damage induction by ion beam irradiation

Adapting the frequency of the ion flux with respect to the scanning speed allowed to observe cells during and shortly after irradiation at conditions that are similar to

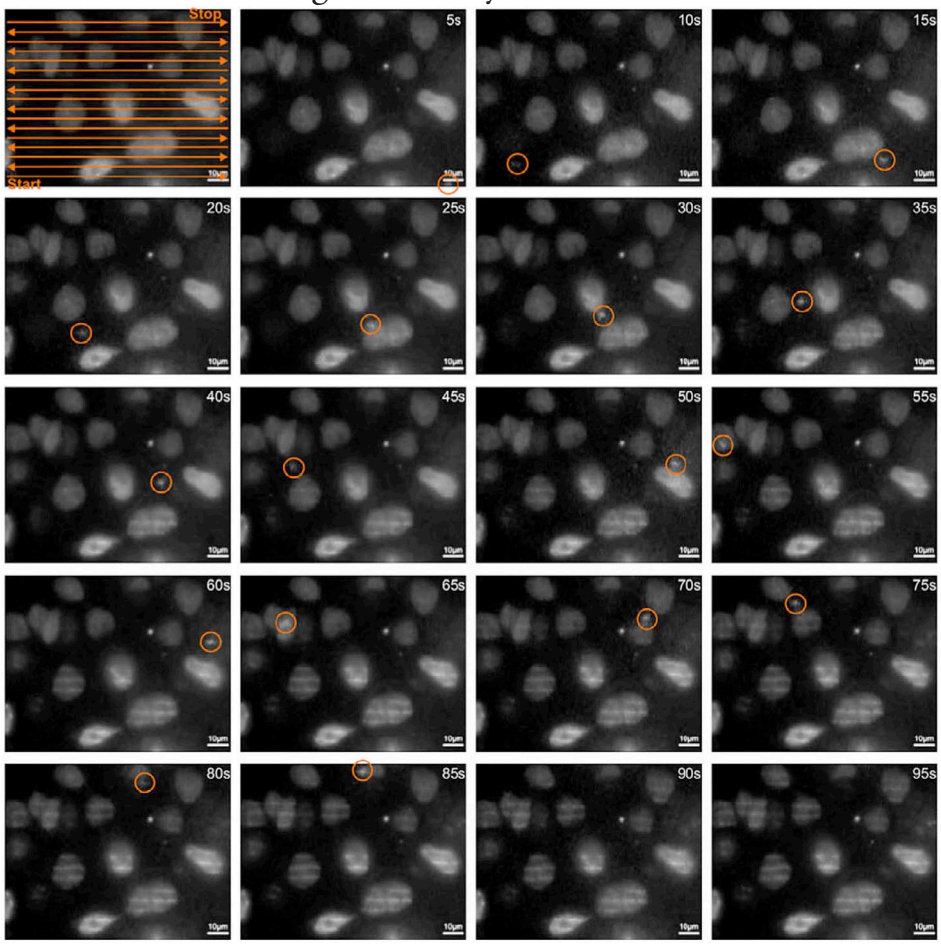

Fig. 4-54: Irradiation of U2OS cells expressing MDC1-GFP. The beam scans slowly over the cell sample as shown in the first image (shown by a circle in the following images). There are 5 s between two images; the scale bar is 10 µm. Foci formation in cell nuclei can be observed a few seconds after they were hit by the beam. Taken from (Hable et al., 2009).

those of single ion irradiation. Irradiation of a U2OS MDC1-GFP cell-line impressively demonstrated the speed at which DNA damages produced by irradiation with ions are detected by proteins of the DNA-damage response (DDR). Fig. 4-54 shows the position of the ion beam and the MDC-GFP signal within the cells constantly lagging ca. 20 seconds behind (compare movie S7). Using an irradiation pattern as shown in fig. 4-54 allows a lot of measurements within one experiment by determining the time that elapsed after irradiation of each point before the signal emerges. Only the MDC1 construct (out of all constructs that were used, yet) showed such fast binding kinetics that simultaneous irradiation and recording of the fluorescent signals were necessary.

4.2.2.4 Sequential irradiation using transgenic cells expressing fluorescent repair proteins don't show the competition effect

While (Greubel et al., 2008a; Greubel et al., 2008b) could find a striking difference in the distribution of the repair factors 53BP1 and Rad51 at sites within a nucleus that were irradiated ca. 45 min after a first irradiation was performed, this so called "competition effect" could not be observed using transgenic cells expressing 53BP1-GFP, (neither at the ion-microbeam (HeLa 53-BP1-GFP) nor at the laser-microbeam (RPE1 53BP1-GFP, see fig. 4-67), yet. However this doesn't completely rule out that the effect isn't reproducible with cells expressing big pools of transgenic repair-proteins at all. Previous experiments have shown that this effect varied strongly between different cell lines.

4.2.2.5 High doses of irradiation lead to saltatory phosphorylation of chromatin

Repeating the experiment mentioned above (4.2.2.3) with a much higher ion flux (ca. 50 ions/position) led to a continuous broadening of the irradiation-damage signal which resulted in the end in homogeneously stained cell-nuclei that didn't show any of the discretely irradiated lines any more (fig. 4-55). Immunofluorescence stains with γ-H2AX, that were performed on the irradiated cells later (not shown) confirmed the in-vivo observations showing nuclei that were completely positive for γ-H2AX.

The observations made here suggest that exceeding a certain threshold of irradia-

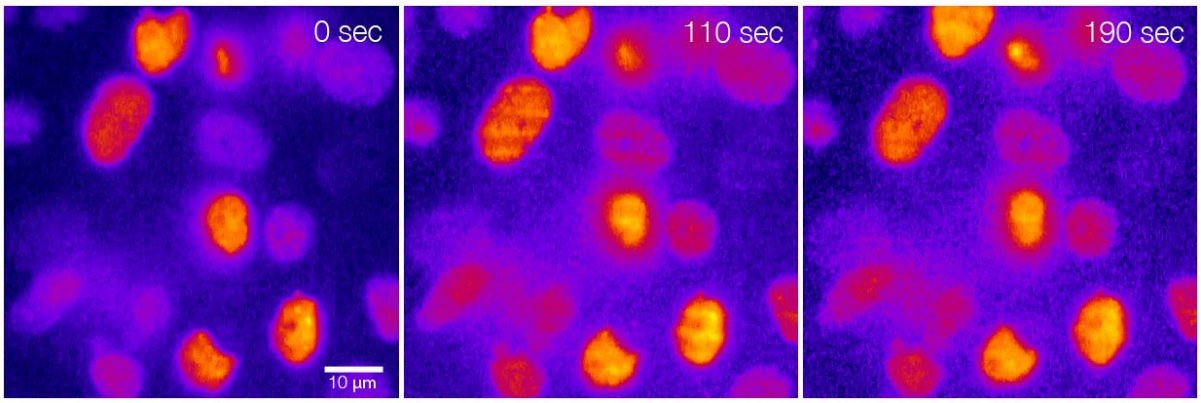

Fig. 4-55: U2OS cells stably expressing MDC1-GFP irradiated by a high dose of ions (≈ 50 ions à 55 MeV/point) show at first expected recruitment of MDC1-GFP to the sites of DNA damage. After a short time the line pattern broaden until they run into each other.

tion leads to saltatory phosphorylation of γ-H2AX all over the chromatin instead of being locally confined to the places that were directly damaged by the highly energetic ions.

Sensing the degree of γ-H2AX phosphorylation might have an influence on the cells's decision to go into repair or apoptosis.

4.2.2.6 Rad 51-GFP generates filaments inside the nucleus at DNA damage foci

Rad51 is known to be a nuclear DNA repair protein whose occurrence is cell cycle dependent. Transfection with expression constructs coding for Rad51 containing strong viral promotors produces a big excess of this protein throughout the cell cycle. At high levels of Rad51 (which result from strong constitutive over-expression) the protein starts to aggregate into crystal-like filaments (Galkin et al., 2006) that span across the nuclear volume building very aesthetic and interesting looking networks (see fig. 4-56 and movie S8). After irradiation of a HeLa Rad51-GFP cell line at the accelerator using 55 MeV C^5 ions that didn't possess visible Rad51 filaments growth of these filaments could be observed during the subsequent time-lapse recording.

It appears that after the first emergence of Rad51-GFP foci (which occurred approximately 10 min after the irradiation) the radiation foci served as crystallization germ, a starting point for the filamentous structures to begin their growth through the nucleus.

Further, already envisaged experiments will aim at the in-vivo observation of the filament growth and/or 3D-FISH experiments to see whether the filaments grow through the interchromatin space along the borders of chromosome territories.

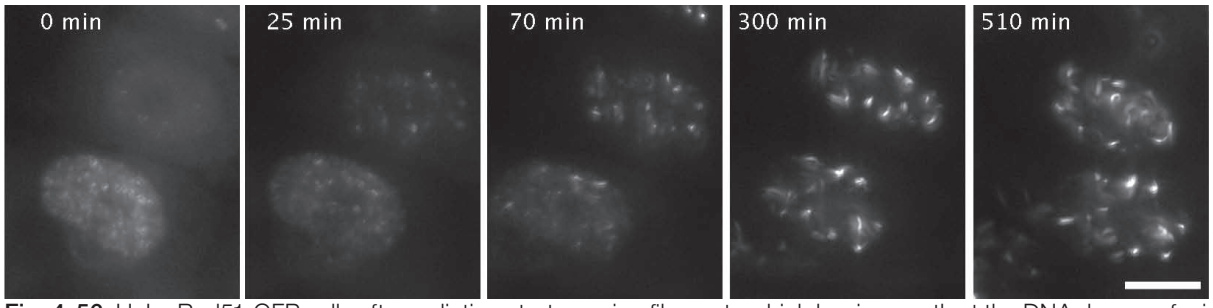

Fig. 4-56: HeLa Rad51-GFP cells after radiation start growing filaments which begin growth at the DNA damage foci.

4.3 Exploring the dynamics of DNA damage response after microirradiation using a continuous laser beam

Laser microirradiation at confocal microscopes produces a broad mix of different damages compared to other irradiation sources like e.g. the ion-micro beam. On the other hand this approach is not so much limited with respect to accessibility of the experimental set-up, provides a much better image quality and is much easier to carry out.

In the following sections DNA damages were induced by irradiation of BrdU sensitized cells (see 3.3.7) using the 405 nm laser line of a spinning disc microscope. This microscope also allowed to explore the dynamics of GFP-tagged repair-proteins in damaged and undamaged cells by FRAP (Fluorescence Recovery After Photobleaching).

4.3.1 Microinjection does not induce visible DNA damage response with respect to single and double strand breaks

Due to poor transfection efficiencies obtained by lipofection of the HeLa cell line that was intended to be used for irradiation experiments at the accelerator, microinjection of expression plasmids into cell nuclei – although very tedious to perform – served as a realistic alternative. Despite the many disadvantages of this method, microinjection of different plasmids into cells (locally separated from each other on one culture dish) allows observation of damage kinetics of different repair proteins under exactly the same experimental conditions.

Microinjection into the nucleus of a cell is thought to expose chromatin to enormous mechanical stress leading to damages that potentially could bias the measurement of the damage kinetics. In order to study to which extent the structural integrity of chromatin is affected by nuclear microinjection a mix of water and 73 kDa dextran-TRITC (10:1) was microinjected into cells stably expressing fluorescent DNA repair proteins. The polysaccharide dextran-TRITC was used as a fluorescent reporter that behaves mostly inert to the chromatin and highlights cells that were successfully injected. To check for the generation of double strand breaks an U2OS MDC1-GFP line was used. A stable HeLa PCNA-GFP

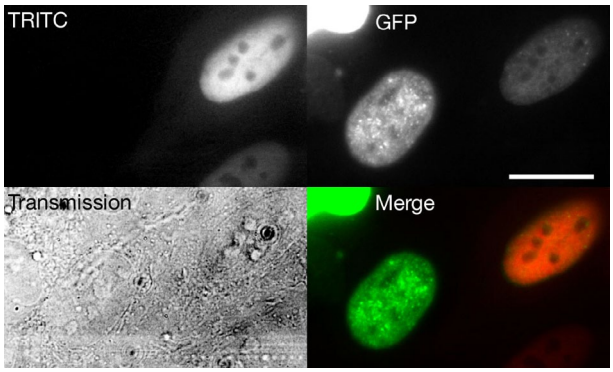

Fig. 4-57: U2OS MDC1-GFP-Cells after microinjection do not show signs of DNA damage (recorded at a widefield fluorescence microscope (Axiovert 200M)).

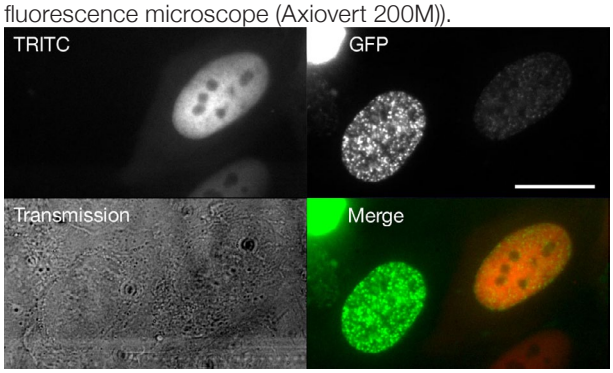

Fig. 4-58: Cells shown in fig 4-57 after 10 min Neocarzinosstatin treatment show that DNA damage response is not impaired by the microinjectinon (recorded at a widefield fluorescence microscope (Axiovert 200M)).

cell line (kindly provided by HEINRICH LEONHARDT) was used to check for the generation of single strand breaks.

Surprisingly injection into the cell nuclei – even when stirring the nucleoplasm with the inserted needle (!) – didn't lead to any visible damage response in both cell lines (U2OS MDC1-GFP and HeLa PCNA-GFP) (fig. 4-57 and fig. 4-59) although presence of the dextran-TRITC indicates a proper nuclear injection.

Although this experiment suggests that microinjection is not affecting the genomic integrity to an extent that is measurable by the used experimental set-up, it must be ruled out that this result was obtained due to an impairment of the DNA damage response by the injection process irself or the injected dextran-TRITC.

To test for this the U2OS MDC1-GFP cells were treated with the radiomimetic drug neocarzinostatin which was added into the medium (200 nM) to generate radicals that lead to double strand breaks. After a 10 min treatment one could clearly see (fig. 4-58) that the DNA damage response system seemed to work fine, producing focal accumulation of MDC1-GFP in the nucleoplasm of microinjected and not injected nuclei.

To test the functionality of PCNA-GFP as a sensor for unscheduled DNA synthesis the HeLa cells were moved and relocated at a confocal microscope (fig. 4-60) in order to generate single strand damages by laser micro irradiation

Fig. 4-61 shows apart from the difference in image quality between a wide field and a confocal fluorescence microscope that DNA damage response for single strand breaks was not impaired by nuclear micro injection, too. Accumulation of PCNA-GFP at the laser irradiated sites was visible in microinjected and in not microinjected cell nuclei.

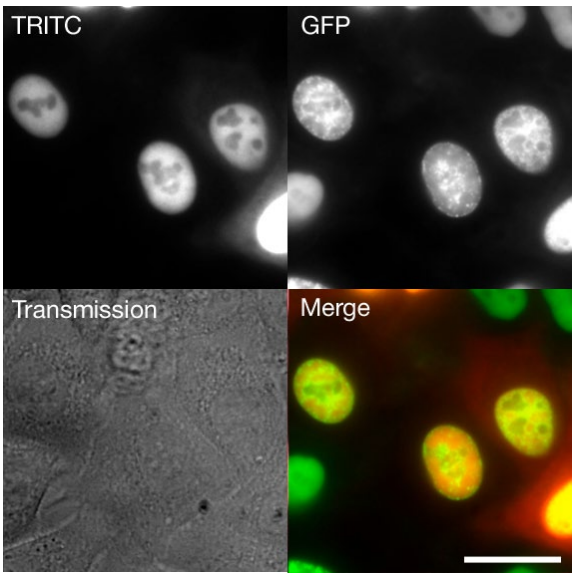

Fig. 4-59: HeLa PCNA-GFP cells directly after microinjection observed at a widefield microscope (Axiovert 200M) show no traces of damage in injectied nuclei.

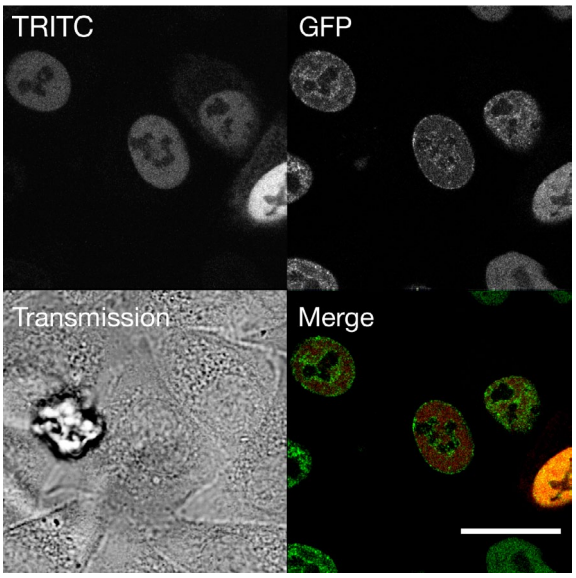

Fig. 4-60: Cells shown in fig. 4-59 relocatied at a confocal microscope (Leica SP5).

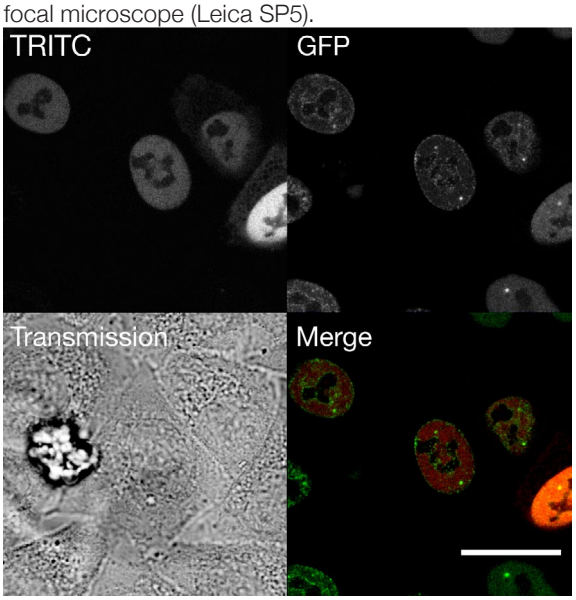

Fig.4-61: HeLa PCNA-GFP cells after damaging the chromatin by lase micro irradiation with a 405 nm laser at a confocal microscope (Leica SP5). The nuclei clearly show recruitment to the irradiated sites.

4.3.2 Kinetics of the repair-proteins MDC1-GFP, 53-BP1-GFP, Rad51-GFP, Rad52-GFP in the undamaged nuclei and after damage induction by a laser microirradiation

In experiments focussing at the nuclear dynamics of Rad51, Rad52, MDC1 and 53BP1 (members of the DNA damage response), cells expressing GFP tagged versions of these proteins were damaged by high energetic laser light as described in 3.5.2.3.

4.3.2.1 MDC1-GFP

Cells stably expressing MDC1-GFP show a phenotype that looks similar to normal chromatin distribution vizualized by e.g. H2B-GFP or DAPI (see fig. 4-22) with exception of some bright spots which will be referred to as *spontaneous* or *cryptic* foci.

Damaging the chromatin by laser microirradiation shows fast recruitment of the MDC1-GFP proteins to the damaged sites (fig. 4-62a). The accumulation of fluorescent proteins becomes visible ca. 35 seconds after irradiation in RPE1 cells (fig. 4-63). Due to the fact that during damage induction by laser irradiation a lot of fluorescent proteins are bleached, too this time value might be overestimated. Measurements performed at the ion microbeam, which doesn't bleach during irradiation showed a sightly faster appearance of damage signals (ca. 20 sec in U2OS cells).

Although diffusion of unbound fluorescent proteins is extremely fast and should't contribute much to a significant delay in appearance of damage recruitment – bleached stripes aside the actual site of damage argue for a high fraction of unspecifically bound MDC1-GFP molecules in the chromatin which might explain the chromatin-like appearance of the protein over big parts of the nuclei. These stripes,

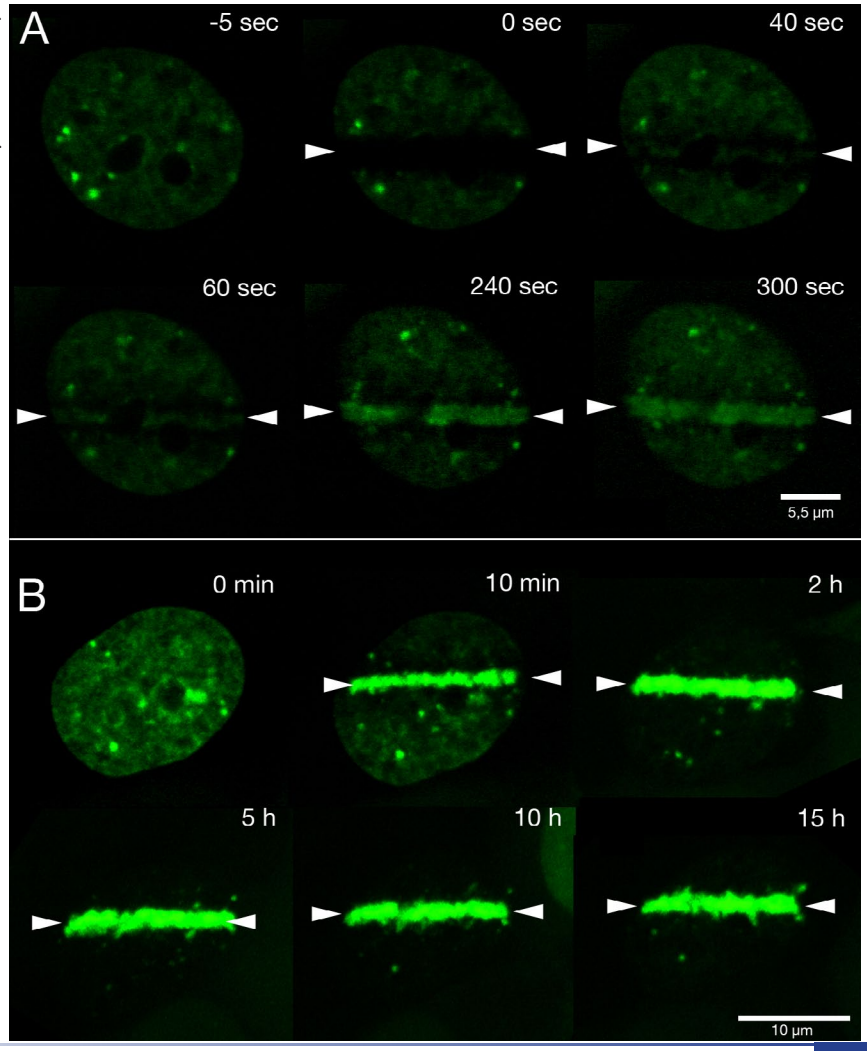

Fig. 4-62: Damage induction in RPE1-MDC1-GFP cells

A: short time observation (mid-sections) of a RPE1-MDC1-GFP cell after damage induction. Note that the spontaneous foci (already visible prior to the damage) don't indicate extraordinary movements of the chromatin in reaction to the damage. In addition chromatin-like distribution of MDC1-GFP in undamaged cells seems to indicate that MDC1-GFP proteins are not diffusing through the nucleoplasm entirely free.

B: long-term observation (z-Projection) of a RPE1-MDC1-GFP-cell after damage induction. Throughout the time, the biggest amount of MDC1-GFP seems to aggregate to the damaged area. Remarkably the shape of the damaged area, as well as the spontaneous foci surrounding it, doesn't change its configuration over time.

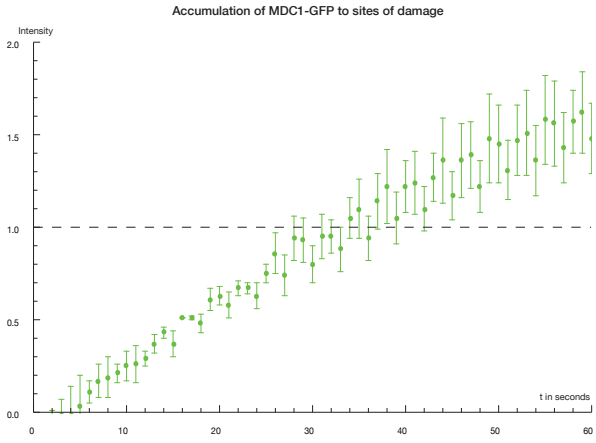

Fig. 4-63: Short time kinetics of MDC1-GFP recruitment to chromatin damaged by laser micro irradiation. (Averaged from 5 RPE1 cells. The zig-zag shape of the line origins from individual measurements with different time intervals)

which could represent bleached MDC1-GFP proteins located at undamaged chromatin adjacent to the damages, are still visible 10 minutes after damage induction (fig. 4-62b). In contrast to the fast recruitment of the MDC1-GFP proteins to the damaged DNA, the pattern of the spontaneous foci, nucleoli (where no foci formation takes place) and centromeres (fig. 4-64 and fig. 4-78) remained unchanged – arguing for the absence of dramatic changes in nuclear architecture caused by the induction of DNA damages. Long-term observations seem to support this point of view and show except from the spontaneous foci a nearly complete recruitment of the MDC1-GFP protein pool to the damaged chromatin. Fig. 4-65 shows the recruitment kinetics of MDC1-GFP as well as the FRAP kinetics of spontaneous foci, damaged and undamaged chromatin.

In contrast to the curve describing a massive recruitment of MDC1-GFP to damaged sites (red), the FRAP curves – as expected converge towards full recovery. The difference between the FRAP curves reflect the affinity of MDC1-GFP towards the bleached structures. While unspecifically bound chromatin has as expected the fastest recovery (shortest residence time) the cryptic foci seem to have the strongest affinity. Since ongoing recruitment at damaged chromatin might strongly bias the fluorescence recovery of damaged chromatin this shown data-set remains speculative.

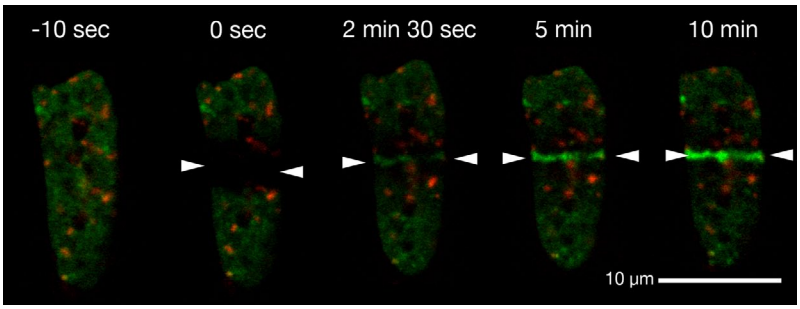

Fig. 4-64: U2OS MDC1-GFP CENP-B-mRFP cells before and after irradiation. Within the observed time interval positioning of the centromeres doesn't seem to be affected by the introduction of DNA damage.

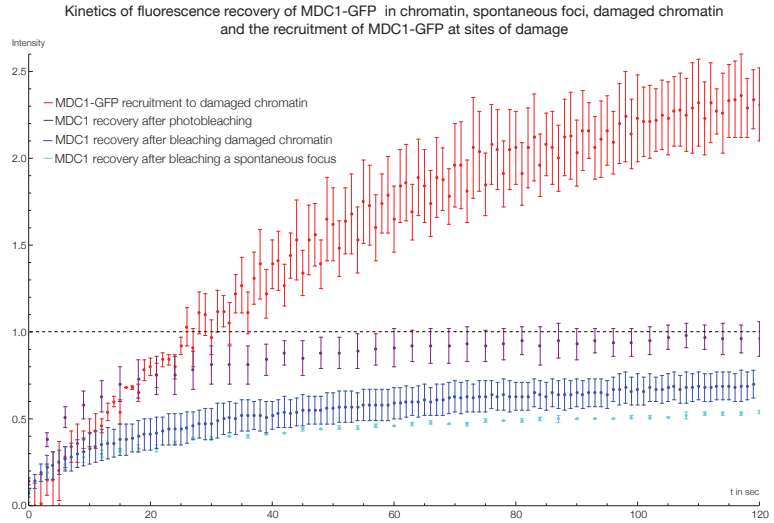

Fig. 4-65: The kinetics of MDC1-GFP generated in RPE1 cells. (fluorescence recovery of spontaneous foci (n = 3), fluorescence recovery from damages (n = 4), damage induction (n = 5), fluorescence recovery from undamaged chromatin (n = 4)). The zig-zag-like nature of the damage induction curves comes from experiments with different time intervals of image acquisition after photobleaching. Because not all time points have the same number of observations the average mean and the standard error might differ between two subsequent time-points. Interestingly the differences lie within the range of the standard error.

4.3.2.2 53BP1-GFP

Distribution of 53BP1-GFP protein in stably transfected RPE1 nuclei differs clearly from that of MDC1-GFP. Apart from the nucleoli, the whole nuclear volume seems to be equally filled with the fluorescent protein – in stark contrast to the chromatin-like appearance of MDC1-GFP. An exception to this uniformity are the big spontaneous (or cryptic) foci that are located almost exclusively attached to the periphery of nucleoli or the nuclear rim (fig. 4-66). These foci which look similar to the perinucleolar compartment (Pollock and Huang, 2009), are rather a wild-type feature of mammalian cells than an artifact produced by over-expression of the transgenic protein, since spontaneous 53BP1 foci are observed in immunofluorescence preparations of human and mouse cells, too (Bekker-Jensen, 2005). Interestingly, after damaging the chromatin by laser or ion microirradiation, these spontaneous foci seem to shrink until they completely disappear while the irradiation induced foci seem to grow. Fig. 4-67(a) and (b) show two examples of this phenomenon. In the example shown in fig. 4-67(a) a spontaneous focus was bleached ca. 30 seconds after damage induction. Surprisingly the recovery in fluorescence of the spontaneous focus appears faster than the recruitment of the 53BP1-GFP proteins to the damaged chromatin.

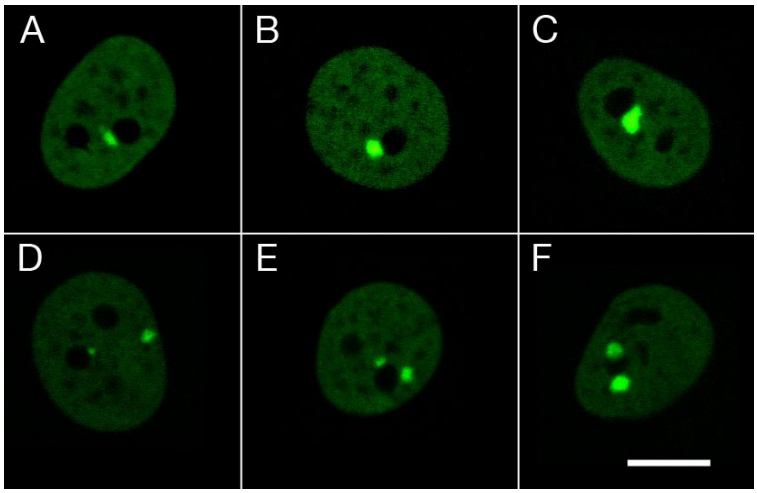

Fig. 4-66: Nuclei of RPE1 53-BP1-GFP cells show a rather homogenous staining pattern except for spontaneous foci located at the periphery of the nucleoli or the nuclear envelope.

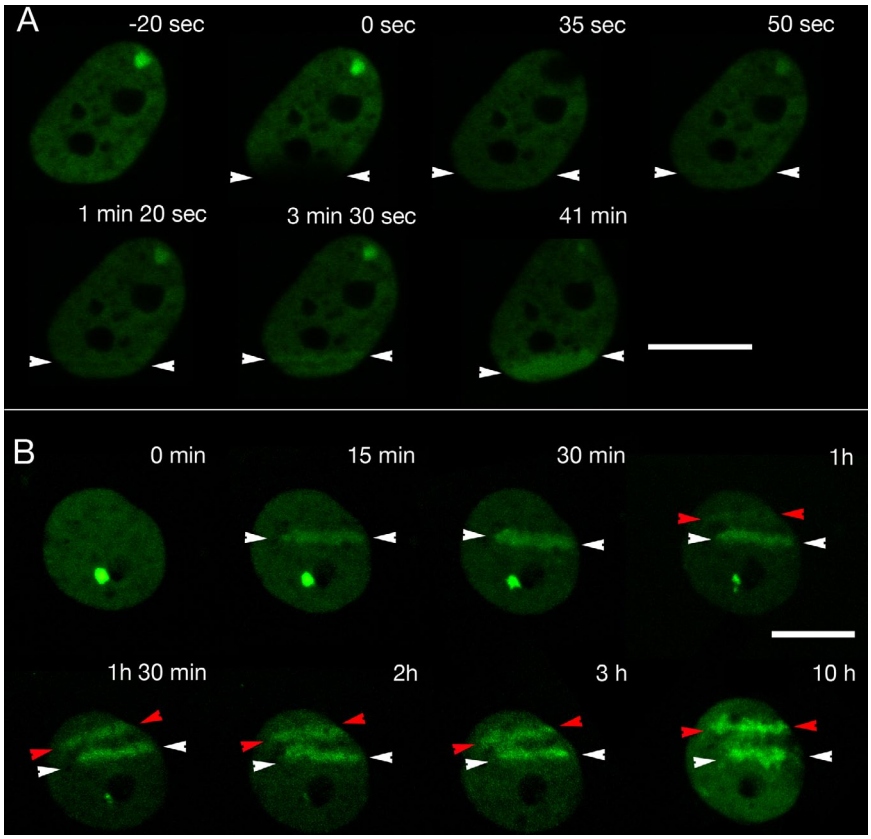

Fig. 4-67: Nuclei of RPE1 53-BP1-GFP cells after damage induction with the laser microbeam. While panel (A) shows a live-cell series over a shorter time interval to focus on 53BP1-GFP recruitment kinetics and dissociation from spontaneous foci, panel (B) shows a long-term observation of a damaged nucleus. This example not only shows that only very little movements occur over time but also that a second damage which was induced 1h after the first one recruits 53BP1-GFP to the same extent as the first one (see 4.2.2.4).

At first glance this somehow generates the impression that 53BP1-

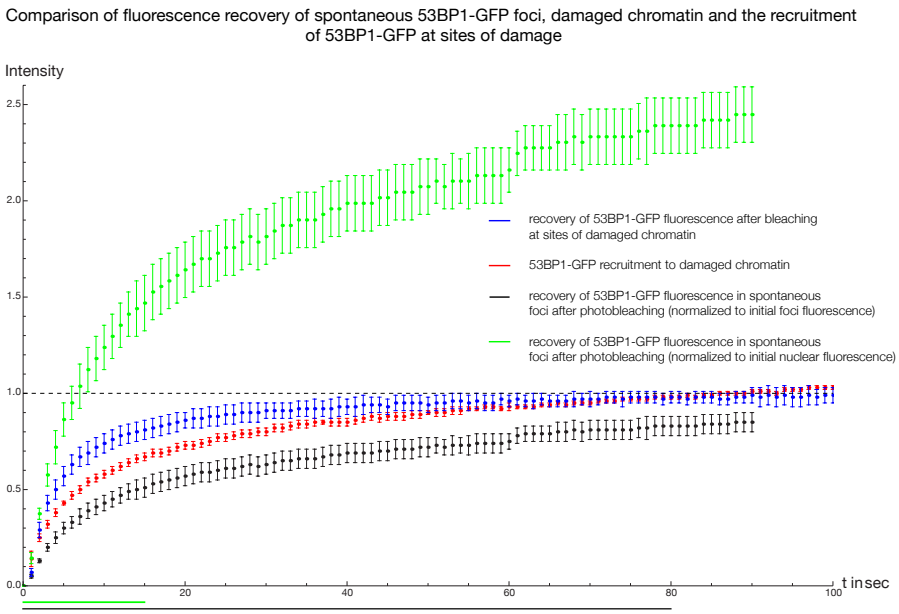

Fig. 4-68: Comparison between FRAP experiments in RPE1-nuclei at sites of damaged chromatin, spontaneous foci and recruitment of 53BP1-GFP to damaged chromatin after laser micro irradiation. The steps that are visible in some curves are caused by image acquisition of different interval lengths (fluorescence recovery of spontaneous foci (n = 8), fluorescence recovery from damages (n = 5), damage induction (n = 5)) the different number of observations influences the average mean value and the standard error.

GFP has a higher affinity towards spontaneous foci than to damaged DNA. Visual impression can be sometimes misleading since it is based on absolute intensity levels. Spontaneous 53BP1-GFP foci possess an approx. 3-fold higher fluorescence intensity than the rest of the nucleus. This is why (normalizing the fluorescence recovery to the average fluorescence of a nucleus) the sponaneous foci re-emerge as soon as after 15 seconds (fig. 4-68 green curve). Performing accurate FRAP (which normalizes to the initial fluorecence level of the measured object) revealed that spontaneous foci in fact have the slowest recovery kinetics (compared to 53BP1-GFP at damaged chromatin and the unbound protein) and thus the highest affinity for 53BP1-GFP. This is somehow surprising, since spontaneous foci disappear after DNA damage induction and therefore a lower affinity for 53BP1-GFP at the spontaeous foci compared to that of damaged chromatin was expected.

Recruitment of 53BP1-GFP to DNA damages is a process that extends over long time periods (fig. 4-67&70). While ongoing recruitment certainly affects FRAP curves to some extent, its contribution to the 53BP1-GFP FRAP curves in fig. 4-68&69 ap-

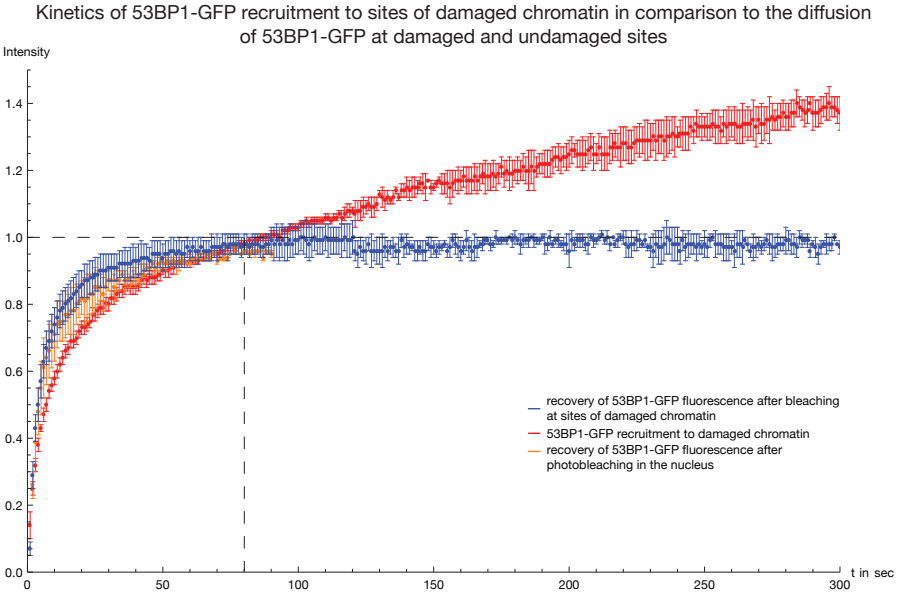

Fig. 4-69: Comparison between 53BP1 damage curve and 53BP1 FRAP-curves show that the damage signal is first observable ca. 80 s after damage induction in RPE1 cells. (fluorescence recovery in normal chromatin (n=4), fluorescence recovery from damages (n = 5), damage induction (n = 5))

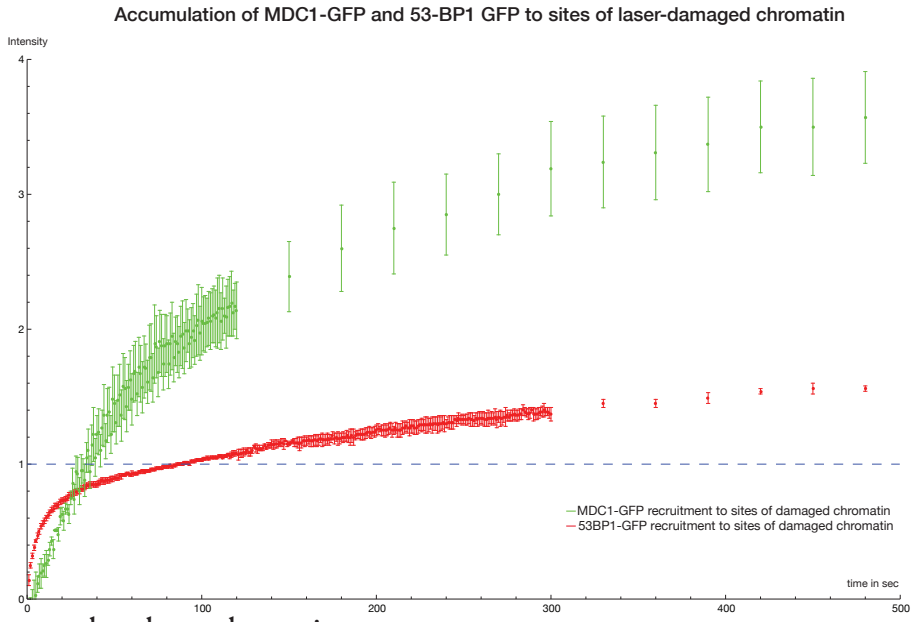

Fig. 4-70: Direct comparison between the recruitment of MDC1-GFP (**green**) and 53BP1-GFP (**red**) to damaged DNA. While MDC1-GFP lags behind the 53BP1-GFP curve (which is most likely due to a smaller immobile fraction) it overtakes the 53BP1-GFP curve, soon and exceeds it by far. Because of the photobleaching effects during laser microirradiation it is hard to draw conclusions about the early dynamics of the proteins.

peared to be rather minor.

The unexpected behavior of 53BP1-GFP spontaneous foci in terms of recovery kinetics opens some room for speculations about their biological purpose. They appear to be storage compartments, somehow like fire departments that store fire engines which otherwise would represent an obstacle for the traffic. Only when needed the "fire engines" swarm out to the places where their help is badly needed. After successfully completing their job they are ordered home again. This model is for sure based on the assumption that after damage induction the affinity properties for repair proteins don't change cell-wide. To test for this appears to be rewarding for future experiments.

To unveil the mysteries of spontaneous focim, it would be tempting, to image these structures at a nanometer scale with the new light optical super-resolution microscopes or by three dimensional electron microscopy, too. This could help to answer the question at which (presumably heterochromatic) structures they form and how they are organized.

As already seen in long-term observations of MDC1-GFP expressing cells (fig. 4-62) the geometry of nucleoli and irradiation patterns doesn't significantly change over time (except from some blur) arguing against major changes in nuclear architecture caused by DNA damage.

In fig. 4-70 the curves describing the damage kinetics of MDC1-GFP and 53BP1-GFP are plotted into the same diagram. It can easily be seen, that MDC1-GFP gets visible significantly earlier than 53BP1-GFP. During the first seconds the 53BP1-GFP curve seems to grow much faster than its MDC1-GFP counterpart. This might be due to a higher mobility of unbound 53BP1-GFP proteins compared to MDC1-GFP proteins which generally seem to be bound to the chromatin tighter as seen by their chromatin-like distribution pattern and by the bleached structures flanking the damages.

Another prominent feature of fig. 4-70 is the pronounced difference in fluorescence intensity (and thus in protein stoichiometry) between both repair proteins that is already established a few minutes after damage induction. This finding is supported by the long-term observations shown in fig. 4-62(b) and fig. 4-67(b).

4.3.3 Rad51-GFP polymerizes into complex filamentous networks

The ability of Rad51-GFP to polymerize into large, bright, fluorescent filaments impaired to obtain useful data on its recruitment kinetics to DNA damages to such an extent, that it was not possible to generate useful data. However looking at the aesthetic filamentous structures seemed to be rewarding in terms of nuclear architecture (see also 4.2.2.6).

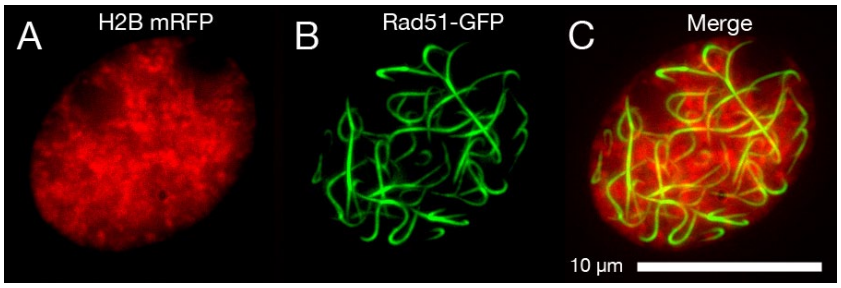

Fig. 4-71: Maximum z-projection of a V79 nucleus with Rad51-GFP filaments and H2B-mRFP labeled chromatin. The filaments show a three dimensional network that spreads across the nuclear space, except for places in which nucleoli are located. The filaments seem to process within areas in which the density of the chromatin is not maximal.

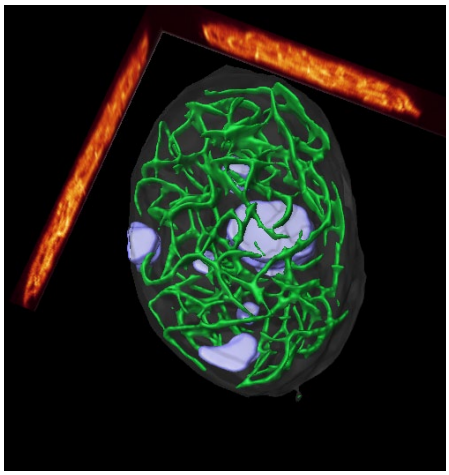

Looking at Rad51-GFP filaments in cells that in addition express H2B-mRFP (fig. 4-71 and fig. 4-72) shows that the filaments do not penetrate through nucleoli and seem to be located preferentially at areas of a lower chromatin density. However it is unclear at present whether this represents a hint for travel routes through the interchromatin space or a just aconsequence of the crystallization process.

Fig. 4-72: 3D reconstruction of a nucleus in which the nucleoli and the Rad51-GFP filaments are displayed. The volumes of nucleoli and Rad51-GFP seem to be mutually exclusive.

4.3.4 Rad52-GFP dissociates from DNA damage foci after highly dynamic processes in the nucleus

To explore the long-term kinetics of Rad52-GFP, nuclei of a stable U2OS Rad52-GFP cell-line were damaged by laser microirradiation and recorded at the microscope for nearly 19 h acquiring 3D stacks (Δz = 500 nm) every 10 minutes.

Unlike in the experiments performed with cells expressing MDC1-GFP and 53BP1-GFP (respectively Rad52-GFP at the ion microbeam see fig. 4-53) the aggregation of Rad52-GFP at sites of DNA-damage didn't occur synchronously. This behaviour could also be observed in RPE1 cells co-expressing Rad52-GFP and CENP-B mRFP. As already seen at the particle accelerator the Rad52-GFP foci (as well as the Rad51-GFP foci) are dot-like structures and much smaller than the foci of 53BP1-GFP and MDC1-GFP. While ca. 92% of the irradiated nuclei (37 out of 40) didn't show a remarkable change in position and width of the damage track three cells showed interesting changes that finally resulted in the disappearance of all Rad52-GFP foci. Interestingly the foci didn't just fade away by decreasing their fluorescence, they disintegrated all simultaneously after a dramatic increase in foci number that surprisingly appeared adjacent from the original damage track, too.

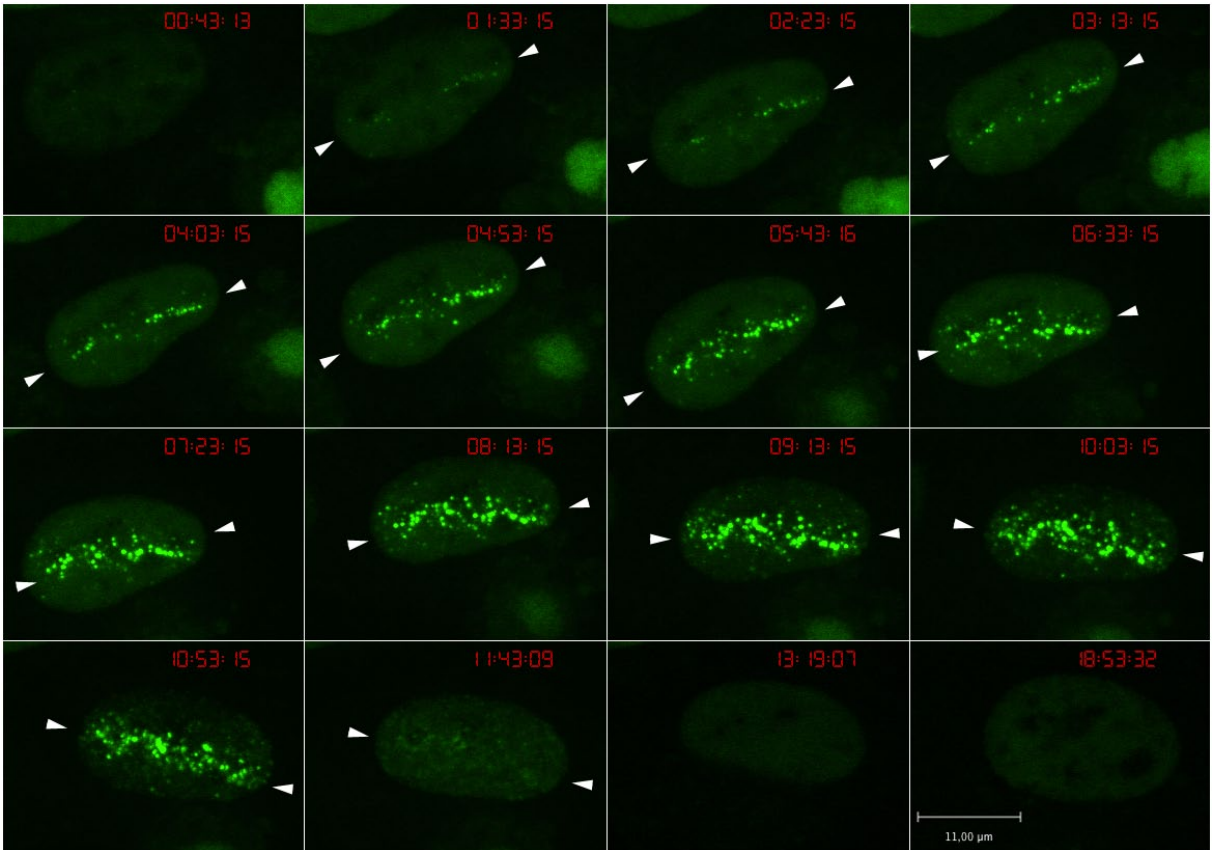

Fig.4-73: U2OS cell stably expressing Rad52-GFP after DNA damage induction by laser microirradiation. Note the increase in the number and distribution of the foci occurs over a period of approx. 11h before most of the foci simultaneously fade away in less than an hour. (Arrowheads point at the damage track)

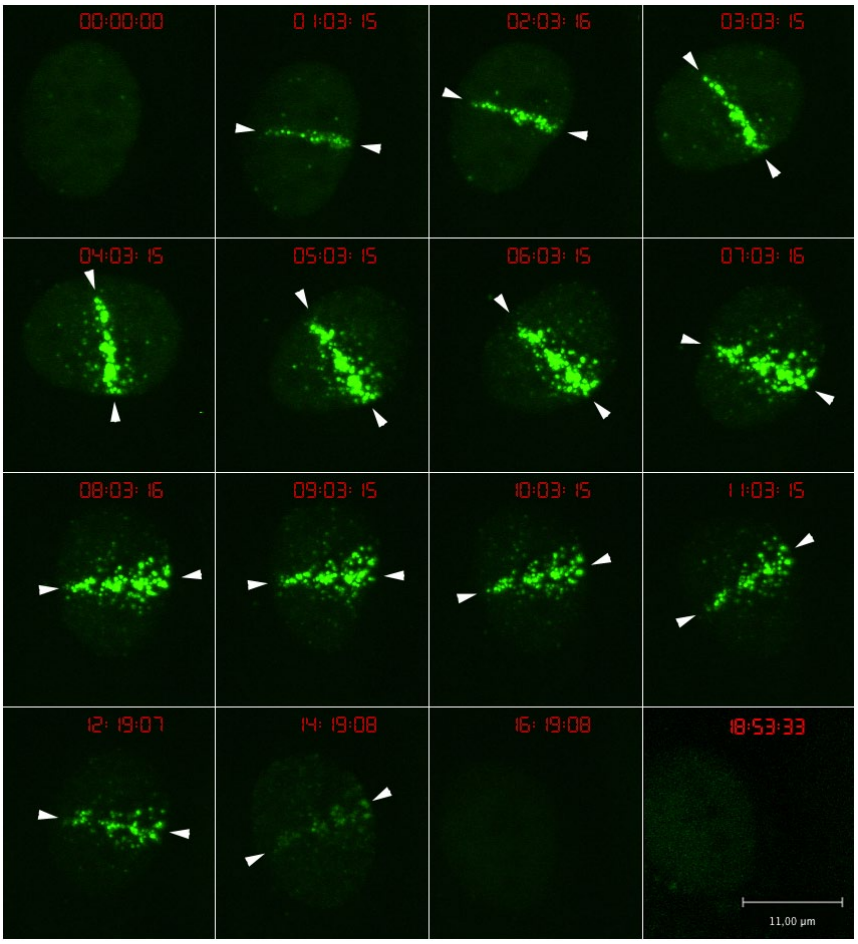

Fig. 4-74: Nucleus of a U2OS cell stably expressing Rad52-GFP damaged by laser microirradiation. After damage induction, a huge recruitment of Rad52-GFP towards the damaged chromatin was visible followed by a complete dissociation of Rad52-GFP leading to a homogeneously stained inconspicuous looking nucleus. (Arrowheads point at the damage track)

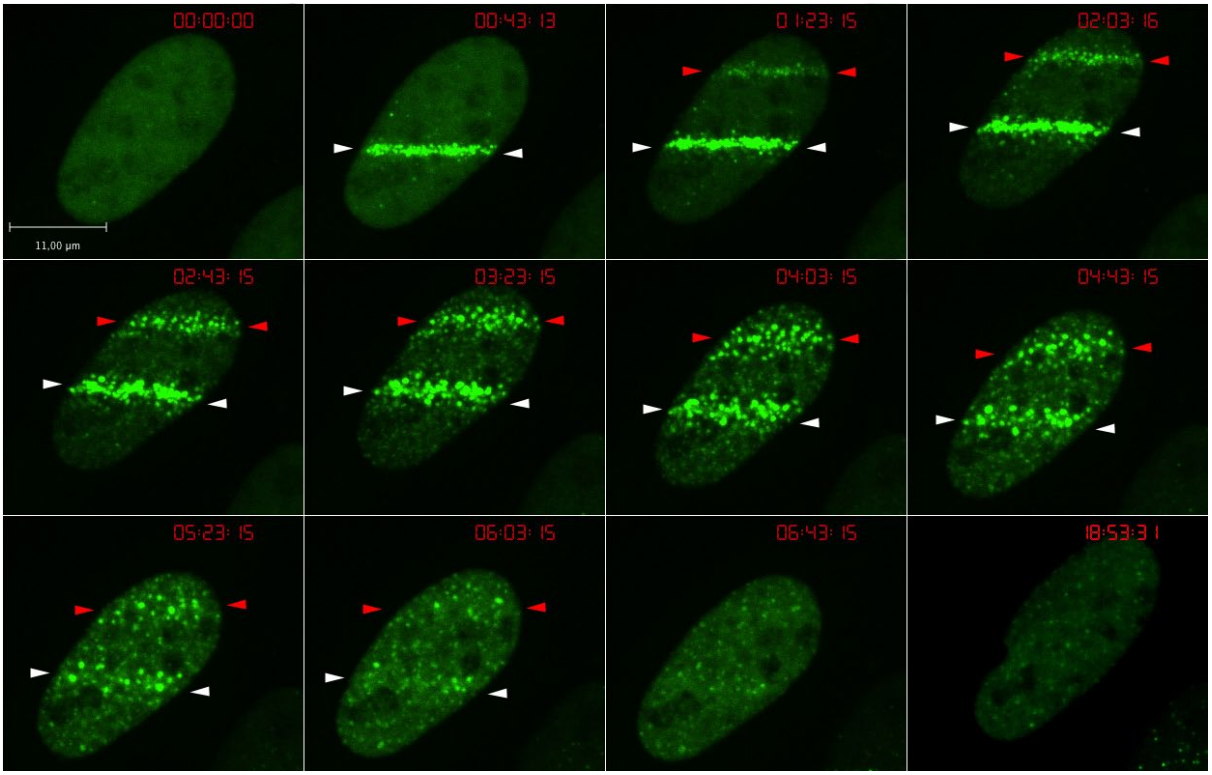

Fig. 4-75: Nucleus of an U2OS Rad52-GFP cell showing disappearance of damage foci from two independently induced damage tracks. Note that of both damage tracks dissappear simultaneously (marked by white (1st damage) and red (2nd damage) arrowheads) although they were induced at different time points. (Arrowheads point at the damage track).

Fig. 4-76 shows a diagram in which the sequence of events in the three shown examples (fig. 4-73 – fig. 4-75 and movie S9(a-c)) are compared on a time scale. Except for the order of events no general temporal pattern could be detected. Of particular interest is, that in fig. 4-75 the foci of both damage tracks, which were induced at separate times, disappear simultaneously. This argues for a nucleus-wide control of this phenomenon similar to the system that switches the cell cycle from one phase to the next. Although the positioning of nucleoli and damage tracks didn't seem to change dramatically, 3D analysis revealed a change in nuclear shape during the phase in which the foci emerged adjacent to the original damage tracks (also visible in fig. 4-77 (click on the figure for rotatable 3D reconstructions in the 3D PDF version)). This change was expressed by an increased nuclear height and a decreased area covered by the nucleus.

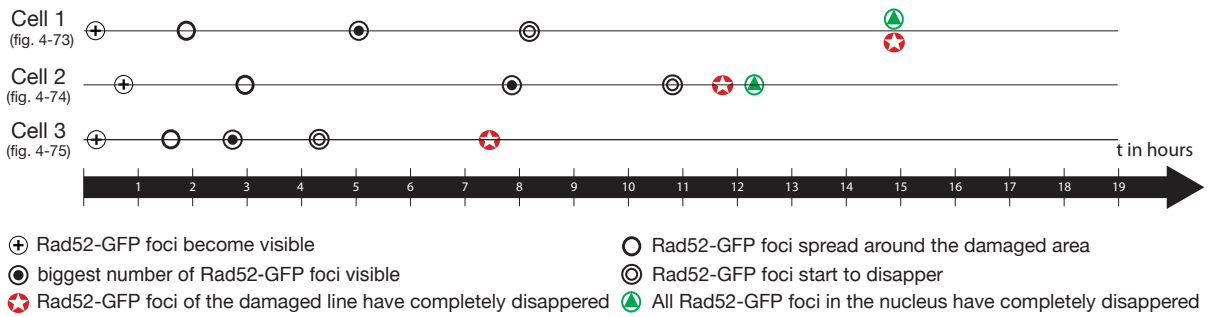

Fig. 4-76: Time line comparing the incidence of events in the irradiated U2OS Rad52-GFP cells, shown in the last three figures. The diagram shows that apart from the order of events no similarity is detectable in timing between the three observations.

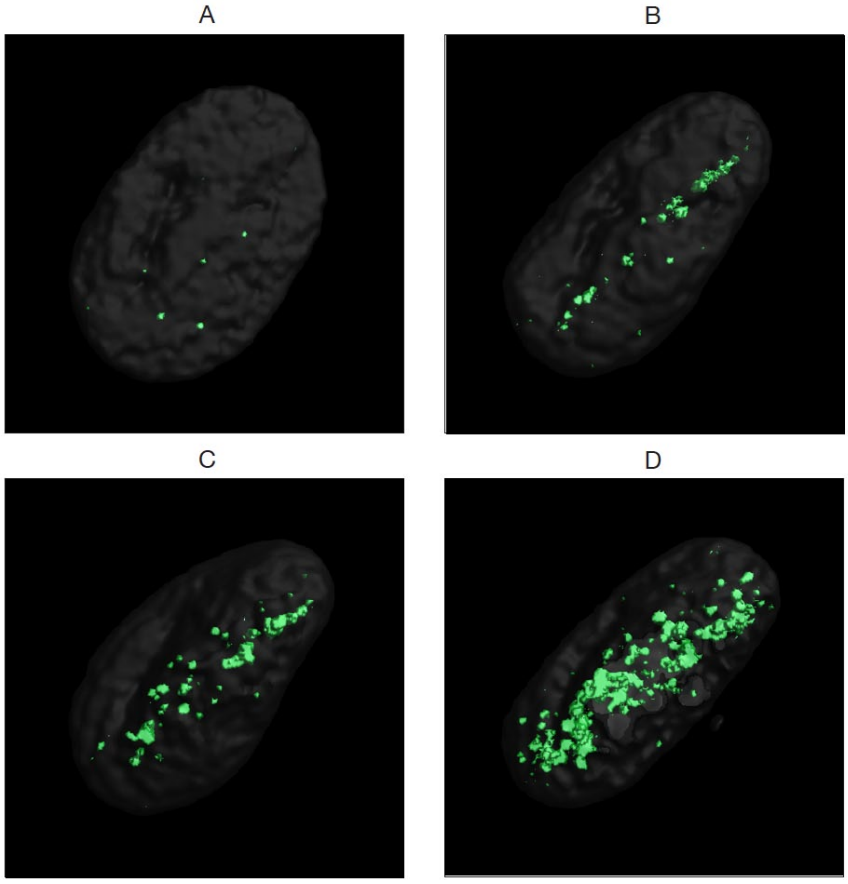

Fig. 4-77: 3D Reconstructions of the U2OS Rad52-GFP nucleus (shown in 4-73) after (A) 0 min, (B) 3 h 10 min, (C) 6 h 36 min, (D) 10h. In this example the nucleus enters a phase in which the number of Rad52-GFP foci dramatically increases even distant from the microirradiated part of the nucleus. This figure focusses on the changes in nuclear shape that happen during this phase. (click on the figure in the 3D version to start 3D mode).

4.3.5 Increased chromatin mobility after DNA damage isn't a general feature in cells

As already mentioned in the last section, the cells in which the Rad52-GFP foci disappear, show strange dynamics in foci distribution just before they become invisible. Numerous publications (Abdel-Halim et al., 2004; Abdel-Halim et al., 2006; Abdel-Halim et al., 2005; Monajembashi et al., 2005) reported specific pairing of homologs (close to the centromers) shortly after DNA damage by ionizing radiation, H_2O_2 or Mitomycin C, which argues for a cellular mechanism carrying out big and directed changes in nuclear architecture. Encouraged by the preceding findings which demonstrate reversible changes in nuclei caused by nuclear rotations (see 4.1.2.4) and the observation of dramatic Rad52-GFP foci disappearance in U2OS Rad52-GFP cells, it seemed promising to check whether the strong dynamics in fig. 4-73, fig. 4-74 and fig. 4-75 are accompanied by pronounced nuclear changes. To test for this, a cell line (RPE1 stably co-expressing Rad52-GFP and CENP-B mRFP) in which kinetochores were used as land marks, was laser microirradiated and observed over an extended period of time.

Of about 100 observed cells not one single cell showed complete disappearance of all damage induced foci although the observation period comprised nearly 60 h. A smaller fraction of nuclei (four) at least showed disappearance of most of the foci. The time series in fig. 4-78 shows one of these nuclei that was imaged for nearly 60 h and in which most of the damage induced foci (except for some at the nuclear rim) disappeared during the observation period. Unfortunately the image acquisition was interrupted for 12 h (microscope was booked by somebody else) but due to the very little movements of the centromeres over time it was still possible to identify individual

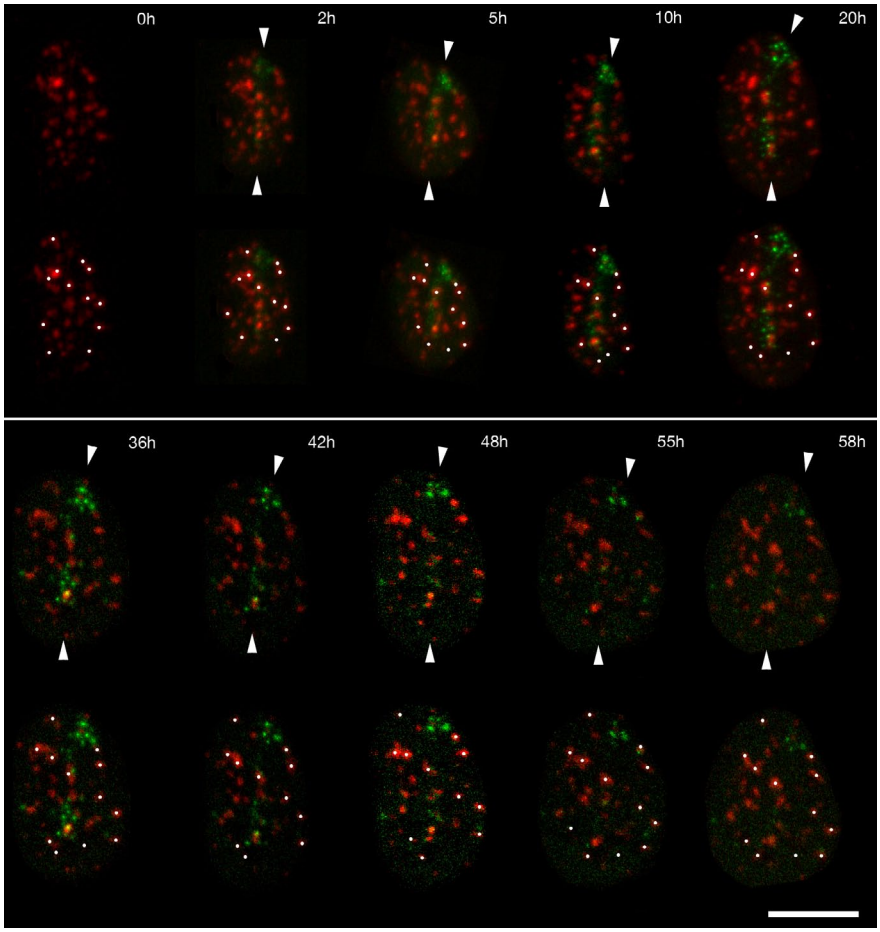

Fig. 4-78: Long-term live-cell observation of a RPE1 Rad52-GFP CENP-B-mRFP nucleus that was damaged using laser micro irradiation. While the damage foci along the track (**green**) nearly completely disappear over time, the patterns of the kinetochores (**red**) that are used as landmarks in this experiment remain almost unchanged. In the **upper row of each panel** the damage track is visualized by two arrow heads pointing at each other, the **lower panels** emphasize on the geometry of selected centromeres).

centromeres at each recorded time point.

In contrast to the observation of the U2OS Rad52-GFP cells this cell behaved differently in several ways:

1. after nearly 60 hours some of the initial foci were still visible
2. Rad52-GFP foci did not disappear simultaneously
3. the phase in which foci emerge aside of the original damage track is absent or by far much less pronounced than in the U2OS Rad52-GFP line
4. the nucleus broadens (flattens) continuously during the whole observation period.

It is at present not clear, why this cell line behaves so differently from the U2OS Rad52-GFP line. Maybe the different behavior reflects differences in the used cell types or the use of an additional fluorescence channel. Despite of that – and focussing again at the original goal of the experiment – it can be stated that the pattern of centromeres remained stable over the whole time lapse series except for some minor changes that can be explained by changes in the nuclear shape (especially within the first 20 h) and continuos broadening accompanied by flattening of the nuclei. This result is in concordance with other long-term observations after DNA damage induction presented in this thesis. A large-scale movement of a single kinetochore after DNA damage could not be observed neither shortly after damage induction, nor over extended time intervals. In terms of nuclear architecture these findings argue against active large-scale movements of chromatin domains towards preassembled DNA repair factories (time-stable irradiation pattern) and against an active movement of repair factories towards the damage (damage foci appear at the expected sites). The present observations rather argue for a model in which the repair machinery assembles directly at the DNA lesions (Solimando et al., 2009).

4.3.6 Fluorescence signals of damaged chromatin and kinetochores are mutually exclusive

While observing the damaged nuclei of the RPE1 Rad52-GFP CENP-B-mRFP line shown in the previous section it became apparent that Rad52-GFP foci and signals of the centromeres seem to exclude each other mutually in all observed nuclei.

To test for mutual exclusion mathematically the evaluation method "Product of the Differences of the Mean" PDM (Li et al., 2004) (see fig. 4-79) was applied to 3D stacks containing pictures of laser damaged nuclei taken from the cell line mentioned above. The method which is implemented in the ImageJ plug-in "Intensity Correlation Analysis" (which was used to generate the diagrams in fig. 4-80) works as follows: for each voxel a PDM value is generated that is defined by the equation:

$$PDM = [RedIntensity(Current\_Voxel) - RedIntensity(Average)] \times [GreenIntensity(Current\_Voxel) - Green\ Intensity(Average)]$$

Surprisingly the first impression obtained by visual inspection is also reflected by quantitative 3D evaluation. In fig. 4-80 the evaluated nuclei are shown as a z-projection in the left column. Since both of the signals to be evaluated represent distinct structures of high fluorescence intensity and since excessive fluorescent proteins often contribute to the background level, the nuclei were pre-processed by applying a modest threshold. The two middle columns of fig. 4-80 show diagrams in which the intensity values of the red (second column) and the green (third column) channel are plotted as functions of the PDM value. The right column of fig. 4-80 shows the in-situ distribution of the PDM values. Outlines of the cell nuclei are depicted by dotted lines. The diagrams shown in the central columns clearly indicate that voxels at high intensity levels possess negative PDM values in both channels – and that voxel intensity and PDM values are inversely correlated.

In order to demonstrate of how the diagrams look in case of positive PDMs the Rad52-GFP channel of example G was evaluated against itself in G'.

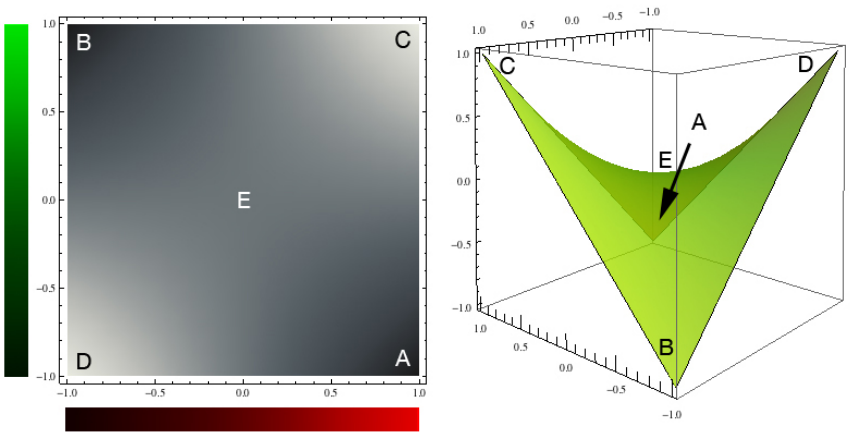

Fig. 4-79: Density and 3D Plot to explain the PDM equation. For reasons of demonstration both channels (red and green) were chosen here to have the same dynamic range and average intensity distribution. The mean value of the red and the green channel was set to half of the maximal intensity. Bright areas indicate positive PDM values; dark areas indicate negative PDM values. Assumed a voxel is exclusively red (A) then the first factor of the PDM term is positive, the second negative so the PDM value will be negative. In exclusively green voxels (B) the first factor is negative, the second positive; the PDM is negative again. Voxels which are bright for both channels (C) or both by far darker than the average brightness values (D) have positive values When a voxel has the average green and the average red value then the PDM is zero (E).

Distribution of the PDM values in the nucleus, shown in the right column indicate additionaly, that both of the signals (kinetochores and Rad52-GFP foci) have negative PDM values – even if they are in close vicinity.

Whether Rad52-GFP is the only protein that locates

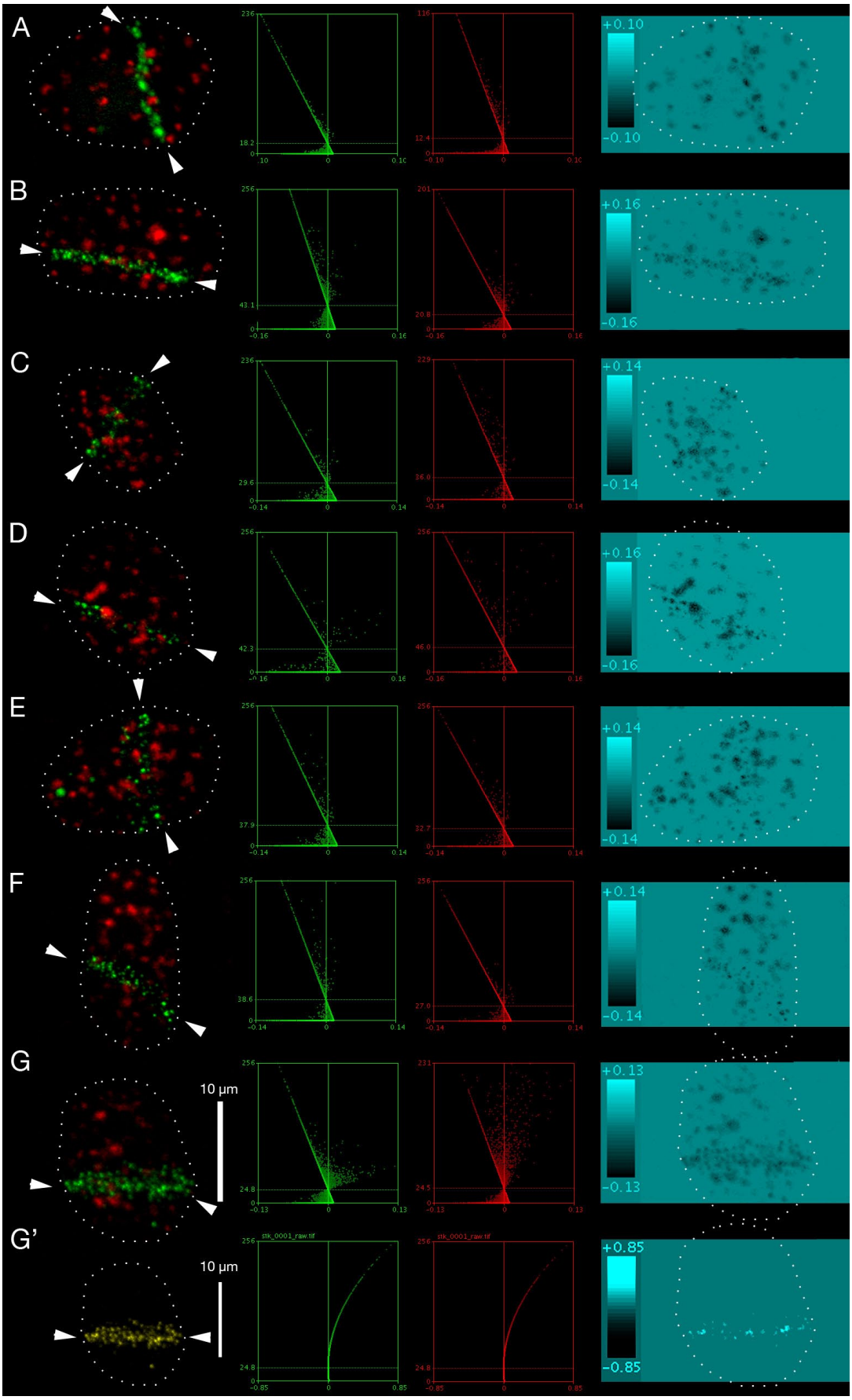

Fig. 4-80: PDM evaluation of laser micro irradiated RPE1 Rad52-GFP CENP-B mRFP nuclei. While the first column shows pictures of the nuclei that were evaluated, the two middle columns show diagrams in which the voxels of the green and red channels are plotted according to their intensity (y-axis) and their PDM values (x-axis). Example G' serves as a control and shows throughout positive PDM values generated by using the PDM-method on identical pixel distributions (two times green channel of example G.). The right column shows the localization of the different PDM values in-situ (z-projection). (Arrowheads point at the damage track)

mutually exclusive with respect to CENP-B mRFP has to be found out in future experiments. Preliminary studies in which nuclei of U2OS CENP-B-GFP cells were irradiated with a line pattern at the particle accelerator showed hints for a mutual exclusiveness between γ-H2AX and CENP-B-GFP, too (fig. 4-81).

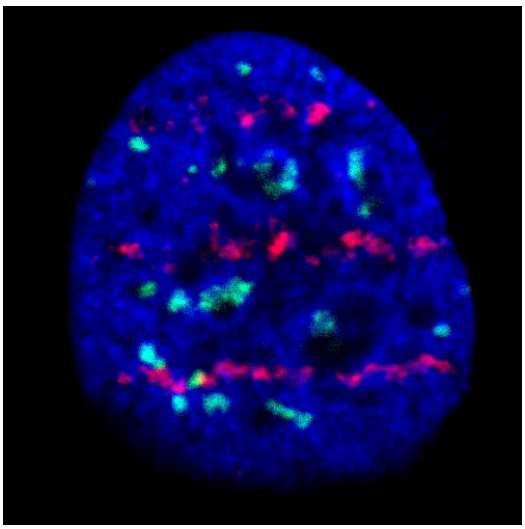

Fig. 4-81: U2OS nucleus irradiated at the Ion microbeam with C^{5+}-ions in a line pattern (1 µm x 5 µm) shows mutual exclusion of γ-H2AX signals (red) and centromere signals (green) (taken from a confocal image mid section).

Since it can be assumed that centromeres (DNA sequences at which the kinetochore-proteins like CENP-B bind) are damaged by irradiation with intensive laser light (or high energetic particles) to a similar extent as other parts of the genome it is unclear why Rad52-GFP damage foci have not been observed at these structures. Due to the fact that centromeres comprise highly repetitive sequences which are often in close association with centromeres of other chromosomes and embedded within constitutive heterochromatin it is possible that damages in this regions are repaired by other repair proteins than those involved in homologous repair. Homologous repair of highly repetitive clustered DNA sequences could easily result in genetic instability (deletion or translocation of chromosome parts).

The same might be true for nucleoli which represent another nuclear compartment that contains large amounts of repetitive rDNA and which is void of DNA damage foci (produced by the proteins and modifications mentioned in this work), too. Both centromeric chromatin and nucleoli are nuclear structures of high density. Apart from the possibility that these structures might be repaired by other proteins, it is tempting to speculate whether establishing a nuclear environment like it is assumed for repair foci might be lesser required at these places, too.

5 Discussion

In the course of this thesis cellular dynamics were studied *in vivo* over extended time periods up to 60 hours. Thanks to these observations it was possible to obtain new insights into the dynamics of interphase, DNA damage repair, and mitosis. As already mentioned in the *Introduction* and demonstrated in the *Results*, live-cell microscopy can help to augment the understanding of dynamic cellular processes and complement/verify results that were obtained from approaches using fixed cells. But before the results of this thesis will be discussed in detail, it is worth while to make some general remarks about cell lines and cell culture conditions since these represent the fundament of this work.

5.1 Working with cultured cells

Today most of the research performed in the biosciences intends to draw general conclusions from experiments performed with a model organism. This model organism represents per definition the wild-type case. While for a multitude of explored aspects this might be unproblematic, there might be some other instances in which the used model organism represents an exception to the rule or behaves differently under the used experimental conditions. This might bias the results and lead to wrong conclusions.

Since culturing of cells derived from multicellular organisms was first successful in 1907 (Harrison, 1907), it was possible to grow and study different cell-types isolated from their host organism. While this achievement represents a big milestone in biomedical research and has become a standard technique, most of the researchers take it for granted and don't pay too much attention to its influence on the experiment. However there is little doubt that for e.g. the majority of metabolic experiments might deliver solid results with most of the established culture cell lines under standard cell culture conditions but results for answering other questions e.g. on nuclear architecture or signal transduction might be biased by certain oddities of a cell line which do not represent the general case. Apart from the various cell types of different tissues in an organism that behave differently because of their specialization to (to fulfill a certain function), cell culture conditions might change properties and behavior of cells profoundly because they are different from the conditions that prevail in a living organism.

Although cell culture tries to simulate the situation as it is in an organism e.g. by using the same temperature and pH, it clearly differs from the natural *in-vivo* environment with respect to the following points:

Whereas most of the adherent non-cancer cell lines grow in cell culture as a contact inhibited single layer, they are surrounded by other cells in a three dimensional context in their original tissue. This has the advantage that they are not exposed so much to oxidative stress radicals from the surrounding medium (Halliwell, 2003) and that they are able to exchange information via cell-cell contacts with cells of another (or the same) kind.

Although a lot of work has been invested in creating (sometimes cell type specific) growth media, the supply with nutritions differens profoundly between cell culture and organism. While the cells in an organism are constantly fed and constantly obtain factors that are optimized for the organism/tissue they are living in, cells in culture are usually fed once per subculturing step with medium that is supplemented with fetal calf serum. This – beyond doubt – contains a multitude of growth factors but certainly not the cell type specific ones at the same concentrations which are present in the original tissue. During the time until the next subculturing the amount of nutrients within the medium constantly drops while metabolic degradation products accumulate and are not constantly removed as in a living organism. While this circumstance can have an effect on the cell's behavior and gene expression, additional stress can be caused by colored pH indicators like phenol red that are used indicate when the nutrients are metabolized and the medium should be exchanged. Especially for live-cell observations this can cause a problem since phenol red can cause oxidative stress while being exposed to bright light.

While cells in an organism are accessible for the immune defense system which eliminates cells that do not conform to the demands of the tissue any more, mutations in cultured cells can accumulate. Some of these mutations represent successful adaptions to the selection pressures of cell culture and thus represent an advantage over other cells which still show the wild-type features.

Since the consequences of this "micro-evolution" result in only little or no morphological changes in many immortalized, tumor derived and cultured wild type cell

Fig. 5-1: M-FISH performed on three metaphase spreads of the same U2OS cell line. Note the substantial differences between the karyotypes although the metaphases were obtained from the same culture flask.

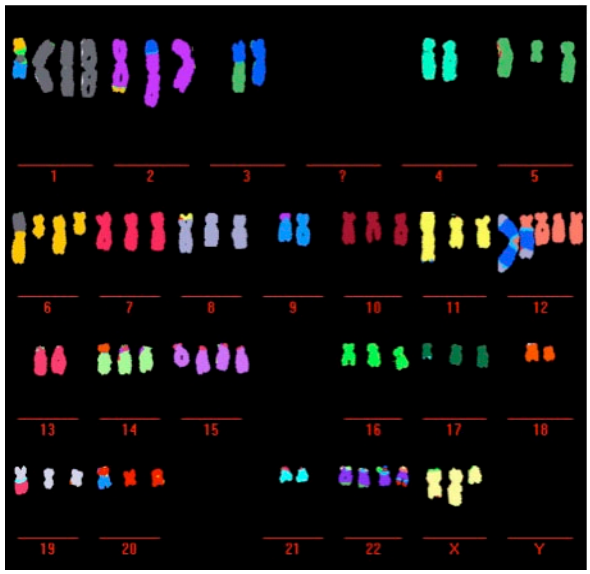

Fig. 5-2: Karyotype of a HeLa cell line with ca. 70 chromosomes.

lines (that underly the HAYFLICK limit), the genome of many cell lines, often show numerous and complex rearrangements (fig. 4-5, fig. 5-1 and fig. 5-2).

Fig. 5-1 shows three karyograms that were obtained applying multicolor FISH (LICHTER, 1997) on metaphases of one and the same an U2OS "cell line" (from even one and the same culture dish!). The pronounced differences seen within these three karyograms serve as an example of how big the genetic variability within one "cell line" can be at the single cell level.

The U2OS-line is a popular bone cancer derived cell line that is frequently used in cell biology, molecular biology and radiation biology. It is esteemed for its easy handling, its wild-type p53 and its ability to easily take up transgenic DNA into its genome. This property and also the reason for its grossly rearranged karyotype most probably relies on the way this cell lines has gained immortality. In contrast to most tumor derived cell lines the U2OS line is telomerase negative and its immortalization is achieved by a mechanism called "alternative lengthening of telomeres" or ALT-mechanism (HENSON ET AL., 2002). This mechanism comprises the lengthening of telomeres using APBs (ALT associated PML-bodies containing PML bodies, extrachromosomal telomeric DNA, telomere specific binding proteins and proteins involved in recombination and DNA repair) (NABETANI AND ISHIKAWA, 2009).

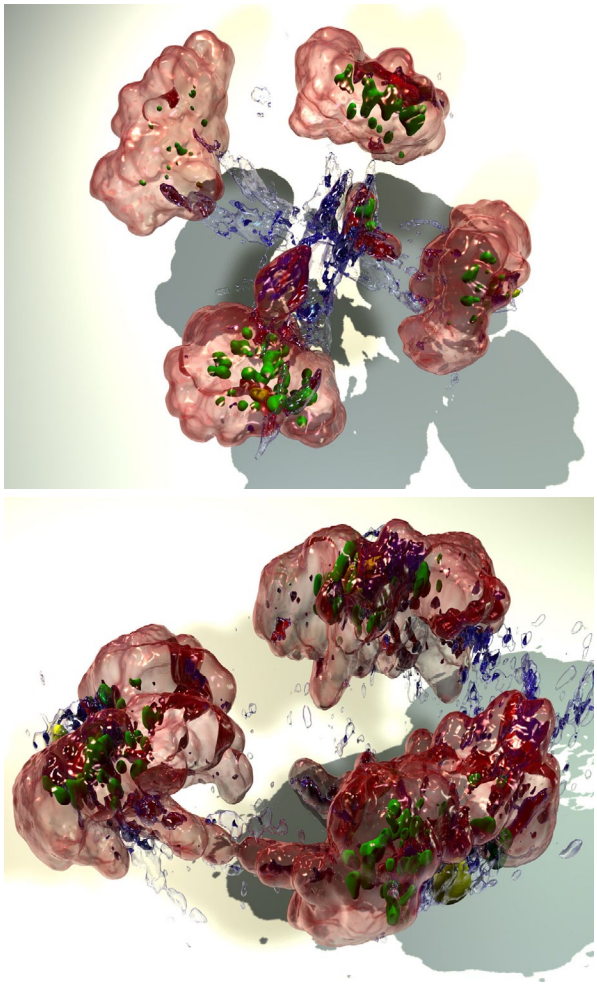

Fig. 5-3: Abnormal mitotic divisions in cultured tumor cells can sometimes lead to more than two daughter nuclei resulting in cells with different karyotypes within the same population. This complicates conclusions about nuclear architecture – especially when analysis is carried out by methods that need thoudsands of cells. (Pictures own work, rendered with Blender. Red: chromatin, blue: microtubules, green: kinetochores, yellow: centrosomes)

Because a lot of assays used in biochemistry and molecular biology require thousands or millions of cells, they cannot detect individual differences between cells or even multiple cell sub-populations (like presented in fig. 5-1). This can lead to problematic results and scientific confusion when information obtained from those assays (performed on heterogeneous abnormal cells) are generalized.

Another example which shows the problems of using cultured tumor cells for generation of general results can bee seen in fig. 4-32 and fig. 5-3.

Abnormal mitotic divisions resulting in three or four daughter nuclei can be observed in many cultured tumor cell lines. Since the products of multipolar mitoses in healthy organisms are doomed because of their incomplete and aneuploid genome, the redundancy in the (often) mixed-up genome of cultured tumor cells, their collapsed check-points,

broken cell signaling pathways and the minimum of functions that are required for cells to grow in culture allow those *"freaks"* to survive. It doesn't take much to realize that evaluations on e.g. nuclear chromosome distributions based on an inhomogenous culture containing genetically different sub-populations of cells might lead to problems.

Despite of being fully aware about these problems and despite of the use of cell friendly culture conditions and cutting-edge imaging equipment it cannot completely ruled out that some of the results presented in this thesis (and most of all other theses) represent exceptions to the rule and cannot be generalized!

5.2 Evidence for Boveri's hypotheses (1909)

The following paragraphs contain text fragments that are also used in (Strickfaden et al., 2010).

The live cell study of cycling RPE1 cells presented in this thesis gives direct experimental support for four hypotheses first proposed by Theodor Boveri with respect to the dynamics of chromosome territory arrangements in cycling blastomeres of *Parascaris equorum* (Boveri, 1909, see Introduction). In support of hypothesis I it was possible to provide evidence for the already widely accepted concept of chromosome territories (see 4.1.2.1). Also hypothesis II which states persistent proximity patterns of CTs during interphase could experimentally be verified for most of the RPE1 cell nuclei (see 4.1.2.2-3). Unexpectedly, however, complex nuclear rotations could occasionally be observed in cells, which led to at least transient, major changes of chromatin proximity patterns, whereas chromosome neighborhood arrangements were always maintained (see 4.1.2.4-5) (Strickfaden et al., 2010). Possible implications of this finding for the formation of specific long-range DNA interactions in trans (Lieberman-Aiden et al., 2009; Lin et al., 2009; Schoenfelder et al., 2010) are discussed below.

In support of hypothesis III profound changes of chromosome proximity patterns during prometaphase could be demonstrated (see 4.1.2.6-8). A randomizing effect of prometaphase on chromosome proximity patterns was well established in previous studies and can be explained by a random order of spindle attachment to the kinetochores of individual prometaphase chromosomes (Alexander and Rieder, 1991; Chaly and Brown, 1988; Kanda et al., 1998; Manders et al., 1999). Due to the stochastic nature of the spindle attachment, widely separated kinetochores can become attached at an earlier time point than juxtaposed kinetochores. Prometaphase chromosomes connected to the spindle apparatus immediately start to move and thus are driven away from originally juxtaposed, but still unconnected neighbors. The varying positions of centrosomes introduce another stochastic component. In some prophase cells the centrosomes were observed close to each other at one side of the nucleus, in other cells they were found in deep invaginations of the nuclear envelope or at opposite sites of the nucleus (see 4.1.2.11).

In experiments, in which the two halves of prophase nuclei were bleach-labeled in different colors, (Gerlich et al., 2003) claimed that the relative positions of chromosomes "both during prometaphase congression, as well as in anaphase and telo-

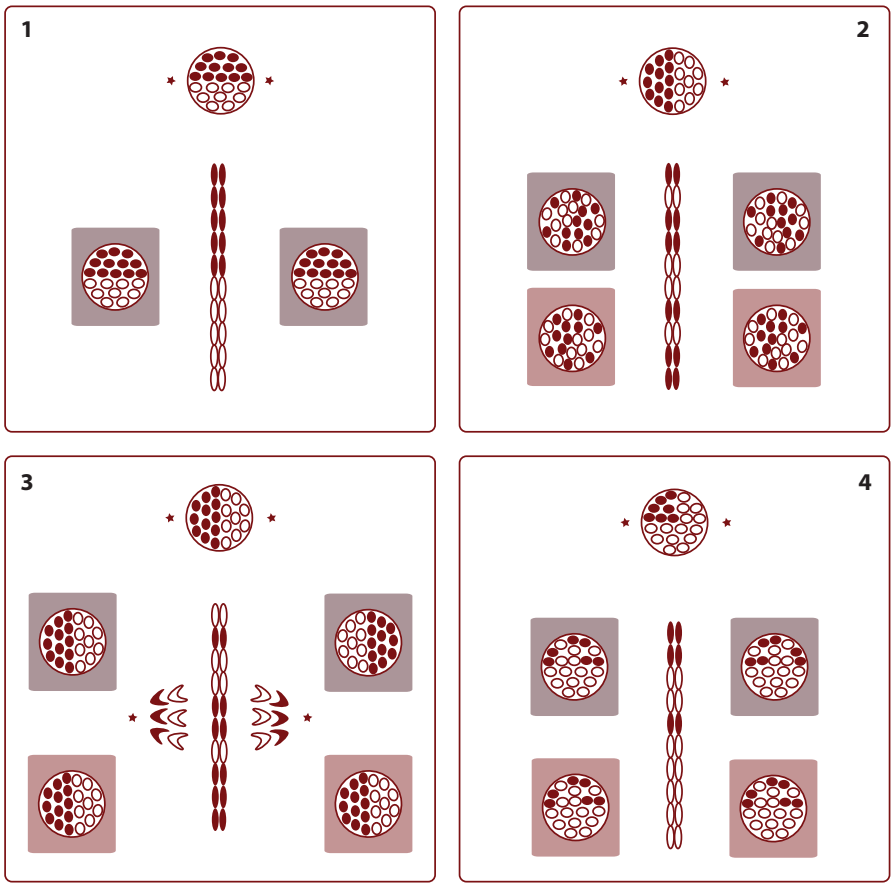

Fig. 5-4: Schematic drafts of different models on how chromosomes might be distributed through mitosis. While model (1), (2) and (4) could be experimentally confirmed within this thesis, no evidence could be found for model (3) proposed by (Gerlich et al., 2003).

phase" were preserved, when the orientation of the labeling boundary was chosen parallel to the spindle axis (fig. 5-4(1)). In contrast, when the labeling boundary was chosen perpendicular to the spindle axis, they reported that the differently labeled chromosomes became "intermixed" from prometaphase to metaphase. In anaphase and telophase, however, (fig. 5-4(3)) "the original global pattern of the mother cell was restored." The results of this study are in disagreement with the interpretation proposed by (Gerlich et al., 2003), who apparently took for granted that contiguous areas of labeled chromatin transmitted from a mother nucleus to its daughters indicate a high preservation of CT proximity patterns within these contiguous areas. Instead, the experiments presented in this thesis unveil that the extent of changes of proximity patterns observed during prometaphase was independent from the spindle position and that both parallel and perpendicular labeling patterns in prophase nuclei yielded the same extent of intermixing (see 4.1.2.8).

In support of hypothesis IV it could be demonstrated that the new proximity patterns of chromosomes established in the metaphase plate persisted largely through anaphase and telophase yielding similar CT proximity patterns in RPE1 daughter cell nuclei (see 4.1.2.9, fig. 4-27&35). In agreement with previous studies (Cvacková et al., 2009; Walter et al., 2003), the patterns observed in daughter nuclei differed considerably and often strikingly from the pattern originally induced in the mother nucleus (see 4.1.2.6). Although chromosome proximity patterns in mother nuclei were not entirely randomized in the resulting daughter nuclei (Cvacková

et al., 2009; Walter et al., 2003), it was not possible to confirm the anaphase-mechanism proposed by (Gerlich et al., 2003) as a means to counteract the loss of proximity patterns at prometaphase. Although these authors conceded, "that the accuracy of transmission is not 100% and that strict transmission of order will be diluted further over several cell cycles", they emphasized that the proposed anaphase mechanism would "facilitate the maintenance of global patterns of gene expression in mammalian cells" (Gerlich et al., 2003; Gerlich and Ellenberg, 2003). The kind donation of the NRK cell line (by jan ellenberg EMBL, Heidelberg) studied in Gerlich and Ellenberg, (2003) allowed to test whether a substantial difference in the transmission of CT proximity patterns exists between cycling RPE1 cells and NRK cells. In agreement with previous results of bleach-labeling experiments performed with HeLa cells (Walter et al., 2003), bleach-labeling experiments of small areas in NRK prophase nuclei, affecting segments from several vicinal prophase chromosomes, yielded daughter nuclei with more or less widely scattered bleach-labeled chromatin segments (fig. 4-26).

In a complementary study performed by thomas cremer's group in collaboration with the group of roland eils (Heidelberg) a landmark-based registration method was used to measure the similarity of CT arrangements visualized by multicolor 3D FISH in cell clones from different human cell types (2-cell clones from diploid human fibroblasts, 4-cell clones from diploid human mammary epithelial cells (HMEC) and HeLa cell clones (up to 32 cells). In order to distinguish pairs of daughter cells unequivocally from 1st grade cousins, the growth of 4-cell clones was monitored in vivo (Köhler et al., 2011) (in preparation). Although far from perfect the similarity was significantly higher in daughter nuclei compared to 1st grade cousins. Two or three mitotic events were sufficient to dilute the global transmission of chromosome proximity patterns to an extent that the similarity within a given clone was not significantly higher than between unrelated clones from the same culture.

Taking a look at fig. 4-27 shows that the similarity between both daughter cells can partially be decreased by the different positions which nascent daughter nuclei can take during the decondensation of the mitotic chromosomes when the cells begin to flatten in telophase. While the left nucleus shown in fig. 4-27 origins from an anaphase rosette falling freely to one side, the right anaphase rosette decondenses in a still upright position and just flattens from this starting position. It appears like during this kind of flattening the chromatin is dispersed like a doe and the photoactivated chromatin are pushed shuffled to some extent during this dispersion process. This gives room for speculations to which extent the degree of similarity in daughter cells depends on the symmetry between the separated daughter - nuclei in the second half of mitosis.

5.3 Probabilistic CT proximity patterns and non-random radial arrangements

In contrast to probabilistic CT proximity patterns, radial chromatin arrangements seem to be stably maintained in nuclei of cycling cells from evolutionary distant animals, including mammals (Bolzer et al., 2005; Grasser et al., 2008; Küpper et al., 2007; Neusser et al., 2007), birds (Habermann et al., 2001), *Drosophila melanogaster* (Lowenstein et al., 2004), the early metazoan *Hydra vulgaris* (Alexandrova et al., 2003) and the spirotrichous ciliate *Stylonychia lemnae*, as an example of a single cell eukaryote (Postberg et al., 2005). Gene poor, mid–late replicating facultative heterochromatin as well as clusters of constitutive heterochromatin is typically enriched beneath the nuclear lamina, while early replicating, gene dense, transcriptionally active chromatin is located in the nuclear interior.

While the publications mentioned above were performed mostly by 3D FISH chromosome painting of single pairs of distinct, whole chromosomes in fixed cells, the experiments presented in chapter 4.1 show cases in which chromatin in flat-shaped RPE1 nuclei was photoactivated at various positions proximal or distal to the nuclear rim and then subsequently traced through mitosis. It is important to point out that these two kinds of experiments are different from each other.

Since distribution curves for pairs of painted chromosomes origin from averaged information (in general from about 30 cells), they exhibit a pronounced variance with respect to their radial position in the nuclear volume. This indicates that in principle chromosomes that are e.g. more frequently located in the interior of a nucleus might – in some less frequent cases – also be found at the nuclear rim and vice versa. Radial distribution curves are most often produced from the measurement of only one (or few), painted chromosome pairs at a given – frozen – time point and show the distribution of these chromosomes in interphase cells, in general regardless of their cell cycle phase, their genealogical background and other individual properties that can differ between cells.

In contrast to this, the experiments performed in this thesis trace arbitrarily photolabeled chromatin belonging to multiple, unknown chromosomes from the mother nucleus to its daughter nuclei.

The big differences between both approaches are: while the 3D FISH approach maps the distribution density of individual chromosomes within the nuclear volume, the *in vivo* approach allows the comparison of the distribution of multiple, unknown chromatin domains between mother and daughter nuclei in a single observation.

Because the *in vivo* approach can hardly discriminate between eu- and heterochromatin without further modifications and due to the fact that with every new experiment another set of chromatin domains is photoactivated, this approach appears *not* to be appropriate to make conclusions about the radial distribution or its conservation.

Despite the problems mentioned above, the experiments illustrated in fig. 4-24 in which chromatin was photoactivated at the nuclear rim of a living RPE1 cell in prophase, showed an interesting feature. Although scattered fluorescent patches were distributed all over the 2D projected nuclear area, they were nearly all still associated

with the nuclear envelope (fig. 4-24(f)). It is tempting to interpret this observation in a way that the topography of chromatin associated with the nuclear envelope is stably maintained in cycling RPE1 cells. However, since the nuclei of these cells are flat-shaped, RPE1 cells don't seem well suited for studying 3D radial arrangements of chromatin for different reasons:

- Having a hight of ca. only 3 µm makes it difficult for conventional light microscopes which have an axial optical resolution of about 500–800 µm to segment the flat nuclei into a number of different shells that would allow a reasonable evaluation of 3D radial distribution.
- Looking at tree dimensional nuclei of this cell type (fig. 4-20) shows that the nuclei seem to be composed to a big extent of only a bottom- and a top layer of chromosomes (one shell of chromosomes). Assuming that this is also true for interphase nuclei with decondensed chromosome territories, it would be trivial to speak of a radial distribution, since most of the chromosome territories would belong to the "exterior" and the "interior" of the nucleus simultaneously.

Nevertheless there is one thing that could be explored with respect to radial distribution using a female celline featuring photoactivatable chromatin like the one that was used in this thesis.

There are studies that implicate that tethering of heterochromatin to the lamina might play a general role in nuclear architecture (Kumaran and Spector, 2008; Malik et al., 2010; Reddy and Singh, 2008). barr bodies (inactive X-chromosomes in female cells) are visible in interphase nuclei due to the high compaction level of their chromatin in cells expressing a fluorochrome tagged histone proteins (see 4.1.1.2). Very often they take a position within the nucleus that is situated next to the nuclear envelope (in other cases they are associated with the nucleoli). At present the mechanism how these structures maintain their radial position through mitosis is mostly unknown.

One possibility to approach this problem could be to use a female cell line, that expresses a histone tagged to a photoactivatable GFP and another histone that is tagged to another fluorescent protein (like the RPE1 H4 PA-GFP H2B-mRFP line). While one or multiple barr bodies are visible in interphase, one of them could be photoactivated and traced through mitosis. During mitosis when the other chromosomes are condensed and cannot be distinguished from the barr bodies, the photoactivated chromatin of the marked X-chromosome would allow identication of the chosen barr body until it gets visible again in the interphase chromatin of the daughter cells. Tracing of the barr body from one cell generation to the next could show when and how the silenced X-chromosomes are positioned at their place close to the nuclear envelope.

Unfortunately photoactivatable H4-GFP seems to be much lesser present in the inactivated X-chromosomes than in the rest of the chromatin (see 4.1.1.2). In case that its presence is too low in the barr bodies to perform the experiment described above PA-GFP might be fused to other histones like H3 (Müller et al., 2010). Whether the lack of H4-PA-GFP is an epigenetic peculiarity of the inactivated X-chromosome like the strong presence of macro H2A or the Histone 3 modification H3K27 is currently not clear.

5.4 The case for long-range chromatin movements

Several groups reported chromatin loops carrying specific clusters of genes expanding up to several micrometers away from the surface of their home CTs (Mahy et al., 2002b; Ragoczy et al., 2003; Volpi et al., 2000; Williams et al., 2002). Such an extrusion of a gene locus from a CT is not necessarily indicative of transcriptional activity, but also can reflect a poised state for activation (Ragoczy et al., 2003). Notably, the compaction level of one such giant loop studied in detail was about one order of magnitude higher than that of an extended 30 nm thick chromatin loop (Albiez et al., 2006). While protein diffusion of soluble proteins in the nucleus is sufficient to recruit proteins quickly to places where they are needed it is unclear which fundamental advantage the close association of chromatin originating from different chromosomes in trans might have.

It has been shown in many fluorescence microscopic studies that vital processes like DNA replication, DNA repair, transcription, splicing and processing of DNA take place in so-called "foci" which consist of huge accumulations of the same proteins. It could be shown that molecular crowding of macromolecules can influence the rate of biochemical reactions by mimicking higher concentrations caused by a virtually decreased volume (in the presence of many macromolecules) (Minton, 2006; Richter et al., 2008). Maybe the spatial organization of nuclear functions into foci represents some kind of compartmentalization into nuclear micro-environments in absence of membranes where the respective biochemical processes can be executed under optimal conditions or even exclusively. Maybe the organization of chromatin from different chromosomes in close proximity represents an effect that rises from a limited number of reaction foci. Once established, such foci could help to stabilize interactions in trans.

Except for a very small number of live cell studies (Chuang et al., 2006; Kumaran and Spector, 2008) (which all report that the formation of large scale chromatin interactions in trans is massively impaired by phototoxic effects), most of the data about giant loops origin from studies of fixed cells, thus very little about their temporal existence is known. While some studies report fast (sometimes transient) specific associations of certain genes upon stimulation with a certain substance (Hu et al., 2008; Mehta et al., 2010), others report positioning of chromosomes to be rather typical for a certain cell-line, differentiation (Brown et al., 2006; Kim et al., 2004) or developmental stage (Xu et al., 2006). The case of transitory long-range interactions would ask for an actively guided mechanism that navigates the genes of different chromosomes together. In case of the permanent loops early processes like gene transcription immediately at the end of mitosis could be thinkable for this phenomenon (which then might contribute to the fact, that genes of highly expressed genes have a tendency to move to the nuclear interior).

5.5 Chromatin diffusion

Live-cell microscopy performed with cultured mammalian and *Drosophila* cells directly demonstrated constrained movements (<2 µm) of sub-chromosomal domains (Abney et al., 1997; Bornfleth et al., 1999; Marshall et al., 1997), as well as long-range movements (<2 µm) (Bornfleth et al., 1999; Chuang et al., 2006). This distinction between short- and long-range movements, although, somewhat arbitrary, is based on the assumption that constrained Brownian motions may suffice for interactions between DNA segments with distances <2 µm, while movements >2 µm require more elaborate mechanisms, including energy dependent directed movements (Chuang and Belmont, 2007; Edelmann et al., 2001; Levi et al., 2005) and/or rotational movements (see below). Live cell data have strongly supported the results of 3D FISH experiments.

The chromatin diffusion that was observed in long-term observations of photoactivated lines in interphase cell nuclei (4.1.2.3) has confirmed and extended the findings of Wiesmeijer et al., (2007). Except for some confined diffusion the lines persisted nearly unchanged over extended periods during interphase. In some instances it was possible to observe smaller globular structures looping out about 2 µm from the edge of the photoactivated line. While this distance is possibly sufficient to establish "long-range interactions" in small, relatively unorganized yeast nuclei, it is by far too small to be called "giant loop" in mammalian nuclei which are in general 1000 fold bigger in volume than yeast nuclei (Misteli and Soutoglou, 2009).

Quantitative evaluations measuring the width of the lines over time based on a physical diffusion model allowed to quantify the average diffusion coefficient for chromatin (comprising hetero- and euchromatin). The physical model used here was derived from a work performed by volker hable and günther dollinger in which the diffusion of chromatin, damaged by high energetic ions at the SNAKE facility, was evaluated using HeLa cells, fixed and immunostained at multiple intervals after ion-beam irradiation. In contrast to this, cells used for this thesis were taken from a RPE1 line, growing almost confluent on an observation chamber in order to reduce pronounced cellular motility and cell cycle dependent effects that could bias the measurement. To answer the question whether chromatin diffusion is cell type dependent (e.g. different in ES cells in which the chromatin is rumored to "breathe" (Bhattacharya et al., 2009; Meshorer et al., 2006) from terminal differentiated cells with globular nuclei), or whether if there are functionally relevant differences in diffusion between eu- and heterochromatin, represents rewarding tasks for future research.

Searching the literature for chromatin diffusion constants shows that the values stated there are not homogenous but vary over a large range (Hable, 2004; Wachsmuth et al., 2008). One reason for this might be that the physical description of chromatin diffusion is much more difficult than it is for a simple liquid. Therefore it is crucial to find a mathematical model that includes as much of the physical data that known about chromatin in a living cell. In contrast to previously published conventional models it might be of advantage to generate new models taking into account the macromolecular nature of the nucleoplasm and molecular crowding. It would be interesting to see whether these new models might change the way we look at intracellular diffusion today.

5.6 Comments on Chromatin Conformation capturing methods

Chromosome conformation capture, first introduced by (Dekker et al., 2002), has provided compelling evidence for specific DNA-DNA interactions in cis and trans in cycling cells (Göndör and Ohlsson, 2009; Hu et al., 2008; Lin et al., 2009; Ling and Hoffman, 2007; Lomvardas et al., 2006; Noordermeer et al., 2008; Nunez et al., 2008; Osborne et al., 2007; Sexton et al., 2009; Simonis and De Laat, 2008; Simonis et al., 2006; Tiwari et al., 2008; Williams and Flavell, 2008; Zhao et al., 2006). The combination of circular chromosome conformation capture (4C) with DNA microarrays (Göndör and Ohlsson, 2009; Schoenfelder et al., 2010) or massively parallel sequencing (Lieberman-Aiden et al., 2009) has allowed for the first time mapping of DNA-DNA interactions in cis and trans at a genome wide level. Although DNA interactions in cis were found to abound, significant interactions in trans were detected in agreement with other studies cited above. This wealth of data, often substantiated by 3D FISH assays, has provided strong support for long-range interactions in cis, i.e. between genes located many Mbs apart on the same chromosomes, or trans, i.e. between genes located on different chromosomes.

Although the chromatin capturing methods offer new ways to examine chromatin interactions in cis and in trans it should be pointed out that these methods have to be applied very thoroughly in order to generate solid results. As this method uses big populations of fixed cells (ca. 20 million cells) (Hou et al., 2008; Schones and Zhao, 2008), results obtained from chromatin capturing thus represent an average of the interaction frequencies between different chromatin regions in a population. Since it was found in this thesis that chromosome proximity patterns are highly variable, and since during the protocol unspecific cross-links might occur, it is crucial to define a threshold mechanism that reliably separates significant (but possibly infrequent) interactions from background noise or unspecific interactions.

5.7 Implications of probabilistic CT proximity patterns for large-scale, non-random DNA-DNA interactions

In search for a mechanism, which explains the formation of specific, long-range DNA-DNA interactions in trans, the evidence discussed above for probabilistic CT proximity patterns in cycling cells, which result from the randomizing effect of mitosis, must be considered. A mechanism for such interactions requires long-range movements (> 2 µm) of the respective CTs and/or of chromatin loops carrying the genes in question. In an attempt to reconcile present evidence for long-range gene "kissing" events in trans during interphase with evidence for probabilistic CT neighborhood arrangements we consider four gene "kissing" scenarios (fig. 5-5(a–d)). In scenarios A and B we consider the demanding problems of directed long-range chromatin movements for gene "kissing" events in trans in such nuclei. It is utterly speculative at pre-

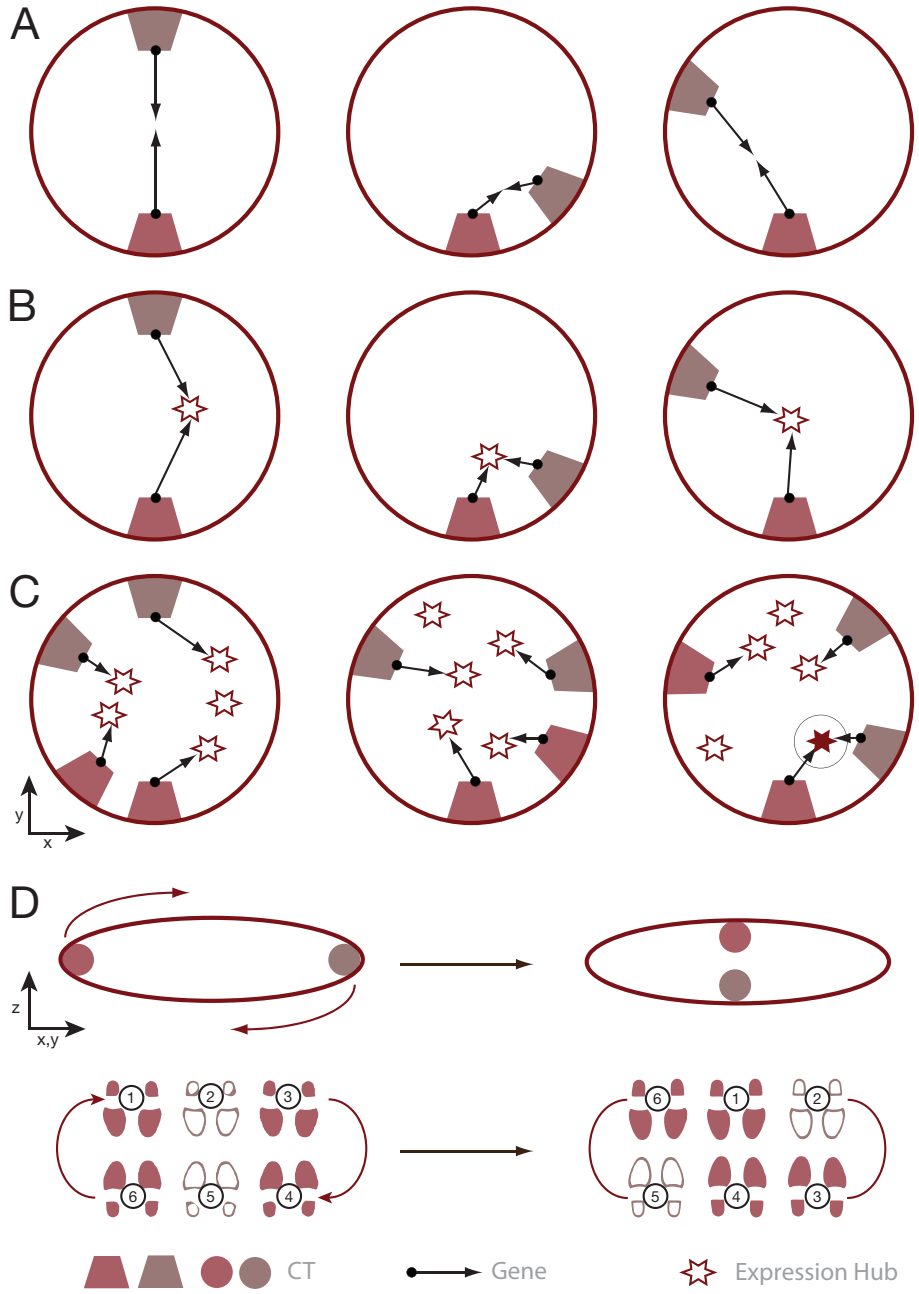

Fig. 5-5: Different models for long range interactions between chromosomes in trans. (A) Contact first model, (B) Factory first model, (C) Multiple factories model, (D) Shows how nuclear rotaion is able to bring chromatin domains that initially are distant from each other into close vincinity that allows direct interaction (see text for further explanation).

sent how the topographical information required for directed movements in trans can be gained and used. Scenario C considers a possibility, where constrained Brownian chromatin motions may suffice for the formation of functionally relevant DNA-DNA interactions in trans. In order to explain "kissing" events between primarily widely separated genes (>2 µm) (Chuang and Belmont, 2007; Wachsmuth et al., 2008) scenario D assumes a combination of large-scale rotational chromatin movements and short-scale constrained Brownian chromatin motions.

Scenario A (fig. 5-5(a)) describes a "contact first" model, which considers the possibility that widely separated genes initially need to come together and then form a

hub or specialized transcription factory at their meeting point (Alberts et al., 2008; Fraser and Bickmore, 2007; Kosak and Groudine, 2004) (compare fig. 4-66 in Alberts et al.). To some extent non-random radial chromatin arrangements may favor the de novo formation of preferential proximity patterns, since genes positioned in the nuclear interior are on average located closer to each other than genes located in the nuclear periphery and thus should have a better chance to be positioned close enough to each for a kiss enabled by constrained Brownian motions. Taking into account that the relative positions of the CTs carrying the genes involved in the requested "kissing" event can change strongly from nucleus to nucleus, the mechanism for large-scale movements requires information about the direction into which the CTs and/or giant loops expanding from the respective CT surfaces should move. The congression of two widely separated CTs necessitates major rearrangements of other CTs as well, since CTs located in-between need to move aside affecting in turn other neighboring CTs. The demand for major chromatin rearrangements could be minimized by the congression of giant chromatin loops, which carry the genes of interest (see for example fig. 2 in Göndör and Ohlsson, 2009). In this case physical constraints need to be overcome that hinder long distance passages of giant loops through the nuclear space. On their route giant loops must penetrate through or pass around one or several other CTs forming obstacles between the site of departure and the site of arrival of genes traveling with giant loops. Although interchromatin channels could serve as routes for expanding loops to remote nuclear sites (Albiez et al., 2006; Bouchet-Marquis et al., 2006; Rouquette et al., 2009), we need to take into account that the IC is crowded with macromolecules and non-chromatin domains, which provide physical obstacles in addition to chromatin clusters for expanding and retracting giant chromatin loops (Bancaud et al., 2009; Hancock, 2007; Richter et al., 2008). At the onset of mitosis the undisturbed retraction of a giant loop towards its corresponding chromosome generates a further potential problem.

In contrast, **scenario B** (fig. 5-5(b)) presents a "factory first" model, where a specialized expression hub/transcription factory already exists and recruits specific genes, which are co-regulated for high expression at such a factory. The same topographical problems discussed for scenario A hold for scenario B. To use a more martial comparison than kissing, the problem resembles the task of duelists with pistols in hand (representing the CTs and the respective genes).

To know where the opponent stands is a minimum requirement for each duelist. In the nucleus this requirement would be served best by strictly deterministic relative positions of the two CTs carrying genes involved in a kissing event. In case that the relative positions change strongly from nucleus to nucleus, the mechanism for a successful kissing event requires information about the direction into which a given CT and/or a giant loop expanding from these CTs should move. It is unlikely that such a complex scenario could successfully evolve in cells since such a complex navigating system for trans interactions would need lots of information implemented within the the genome and thus would be susceptible to mutations. In this case it would have made it easier for evolution to increasing the probability for certain genes to interact with each other by positioning them onto one and the same chromosome.

Scenario C (fig. 5-5(c)) assumes random CT proximity patterns and argues that

DNA-DNA interactions in trans are limited to CTs, which by chance are located sufficiently close to each other. This chance increases with the number of pre-existing special expression hubs/transcription factories (compare fig. 8 (h) in (Schoenfelder et al., 2010). A set of genes involved in a distinct gene network functions as long as each gene is able to get access to one of multiple specialized hubs/factories, the more the better, which may be widely dispersed in the nuclear space. Probabilistic CT proximity patterns should yield a fraction of cells where two or even more genes, which are involved in the same regulatory gene network, but located on different CTs, are by chance located near enough to each other to explore their immediate nuclear environment by constrained Brownian motions and attach to the same hub/factory. Genes located far away from each other will explore different nuclear sub-volumes and attach to different hubs/factories suitable for their special needs of regulatory factors.

Scenario D (fig. 5-5(d)) attempts to explain long-range gene "kissing" events starting with random CT proximity patterns by a two-step mechanism. Clockwise and anti-clockwise rotational movements of CT assemblies provide the means to bring widely separated CTs carrying genes involved in a required "kissing" event into proximity close enough to interact thereafter by constrained Brownian movements. While simple rotational movements of whole spherical nuclei would not change the relative positions of CTs, the situation is different for complex rotational movements of flatly shaped nuclei and/or CT assemblies within such nuclei. In this case global, large-scale, rotational chromatin movements around an axis parallel to the growth surface resemble a moving device built up from an endless belt (representing the CTs) rotating around sprocket wheels (representing the unknown molecular mechanism) (fig. 5-5(d), upper panel). Importantly, in contrast to scenarios A and B, scenario D does not require a priori information on the topography of two CTs involved in a gene-"kissing" event. It is possible with any starting assembly of the individuals to bring a desired pair of dancers into a directly opposite position by a clockwise or anti-clockwise rotation of the whole assembly.

To illustrate this point, we compare the necessary dance of CTs with a group of square dancers (fig. 5-5, lower panel). Consider for example dancers 1 and 4. In the starting configuration they stand widely apart from each other, whereas in the later configuration they occupy directly opposite positions. The larger the group of dancers or the number of chromosomes in a given chromosome complement, the more obvious is the need for choreography in order to enable positional changes without chaos. Such choreography seems essential for an ordered mechanism of homologous alignment during meiotic prophase and it is tempting to speculate that some part of the meiotic pairing mechanism (Moore and Shaw, 2009) is also used in somatic cells to achieve homologous chromosome pairing during *Drosophila melanogaster* embryogenesis (Hiraoka et al., 1993), as well as homologous and heterologous chromatin alignments necessary for intranuclear DNA–DNA interactions in trans. Since the necessary dance of CTs in assemblies takes place within a 3D nuclear space, which can change shape transiently or permanently, the possibilities for choreographies may be exceedingly more complex than the simple choreographic example of some square dancers.

An obvious difference of the meiotic mechanism for the alignment and pairing of homologous chromosomes and the proposed mechanism for the alignment and connection of chromatin segments in trans proposed here for somatic cells is given by the fact that the mechanism in meiosis acts during meiotic prophase, while the mechanism proposed here for somatic cells arguably acts in nuclei during interphase or in postmitotic cell nuclei. These processes, however, differ with regard to their functional implications. The meiotic process has evolved, since it allows the portioning of two full sets of homologous chromosomes. The proximity patterns of the heterologous chromosomes in the cells generated by meiosis I, however, may be probabilistic, if not fully random.

An envisaged mechanism for the specific alignment of chromosomes in trans during mitotic prophase would need to explain how the randomizing effect of a chance sequence of connections between the kinetochores of individual chromosomes and the spindle could be avoided. Since chromosomes start to move as soon as they are connected to the spindle, they are typically driven away from other neighboring chromosomes, which by chance are not yet connected. For all what is presently known about this process it seems very difficult to propose a mechanism by which chromosomes could be connected to the spindle in a non-random order.

Simple and complex nuclear rotation (NR) with and without changes of CT proximity patterns has been observed in various cell types, including neurons (De Boni and Mintz, 1986; Park and De Boni, 1991). De Boni and co-workers described saltatory, rotational movements with changes in direction including reversals and were the first, who argued for a link between NR and the positioning of specific chromatin domains into cytotypic, nonrandom chromosome pattern in cycling and even in terminal differentiated cells. In multinucleolate neurons studied by time-lapse imaging they observed examples of nucleolar fusion, where nucleoli moved along curvilinear trajectories within the 3D nuclear space prior to the fusion event. Since large-scale movements of nucleoli require concomitant large-scale movements of NOR-bearing CTs and likely also of other CTs carrying chromatin domains specifically associated with perinucleolar heterochromatin, they provide a case in point for the necessity of a choreography, in which CTs move in assemblies rather than as independent individuals.

An important question with respect to the mechanism(s) involved in NR is whether NR represents motion of nuclei in toto, including the nuclear envelope, or independent motion of subnuclear structures, relative to each other, while the nuclear envelope stays fixed. In contrast to rotations of whole nuclei, where motor mechanism acting from outside would clearly suffice, intranuclear chromatin rotations require an intranuclear motor mechanism a motor fiber system, which passes from the cytoplasm through the nuclear envelope. Furthermore, interactions of chromatin with lamin receptors must be highly dynamic in order to free peripheral chromatin transiently for rotational movements. Reports on significant changes of chromatin domains relative to stationary cytoplasmic structures with a juxtanuclear position have provided circumstantial evidence that the interface for NR may lie on the karyoplasmic side of the nuclear envelope (De Boni, 1988).

Complex rotational movements of CTs in assemblies, followed by constrained

Brownian motions of chromatin domains or loops harboring specific genes provide an experimentally testable hypothesis how log-range DNA–DNA interactions in trans can be established in a population of cells starting with random CT proximity patterns. The stabilization of useful DNA–DNA interactions requests a molecular part for the mutual recognition and stabilization of aligned chromatin segments. This task may involve connecting filaments (see below) analogous to meiotic transverse filaments (Heyting, 2005) or an IC channel specifically connecting two CTs or loci of interest. Although both assumptions are presently not supported by experimental data, they are fully testable by *state of the art* methods. In case that CTs connected in trans by such filaments move apart from each other because of continued rotational CT movements, connected giant loops expanding from different CTs would be the consequence rather than the cause of "gene kissing" events. If such connecting filaments become sufficiently long, they could even help to permanently widely separated genes once connected by a "kissing" event and trigger directed movements of such genes towards each other upon a stimulus provided by a signaling pathway (Lin et al., 2009). Connecting fibers could even provide a possibility to re-establish functionally important patterns of co-localized genes present in a mother nucleus in its daughters.

Except for a few candidates the numerous molecular components expected to participate in mechanism(s) for long-range DNA–DNA interactions in trans complex have not yet been identified. In addition to cytoplasmic and/or nuclear actin and myosin (Chuang et al., 2006; Hu et al., 2008; Mehta et al., 2008; Pederson, 2008; Pederson and Aebi, 2005), other proteins should be considered for a role in such movements, including dynein (Levy and Holzbaur, 2008). A disturbance in the connection between the nucleus and the cytoskeleton and a concomitant loss of RT was observed in A-type lamin-deficient (lmna –/–) fibroblasts isolated from lmna knockout mice, as well as in 3T3 cells with RNAi induced reduction of lmna expression (Houben et al., 2009).

A single choreography of dancing CTs as exemplified in fig. 5-5(d) is certainly not sufficient to serve all requirements for large-scale changes of CTs in cycling or postmitotic cell nuclei. Movements of chromatin loops expanding from or retracting towards a CT (Albiez et al., 2006; Mahy et al., 2002a; Volpi et al., 2000), which likely serve functional demands to move genes from a compartment of silent into a nearby compartment of active chromatin (and vice versa), are less complex than movements necessary for long-range "kissing" events between genes in trans. Long-range movements of chromatin away from the nuclear periphery into the nuclear interior (and vice versa) (Barr and Bertram, 1951; Borden and Manuelidis, 1988; Chuang and Belmont, 2007; Solovei et al., 2009; Solovei et al., 2004) apparently require a choreography different from the example presented in fig. 5-5(d). Using live-cell microscopy, (Chuang et al., 2006) observed long-range directional movements of a chromosome locus undergoing an inducible repositioning from the nuclear periphery to the interior 1–2 h after targeting a transcriptional activator to this site. Extended periods of chromosome immobility were interspersed with several minute periods in which chromosomes moved unidirectionally along curvilinear paths oriented roughly perpendicular to the nuclear envelope at velocities of 0.1–0.9

µm/min over distances of 1–5 µm. We suggest that this movement implied movements of higher order chromatin assemblies rather than the isolated movement of a single locus (compare fig. 4-20 and fig. 4-21).

The complete inversion of heterochromatin and euchromatin arrangements during postnatal terminal differentiation of photoreceptor cells in nocturnal mammals (Solovei et al., 2009) provides the most complex case detected so far. This inversion may be the result of rotations of CTs with a polarized arrangement of gene dense and gene poor chromatin. If the concept that during ontogeny an omnipotent 3D architecture of early blastomere nuclei yields a large variety of 3D nuclear architectures in differentiated cell types (Blobel, 1985) a similar diversity of choreographies is required to achieve the necessary multitude of higher order chromatin arrangements.

5.8 Dynamics of DNA repair

The installation of a live-cell observation facility at the ion-microbeam SNAKE represents a big progress for radiobiological research using corpuscular irradiation. Although the development of this unique device (Gerardi, 2006) is still at an early stage with respect to handling and image quality – the first pilot experiments performed here demonstrate the potential of live-cell imaging biological specimen microirradiated by highly energetic ions. Due to the exactly choosable energy of the used ions and the fact that ion irradiation doesn't produce bleaching of GFP, in-vivo experiments performed here might not only substantiate results that were obtained by laser micro irradiation experiments but also lead to the discovery of new effects as it was already demonstrated by the discovery of the the competition effect for fixed cells (Greubel et al., 2008a; Greubel et al., 2008b).

Induction of damages using both ion- and laser microirradiation followed by long term live-cell observation showed that damages induced into the chromatin of living cells retain their position until the end of the observation period or until the irradiation induced foci disappear from the chromatin (see 4.2.2.2 and 4.3.4). This argues against reports from different groups that measured a significantly increased amount of chromosome pairs between the pericentric regions of homologous chromosomes soon after DNA damage (Abdel-Halim et al., 2004; Abdel-Halim et al., 2006; Abdel-Halim et al., 2005; Monajembashi et al., 2005), which would imply measurable changes in the nuclear architecture of the affected cells. These findings and the observation that the repair protein 53BP1 is transported from spontaneous (storage) foci to the damaged DNA also argue against models that claim the transport of damaged DNA towards repair factories. Moreover the results of this study and support the point of view that DNA damages are repaired in-situ – probably within micro environments that form at the surface of chromosome territories (Solimando et al., 2009).

The concept of membraneless micro compartments in form of transient nuclear bodies that was mentioned earlier in this discussion is fueled further by the observation of DNA damage foci. While components of DNA repair-protein factors like 53BP1, MDC1 and γ-H2AX seem to accumulate within the chromatin in a wider radius around the actual damage and might function as a scaffold, the components

of the homologous repair Rad51 and Rad52 seem to be directly located within micro-foci at the DNA lesions (Bekker-Jensen, 2006). In this context future work should address the purposes of damage and storage-foci, and how they are embedded into the context of nuclear topography. The new developments in light and electron microscopy might strongly support the answering of these questions.

One of the most interesting observations within this thesis is the disintegration of Rad52-GFP foci from the sites at which the DNA was damaged before using laser-microirradiation (see 4.3.4). Especially interesting is the observation that in this cell line the foci (regardless whether they stem from differently old damages) seem to disappear all at once after a phase of dramatic changes in which new foci emerged far aside from the damaged sites. While transient changes in width of the damage track, hight and base area of the nuclei during this dramatic phase might argue for larger changes in chromatin architecture (e.g. caused by nuclear rotations) the stability in the pattern of nucleoli (used here in this experiment as landmarks) argue against large-scale changes in the nuclear architecture.

However as these observations were obtained using the highly abnormal U2OS cell line conclusions about the observed phenomena have to be drawn with caution. Because of the way this cell line is immortalized (ALT-mechanism) involves homologous repair, the emergence of Rad52-GFP foci aside the damaged track could also reflect features of the homologous telomere lengthening, which (although it is a special feature of this cell line) cannot be generalized as a common phenomenon which is observable in the vast majority of cells.

In another cell line that was not tumor derived, the repair dynamics observed in the U2OS cell line were much less pronounced and the kinetics of Rad52-GFP foci dissapearance were slower, not synchronous and (using the laser micro irradiation parameters described in 3.5.2.3) not entirely finished after an observation period of ca. 60h. But also here only small changes in the arrangement of the damage foci and the centromeres could be observed.

Apart from the kinetics of DNA damage repair this cell line also showed an interesting structural phenomenon. All analyzed cells showed the mutual exclusion of Rad52-GFP foci and CENP-B-mRFP signals. Although it is very unlikely that the centromeric DNA to which CENP-B as a component of the kinetochore complex binds is spared from damage, it is possible that DNA repair of this highly repetitive sequences is performed by other components of the DNA repair machinery than by those of the homologous repair pathway.

5.9 Concluding remarks: mapping and understanding the dynamic nuclear architecture requires a systems biological approach

The above considerations encourage a new perspectives of dynamic chromatin arrangements in somatic cell types. The envisaged complexity of the mechanism(s) responsible for dynamic chromatin arrangements in somatic cell nuclei involves a great number of proteins assembled in molecular machines, potentially including proteins also involved in alignment and pairing events in meiotic prophase. The hypothesis that chromosome territories dance in assemblies in order to establish transient or permanent cell type specific DNA–DNA interactions implies that mapping the dynamic nuclear architecture may become an exceedingly demanding task. Genome wide mapping of DNA–DNA interactions is only the beginning paving the way to even more demanding problems. What do these interactions mean in functional terms and what molecular mechanisms are required to establish, maintain and disassemble such interactions? How are dynamic DNA–DNA interactions in *cis* and *trans* related to the topography of protein machineries involved in transcription, splicing, DNA replication and repair, or to the topographical aspects of the nuclear import and export of macromolecules?

Major progress of our insight into the complex relationships between cell type-specific nuclear architectures and cell-type specific gene expression patterns requires a systems biology approach. The complementary capabilities of both high throughput methods and single cell assays are needed to explore the nuclear topography and dynamic interactions of chromatin and non-chromatin assemblies. Genome-wide screening methods are required not only to establish DNA–DNA interactions in cis and trans, but also DNA–protein and DNA–RNA interactions. (Göndör and Ohlsson, 2009) have emphasized the importance of combining 4C methods with chromatin immune precipitation (ChIP) technology. Although these authors called this combination the Rosetta stone to explore a general link between genome biology and the nuclear architecture, one Rosetta stone will not suffice to decipher the topographical implications of the chromatin language. An approach, which allows the construction of genome-wide maps of DNA sequences interacting in vivo with DNA binding proteins was introduced by (van Steensel and Henikoff, 2000). A recent breakthrough achieved with this elegant method was the genome wide characterization of DNA sequences interacting with the lamina underpinning the nuclear envelope in *Drosophila melanogaster* and human cells (Guelen et al., 2008; Pickersgill et al., 2006).

Genome wide high-throughput assays, such as Hi-C (Lieberman-Aiden et al., 2009), require, by principle, a high cell number. They are therefore not suited to discriminate between the many different cell types present in complex tissues, which may be at different stages of cell cycle or terminal differentiation. Such studies will remain the domain of single cell assays and require advanced 3D and 4D microscopic

techniques. New concepts of fluorescence microscopy have been conceived and realized for cell imaging with a resolving power beyond the Abbe limit of conventional light microscopy (Cremer and Cremer, 1978; Gunkel et al., 2009; Hell, 2007). This methodological breakthrough has been accentuated by the term light optical nanoscopy. Its applicability for live cell studies is an urgently awaited further breakthrough, because such an approach besides its impact for high resolution studies of nuclear dynamics would allow rigorous tests how certain fixation and post-fixation procedures alter fine structural features present in the living cell. New 3D EM approaches combining scanning EM either with ultramicrotomy or with focused ion beam milling show also great promise for novel achievements (Rouquette et al., 2009). Genome wide assays will greatly help to decide, which interactions should be studied in detail.

6 References

Abdel-Halim, H.I., Imam, S.A., Badr, F.M., Natarajan, A.T., Mullenders, L.H.F. and Boei, J.J.W.A. (2004). Ionizing radiation-induced instant pairing of heterochromatin of homologous chromosomes in human cells. *Cytogenet Genome Res* **104**, 193-199.

Abdel-Halim, H.I., Mullenders, L.H.F. and Boei, J.J.W.A. (2006). Pairing of heterochromatin in response to cellular stress. *Experimental Cell Research* **312**, 1961-1969.

Abdel-Halim, H.I., Natarajan, A.T., Mullenders, L.H.F. and Boei, J.J.W.A. (2005). Mitomycin C-induced pairing of heterochromatin reflects initiation of DNA repair and chromatid exchange formation. *J Cell Sci* **118**, 1757-1767.

Abney, J.R., Cutler, B., Fillbach, M.L., Axelrod, D. and Scalettar, B.A. (1997). Chromatin dynamics in interphase nuclei and its implications for nuclear structure. *The Journal of Cell Biology* **137**, 1459-1468.

Abraham, R.T. and Tibbetts, R.S. (2005). Cell biology. Guiding ATM to broken DNA. *Science* **308**, 510-511.

Adams M.M. and Carpenter P.B. (2006). Tying the loose ends together in DNA double strand break repair with 53BP1. *Cell Div* **31**, 1-19

Akhtar, A. and Gasser, S.M. (2007). The nuclear envelope and transcriptional control. *Nat Rev Genet* **8**, 507-517.

Alberts, B., Johnson, A., Lewis, J., Raff, M., Roberts, K. and Walter, P. (2008). Molecular Biology of the Cell, Fifth Edition.

Albiez, H., Cremer, M., Tiberi, C., Vecchio, L., Schermelleh, L., Dittrich, S., Küpper, K., Joffe, B., Thormeyer, T., Hase, J. et al. (2006). Chromatin domains and the interchromatin compartment form structurally defined and functionally interacting nuclear networks. *Chromosome Res* **14**, 707-733.

Alexander, S.P. and Rieder, C.L. (1991). Chromosome motion during attachment to the vertebrate spindle: initial saltatory-like behavior of chromosomes and quantitative analysis of force production by nascent kinetochore fibers. *The Journal of Cell Biology* **113**, 805-815.

Alexandrova, O., Solovei, I., Cremer, T. and David, C.N. (2003). Replication labeling patterns and chromosome territories typical of mammalian nuclei are conserved in the early metazoan Hydra. *Chromosoma* **112**, 190-200.

Bancaud, A., Huet, S., Daigle, N., Mozziconacci, J., Beaudouin, J. and Ellenberg, J. (2009). Molecular crowding affects diffusion and binding of nuclear proteins in heterochromatin and reveals the fractal organization of chromatin. *EMBO J* **28**, 3785-3798.

Barr, M.L. and Bertram, E.G. (1951). The behaviour of nuclear structures during depletion and restoration of Nissl material in motor neurons. *J Anat* **85**, 171-181.

Bekker-Jensen, S., Lukas, C., Melander, F., Bartek, J. and Lukas, J. (2005). Dynamic assembly and sustained retention of 53BP1 at the sites of DNA damage are controlled by Mdc1/NFBD1. *The Journal of Cell Biology* **170**, 201-211.

Bekker-Jensen, S., Lukas, C., Kitagawa. R., Melander, F., Kastan, M.B., J. and Lukas, J. (2006). Spatial organization of the mammalian genome surveillance machinery in response to DNA strand breaks. *The Journal of Cell Biology* **173**, 195-206.

Bernardi, R. and Pandolfi, P.P. (2007). Structure, dynamics and functions of promyelocytic leukaemia nuclear bodies. *Nat Rev Mol Cell Biol* **8**, 1006-1016.

Betzig, E., Patterson, G.H., Sougrat, R., Lindwasser, O.W., Olenych, S., Bonifacino, J.S., Davidson, M.W., Lippincott-Schwartz, J. and Hess, H.F. (2006). Imaging intracellular fluorescent proteins at nanometer resolution. *Science* **313**, 1642-1645.

Bhattacharya, D., Talwar, S., Mazumder, A. and Shivashankar, G.V. (2009). Spatio-temporal plasticity in chromatin organization in mouse cell differentiation and during Drosophila embryogenesis. *Biophys J* **96**, 3832-3839.

Blobel, G. (1985). Gene gating: a hypothesis. *Proc Natl Acad Sci USA* **82**, 8527-8529.

Bolzer, A., Kreth, G., Solovei, I., Koehler, D., Saracoglu, K., Fauth, C., Müller, S., Eils, R., Cremer, C., Speicher, M.R., et al. (2005). Three-dimensional maps of all chromosomes in human male fibroblast nuclei and prometaphase rosettes. *PLoS Biol* **3**, e157.

Borden, J. and Manuelidis, L. (1988). Movement of the X chromosome in epilepsy. *Science* **242**, 1687-1691.

Bornfleth, H., Edelmann, P., Zink, D., Cremer, T. and Cremer, C. (1999). Quantitative motion analysis of subchromosomal foci in living cells using four-dimensional microscopy. *Biophys J* **77**, 2871-2886.

Bouchet-Marquis, C., Dubochet, J. and Fakan, S. (2006). Cryoelectron microscopy of vitrified sections: a new challenge for the analysis of functional nuclear architecture. *Histochem Cell Biol* **125**, 43-51.

Boveri, T. (1909). Die Blastomerenkerne von Ascaris megalocephala und die Theorie der Chromosomenindividualität. *Arch Zellforsch* **3**, 181-268.

Brown, J.M., Leach, J., Reittie, J.E., Atzberger, A., Lee-Prudhoe, J., Wood, W.G., Higgs, D.R., Iborra, F.J. and Buckle, V.J. (2006). Coregulated human globin genes are frequently in spatial proximity when active. *J Cell Biol* **172**, 177-187.

Bulina, M., Chudakov, D., and Britanova, O., Yanushevich, Y., Straroverov, D., Chepurnykh, T., Merzlyak, E., Shrkrob, M., Lukyanov, S. and Lukyanov, K. (2006). A genetically encoded photosensitizer. *Nat Biotechnol*. **24**, 95-99.

Chagin, V.O., Stear, J.H. and Cardoso, M.C. (2010). Organization of DNA replication. *Cold Spring Harb Perspect Biol* **2**, a000737.

Chalfie, M., Tu, Y., Euskirchen, G., Ward, W.W. and Prasher, D.C. (1994). Green fluorescent protein as a marker for gene expression. *Science* **263**, 802-805.

Chaly, N. and Brown, D.L. (1988). The prometaphase configuration and chromosome order in early mitosis. *Journal of Cell Science* **91** (Pt 3), 325-335.

Chambeyron, S. Da Silva, N.R., Lawson, K.A., and Bickmore, W.A. (2005). Nuclear re-organisation of the Hoxb complex during mouse embryonic development. *Development* **132**, 2215-2223.

Choi, K.H., Basma, H., Singh, J. and Cheng, P.-W. (2005). Activation of CMV promoter-controlled glycosyltransferase and beta -galactosidase glycogenes by butyrate, tricostatin A, and 5-aza-2‘-deoxycytidine. *Glycoconj J* **22**, 63-69.

Chuang, C.-H. and Belmont, A.S. (2007). Moving chromatin within the interphase nucleus-controlled transitions? *Semin Cell Dev Biol* **18**, 698-706.

Chuang, C.-H., Carpenter, A.E., Fuchsova, B., Johnson, T., de Lanerolle, P. and Belmont, A.S. (2006). Long-range directional movement of an interphase chromosome site. *Curr Biol* **16**, 825-831.

Cmarko, D., Verschure, P.J., Martin, T.E., Dahmus, M.E., Krause, S., Fu, X.D., Van Driel, R. and Fakan, S. (1999). Ultrastructural analysis of transcription and splicing in the cell nucleus after bromo-UTP microinjection. *Mol Biol Cell* **10**, 211-223.

Cmarko, D., Verschure, P.J., Otte, A.P., van Driel, R. and Fakan, S. (2003). Polycomb group gene silencing proteins are concentrated in the perichromatin compartment of the mammalian nucleus. *J Cell Sci* **116**, 335-343.

Cremer, C. and Cremer, T. (1978). Considerations on a laser-scanning-microscope with high resolution and depth of field. *Microscopica acta* **81**, 31-44.

Cremer, T. and Cremer, C. (2006). Rise, fall and resurrection of chromosome territories: a historical perspective. Part I. The rise of chromosome territories. *Eur J Histochem* **50**, 161-176.

Cremer, T. and Cremer, M. (2010). Chromosome Territories. *Cold Spring Harb Perspect Biol* **2**, a003889-a003889.

Cvacková, Z. Masata, M., Staněk, D., Fidlerová, H., and Raska, I. (2009). Chromatin position in human HepG2 cells: although being non-random, significantly changed in daughter cells. *J Struct Biol* **165**, 107-117.

D. Goldman, R. and L. Spector, D. (2005). Live cell imaging: a laboratory manual. 631.

De Boni, U. (1988). Chromatin motion in interphase nuclei, its modulation and its potential role in gene expression. *Anticancer Res* **8**, 885-898.

De Boni, U. and Mintz, A.H. (1986). Curvilinear, three-dimensional motion of chromatin domains and nucleoli in neuronal interphase nuclei. *Science* **234**, 863-866.

Dechat, T., Pfleghaar, K., Sengupta, K., Shimi, T., Shumaker, D.K., Solimando, L. and Goldman, R.D. (2008). Nuclear lamins: major factors in the structural organization and function of the nucleus and chromatin. *Genes & Development* **22**, 832-853.

Dekker, J., Rippe, K., Dekker, M. and Kleckner, N. (2002). Capturing chromosome conformation. *Science* **295**, 1306-1311.

Ditullio, R.A., Mochan, T.A., Venere, M., Bartkova, J., Sehested, M., Bartek, J. and Halazonetis, T.D. (2002). 53BP1 functions in an ATM-dependent checkpoint pathway that is constitutively activated in human cancer. *Nat Cell Biol* **4**, 998-1002.

Donnert, G., Keller, J., Medda, R., Andrei, M.A., Rizzoli, S.O., Lührmann, R., Jahn, R., Eggeling, C. and Hell, S.W. (2006). Macromolecular-scale resolution in biological fluorescence microscopy. *Proc Natl Acad Sci USA* **103**, 11440-11445.

Dunn, G.A. and Jones, G.E. (2004). Timeline: Cell motility under the microscope: Vorsprung durch Technik. *Nat Rev Mol Cell Biol* **5**, 667-672.

Edelmann, P., Bornfleth, H., Zink, D., Cremer, T. and Cremer, C. (2001). Morphology and dynamics of chromosome territories in living cells. *Biochim Biophys Acta* **1551**, M29-39.

Essers, J., van Cappellen, W.A., Theil, A.F., van Drunen, E., Jaspers, N.G.J., Hoeijmakers, J.H.J., Wyman, C., Vermeulen, W. and Kanaar, R. (2005). Dynamics of relative chromosome position during the cell cycle. *Mol Biol Cell* **16**, 769-775.

Fraser, P. and Bickmore, W. (2007). Nuclear organization of the genome and the potential for gene regulation. *Nature* **447**, 413-417.

Fujimori, A., Tachiiri, S., Sonoda, E., Thompson, L.H., Dhar, P.K., Hiraoka, M., Takeda, S., Zhang, Y., Reth, M. and Takata, M. (2001). Rad52 partially substitutes for the Rad51 paralog XRCC3 in maintaining chromosomal integrity in vertebrate cells. *EMBO J* **20**, 5513-5520.

Galkin, V.E., Wu, Y., Zhang, X.-P., Qian, X., He, Y., Yu, X., Heyer, W.-D., Luo, Y. and Egelman, E.H. (2006). The Rad51/RadA N-terminal domain activates nucleoprotein filament ATPase activity. *Structure* **14**, 983-992.

Gasior, S.L., Wong, A.K., Kora, Y., Shinohara, A. and Bishop, D.K. (1998). Rad52 associates with RPA and functions with rad55 and rad57 to assemble meiotic recombination complexes. *Genes Dev* **12**, 2208-2221.

Gerardi, S. (2006). A comparative review of charged particle microbeam facilities. *Radiation Protection Dosimetry* **122**, 285-291.

Gerlich, D., Beaudouin, J., Kalbfuss, B., Daigle, N., Eils, R. and Ellenberg, J. (2003). Global chromosome positions are transmitted through mitosis in mammalian cells. *Cell* **112**, 751-764.

Gerlich, D. and Ellenberg, J. (2003). Dynamics of chromosome positioning during the cell cycle. *Curr Opin Cell Biol* **15**, 664-671.

Gluckman, P.D. and Hanson, M.A. (2004). Living with the past: evolution, development, and patterns of disease. *Science* **305**, 1733-1736.

Goldberg, M., Stucki, M., Falck, J., D'amours, D., Rahman, D., Pappin, D., Bartek, J. and Jackson, S.P. (2003). MDC1 is required for the intra-S-phase DNA damage checkpoint. *Nature* **421**, 952-956.

Göndör, A. and Ohlsson, R. (2009). Chromosome crosstalk in three dimensions. *Nature* **461**, 212-217.

Grasser, F., Neusser, M., Fiegler, H., Thormeyer, T., Cremer, M., Carter, N.P., Cremer, T. and Müller, S. (2008). Replication-timing-correlated spatial chromatin arrangements in cancer and in primate interphase nuclei. *Journal of Cell Science* **121**, 1876-1886.

Gray, H. (1989). Gray's anatomy (37th ed.) (P. L. Williams, Ed.). Edinburgh: C. Livingstone.

Greubel, C., Hable, V., Drexler, G.A., Hauptner, A., Dietzel, S., Strickfaden, H., Baur, I., Krücken, R., Cremer, T., Dollinger, G., et al. (2008a). Competition effect in DNA damage response. *Radiat Environ Biophys* **47**, 423-429.

Greubel, C., Hable, V., Drexler, G.A., Hauptner, A., Dietzel, S., Strickfaden, H., Baur, I., Krücken, R., Cremer, T., Friedl, A.A., et al. (2008b). Quantitative analysis of DNA-damage response factors after sequential ion microirradiation. *Radiat Environ Biophys* **47**, 415-422.

Guelen, L., Pagie, L., Brasset, E., Meuleman, W., Faza, M.B., Talhout, W., Eussen, B.H., de Klein, A., Wessels, L., De Laat, W., et al. (2008). Domain organization of human chromosomes revealed by mapping of nuclear lamina interactions. *Nature* **453**, 948-951.

Gunkel, M., Erdel, F., Rippe, K., Lemmer, P., Kaufmann, R., Hörmann, C., Amberger, R. and Cremer, C. (2009). Dual color localization microscopy of cellular nanostructures. *Biotechnol J* **4**, 927-938.

Gustafsson, M.G.L., Shao, L., Carlton, P.M., Wang, C.J.R., Golubovskaya, I.N., Cande, W.Z., Agard, D.A., and Sedat, J.W. (2008). Three-dimensional resolution doubling in wide-field fluorescence microscopy by structured illumination. *Biophys J* **94**, 4957-4970.

Habermann, F.A., Cremer, M., Walter, J., Kreth, G., von Hase, J., Bauer, K., Wienberg, J., Cremer, C., Cremer, T. and Solovei, I. (2001). Arrangements of macro- and microchromosomes in chicken cells. *Chromosome Res* **9**, 569-584.

Hable, V. (2004). Untersuchung der Dynamik von DNA-Reparaturproteinen nach Bestrahlung lebender Zellen am Rasterionenmikroskop SNAKE. Diplomarbeit, 1-68.

Hable, V., Greubel, C., Bergmaier, A. and Reichart, P. (2009). The live cell irradiation and observation setup at SNAKE. *Nuclear Inst and Methods in Physics Research* **267**, 2090-2097.

Halliwell, B. (2003). Oxidative stress in cell culture: an under-appreciated problem? *FEBS Lett* **540**, 3-6.

Hancock, R. (2007). Packing of the polynucleosome chain in interphase chromosomes: evidence for a contribution of crowding and entropic forces. *Semin Cell Dev Biol* **18**, 668-675.

Harrison, R.G. (1907). Observations on the living developing verve fiber. *The anatomical Record* **1**, 116-118.

Hauptner, A., Dietzel, S., Drexler, G.A., Reichart, P., Krücken, R., Cremer, T., Friedl, A.A. and Dollinger, G. (2004). Microirradiation of cells with energetic heavy ions. *Radiat Environ Biophys* **42**, 237-245.

Heessen, S. and Fornerod, M. (2007). The inner nuclear envelope as a transcription factor resting place. *EMBO Rep* **8**, 914-919.

Heisel, S., Hoffmann, J., Strickfaden, H., Chang, P. and Meese, E. (2010). The glioma-amplified sequence 41 as centrosome associated protein essential for spindle formation. *FasebJ Jounal* (submitted).

Hell, S.W. (2007). Far-field optical nanoscopy. *Science* **316**, 1153-1158.

Henson, J.D., Neumann, A.A., Yeager, T.R. and Reddel, R.R. (2002). Alternative lengthening of telomeres in mammalian cells. *Oncogene* **21**, 598-610.

Heyting, C. (2005). Meiotic transverse filament proteins: essential for crossing over. *Transgenic Res* **14**, 547-550.

Hiraoka, Y., Dernburg, A.F., Parmelee, S.J., Rykowski, M.C., Agard, D.A. and Sedat, J.W. (1993). The onset of homologous chromosome pairing during Drosophila melanogaster embryogenesis. *The Journal of Cell Biology* **120**, 591-600.

Hou, C., Zhao, H., Tanimoto, K. and Dean, A. (2008). CTCF-dependent enhancer-blocking by alternative chromatin loop formation. *Proc Natl Acad Sci USA* **105**, 20398-20403.

Houben, F., Willems, C.H.M.P., Declercq, I.L.J., Hochstenbach, K., Kamps, M.A., Snoeckx, L.H.E.H., Ramaekers, F.C.S. and Broers, J.L.V. (2009). Disturbed nuclear orientation and cellular migration in A-type lamin deficient cells. *Biochim Biophys Acta* **1793**, 312-324.

Hu, Q., Kwon, Y.-S., Nunez, E., Cardamone, M.D., Hutt, K.R., Ohgi, K.A., Garcia-Bassets, I., Rose, D.W., Glass, C.K., Rosenfeld, M.G., et al. (2008). Enhancing nuclear receptor-induced transcription requires nuclear motor and LSD1-dependent gene networking in interchromatin granules. *Proceedings of the National Academy of Sciences* **105**, 19199-19204.

Ismail, I.H. and Hendzel, M.J. (2008). The gamma-H2AX: is it just a surrogate marker of double-strand breaks or much more? *Environ Mol Mutagen* **49**, 73-82.

Jackson, D., Dhar, K., Wahl, J.K., Wold, M.S. and Borgstahl, G.E.O. (2002). Analysis of the human replication protein A:Rad52 complex: evidence for crosstalk between RPA32, RPA70, Rad52 and DNA. *Journal of Molecular Biology* **321**, 133-148.

Kanda, T., Sullivan, K.F. and Wahl, G.M. (1998). Histone-GFP fusion protein enables sensitive analysis of chromosome dynamics in living mammalian cells. *Curr Biol* **8**, 377-385.

Kao, G.D., McKenna, W.G., Guenther, M.G., Muschel, R.J., Lazar, M.A. and Yen, T.J. (2003). Histone deacetylase 4 interacts with 53BP1 to mediate the DNA damage response. *J Cell Biol* **160**, 1017-1027.

Kim, S.H., McQueen, P.G., Lichtman, M.K., Shevach, E.M., Parada, L.A. and Misteli, T. (2004). Spatial genome organization during T-cell differentiation. *Cytogenet Genome Res* **105**, 292-301.

Kleinig, H. and Sitte, P. (1999). Zellbiologie. 4th edition, Spektrum

Köhler, D., Gao, J., Mattes, J., Cremer, T., Joffe, B., Eils, R. and Solovei, I. (2011). Inheritance and Diversification of Spatial Chromosome Arrangement in Growing Cell Clones of Human Cells. (in preparation).

Kosak, S.T. and Groudine, M. (2004). Gene order and dynamic domains. *Science* **306**, 644-647.

Kumaran, R.I. and Spector, D.L. (2008). A genetic locus targeted to the nuclear periphery in living cells maintains its transcriptional competence. *The Journal of Cell Biology* **180**, 51-65.

Küpper, K., Kölbl, A., Biener, D., Dittrich, S., Von Hase, J., Thormeyer, T., Fiegler, H., Carter, N.P., Speicher, M.R., Cremer, T., et al. (2007). Radial chromatin positioning is shaped by local gene density, not by gene expression. *Chromosoma* **116**, 285-306.

Lamond, A.I. and Spector, D.L. (2003). Nuclear speckles: a model for nuclear organelles. *Nat Rev Mol Cell Biol* **4**, 605-612.

Levi, V., Ruan, Q., Plutz, M., Belmont, A.S. and Gratton, E. (2005). Chromatin dynamics in interphase cells revealed by tracking in a two-photon excitation microscope. *Biophysical Journal* **89**, 4275-4285.

Levy, J.R. and Holzbaur, E.L.F. (2008). Dynein drives nuclear rotation during forward progression of motile fibroblasts. *J Cell Sci* **121**, 3187-3195.

Li, Q., Lau, A., Morris, T.J., Guo, L., Fordyce, C.B. and Stanley, E.F. (2004). A syntaxin 1, Galpha(o), and N-type calcium channel complex at a presynaptic nerve terminal: analysis by quantitative immunocolocalization. *J Neurosci* **24**, 4070-4081.

Lichter, P. (1997). Multicolor FISHing: what's the catch? *Trends Genet* **13**, 475-479.

Lieberman-Aiden, E., van Berkum, N.L., Williams, L., Imakaev, M., Ragoczy, T., Telling, A., Amit, I., Lajoie, B.R., Sabo, P.J., Dorschner, M.O., et al. (2009). Comprehensive mapping of long-range interactions reveals folding principles of the human genome. *Science* **326**, 289-293.

Limoli, C.L. and Ward, J.F. (1993). A new method for introducing double-strand breaks into cellular DNA. *Radiation Research* **134**, 160-169.

Lin, C., Yang, L., Tanasa, B., Hutt, K., Ju, B.-g., Ohgi, K., Zhang, J., Rose, D.W., Fu, X.-D., Glass, C.K., et al. (2009). Nuclear receptor-induced chromosomal proximity and DNA breaks underlie specific translocations in cancer. *Cell* **139**, 1069-1083.

Ling, J.Q. and Hoffman, A.R. (2007). Epigenetics of long-range chromatin interactions. *Pediatr Res* **61**, 11R-16R.

Liu, Y. and Maizels, N. (2000). Coordinated response of mammalian Rad51 and Rad52 to DNA damage. *EMBO Rep* **1**, 85-90.

Lloyd, C. and Chan, J. (2006). Not so divided: the common basis of plant and animal cell division. *Nat Rev Mol Cell Biol* **7**, 147-152.

Lomvardas, S., Barnea, G., Pisapia, D.J., Mendelsohn, M., Kirkland, J., and Axel, R. (2006). Interchromosomal interactions and olfactory receptor choice. *Cell* **126**, 403-413.

Lowenstein, M.G., Goddard, T.D. and Sedat, J.W. (2004). Long-range interphase chromosome organization in Drosophila: a study using color barcoded fluorescence in situ hybridization and structural clustering analysis. *Mol Biol Cell* **15**, 5678-5692.

Lukas, C., Bartek, J. and Lukas, J. (2005). Imaging of protein movement induced by chromosomal breakage: tiny ‚local' lesions pose great ‚global' challenges. *Chromosoma* **114**, 146-154.

Lukyanov, K.A., Chudakov, D.M., Lukyanov, S. and Verkhusha, V.V. (2005). Innovation: Photoactivatable fluorescent proteins. *Nat Rev Mol Cell Biol* **6**, 885-891.

Lyon, M.F. (1962). Sex chromatin and gene action in the mammalian X-chromosome. *Am J Hum Genet* **14**, 135-148.

Mahy, N.L., Perry, P.E. and Bickmore, W.A. (2002a). Gene density and transcription influence the localization of chromatin outside of chromosome territories detectable by FISH. *The Journal of Cell Biology* **159**, 753-763.

Mahy, N.L., Perry, P.E., Gilchrist, S., Baldock, R.A. and Bickmore, W.A. (2002b). Spatial organization of active and inactive genes and noncoding DNA within chromosome territories. *J Cell Biol* **157**, 579-589.

Malik, P., Zuleger, N. and Schirmer, E.C. (2010). Nuclear envelope influences on genome organization. *Biochem Soc Trans* **38**, 268-272.

Manders, E.M., Kimura, H. and Cook, P.R. (1999). Direct imaging of DNA in living cells reveals the dynamics of chromosome formation. *The Journal of Cell Biology* **144**, 813-821.

Marshall, W.F., Straight, A., Marko, J.F., Swedlow, J., Dernburg, A., Belmont, A., Murray, A.W., Agard, D.A. and Sedat, J.W. (1997). Interphase chromosomes undergo constrained diffusional motion in living cells. *Curr Biol* **7**, 930-939.

Mehta, I.S., Amira, M., Harvey, A.J. and Bridger, J.M. (2010). Rapid chromosome territory relocation by nuclear motor activity in response to serum removal in primary human fibroblasts. *Genome Biol* **11**, R5.

Mehta, I.S., Elcock, L.S., Amira, M., Kill, I.R. and Bridger, J.M. (2008). Nuclear motors and nuclear structures containing A-type lamins and emerin: is there a functional link? *Biochem Soc Trans* **36**, 1384-1388.

Meshorer, E., Yellajoshula, D., George, E., Scambler, P.J., Brown, D.T. and Misteli, T. (2006). Hyperdynamic plasticity of chromatin proteins in pluripotent embryonic stem cells. *Dev Cell* **10**, 105-116.

Minton, A.P. (2006). How can biochemical reactions within cells differ from those in test tubes? *Journal of Cell Science* **119**, 2863-2869.

Misteli, T. (2007). Beyond the sequence: cellular organization of genome function. *Cell* **128**, 787-800.

Misteli, T. and Soutoglou, E. (2009). The emerging role of nuclear architecture in DNA repair and genome maintenance. *Nat Rev Mol Cell Biol* **10**, 243-254.

Mochan, T.A., Venere, M., Ditullio, R.A. and Halazonetis, T.D. (2003). 53BP1 and NFBD1/MDC1-Nbs1 function in parallel interacting pathways activating ataxia-telangiectasia mutated (ATM) in response to DNA damage. *Cancer Res* **63**, 8586-8591.

Monajembashi, S., Rapp, A., Schmitt, E., Dittmar, H., Greulich, K.-O. and Hausmann, M. (2005). Spatial association of homologous pericentric regions in human lymphocyte nuclei during repair. *Biophysical Journal* **88**, 2309-2322.

Moore, G. and Shaw, P. (2009). Improving the chances of finding the right partner. *Current Opinion in Genetics & Development* **19**, 99-104.

Mortusewicz, O., Amé, J-C., Schreiber, V. and Leonhardt, H. (2007) Feedback-regulated poly(ADP-ribosyl)ation by PARP-1 is required for rapid response to DNA damage in living cells. *Nucleic Acids Res.* **35**, 7665-7675.

Müller, I., Boyle, S., Singer, R.H., Bickmore, W.A. and Chubb, J.R. (2010). Stable morphology, but dynamic internal reorganisation, of interphase human chromosomes in living cells. *PLoS ONE* **5**, e11560.

Murr, R., Loizou, J.I., Yang, Y.-G., Cuenin, C., Li, H., Wang, Z.-Q. and Herceg, Z. (2006). Histone acetylation by Trrap-Tip60 modulates loading of repair proteins and repair of DNA double-strand breaks. *Nat Cell Biol* **8**, 91-99.

Nabetani, A. and Ishikawa, F. (2009). Unusual telomeric DNAs in human telomerase-negative immortalized cells. *Molecular and Cellular Biology* **29**, 703-713.

Neusser, M., Schubel, V., Koch, A., Cremer, T. and Müller, S. (2007). Evolutionarily conserved, cell type and species-specific higher order chromatin arrangements in interphase nuclei of primates. *Chromosoma* **116**, 307-320.

Noordermeer, D., Branco, M.R., Splinter, E., Klous, P., van Ijcken, W., Swagemakers, S., Koutsourakis, M., van der Spek, P., Pombo, A. and De Laat, W. (2008). Transcription and chromatin organization of a housekeeping gene cluster containing an integrated beta-globin locus control region. *PLoS Genet* **4**, e1000016.

Nunez, E., Kwon, Y.-S., Hutt, K.R., Hu, Q., Cardamone, M.D., Ohgi, K.A., Garcia-Bassets, I., Rose, D.W., Glass, C.K., Rosenfeld, M.G., et al. (2008). Nuclear receptor-enhanced transcription requires motor- and LSD1-dependent gene networking in interchromatin granules. *Cell* **132**, 996-1010.

Ormö, M., Cubitt, A.B., Kallio, K., Gross, L.A., Tsien, R.Y. and Remington, S.J. (1996). Crystal structure of the Aequorea victoria green fluorescent protein. *Science* **273**, 1392-1395.

Osborne, C.S., Chakalova, L., Mitchell, J.A., Horton, A., Wood, A.L., Bolland, D.J., Corcoran, A.E. and Fraser, P. (2007). Myc dynamically and preferentially relocates to a transcription factory occupied by Igh. *PLoS Biol* **5**, e192.

Park, P.C. and De Boni, U. (1991). Dynamics of nucleolar fusion in neuronal interphase nuclei in vitro: association with nuclear rotation. *Exp Cell Res* **197**, 213-221.

Patterson, G.H. and Lippincott-Schwartz, J. (2002). A photoactivatable GFP for selective photolabeling of proteins and cells. *Science* **297**, 1873-1877.

Patterson, G.H. and Lippincott-Schwartz, J. (2004). Selective photolabeling of proteins using photoactivatable GFP. *Methods* **32**, 445-450.

Pederson, T. (2004). The spatial organization of the genome in mammalian cells. *Curr Opin Genet Dev* **14**, 203-209.

Pederson, T. (2008). As functional nuclear actin comes into view, is it globular, filamentous, or both? *The Journal of Cell Biology* **180**, 1061-1064.

Pederson, T. and Aebi, U. (2005). Nuclear actin extends, with no contraction in sight. *Mol Biol Cell* **16**, 5055-5060.

Pickersgill, H., Kalverda, B., de Wit, E., Talhout, W., Fornerod, M. and van Steensel, B. (2006). Characterization of the Drosophila melanogaster genome at the nuclear lamina. *Nat Genet* **38**, 1005-1014.

Pollock, C. and Huang, S. (2009). The perinucleolar compartment. *J Cell Biochem* **107**, 189-193.

Postberg, J., Alexandrova, O., Cremer, T. and Lipps, H.J. (2005). Exploiting nuclear duality of ciliates to analyse topological requirements for DNA replication and transcription. *J Cell Sci* **118**, 3973-3983.

Prasher, D.C., Eckenrode, V.K., Ward, W.W., Prendergast, F.G. and Cormier, M.J. (1992). Primary structure of the Aequorea victoria green-fluorescent protein. *Gene* **111**, 229-233.

Rabl, C. (1885). Über Zellteilung. *Morph Jb* **10**, 214-330.

Ragoczy, T., Telling, A., Sawado, T., Groudine, M. and Kosak, S.T. (2003). A genetic analysis of chromosome territory looping: diverse roles for distal regulatory elements. *Chromosome Res* **11**, 513-525.

Ranatunga, W., Jackson D., Lloyd J.A., Forget A.L., Knight K.L. and Borgstahl G.E. (2001). Human RAD52 exhibits two modes of self-association. *J Biol Chem* **276**, 15876-15880.

Reddy, K.L. and Singh, H. (2008). Using molecular tethering to analyze the role of nuclear compartmentalization in the regulation of mammalian gene activity. *Methods* **45**, 242-251.

Richter, K., Nessling, M. and Lichter, P. (2008). Macromolecular crowding and its potential impact on nuclear function. *Biochim Biophys Acta* **1783**, 2100-2107.

Rosenblatt, J., Cramer, L.P., Baum, B. and McGee, K.M. (2004). Myosin II-dependent cortical movement is required for centrosome separation and positioning during mitotic spindle assembly. *Cell* **117**, 361-372.

Rothbauer, U., Zolghadr, K., Tillib, S., Nowak, D., Schermelleh, L., Gahl, A., Backmann, N., Conrath, K., Muyldermans, S., Cardoso, M.C., et al. (2006). Targeting and tracing antigens in live cells with fluorescent nanobodies. *Nat Methods* **3**, 887-889.

Rouquette, J., Genoud, C., Vazquez-Nin, G.H., Kraus, B., Cremer, T. and Fakan, S. (2009). Revealing the high-resolution three-dimensional network of chromatin and interchromatin space: a novel electron-microscopic approach to reconstructing nuclear architecture. *Chromosome Res* **17**, 801-810.

Ruault, M., Dubarry, M. and Taddei, A. (2008). Re-positioning genes to the nuclear envelope in mammalian cells: impact on transcription. *Trends Genet* **24**, 574-581.

Sancar, A., Lindsey-Boltz, L.A., Unsal-Kaçmaz, K. and Linn, S. (2004). Molecular mechanisms of mammalian DNA repair and the DNA damage checkpoints. *Annu Rev Biochem* **73**, 39-85.

Schermelleh, L., Carlton, P.M., Haase, S., Shao, L., Winoto, L., Kner, P., Burke, B., Cardoso, M.C., Agard, D.A., Gustafsson, M.G.L., et al. (2008). Subdiffraction Multicolor Imaging of the Nuclear Periphery with 3D Structured Illumination Microscopy. *Science* **320**, 1332-1336.

Schermelleh, L., Solovei, I., Zink, D. and Cremer, T. (2001). Two-color fluorescence labeling of early and mid-to-late replicating chromatin in living cells. *Chromosome Res* **9**, 77-80.

Schoenfelder, S., Sexton, T., Chakalova, L., Cope, N.F., Horton, A., Andrews, S., Kurukuti, S., Mitchell, J.A., Umlauf, D., Dimitrova, D.S., et al. (2010). Preferential associations between co-regulated genes reveal a transcriptional interactome in erythroid cells. *Nature Genetics* **42**, 53-61.

Schones, D.E. and Zhao, K. (2008). Genome-wide approaches to studying chromatin modifications. *Nat Rev Genet* **9**, 179-191.

Schroeder-Reiter, E., Pérez-Willard, F., Zeile, U. and Wanner, G. (2009). Focused ion beam (FIB) combined with high resolution scanning electron microscopy: a promising tool for 3D analysis of chromosome architecture. *J Struct Biol* **165**, 97-106.

Schwarzacher, H.G. and Wachtler, F. (1983). Nucleolus organizer regions and nucleoli. *Hum Genet* **63**, 89-99.

Segal, E. and Widom, J. (2009). What controls nucleosome positions? *Trends Genet* **25**, 335-343.

Service, R.F. (2008). Nobel Prize in chemistry. Three scientists bask in prize's fluorescent glow. *Science* **322**, 361.

Sexton, T., Bantignies, F. and Cavalli, G. (2009). Genomic interactions: chromatin loops and gene meeting points in transcriptional regulation. *Semin Cell Dev Biol* **20**, 849-855.

Shiloh, Y. (2003). ATM and related protein kinases: safeguarding genome integrity. *Nat Rev Cancer* **3**, 155-168.

Shimomura, O., Johnson, F.H. and Saiga, Y. (1962). Extraction, purification and properties of aequorin, a bioluminescent protein from the luminous hydromedusan, Aequorea. *J Cell Comp Physiol* **59**, 223-239.

Shinohara, A., Shinohara, M., Ohta, T., Matsuda, S. and Ogawa, T. (1998). Rad52 forms ring structures and co-operates with RPA in single-strand DNA annealing. *Genes Cells* **3**, 145-156.

Shu, X., Royant, A., Lin, M.Z., Aguilera, T.A., Lev-Ram, V., Steinbach, P.A. and Tsien, R.Y. (2009). Mammalian expression of infrared fluorescent proteins engineered from a bacterial phytochrome. *Science* **324**, 804-807.

Simonis, M. and De Laat, W. (2008). FISH-eyed and genome-wide views on the spatial organisation of gene expression. *Biochim Biophys Acta* **1783**, 2052-2060.

Simonis, M., Klous, P., Splinter, E., Moshkin, Y., Willemsen, R., de Wit, E., van Steensel, B. and De Laat, W. (2006). Nuclear organization of active and inactive chromatin domains uncovered by chromosome conformation capture-on-chip (4C). *Nat Genet* **38**, 1348-1354.

Solimando, L., Luijsterburg, M.S., Vecchio, L., Vermeulen, W., Van Driel, R. and Fakan, S. (2009). Spatial organization of nucleotide excision repair proteins after UV-induced DNA damage in the human cell nucleus. *Journal of Cell Science* **122**, 83-91.

Solovei, I., Kreysing, M., Lanctôt, C., Kösem, S., Peichl, L., Cremer, T., Guck, J. and Joffe, B. (2009). Nuclear architecture of rod photoreceptor cells adapts to vision in mammalian evolution. *Cell* **137**, 356-368.

Solovei, I., Schermelleh, L., Düring, K., Engelhardt, A., Stein, S., Cremer, C. and Cremer, T. (2004). Differences in centromere positioning of cycling and postmitotic human cell types. *Chromosoma* **112**, 410-423.

Spector, D.L. (2006). SnapShot: Cellular bodies. *Cell* **127**, 1071.

Strickfaden, H., Zunhammer, A., van Koningsbruggen, S., Köhler, D. and Cremer, T. (2010). 4D Chromatin dynamics in cycling cells: Theodor Boveri's hypothesis revisited *Nucleus* **1,** 284-297.

Stucki, M., Clapperton, J., Mohammad, D., Yaffe, M., Smerdon, S. and Jackson, S. (2005). MDC1 Directly Binds Phosphorylated Histone H2AX to Regulate Cellular Responses to DNA Double-Strand Breaks. *Cell* **123**, 1213-1226.

Subach, F.V., Patterson, G.H., Manley, S., Gillette, J.M., Lippincott-Schwartz, J. and Verkhusha, V.V. (2009). Photoactivatable mCherry for high-resolution two-color fluorescence microscopy. *Nat Methods* **6**, 153-159.

Taddei, A., Hediger, F., Neumann, F.R. and Gasser, S.M. (2004). The function of nuclear architecture: a genetic approach. *Annu Rev Genet* **38**, 305-345.

Takahashi, A. and Ohnishi, T. (2005). Does gammaH2AX foci formation depend on the presence of DNA double strand breaks? *Cancer Lett* **229**, 171-179.

Tashiro, S., Walter, J., Shinohara, A., Kamada, N. and Cremer, T. (2000). Rad51 accumulation at sites of DNA damage and in postreplicative chromatin. *J Cell Biol* **150**, 283-291.

Tiwari, V.K., Cope, L., McGarvey, K.M., Ohm, J.E. and Baylin, S.B. (2008). A novel 6C assay uncovers Polycomb-mediated higher order chromatin conformations. *Genome Research* **18**, 1171-1179.

van Steensel, B. and Henikoff, S. (2000). Identification of in vivo DNA targets of chromatin proteins using tethered dam methyltransferase. *Nat Biotechnol* **18**, 424-428.

van Thor, J.J., Gensch, T., Hellingwerf, K.J. and Johnson, L.N. (2002). Phototransformation of green fluorescent protein with UV and visible light leads to decarboxylation of glutamate 222. *Nat Struct Biol* **9**, 37-41.

van Thor, J.J., Pierik, A.J., Nugteren-Roodzant, I., Xie, A. and Hellingwerf, K.J. (1998). Characterization of the photoconversion of green fluorescent protein with FTIR spectroscopy. *Biochemistry* **37**, 16915-16921.

Varmark, H. (2004). Functional role of centrosomes in spindle assembly and organization. *J Cell Biochem* **91**, 904-914.

Virchow, R.L.K. (1858). Cellular pathology as based upon physiological and pathological histology. August Hirschwald, Berlin.

Volpi, E.V., Chevret, E., Jones, T., Vatcheva, R., Williamson, J., Beck, S., Campbell, R.D., Goldsworthy, M., Powis, S.H., Ragoussis, J., et al. (2000). Large-scale chromatin organization of the major histocompatibility complex and other regions of human chromosome 6 and its response to interferon in interphase nuclei. *Journal of Cell Science* **113** (Pt 9), 1565-1576.

Wachsmuth, M., Caudron-Herger, M. and Rippe, K. (2008). Genome organization: balancing stability and plasticity. *Biochim Biophys Acta* **1783**, 2061-2079.

Walter, J., Schermelleh, L., Cremer, M., Tashiro, S. and Cremer, T. (2003). Chromosome order in HeLa cells changes during mitosis and early G1, but is stably maintained during subsequent interphase stages. *Journal of Cell Biology* **160**, 685-697.

Wiedenmann, J. and Nienhaus, G.U. (2006). Live-cell imaging with EosFP and other photoactivatable marker proteins of the GFP family. *Expert review of proteomics* **3**, 361-374.

Williams, A. and Flavell, R.A. (2008). The role of CTCF in regulating nuclear organization. *J Exp Med* **205**, 747-750.

Williams, R.R.E., Broad, S., Sheer, D. and Ragoussis, J. (2002). Subchromosomal positioning of the epidermal differentiation complex (EDC) in keratinocyte and lymphoblast interphase nuclei. *Experimental Cell Research* **272**, 163-175.

Williams, R.R.E. and Fisher, A.G. (2003). Chromosomes, positions please! *Nat Cell Biol* **5**, 388-390.

Wyman, C. and Kanaar, R. (2006). DNA double-strand break repair: all's well that ends well. *Annu Rev Genet* **40**, 363-383.

Xu, N., Tsai, C.-L. and Lee, J.T. (2006). Transient homologous chromosome pairing marks the onset of X inactivation. *Science* **311**, 1149-1152.

Yokoe, H. and Meyer, T. (1996). Spatial dynamics of GFP-tagged proteins investigated by local fluorescence enhancement. *Nat Biotechnol* **14**, 1252-1256.

Yuan, S.-S.F., Chang, H.-L. and Lee, E.Y.-H.P. (2003). Ionizing radiation-induced Rad51 nuclear focus formation is cell cycle-regulated and defective in both ATM(-/-) and c-Abl(-/-) cells. *Mutat Res* **525**, 85-92.

Zgheib, O., Huyen, Y., Ditulliojr, R., Snyder, A., Venere, M., Stavridi, E. and Halazonetis, T. (2005). ATM signaling and 53BP1. *Radiotherapy and Oncology* **76**, 119-122.

Zhao, R., Bodnar, M.S. and Spector, D.L. (2009). Nuclear neighborhoods and gene expression. *Curr Opin Genet Dev* **19**, 172-179.

Zhao, Z., Tavoosidana, G., Sjölinder, M., Göndör, A., Mariano, P., Wang, S., Kanduri, C., Lezcano, M., Sandhu, K.S., Singh, U., et al. (2006). Circular chromosome conformation capture (4C) uncovers extensive networks of epigenetically regulated intra- and interchromosomal interactions. *Nat Genet* **38**, 1341-1347.

Curriculum Vitae

Hilmar Strickfaden
Rosskopfweg 12
79194 Gundelfingen
Germany

Hilmar.Strickfaden@lrz.uni-muenchen.de
Hilmar.Strickfaden@googlemail.com

Born: 12/30/1974
in Freiburg im Breisgau
(Baden-Württemberg), Germany

Nationality: German

Education:

09/81 – 07/85 Johann-Peter-Hebel elementary school in Gundelfingen (Baden-Württemberg)

09/85 – 06/94 Albert-Schweitzer-Gymnasium (high school) in Gundelfingen; finished with Abitur

Civilian service:

08/94 – 10/95 Schwarzwaldverein e.V. (Baden-Württemberg)

University:

Taking courses in Biology, Mathematics/Statistics, Philosophy and Computer Science

10/95 – 10/97 basic study period at the Albert-Ludwigs-Universität Feiburg im Breisgau (Baden-Württemberg) finished with “Vordiplom” in Biology

10/97 – 05/01 main study period at the Albert-Ludwigs-Universität Feiburg im. Breisgau (Baden-Württemberg) with focus on Molecular Biology & Genetics, Biochemistry and Cell-Biology
Also taking courses in Developmental Biology, Mathematics, Computer-Science, Statistics and Philosophy.

10/97 – 05/01 several student jobs as computer-pool administrator, computer administrator/webmaster of several workgroups.

05/01 – 05/02 recovering from a nearly lethal septic meningitis

05/02 – 12/02 preparing for the diploma-exams

01/03 – 12/03 Diploma Thesis: “Die Anwendung von Petri-Netzen bei der Erforschung genetischer und molekularer Netzwerke am Beispiel der lichtregulierten Sporulation von *Physarum polycephalum*.”

03/04 graduating from university with an overall average grade of 1,1 (very good)

03/04 – 12/04 working as a private computer consultant / looking for a Ph. D student position.

01/05 – 06/10 Ph. D. thesis at the department of biology II, chair for Human Genetics, Ludwigs-Maximilins University Munich (Bavaria) under supervision of Prof. Dr. Thomas Cremer: “Nuclear architecture explored by live-cell fluorescence microscopy using laser- and ion beam microirradiation”.

01/08 – 12/08 funded by CIPSM (Center for Integrated Protein Science Munich) Munich center of excellence

Laboratory skills

- cell culture of mammalian cells
- Immuno fluorescence preparation
- 2D- and 3D-FISH
- Microinjection of adherent cells (into the nucleus and into the cytoplasm)
- Transfection of mammalian cells by lipofection and electroporation and making stable cell lines.
- 4D in vivo microscopy
- Fluorescence microscopy
- widefield fluorescence microscopy
- widefield live-cell fluorescence microscopy
- laser scanning confocal fluorescence microscopy
- laser scanning confocal fluorescence live-cell microscopy
- spinning disc confocal fluorescence microscopy
- spinning disc confocal fluorescence live cell microscopy

Computer skills

Proficient in:

Operating systems:

- Apple Mac OS X
- GNU/Linux
- MS Windows XP/Windows 7

Office solutions:

- iWork '09 (Apple)
- Microsoft Office 2004
- Open Office

Image Processing

- ImageJ
- Huygens
- Adobe CS4
- Amira 5
- Blender

Microscopy Software

- Metamorph 6.0
- Volocity 5.3
- Leica Application Suite
- Axiovision (Zeiss)

- R (statistics package)
- Mathematica (computer algebra package)

Languages

- German (mother-tongue)
- English (advanced)
- French (school level)

Hobbies:

Music Instruments:	**Hobbies:**	
piano	hiking	photography
guitar	swimming	astronomy
electric bass	technology	chaos theory

Presentations:

12/05	Altleiningen: Workshop "Cell Biology and Microscopy": (Germany)
06/06	Erasmus MC Rotterdam (During a 4 weeks visit in the Lab of Prof. Roland Kanaar) (The Netherlands)
09/06	Reimlingen: Transregio Chromatin Summer School 2006 (Germany)
05/08	3rd Marie Curie Conference Madrid (Spain)
05/08	3rd EuroDyna Meeting Cambridge (England)
04/09	4th Marie Curie Conference Edinburgh (Scotland)
09/09	21st Wilhelm Bernhard Nuclear Workshop Ustron (Poland)
11/09	Laboratoire de Biologie Moléculaire Eucaryote à l' Université de Toulouse (France)

Other qualifications:

06/06	Learned establishing stable cell-lines during a three weeks stay in the Lab of Prof. Roland Kanaar (Erasmus MC Rotterdam)
12/07	Micro injcection-Workshop EMBL Heidelberg
09/08	Visit at the Max-Planck-Institute of Molecular Cell Biology and Genetics Dresden to learn microinjection of beads into cell nuclei.
12/08	Network administration TCP/IP Seminar
05/09	Received 5000 □ together with Thomas Cremer from the U of A LMU Partnership Fund to start a cooperation project between Thomas Cremer's and Michael J. Hendzel's lab.
05/10	Awarded "Lab of the Month" by Perkin Elmer

List of Publications:

- H. Strickfaden, T. Cremer, K. Rippe (2010) Chapter 17 Chromosome organization and dynamics Genome organization and function in the cell nucleus (2011).
- H. Strickfaden, A. Zunhammer, D. Köhler, S. von Koeningsbruggen, T. Cremer (2010) 4D chromatin dynamics in cycling cells: Theodor Boveri's Hypotheses revisited. Nucleus 1(3): (published online).
- S. Heisel, J. Hoffmann, H. Strickfaden, P. Chang, A. Ruggeri and E. Meese (2011) The glioma-amplified sequence 41 as centrosome associated protein essential for spindle formation (submitted to FASEB J).
- D.M. Seiler, J. Rouquette, C. Ottmann, H. Strickfaden, G.A. Drexler, B. Mazurek, C. Greubel, V. Hable, G. Dollinger, T. Cremer, A.A. Friedl (2011) Histone H3 lysine 4 trimethylation and radiation-induced double-strand breaks marked by γ-H2AX are mutually exclusive in human cells (in preparation).
- D. Illner, R. Zinner, V. Handtke, J. Rouquette, H. Strickfaden, C. Lanctôt, M. Conrad; A. Seiler; A. Imhof; T. Cremer; M. Cremer (2010) Remodeling of nuclear architecture by the thiodioxoxpiperazine metabolite chaetocin Experimental cell research 316:1662-80.
- B. Hübner, H. Strickfaden, S. Müller, M. Cremer, T. Cremer (2009) Chromosome shattering: an early observation of mitotic cell death revisited by live cell microscopy. Eur Biophys J 38(6):729-47.
- V. Hable, C. Greubel, A. Bergmaier, P. Reichart, A. Hauptner, R. Krücken, H. Strickfaden, S. Dietzel, T. Cremer, G.A. Drexler, A.A. Friedl, G. Dollinger. (2009). The live cell irradiation and observation set-up at SNAKE. Nucl. Instr. and Meth. B 267:2090-2097.
- C. Greubel, V. Hable, G.A. Drexler, A. Hauptner, S. Dietzel, H. Strickfaden, I. Baur, R. Krücken, T. Cremer, G. Dollinger, and A.A. Friedl;Competition effect in DNA damage response. (2008a) Radiat Environ Biophys. 47:423-429.

- Greubel, C., V. Hable, G.A. Drexler, A. Hauptner, S. Dietzel, **H. Strickfaden**, I. Baur, R. Krücken, T. Cremer Quantitative analysis of DNA-damage response factors after sequential ion microirradiation. (2008b) Environ Biophys. 47:415-422.
- Friedl, A.A., G.A. Drexler, M. Deutsch, **H. Strickfaden**, S. Dietzel, T. Cremer, A. Hauptner, R. Krücken, C. Greubel, V. Hable, and G. Dollinger. (2006). Radiobiological Experiments at the Munich Microprobe SNAKE. Radiation Research. 166:652-689.
- Hauptner, A., T. Cremer, M. Deutsch, S. Dietzel, G.A. Drexler, C. Greubel, V. Hable, R. Krücken, R. Löwe, **H. Strickfaden**, G. Dollinger, and A.A. Friedl. (2006a). Irradiation of Living Cells with Single Ions at the Ion Microprobe SNAKE. Acta Physica Polonica. 109:273-278.
- Hauptner, A., W. Friedland, S. Dietzel, G.A. Drexler, C. Greubel, V. Hable, **H. Strickfaden**, T. Cremer, A.A. Friedl, R. Krücken, H.G. Paretzke, and G. Dollinger. (2006b). Spatial Distribution of DNA Double-Strand Breaks from Ion Tracks. Royal Danish Academy of Sciences and Letters, Copenhagen:59-85.
- Hauptner A, Krücken R, Greubel C, Hable V, Dollinger G, Drexler GA, Deutsch M,Löwe R, Friedl AA, Dietzel S, **Strickfaden H**, Cremer T. DNA-repair protein distribution along the tracks of energetic ions. Radiat Prot Dosimetry. (2006);122(1-4):147-9. Epub 2006 Nov 28.

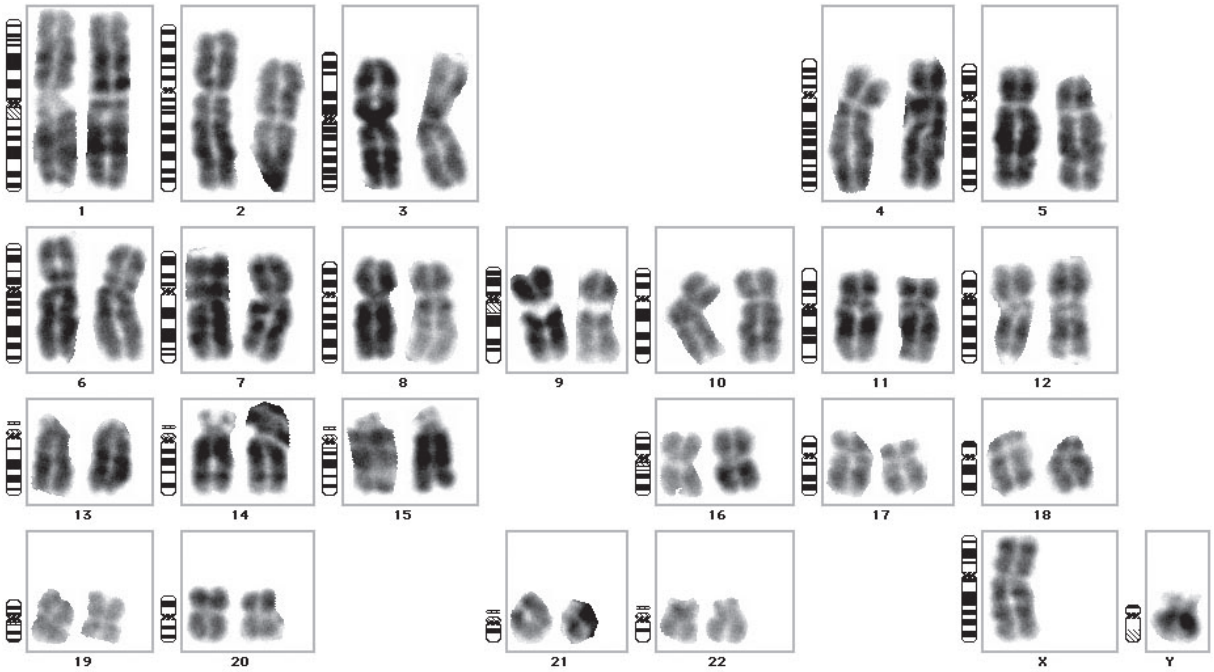

Karyogram of Hilmar Strickfaden ;-)

Appendix A

Abbreviations:

2D, 3D, 4D	2-dimensional, 3-dimensional, 4-dimensional
Ab	antibody
ALT	alternative lengthening of the telomeres
Bp	base pair
BrdU	5-bromo-2'-deoxyuridine
BSA	bovine serum albumine
CAD	computer aided design
CCD	charge-coupled device
CENP-B	centromeric protein B
ChIP	chromatin immunoprecipitation
nm, µm, cm	nanometer, micrometer, centimeter
CP	chromo protein
CT	chromosome territory
DAPI	4',6-diamidino-2-phenylindole
DDR	DNA damage response
dH_2O	de-ionized water
dd H_2O	ultrapure water or H_2O_{bidest}
DMEM	dulbecco's modified eagle medium
DNA	deoxyribo-nucleic acid
DSB	double strand break
dUTP	deoxyuridine-triphosphate
EDTA	ethylendiamintetraaceta
EM	electron microscope
EtOH	ethanol
FA	formaldehyde
FACS	Fluorescence Activated Cell Sorting
FCS	fetal calf serum
FISH	fluorescence In situ hybridization
FITC	fluorescein isothiocyanat
FOP	FGRF1 oncogene partner
FP	fluorescent protein
FRAP	fluorescence recovery after photobleaching
FRET	förster (fluorescence) resonance energy transfer
FWHM	full width half maximum
HAT	histone acetyl transferase

HCC	Hypercondensed Chromatin Condensation
HDAC	histone deacetylase
h.c.a.	highly cross adsorbed
HEPES	N-2-hydroxyethylpiperazin-N'-2-ethanesulfonic acid
HFb	human fibroblasts
HR	homologous recombination
HRR	homologous recombination repair
h-TERT	Human telomerase reverse transcriptase
IF	immunofluorescence
IRIF	irradiation induced foci
kDa	kilodalton
kb	kilobase
MCF-7	mammary carcinoma fibroblasts
M FISH	multicolor FISH
mb	megabase
NA	numerical aperture
NHEJ	non homlogous end joining
NOR	nucleoli organizer regions
NR	nuclear rotation
ON	over night
osm	osmol
PBS	phosphate-buffered saline
PC	perichromatin region
PCNA	Proliferating cell nuclear antigen
PSF	point spread function
RNA	ribonucleic acid
RNP	ribo-nucleo-protein
RPE	Retina pigment epithelium
RPMI	cell culture medium (roswell park memorial institute)
RPM	rotations per minute
RT	room temperature
SSB	single strand brake
Tris	tri(hydroxymethyl)aminomethane
Triton X-100	octylphenoldecaethylenglycolether
Tween 20	polyoxyethylensorbitanmonolaurat
X_a/X_i	Active X-chromosome/inactivated X-chromosome
WT	wildtype

Appendix B

Spectral profiles, Filters, Lasers and Fluorophores used in this Thesis:

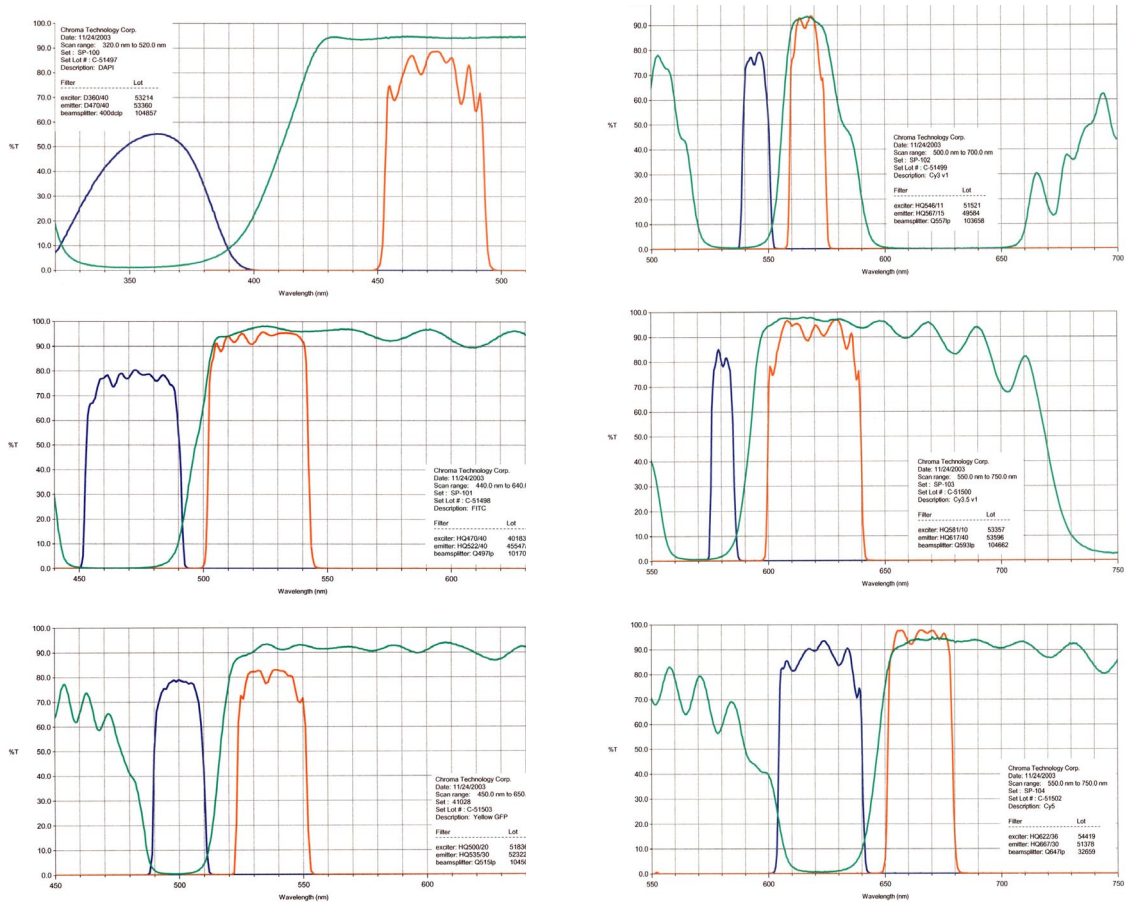

Fig. AB-1: Cell Observer (Axiovert 200 M widefield microscope) fluorescence filter characteristics

Power After Configuration (DPSS only)		405		440		488		514		561		640
Output Dichroic Combiner (PK Mode)	17	mW	23.00	mW	47.25	mW	16.80	mW	29.57	mW	31.30	mW
Power After 4hrs (Units Stacked)		mW		mW		mW		mW		mW		mW
Spec Coupling Efficiency (50%)												

PK Unit Output Test:		405		440		488		514		561		640
Output Power from PK Fibre	6.20	mW	13.50	mW	31.00	mW	10.07	mW	15.40	mW	15.50	mW
Output Power from PK Unit	2.1	mW	6.3	mW	21	mW	7.7	mW	13.22	mW	10.4	mW

Problems/Issues

		405		440		488		514		561		640
Clean Up Filter Fitted		Y		Y		n/a		n/a		n/a		Y
L.E.D. Operation		Y		Y		Y		Y		Y		Y
Raw Power from Laser	51	mW	44	mW	82	mW	28	mW	51	mW	52	mW
Output Power after AOTF/Manipulator		mW		mW		mW		mW		mW		mW
Frequency							122.312		110.141			
Amplitude							5932		5960			
Spec Coupling Efficiency (50%)												

PerkinElmer life sciences

Test Report

Product no. and name:		Changed by :	
UltraVIEW Vox		Revision #	1
		Date :	07/09/2004
Identifier:		Approved by :	
AOTF Laser Modulation System		Date :	
		Name	0
			0

Lasers		0
L7215212 Coherent 488nm 75mW		LDP.1116054.084753
L7215226 Cobolt 561nm 75mW		0561-03-03-2097-0050
L7215228 Cobolt 514nm 25mW		1820
L7215201 Melles Griot 405nm 50mW		00063177
L7215202 Melles Griot 445nm 40mW		00063037
L7215203 Melles Griot 640nm 50mW		00063041

Fig. AB-2: Laser Specs of the Perkin Elmer Ultra View Vox System.

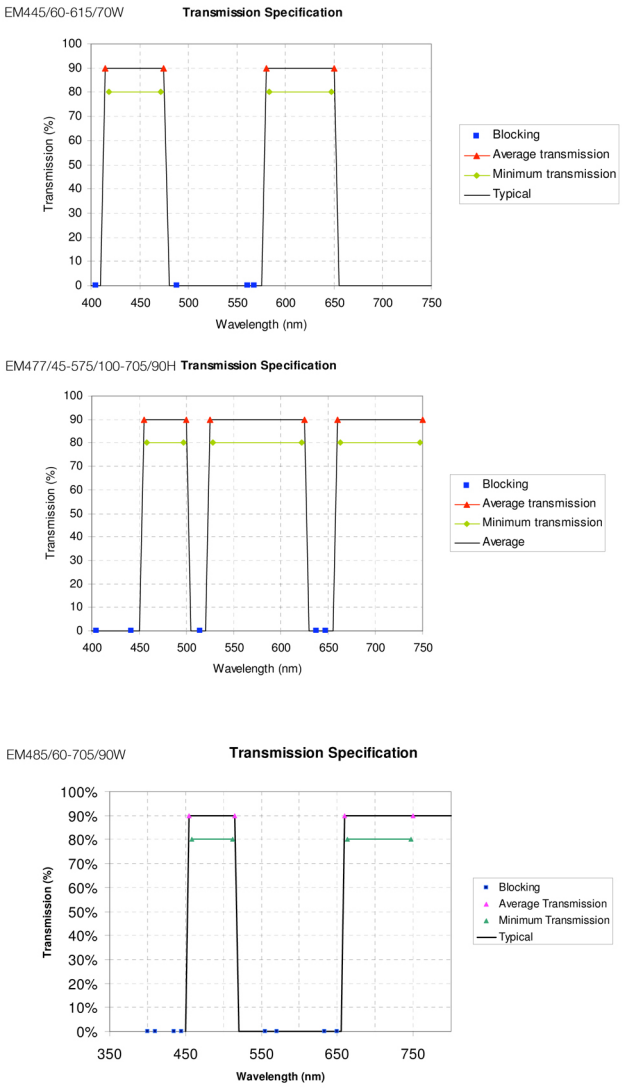

Fig. AB1-3: Emission Filters used at the Ultra *View* VOX system by Perkin Elmer.

Appendix C

Shift Measurements at the Spinning Disc Microscope:

In order evaluate the extent of the chromatic shift in the images recorded at the spinning disc microscope polystyrol beads with diameters of 500 nm and fluorescent in 4 colors were recorded in 3D. The acquired image stacks were then used to determine the intensity centers of recorded beads for each fluorescent color (in this case green and red) Distances (n=20) between these intensity centers were measured and averaged.

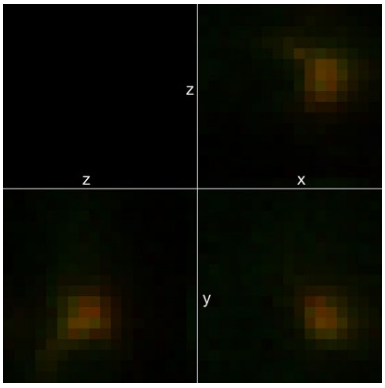

3D Stack of a 500 nm fluorescent “TetraSpeck” bead recorded at a z-stepping of 100 nm using the same light paths that were used in this thesis for imaging the live-cell data (GFP and mRFP). Shift measurements were carried out in ImageJ using the plug-in “Shift Measurement 3D”.
40x Plan-Apochromat objective by Zeiss.
dx = 10 nm
dy = -35.0 nm
dz = 88.2 nm

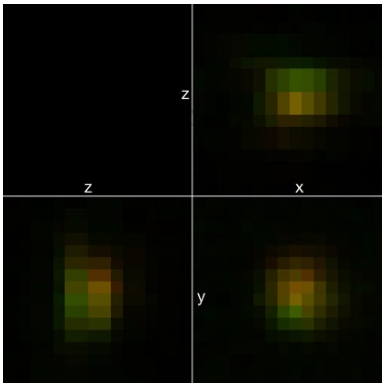

63x Plan-Apochromat objective by Zeiss

dx = 5 nm
dy =-37 nm
dz = 62 nm

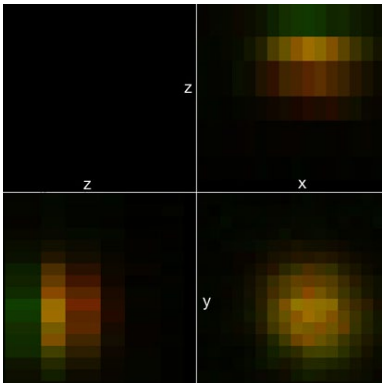

100x Plan-Apochromat objective by Zeiss

dx = 3 nm
dy = -5 nm
dz = 103.95 nm

Fig. AC-1: 3D stacks of a 500 nm fluorescent “TetraSpeck” bead recorded with a z-stepping of 100 nm using the same light paths that were used for imaging the live-cell data in GFP and mRFP. Shift was measured using the plug-in “Shift Measurement 3D”.

Measuring the chromatic shift

Background:

In fluorescence microscopy it is virtually impossible to entirey superimpose the optical focus planes of different color channels at a given axial objective position. Misalignments (shifts) between different fluorescence channels can be measured by 3D recording of single beads that fluoresce in all of the used colors. Knowing the chromatic shifts for a certain fluorescence microscope (and the respective objectives) allows to decrease misalignments in 3D color images by assigning the same slice number to slices of different color channels that physically have the closest vincinity.

Materials:

- Confocal microscope
- Coverslip
- Fluorescent beads: Tetraspeck
- Nail polish
- Object slide
- Vectashield embedding medium (antifade)

Method:

Preparation of a microscope slide for measuring chromatic shift:

- Dilute Tetraspeck bead solution and spot an appropriately volume onto a coverslip
- Wait until the solution on the cover slip has dried. Usually this is enough to adhere the beads permanently on the coverslip. If adherence of beads is an issue Poly-L-Lysine coated coverslips (see 3.2.3) may help.
- Embed coverslip in anti fade mounting medium (Vectashield) on a microscope slide
- Use nail polish to seal the sample

Measureing chromatic shifts:

- Mount the microscope slide with the tetraspeck beads onto the microscope stage
- Focus beads (~10 beads should be visible in the field of view without being too close to each other).
- Record image stacks in all fluorescence channels (leaving some void

space above and below the top and the bottom of the beads, respectively.

Determination of chromatic shift (image processing):

- Load the image stacks of the beads in the different fluorescence channels into ImageJ and determine the chromatic shift using the plugin Sync Measure 3D developed by Dr. J. Walter. This plugin allows to determine the intensity gravity centers of for every bead in every color channel in x,y and z. Comparing the intensity gravity centers of the different channels and calculating the actual physical dimensions yields the shift in all three axes.
- Measuring of at least 20 beads is recommended.
- Save chromatic shift vector information for subsequent shift corrections in an Excel worksheet.

Appendix D

Fluorophores used in this Thesis:

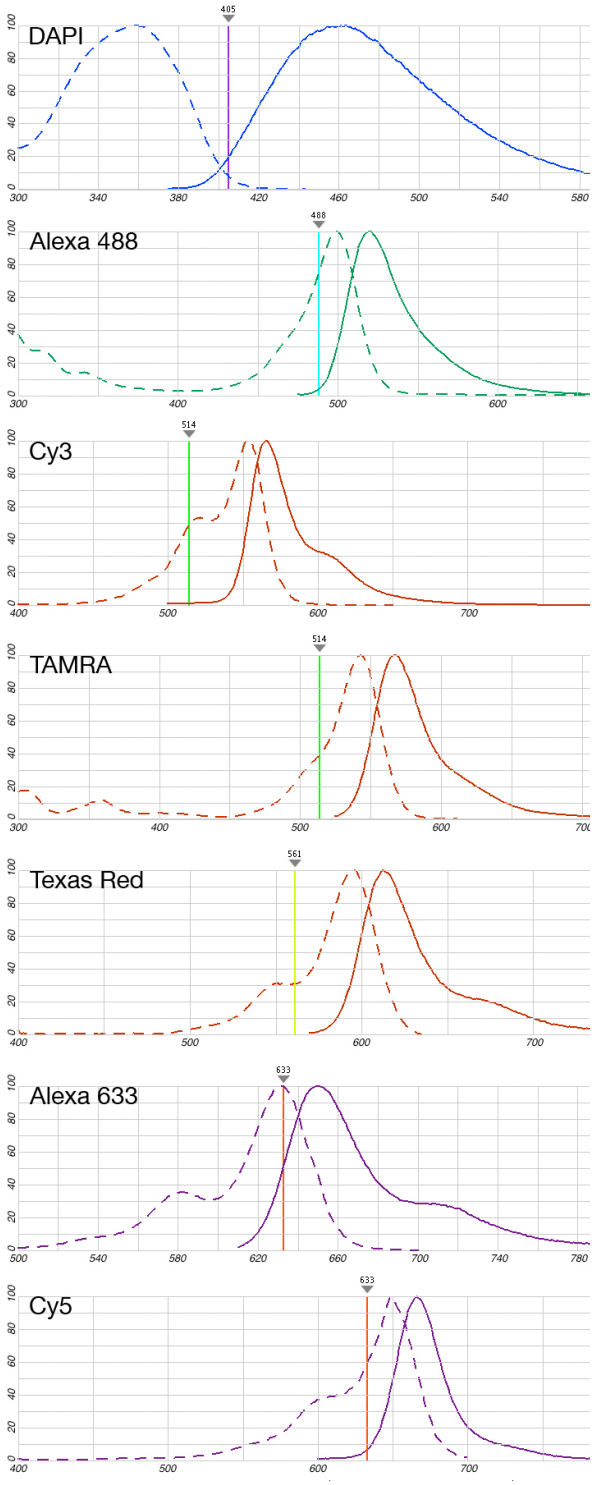

Fig. AD-1: Spectral profiles of the fluorochromes used in this thesis. The dashed lines represent the excitation spectra – the continuos lines the emission spectra. The perpendicular line shows the laser line that was used to excite the respective fluorophore. Profiles were generated by the Fluorescence SpectraViewer on the Invitrogen website.

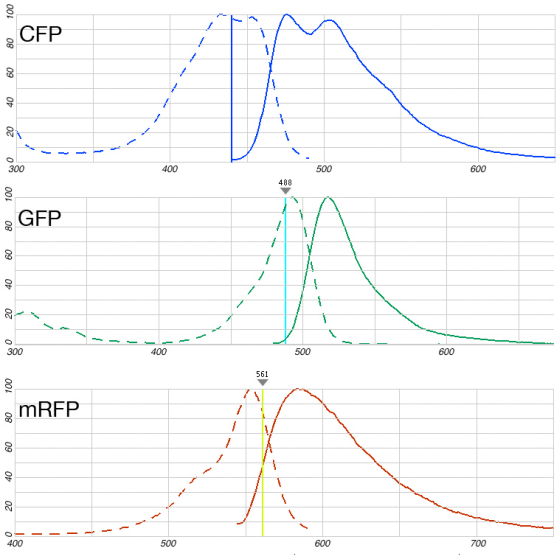

Fig.AD-2: Spectral profiles of the fluorescent proteins used in this thesis. The dashed lines represent the excitation- the continuos lines the emission spectra. The perpendicular line shows the laser line the protein was excited with. Profiles were generated with the Fluorescence SpectraViewer on the Invitrogen website.

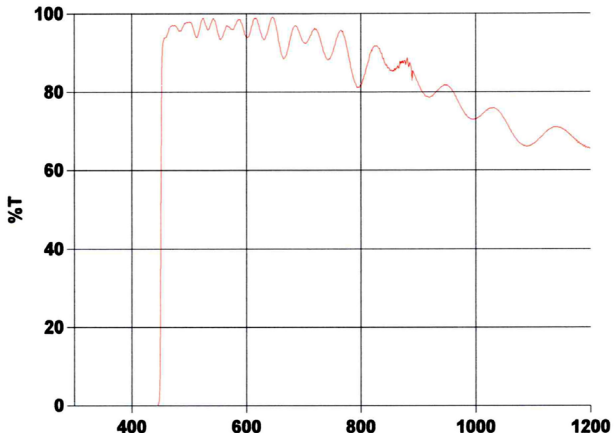

Fig. AC-3a: 3RD Millennium Longpass filter LC-3RD/450LP-25 filter was used to protect the cells from ultra violet light emitted by fluorescence lamps (Halogen lamp,HXP 120, HBO) during live cell observations.

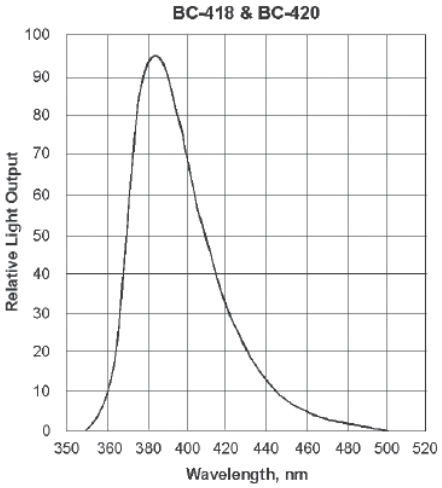

Fig. AC-3b: Light emitted using the BC-418 plastic scintillator.

Appendix E

Used cell lines:

ATCC® Number:	CCL-2™
Designations:	**HeLa**
Biosafety Level:	2 (CELLS CONTAIN PAPOVAVIRUS)
Growth Properties:	adherent
Organism:	*Homo sapiens* (human)
Morphology:	epithelial
Source:	**Organ:** cervix **Disease:** adenocarcinoma **Cell Type:** epithelial
Cytogenetic Analysis:	Modal number = 82; range = 70 to 164. There is a small telocentric chromosome in 98% of the cells. 100% aneuploidy in 1385 cells examined. Four typical HeLa marker chromosomes have been reported in the literature.HeLa Marker Chromosomes: One copy of MI, one copy of M2, four-five copies of M3, and two copies of M4 as revealed by G-banding patterns. M1 is a rearranged long arm and centromere of chromosome 1 and the long arm of chromosome 3. M2 is a combination of short arm of chromosome 3 and long arm of chromosome 5. M3 is an isochromosome of the short arm of chromosome 5. M4 consists of the long arm of chromosome 11 and an arm of chromosome 19.
Age:	31 years adult
Gender:	female
Ethnicity:	Black

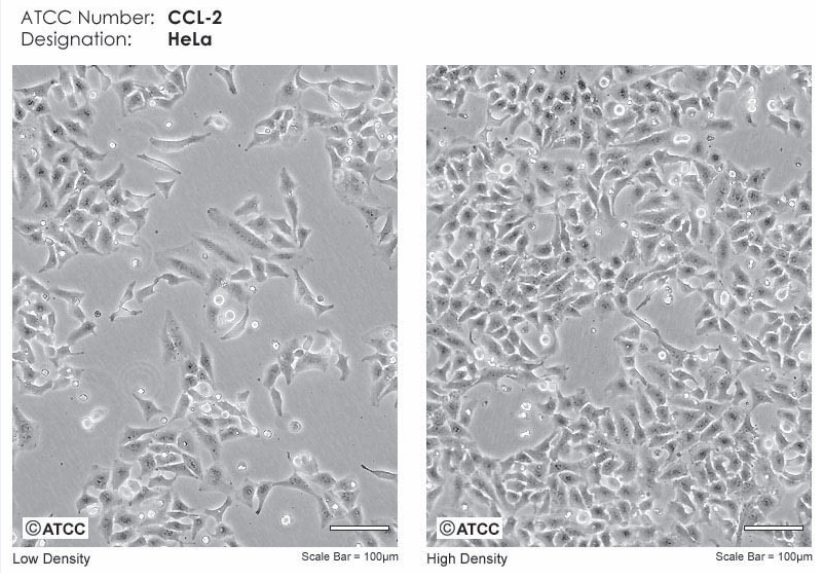

ATCC® Number:	CCL-2™
Comments:	The cells are positive for keratin by immunoperoxidase staining. HeLa cells have been reported to contain human papilloma virus 18 (HPV-18) sequences. P53 expression was reported to be low, and normal levels of pRB (retinoblastoma suppressor) were found.
Propagation:	**ATCC complete growth medium:** The base medium for this cell line is ATCC-formulated Eagle's Minimum Essential Medium, Catalog No. 30-2003. To make the complete growth medium, add the following components to the base medium: fetal bovine serum to a final concentration of 10%. **Atmosphere:** air, 95%; carbon dioxide (CO_2), 5% **Temperature:** 37.0°C
Subculturing:	**Subcultivation Ratio:** A subcultivation ratio of 1:2 to 1:6 is recommended **Medium Renewal:** 2 to 3 times per week
Preservation:	**Freeze medium:** Complete growth medium supplemented with 5% (v/v) DMSO

ATCC® Number:	CRL-4000™
Designations:	**hTERT RPE1**
Biosafety level:	1
Growth Properties:	adherent
Organism:	*Homo Sapiens* (human)
Morphology:	epithelial 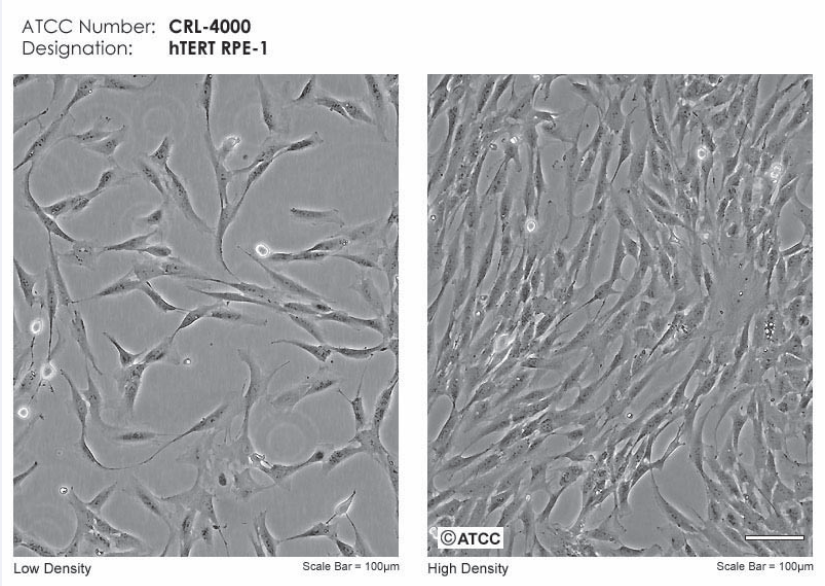
Cytogenetic Analysis:	This is a near-diploid human cell line of female origin with a modal chromosome number of 46 that occurred in 90% of the cells counted. The sex chromosomes consist of a karyotypically normal X-chromosome and a derivative X-chromosome with additional chromosomal material at the terminal end of the q-arm. The derivative X-chromosome was present in all of the cells analyzed.
Gender:	female

ATCC® Number:	CRL-4000™
Comments:	The hTERT-immortalized retinal pigment epithelial cell line, hTERT RPE1, was derived by transfecting the RPE-340 cell line with the pGRN145 hTERT-expressing plasmid (ATCC MBA-141). Cells were cultured in medium containing hygromycin B until stable clones were selected [Pubmed: 9454332, 9916802].
Propagation:	**ATCC complete growth medium:** The base medium for this cell line is ATCC-formulated DMEM:F12 Medium Catalog No. 30-2006.To make the complete growth medium, add the following components to the base medium: • fetal bovine serum to a final concentration of 10% • 0.01 mg/ml hygromycin B **Atmosphere:** air, 95%; carbon dioxide (CO_2), 5% **Temperature:** 37.0°C
Growth Conditions:	Subculture when cell concentration reaches between 2 10^4 and 4 10^4 cells/cm^2.
Subculturing:	**Subcultivation Ratio:** 1:5 to 1:10 twice weekly **Medium Renewal:**
	every 2 days (or as needed)
Preservation:	**Freeze medium:** culture medium, 30%; fetal bovine serum, 60%; DMSO, 10%

ATCC® Number:	HTB-96™
Designations:	**U-2 OS**
Depositors:	Hellstrom
Biosafety Level:	1
Growth Properties:	adherent
Organism:	*Homo sapiens* (human)
Morphology:	epithelial 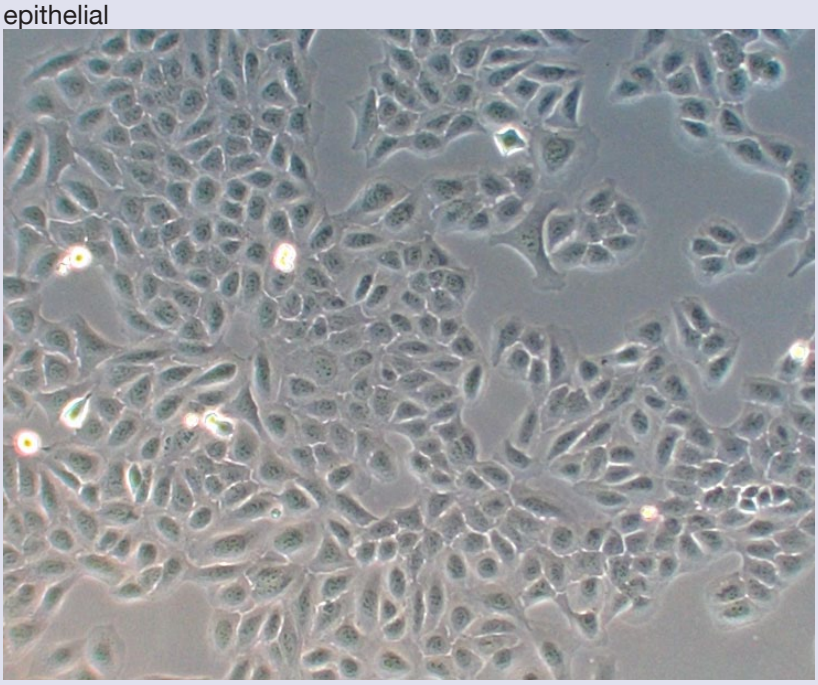
Source:	**Organ:** bone **Disease:** osteosarcoma osteosacoma derived growth factor (ODGF)

ATCC® Number:	HTB-96™
Cytogenetic Analysis:	Cell line U-2 OS is chromosomally highly altered, with chromosome counts in the hypertriploid range. We did not find the hypodiploid cell population described by J. Ponten, et al., Instead, most of the population has slightly higher counts than first described. Very few normal chromosomes are present, but a high number of stable marker chromosomes are identified., Different chromosomal rearrangements involving the same chromosomes (N1, N7, N9, and N11 particularly), are seen. Twenty-two markers are found including: t(9qter → 9q21::1p36 → 1p::?), 7p+, iso(17q), t(15q;?), 4q+, del(3)(q21), 5q(aberrant) and others.
Age:	15 years
Gender:	female
Ethnicity:	Caucasian
Comments:	J. Ponten and E. Saksela derived this line (originally 2T) in 1964 from a moderately differentiated sarcoma of the tibia of a 15 year old girl. Viruses were not detected during co-cultivation with WI-38 cells or in CF tests against SV40, RSV or adenoviruses. Mycoplasma contamination was detected and eliminated in 1972.
Propagation:	**ATCC complete growth medium:** The base medium for this cell line is ATCC-formulated McCoy's 5a Medium Modified, Catalog No. 30-2007. To make the complete growth medium, add the following components to the base medium: fetal bovine serum to a final concentration of 10%. **Temperature:** 37.0°C
Subculturing:	**Subcultivation Ratio:** A subcultivation ratio of 1:3 to 1:6 is recommended **Medium Renewal:** 2 to 3 times per week
Preservation:	**Freeze medium:** Culture medium, 95%; DMSO, 5%

Appendix F

Maps of the used expression plasmids:

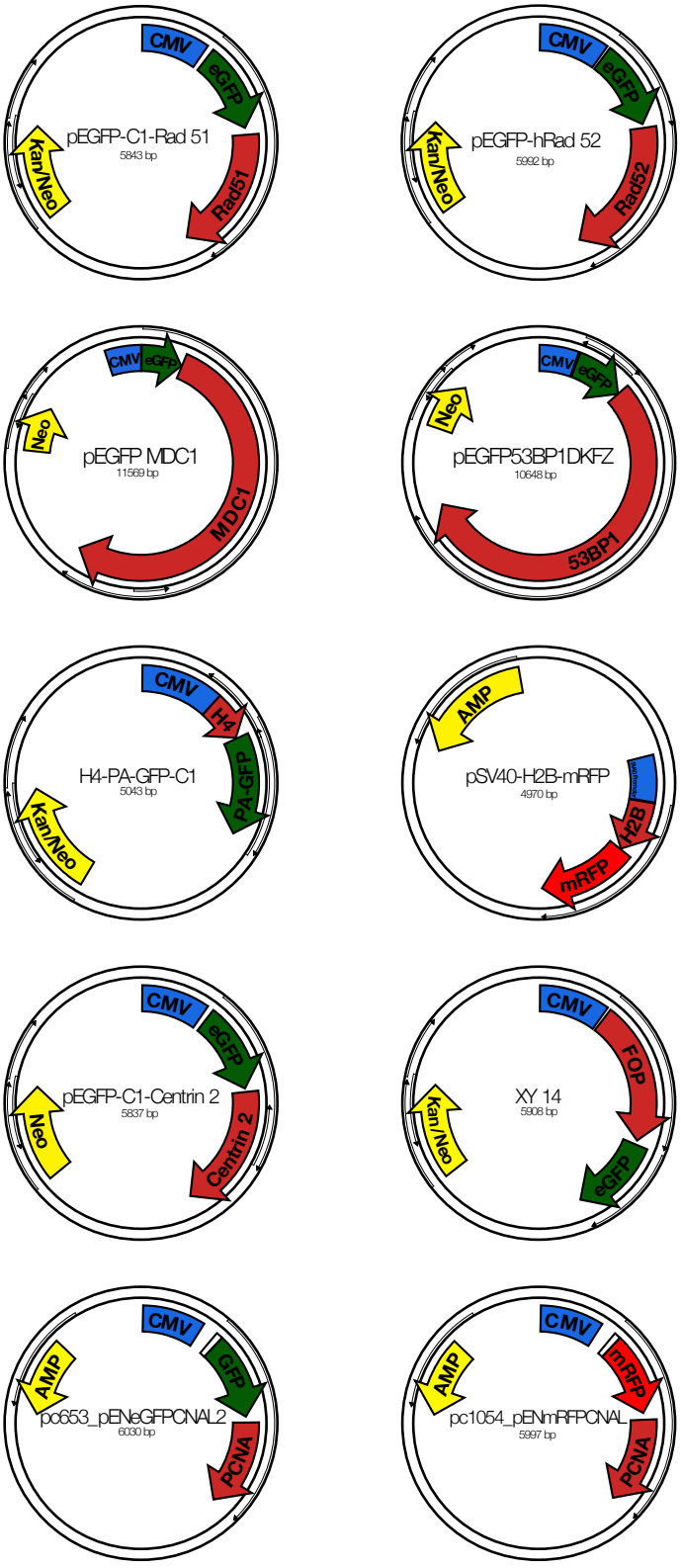

Fig. AF-1: Plasmid maps of the expression constructs used in this thesis. Most of the shown expression vectors are based upon a Clontech backbone containing a Kan/Neo resistance, a CMV promotor and a multi cloning site for generation of N or C-terminal fusion proteins between the GFP (RFP) and a protein sequence of choice. Though being one ORF the sequences of the GFP part and the sequence of the fluorescently tagged protein are displayed seperately in the shown maps.
Green arrows represent the position of the GFP sequences.
Dark red arrows represent the sequence of a mRFPs
Red arrows represent the DNA-sequence of the protein which is inserted into the vector and which is tagged by the fusion to the fluorescent protein GFP or RFP respectively.
Yellow arrows represent the ORF coding for the selection marker (Neo/Kan respct. Amp) for selection in prokaryotes or eukaryotes.
Blue boxes represent the used promotors for the cloned genes.

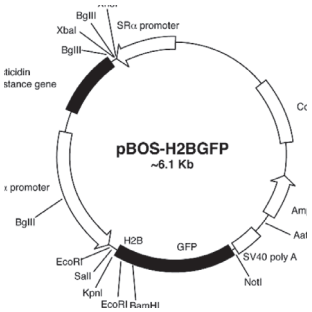

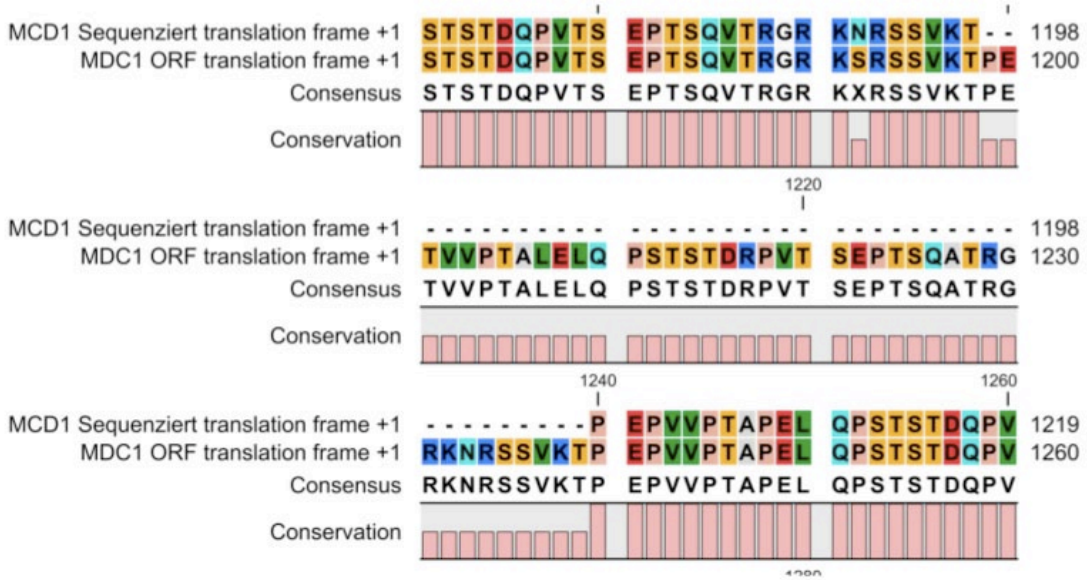

Fig. AF-2: Amino acid sequence of the used MDC1-GFP construct containing a deletion (kindly provided by Dr. Guido Drexler).

Appendix G

Box plots of mitotic events and whole cell cycles based on live-cell observations:

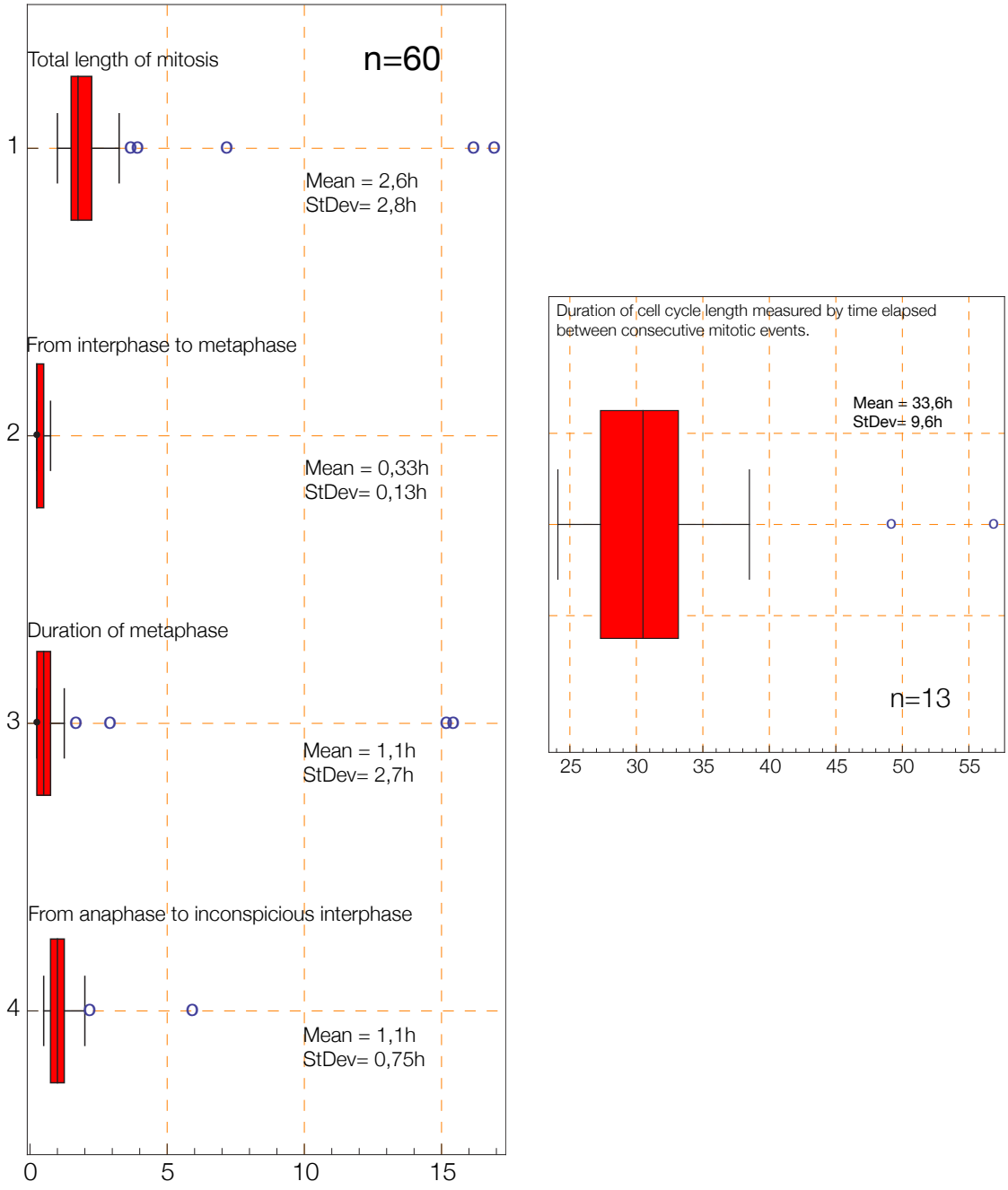

Fig. AG-1: Left column: Box plots of mitotic stage durations in the RPE1 H4 PA-GFP H2B-mRFP cell line. **Right column:** Duration of this line's the cell cycle length measured by tracing cell pedigrees and determining the time between consecutive mitoses. The x-Achsis measures the time in hours.

Appendix H
Die Blastomerenkerne von *Ascaris megalocephala* und die Theorie der Chromosomenindividualität.

Von Theodor Boveri (Würzburg) 1909

Text Color Legend:

I. Chromosomes occupy distinct chromosome territories (CTs) in the cell nucleus.

II. CT order is stably maintained during interphase.

III. These changes occur in particular during prometaphase, when chromosomes become attached to the spindle and move toward the metaphase plate.

IV. Neighborhood arrangements in the fully established metaphase plate are conserved to a considerable extent throughout anaphase and telophase resulting in rather symmetrical arrangements of CTs in the two daughter nuclei.

Einleitung

Die Anschauung, daß im ruhenden Kern der höheren Tiere und Pflanzen eine Anzahl von Territorien bestehen, deren jedes aus einem bestimmten Chromosoma der vorhergehenden Mitose entstanden ist und bei der nächsten Mitose wieder zu einem bestimmten Chromosoma sich zusammenzieht, diese Anschauung hat, seit sie zuerst ausgesprochen worden ist, durch vielfältige und sehr verschiedenartige Studien im Tier- und Pflanzenreich immer neue und kräftigere Stützen gewonnen.

So höchst wertvoll nun aber auch diese im Lauf der Jahre hinzugekommenen Beweismittel sind, in zweierlei Hinsicht ist dasjenige Objekt, für welches die Lehre zuerst klar formuliert worden ist – der junge Keim von *Ascaris megalocephala* –, bisher durch kein andres übertroffen worden. Nirgends anders läßt sich so einfach und sicher die für jene Hypothese unerläßliche Grundlage feststellen, daß nämlich abnorme Chromosomenzahlen sich durch den Ruhezustand des Kerns hindurch erhalten; nirgends sonst bietet ein Kern so sichere Kriterien für die Frage dar, ob an der nämlichen Stelle, wo sich ein Chromosoma in den nicht analysierbaren Ruhezustand umgewandelt hat, auch wieder eines sich herausbildet.

Es ist daher eine für die Individualitätstheorie nicht unwichtige Frage, ob die Angaben, die ich vor 21

Jahren für dieses Objekt gemacht habe (9), zutreffend sind oder nicht. In einem vor kurzem erschienenen kritischen Referat hat R. Fick (23) dies bestritten. Was ich für die Erhaltung abnormer Chromosomenzahlen als vollen Beweis ansehen zu dürfen glaubte, betrachtet er als eine bloße Deutung; die Gründe für die Individualitätshypothese aber, die ich aus meinen Beobachtungen über die Schleifengruppierung abgeleitet habe, bezeichnet er als gänzlich nichtig.

So schien es mir geboten, die *Ascaris*–Kerne speziell mit Rücksicht auf den zweiten Punkt von neuem zu studieren. Ehe ich auf die Ergebnisse dieser Untersuchung eingehe, sei das Problem kurz dargelegt.

Nachdem C. Rabl (30) für Salamanderkerne gezeigt hatte, daß die Stellung der Schleifen in dem zur Teilung sich vorbereitenden Kern ungefähr die gleiche ist wie diejenige der Tochterschleifen, die den Kern gebildet hatten, habe ich mir die Frage vorgelegt, ob sich an den für solche Untersuchungen viel günstigeren Blastomerenkernen von *Ascaris megalocephala* nicht Anhaltspunkte dafür finden ließen, daß jedes neue Chromosoma mit einem bestimmten der in den Kern eingegangenen identisch ist. Der Weg zur Prüfung dieser Frage war folgender. Die Beobachtung der Vorgänge bei der Bildung der ruhenden Kerne lehrt, daß, so lange sich überhaupt der Verlauf der Tochterchromosomen noch er kennen läßt, deren Gestalt und gegenseitige Stellung nicht wesentlich verändert wird. Geht nun jedes neue Chromosoma genau aus dem Kernbezirk hervor, den ein Tochterchromosoma gebildet hatte, der Art, daß jedes frühere Ende wieder zu einem Ende wird, so muß beim Sichtbarwerden der neuen Chromosomen im Prinzip die gleiche Gruppierung auftreten, die vor der Kernbildung bestanden hatte. Die Entscheidung wäre einfach, wenn man diese Verhältnisse im Leben verfolgen könnte. Da dies nicht der Fall ist, handelte es sich darum, ein Mittel zu finden, um die Frage auf indirektem Weg zu entscheiden. Dieses Mittel ist gegeben in der Vergleichung der beiden Schwesterkerne. Da diese beiden Kerne sich aus prinzipiell gleicher Schleifengruppierung ableiten, müssen sie, falls der ruhende Kern die ihm zugrunde liegende Chromosomenanordnung dauernd bewahrt, auch in den Prophasen der nächsten Teilung wieder beide die gleiche Schleifenstellung aufweisen. Und wird nun eine solche Übereinstimmung in der Tat gefunden, so darf es, da die Schleifengruppierung von Ei zu Ei variabel und also innerhalb dieser Grenzen funktionell bedeutungslos ist, als sehr wahrscheinlich bezeichnet werden, daß die Gleichheit der Gruppierung in den Schwesterkernen eine ererbte ist, d. h. daß sich die gegebene Anordnung durch den Ruhezustand hindurch erhalten hat.

Die von mir an einigen günstigen Zweizellenstadien ausgeführte Analyse hatte mich in der Tat zu solchem Schluß geführt. Dieses Ergebnis nun ist es, das Fick in ausführlicher Darlegung als hinfällig erklärt, und zwar sowohl auf Grund einer Prüfung meiner alten Figuren als auch gestützt auf die Angaben andrer Autoren und auf eigene Untersuchungen am gleichen Objekt.

Ein Mangel haftet meinen damaligen Resultaten allerdings an: ich hatte nur eine kleine Zahl analysierbarer Fälle auffinden können. Als daher der Angriff Ficks erschienen war, suchte ich nach günstigerem Material und stieß dabei in einigen, vor 9 Jahren in Alkohol–Essigsäure[1] konservierten Uteri auf Eier, die zur Prüfung unsrer Frage in unübertrefflicher Weise geeignet sind. Ihre Vorzüge gegenüber meinen Präparaten von 1888 bestehen in drei Umständen:

1. gehören sie der Varietät *univalens* an, bei der die Verfolgung der einzelnen Schleifen unvergleichlich viel leichter ist als bei *bivalens*;
2. sind die Kerne der beiden primären Blastomeren fast in allen Keimen in der gleichen Phase ihrer Metamorphose, so daß die für unsre Zwecke notwendige Analyse beider Kerne, die ich früher nur an fünf Objekten hatte ausführen können, nun an zahllosen Eiern möglich ist;
3. endlich zeigen die Eier eine beträchtliche Mannigfaltigkeit sehr charakteristischer Chromosomenstellungen, so daß sieben Haupttypen unterscheidbar sind, die in verschiedenem Mengenverhältnis vorkommen.

Alle im folgenden beschriebenen Befunde beziehen sich, falls nichts andres bemerkt ist, auf den gleichen Wurm, der mit A bezeichnet sein mag.

1 95 Teile Alkohol 70% +5 Teile Eisessig.

I. Die verschiedenen Typen von Äquatorialplatten im Ei von *Ascaris meg. univalens*.

Naturgetreue Abbildungen von Äquatorialplatten, alle von dem Wurm A stammend, sind in Fig. 1a–7a (Taf. VII) wiedergegeben. Diese sieben Haupttypen, zu denen es mancherlei untergeordnete Variationen gibt, werden in sehr verschiedener Häufigkeit angetroffen.

A. Beide Schleifen gestreckt oder leicht gebogen.	
1. Die vier Schleifenenden weit voneinander entfernt	
2. Die beiden Schleifen mit ihrem einen Ende benachbart	
3. Jedes Ende der einen Schleife einem Ende der andern benachbart	
B. Eine Schleife gestreckt oder leicht gebogen, die andre U-förmig zusammengebogen.	
4. Die Enden der gestreckten Schleife von denen der U-förmigen	
5. Das eine Ende der gestreckten Schleife den beiden Enden der U-förmigen benachbart	
C. Beide Schleifen U-förmig gebogen.	
6. Die Enden der einen Schleife von denen der andern weit entfernt	
7. Alle vier Schleifenenden benachbart	

Bei unserm Wurm A ist Typus 6 weitaus am häufigsten, dann folgen, unter sich etwa gleich zahlreich, Typus 4 und 5. Selten sind die Typen 1, 2 und 7. Nur ein einziges Mal habe ich den Typus 3 gefunden

II. Die Entstehung der Tochterkerne. Die Kernfortsätze.

Im Jahr 1883 hat bekanntlich E. Van Beneden (3) im *Ascaris*–Ei die Entstehung der Tochterplatten durch Längsspaltung der Chromosomen der Äquatorialplatte entdeckt und damit die völlig symmetrische Schleifengruppierung in den beiden Tochtergruppen. Betrachtet man ein Ei im Stadium der Metakinese in polarer Ansicht, so erhält man bei verschiedener Einstellung zweimal die gleiche Figur. Bei Van Beneden (3, pl. XIX bis, Fig. 25) ist ein solches Bild von der Varietät *bivalens* wiedergegeben; ein ähnliches in etwas schiefer Ansicht findet sich bei mir (9, Taf. IV, Fig. 80a). Genau das gleiche gilt natürlich für die Varietät univalens. So sind also die sieben oben aufgeführten Typen auch in den Tochterplatten zu unterscheiden. Allerdings lassen sich die Bilder dieser Stadien bei dem Wurm A an Klarheit mit andern Präparaten, die ich gesehen habe, nicht vergleichen. Eine Erscheinung, auf die ich schon früher gelegentlich hingewiesen habe: die große Variabilität des Teilungsvorgangs im *Ascaris*–Ei, soweit es sich um untergeordnete Punkte handelt, zeigt sich auch hier. Das Eigentümliche in unserm Fall besteht darin, daß nur ein ziemlich kleiner mittlerer Abschnitt einer jeden Schleife von Spindelfasern besetzt und also direkt von dementsprechenden Abschnitt der Schwesterschleife wegbewegt wird. Nur dieser kleine Bereich bildet die eigentliche, „Tochterplatte", die größeren Endabschnitte sind in der bekannten Weise gegen den Äquator abgebogen, wo sie oft noch lange mit denen der Schwesterschleife in Zusammenhang stehen (Fig. 9, Taf. VIII).[2] Etwas spätere Stadien nach schon vollzogener Durchschnürung des Protoplasmas sind in Fig. 10 und 11 wiedergegeben. Die abgebogenen Schleifenabschnitte zeigen sich in einer Weise, die ich nur bei diesem Wurm A gefunden habe, gegen die Spindelachse zusammengedrängt, um sich, wenn die passive Bewegung des Auseinanderweichens zu

2 Ich bemerke, daß bei fast allen hier besprochenen Präparaten die Zellenoberfläche mehr oder weniger stark gerunzelt ist. Ich habe diese Artefakte in den Zeichnungen nicht wiedergegeben, sondern überall glatte Konturen gezeichnet, wie wir sie von den lebenden Eiern kennen.

Ende ist, wieder weiter auseinanderzuspreizen, so daß die Anordnung wieder durchsichtig wird.

Ein solches Stadium mit wieder aufgelockerten Chromosomen ist in Fig. 14a wiedergegeben; in 14b sind die bei den Chromosomengruppen in der Richtung der Spindelachse gezeichnet, und zwar beide bei der gleichen Stellung des Eies. Wir haben es hier mit dem Typus 6 zu tun, der oben für die Äquatorialplatte des Eies folgendermaßen charakterisiert worden ist: „Beide Schleifen U–förmig gebogen; die Enden der einen Schleife von denen der andern weit entfernt". In jeder Tochtergruppe ist diese Anordnung leicht zu erkennen, zugleich aber auch, daß die früher so exakte Symmetrie der beiden Antagonisten schon auf diesem Stadium keine vollkommene mehr ist. Es machen sich hier allem Anschein nach schon Eigenbewegungen der Chromosomen geltend, die nicht genau parallel gehen. An diesen Bewegungen ist besonders der Umstand erwähnenswert, daß die mittleren Schleifenabschnitte einer jeden Gruppe, die ursprünglich alle im gleichen Niveau und dem Pol am nächsten standen, sich mehr oder weniger stark gegeneinander verschieben können. Fig. 14a zeigt dies sehr klar, besonders ausgeprägt in der oberen Zelle. Das Rablsche Schema: Schleifenwinkel gegen den Pol gerichtet, gilt hier nicht mehr. Es sieht oft so aus, als wenn die Schleifen sich in einem gegebenen Raum möglichst gleichmäßig zu verteilen suchten und sich dabei einander auswichen. Aus dem früheren flächenhaften Nebeneinander wird ein räumliches Untereinander, so daß die beiden Fäden bei Polansicht (Fig. 14b) einander überschneiden. Alles dies wird uns wichtig werden, wenn wir mit dem oben betrachteten Stadium dasjenige der nächsten Prophasen vergleichen werden.

Ein dem eben betrachteten Bild sehr ähnliches zeigt Fig. 15. Nur ist hier bereits die Kernmembran aufgetreten, in ihrem Verlauf dem Komplex der mittleren Schleifenabschnitte folgend. Die Schleifenenden ragen noch frei ins Protoplasma heraus. Wir treffen hier wieder auf einen Punkt, der bei verschiedenen Individuen des Pferdespulwurms in hohem Grad variabel sein kann, nämlich das zeitliche Verhältnis zwischen dem Erscheinen der Kernmembran und der Metamorphose der Tochterschleifen. In den Eiern, die meiner Arbeit von 1888 zugrunde liegen, beginnen die Chromosomen mit der Umbildung zum Gerüstzustand lange, ehe eine Spur der Kernvacuole zu sehen ist; zur Zeit, wo diese auftritt, sind schon so zahlreiche Anastomosen zwischen den Chromosomen entstanden, daß sich der Bezirk, der jedem dieser Elemente entspricht, nicht mehr feststellen läßt. Bei den Eiern, die uns hier beschäftigen, finden wir die Chromosomen im jungen Kernbläschen noch fast unverändert vor; ihr Verlauf ist mit Leichtigkeit zu bestimmen.

Auch in dem weiter fortgeschrittenen Kern der Fig. 16 ist dies noch der Fall. Die mittleren Teile der Chromosomen erscheinen hier zu blassen, undeutlich und unregelmäßig begrenzten Bändern aufgequollen, die teils ihre breite, teils ihre schmale Seite dem Beschauer zukehren. Bei der Betrachtung der Breitseite zeigen sich die stärker färbbaren Teile sehr häufig zu einer Doppelreihe angeordnet. Anastomosen zwischen den bei den Schleifen oder zwischen verschiedenen Abschnitten der gleichen Schleife sind kaum noch aufgetreten.

Im Gegensatz zu den mittleren Bereichen sind die frei herausragenden Schleifenenden noch wenig verändert; sie sind viel kompakter und stärker färbbar; in ihrem Umkreis erscheinen nun die ersten Spuren schlauchförmiger Membranen, die uns in späteren Stadien als deutliche Blindsäcke der Hauptvacuole wieder begegnen.

Auf das Detail der Chromosomenmetamorphose gehe ich nicht ein; es ist mir zweifelhaft, ob der Konservierungszustand der Präparate eine bis ins einzelne gehende Beschreibung alles Wahrnehmbaren rechtfertigen würde. Doch muß ich kurz der Darstellung gedenken, die in jüngster Zeit K. Bonnevie (5) von den Kernen der *Ascaris*-Blastomeren gegeben hat. Sie findet, daß jedes Tochterchromosoma sich vor dem Übergang in den Ruhezustand zu einem Spiralfaden metamorphosiert. Die mittleren Teile der Schleifen sollen sich als Ganzes, in offenen Spiralwindungen anordnen, während sich in den Schleifenenden die färbbare Substanz zu einem feineren Spiralfaden differenziert, der als Leiste die achromatische Grundsubstanz umwindet und sich kontinuierlich in die offene Spirale des mittleren Schleifenabschnittes fortsetzt.

Bei der Beurteilung dieser Angaben wird man wieder die große Variabilität aller dieser Verhältnisse bei verschiedenen Individuen berücksichtigen müssen. Völlig sicher ist es, daß die spiralige Anordnung der mittleren Schleifenbereiche keine allgemeine und also auch keine wesentliche Erscheinung sein kann; ich habe sie an keinem einzigen der je von mir studierten Blastomerenkerne gesehen; auch bei unserm Wurm A ist sie mir niemals begegnet. Dagegen sind mir die Bilder, auf welche sich Fräulein Bonnevies Beschreibung eines Spiralfadens an den Schleifenenden gründet, wohlbekannt. In etwas schematischer Weise finden sich diese Strukturen bereits bei Van Beneden und Neyt (4, Pl. I, Fig. 6 und 8) abgebildet. Am deutlichsten habe ich sie in Eiern gefunden, die in einem starken Alkoholessiggemisch (20% Eisessig) konserviert waren. Die Bilder, die ich hier gesehen und neuerdings an Präparaten von *bivalens* genauer studiert habe, sind denen K. Bonnevies ungemein ähnlich und lassen sich kaum anders als im Sinn eines chromatischen

Spiralfadens deuten. Nicht unerwähnt darf jedoch bleiben, daß mir viele Präparate speziell von *univalens* vorgekommen sind, die durchaus nicht den Eindruck schlechter Konservierung machen und bei denen der Übergang der Schleifenenden in den Zustand eines groben Gerüstes Schritt für Schritt verfolgbar ist, ohne daß Bilder auftreten, die den Gedanken an eine Spiralstruktur nahelegen könnten. So wird gegenüber einer Generalisierung der von K. Bonnevie betonten Struktur noch eine gewisse Vorsicht geboten sein.

Glücklicherweise sind alle diese Fragen nach der feineren Struktur für das Problem, das uns hier beschäftigt, ohne Belang. Es kommt uns nur auf die gröberen Verhältnisse an, über deren Realität kein Zweifel bestehen kann. In dieser Beziehung seien nun die Kerne der Fig. 16 noch etwas genauer ins Auge gefaßt. Wir haben hier die letzte Phase vor uns, in welcher die Tochterchromosomen in den beiden Kernen noch sicher verfolgt werden können. Wir wollen sie deshalb hier nochmals auf ihre Symmetrie vergleichen. Auf den ersten Blick mag die Anordnung der Fäden in den beiden Kernen recht verschieden erscheinen. Allein genauere Betrachtung zeigt, daß oben wie unten der gleiche Gruppierungstypus besteht, nämlich unser Typus 5, den wir für die Äquatorialplatte des Eies folgendermaßen charakterisiert haben: „eine Schleife gestreckt oder leicht gebogen, die andre U–förmig zusammengebogen; das eine Ende der gestreckten Schleife den beiden Enden der U–förmigen benachbart". An jedem Kern unsrer Fig. 16 finden wir links das isolierte Ende der gestreckten Schleife; verfolgen wir ihren Verlauf, so gelangen wir zu ihrem andern Ende, das neben den beiden Enden der U–förmigen Schleife liegt. Nach diesen Merkmalen sind also die einander entsprechenden Chromosomen der beiden Kerne mit aller Sicherheit zu bestimmen. Und nun ist es wichtig zu beachten, wie verschieden sich die mittleren Schleifenabschnitte oben und unten präsentieren. Zum großen Teil rührt dies freilich daher, daß sich die Kerne nicht mehr völlig symmetrisch gegenüberstehen. Während an dem oberen Kern das isolierte linke und die drei rechten Schleifenenden annähernd in der gleichen optischen Ebene und im größten Durchschnitt der Kernvacuole liegen, befindet sich das linke Schleifenende des unteren Kerns erheblich tiefer als der größte optische Schnitt des Kernbläschens; die drei rechten Enden liegen entsprechend höher. Aber auch abgesehen davon ist der Verlauf der Chromosomen des oberen Kerns demjenigen der unteren nur in den gröberen Zügen vergleichbar. Wir können also auch später, wenn die Chromosomen wieder aus dem Ruhezustand herauskommen, keine größere Übereinstimmung erwarten, als sie hier besteht.

Wir gelangen nun zu einem der wichtigsten Punkte, zu der Frage nach der Bedeutung der Kernfortsätze. Ich habe zuerst 1887 (8) kurz dargelegt, daß diese für die Blastomerenkerne von *Ascaris* so charakteristischen Bildungen ihre Entstehung den Schleifenenden verdanken. Zu dem gleichen Resultat kamen fast gleichzeitig Van Beneden und Neyt (4). Eingehend habe ich sodann diese Verhältnisse 1888 (9) erörtert. Nichts ist leichter zu konstatieren und tritt ja auch wieder an den besprochenen Figuren hervor, als daß die als linsenförmiges Bläschen auftretende Kernvacuole für gewöhnlich die Schleifenenden nicht mit umgreift; vielmehr bilden diese ihre besonderen Kernmembranen aus, wobei es dahingestellt bleiben mag, ob, wie ich es früher beschrieben habe, sich im Umkreis des Chromatinfadens Flüssigkeit ansammelt, gegen die sich das Protoplasma allmählich mit einer Membran abgrenzt; oder ob, wie Bonnevie, im Anschluß an Van Beneden und Neyt, wahrscheinlich gemacht hat, die achromatische Substanz des Chromosomas aufquillt und so die Oberfläche des Chromosomas direkt zur Oberfläche des Blindsackes wird. Mir ist es sehr wahrscheinlich, daß auch dieser Vorgang variabel ist und hier so, dort anders verläuft. Das schließliche Resultat ist jedenfalls überall gleich: der fertige Kern besitzt Blindsäcke, deren Membranen mit der Membran der Hauptvacuole ein Kontinuum bilden.

Was nun die Zahl dieser Fortsätze anlangt, so ist sie variabel, aber nicht etwa in gesetzloser Weise. Da die Tochterplatte bei *bivalens* acht, bei *univalens* vier Schleifenenden besitzt, wären dort acht, hier vier Kernfortsätze zu erwarten; und solche Fälle, die man als die typischen bezeichnen kann, kommen auch in der Tat vor. Ich habe früher für *bivalens* Kerne mit acht Fortsätzen beschrieben; ein solcher Kern ist, wenn auch nicht vollkommen deutlich, in meiner Arbeit von 1888 (9) in Fig. 74 (Taf. IV) zu sehen. Auch K. Bonnevie hat *bivalens*-Kerne mit acht deutlichen Fortsätzen beobachtet. Kerne von *univalens* mit vier aufs beste ausgeprägten Blindsäcken finden sich z. B. bei Herla (24, PI. XVI, Fig. 27). Doch sind diese Fälle, bei denen die Zahl der Aussackungen genau der Zahl der Chromosomenenden entspricht, wenigstens bei *bivalens*, keineswegs häufig; gewöhnlich ist die Zahl der Fortsätze kleiner, ja sie können völlig fehlen.

Die Gründe für diese Verschiedenheiten liegen in Folgendem. Die Kernenden verhalten sich bei der Bildung ihrer Blindsäcke genauso wie die ganzen Chromosomen bei der Bildung ganzer Kerne. Wir wissen, daß wenn die Chromosomen einer Tochterplatte nahe beisammenliegen, sie ein gemeinschaftliches Bläschen bilden; liegen sie weiter von einander entfernt, so bildet jedes Chromosoma für sich ein eignes Bläschen. Der letztere Fall ist z.B. typisch für die Blastomeren der Seeigel.

Allerdings kommen hier diese Partialkerne alsbald mit einander in Berührung und verschmelzen zu einer einzigen Vacuole. In andern Fällen können sie aber dauernd selbständig bleiben; solche Zustände habe ich (9) für *Ascaris*-Eier beschrieben und l. e. in Fig. 45–47, Taf. III abgebildet. Die verschiedenen Erfahrungen auf diesem Gebiet führen zu der Vorstellung, daß eine nachträgliche Verschmelzung der primär gebildeten Bläschen nur bis zu einem gewissen Alter möglich ist; hat die Kernmembran einmal ihre volle Ausbildung erlangt, so tritt eine Verschmelzung nicht mehr ein. So ist es auch offenbar zu erklären, daß in vielen Eiern, z.B. bei *Ascaris*, die beiden Vorkerne gewöhnlich nicht verschmelzen, obgleich sie sich berühren; sie haben eben diesen Kontakt erst erlangt, nach dem die Stärke der Membran ein Zusammenfließen nicht mehr erlaubte.

Übertragen wir diese Ergebnisse auf die Kernfortsätze, so ergibt sich das sehr einfache Resultat: liegen die einzelnen Kernenden zur Zeit der Kernrekonstruktion weit voneinander entfernt, so bildet jedes seinen eignen Blindsack; liegen zwei oder drei oder vier Kernenden nahe zusammen, so bilden sie einen gemeinsamen Blindsack. Dazwischen mag es Übergänge geben, wo die Vacuolen um zwei ziemlich naheliegende Enden zunächst selbständig entstehen, dann aber, ehe ihre Membranen widerstandsfähig geworden sind, in Berührung kommen und verschmelzen.

Zur Illustration des Gesagten ist das Material unseres Wurmes A vorzüglich geeignet. Wenn wir die sieben hier unterschiedenen Gruppierungstypen betrachten, so können wir voraussagen, wie viele Kernfortsätze ein jeder ergeben muß. Beim Typus 1 müssen vier Fortsätze entstehen; beim Typus 2 drei Fortsätze, einer mit zwei Enden, die beiden andern mit je einem; einen ganz ähnlichen Kern wird Typus 4 ergeben. Typus 3 und Typus 6 müssen Kerne liefern mit zwei opponierten Blindsäcken, deren jeder zwei Schleifenenden birgt. Auch Typus 5 wird Kerne mit zwei Fortsätzen ergeben, von denen aber der eine drei, der andre ein Ende umschließt. Endlich aus dem Typus 7 müssen sich Kerne ableiten, die nur einen einzigen Blindsack besitzen.

Die Untersuchung der Eier des Wurms A bestätigt diese Forderungen in der vollkommensten Weise. Vor allem zeigt sich, daß nicht nur alle im vorstehenden aufgeführten Kernformen wirklich vorkommen, sondern daß sie auch ungefähr in dem nämlichen Mengenverhältnis auftreten, das oben für die verschiedenen Typen der Äquatoriaplatten des Eies konstatiert worden ist. Blastomerenkerne mit vier Fortsätzen, wie solche in jenem Material sehr häufig waren, das mir zu meiner Arbeit über die Embryonalentwicklung von *Ascaris* gedient hat, finden sich bei dem Wurm A nur äußerst selten; darum eben, weil Äquatorialplatten und also auch Tochterplatten mit vier weit von einander entfernten Chromosomenenden sehr selten sind. Ungemein häufig dagegen sind die Fälle, wo jeder Blastomerenkern zwei ungefähr opponierte, gleichstarke Fortsätze besitzt; ganz im Einklang mit der großen Häufigkeit des Typus 6. Von den Tochtergruppen der Fig. 14 läßt sich voraussagen, daß sie solche Kerne mit zwei „zweiwertigen" Fortsätzen bilden werden; in Fig. 15 ist dies schon ganz unverkennbar, obgleich die Schleifenenden noch frei im Protoplasma liegen. An diesem Keim läßt sich auch leicht demonstrieren, warum die korrespondierenden Fortsätze der beiden Schwesterkerne nicht immer völlig gleich ausfallen. Infolge der oben besprochenen Eigenbewegungen der Tochterchromosomen ereignet es sich nicht selten, daß beim Auftreten der Kernvacuole die Enden des einen Kerns weiter herausragen als ihre Antagonisten im andern Kern. Dementsprechend müssen auch die Blindsäcke verschieden groß werden. Dies zeigt sich z. B. in den ausgewachsenen Kernen der Fig. 21 (Taf. IX), welche dem gleichen Typus angehören und in denen sich in jedem Fortsatz die beiden Enden noch aufs deutlichste erkennen lassen. Im linken Kern sind beide Blindsäcke sehr wohl entwickelt und deutlich von dem Hauptraum abgesetzt, im rechten ist besonders der obere Blindsack nur schwach ausgeprägt.

Die Kerne der oben eingehend betrachteten Fig. 16 (Taf. VIII) werden, wie ja zum Teil schon erkennbar, auch zwei Fortsätze erhalten, aber zum Unterschied von den bisher betrachteten einen einwertigen und einen dreiwertigen. Entsprechend der beträchtlichen Häufigkeit des Typus 5 sind ruhende Kerne dieser Art oft anzutreffen (Fig. 23, Taf. IX), ebenso solche mit einem zweiwertigen und zwei einwertigen Fortsätzen, die sich aus dem gleichfalls ziemlich häufigen Typus 4 ableiten lassen.

Ich glaube nicht, daß es nötig ist, das Gesagte durch weitere Figuren zu erläutern, umsoweniger, als uns alle diese Kernformen in Stadien, wo die neuen Schleifen bereits erkennbar sind, wieder begegnen werden.

Nur über die Kerne, die eine einzige Aussackung oder gar keine besitzen, ist noch einiges zu sagen. Sie müssen dann entstehen, wenn alle vier Schleifenenden der Tochterplatte bei der Kernrekonstruktion sehr nahe nebeneinanderliegen. Typus 7 muß dazu führen, und zwei eben gebildete Tochterkerne dieses Typus haben wir in Fig. 17 (Taf. VIII) vor uns, sehr wohl charakterisiert durch die vier an der einen Seite zusammengedrängten Schleifenenden, die alle von einem einzigen Blindsack umschlossen werden. Es scheint mir aber, daß Kerne mit nur einer Aussackung in unserm Material auch noch in andrer Weise entstehen

können. Ich habe oben schon darauf hingewiesen, daß in diesen Eiern häufig während der Metaphasen alle Schleifenenden einer Tochtergruppe gegen die Spindelachse zusammengedrängt werden. Fig. 10 u. 11 illustrieren diesen Zustand. Ich habe dieses Verhalten zu oft gesehen, um annehmen zu können, daß es nur aus der so selten gefundenen Äquatorialplatte des Typus 7 hervorgehen kann. Vielmehr scheint mir die Annahme nicht zu umgehen, daß diese kompakten Figuren bei allen Schleifengruppierungen eintreten können, daß sich aber in der Regel später die zusammengedrängten Enden wieder auf die der bestimmten Gruppierung entsprechenden Abstände voneinander entfernen. Man kann sich leicht vorstellen, daß fadenartige Gebilde von gewisser Konsistenz, während sie ziemlich rasch durch eine zähflüssige Substanz hindurchgezogen werden, ihre nicht direkt angegriffenen Enden in der Art, wie Fig. 10 es zeigt, abbiegen, um beim Aufhören der Bewegung wieder in eine mehr lockere Anordnung überzugehen[3]. Allem Anschein nach kann es aber auch vorkommen, daß die in der Metaphase eingetretene enge Zusammenlagerung aller vier Schleifenenden nicht mehr rückgängig gemacht wird. Dann werden sie alle vier von einem einheitlichen weiten Blindsack umschlossen. Ein frühes Stadium dieses Zustands ist in Fig. 18 gezeichnet. Ähnlich wie in Fig. 17 sind alle vier Schleifenenden dicht benachbart, aber nicht, wie dort einseitig, sondern im Umkreis der Spindelachse. Sie werden ohne Zweifel gemeinsam einen einzigen Kernfortsatz bilden, obgleich, nach der ganzen Gruppierung zu schließen, die Schleifenanordnung der Äquatorialplatte nicht dem Typus 7, sondern dem Typus 4 angehörte, bei welchem in der Regel drei Fortsätze auftreten, zwei einwertige und ein zweiwertiger.

Etwas weiter entwickelte Schwesterkerne mit je einem vierwertigen Fortsatz sind in Fig. 19 dargestellt. Es sind nur die Kerne abgebildet, da bei einer und derselben Stellung des ganzen Keimes nicht beide Kerne die gleiche Ansicht darboten, ein Umstand, auf den ich im nächsten Abschnitt zurückkomme. Für diese Kerne halte ich es für möglich, daß sie aus dem Gruppierungstypus 7 herzuleiten sind. Wie es an ihnen zu sehen ist, so findet man auch an den entsprechenden späteren Stadien den vierwertigen Fortsatz gewöhnlich nicht scharf von der Hauptvacuole abgesetzt; der ganze Kern besitzt eine Birnform. In wieder andern Fällen dieser Art ist eine besondere Aussackung für die Enden überhaupt nicht vorhanden, die Kernmembran ist an allen Stellen konvex gerundet. Aber in einem Punkt sind auch diese fortsatzlosen Kerne noch charakteristisch; sie sind nämlich stets in der Achsenrichtung verlängert, wogegen die Kerne, bei denen die Schleifenenden in besonderen Aussackungen liegen, stets in der Richtung ihrer Achse verkürzt sind, eine Differenz, die ja nach der ganzen Genese des Kerns leicht zu verstehen ist.

Es ist nach all dem Gesagten klar, daß sehr geringe Distanzunterschiede darüber entscheiden können, ob zwei Schleifenenden einen gemeinsamen Blindsack bilden oder jedes einen für sich allein. Und so ist es leicht erklärlich, daß man, bei unserm Wurm A allerdings selten, bei manchen andern Individuen aber häufig, Schwesterkerne findet, die in der Zahl ihrer Fortsätze nicht übereinstimmen. Dies gilt besonders für die Varietät *bivalens*, wo die acht Schleifenenden viel gedrängter liegen und somit viel leichter der Fall eintreten wird, daß zwei Enden bei der Rekonstruktion des Kerns so nahe benachbart sind, daß sie von einem gemeinsamen Blindsack umschlossen werden. Es deuten also diese Verschiedenheiten keineswegs darauf hin, daß die Kernfortsätze Bildungen sind, die während der Existenz des Ruhekerns auftreten oder verschwinden können; vielmehr dürfen wir mit Bestimmtheit sagen: so viele Kernfortsätze nach voller Ausbildung der Kernmembran vorhanden sind, so viele erhalten sich an genau gleicher Stelle bis zur Kernauflösung; es kommt keiner weg und keiner dazu. Sind Schwesterkerne in der Zahl ihrer Fortsätze verschieden, so rührt dies ausschließlich daher, daß schon vor der Kernbildung die Stellung der Schleifenenden in den beiden Tochtergruppen eine verschiedene war.

Dies mag noch an ein paar Beispielen näher erläutert sein. In Fig. 9 (Taf. VIII) ist ein Ei in Durchschnürung abgebildet. Die Tochterchromosomen stehen sich im ganzen symmetrisch gegenüber. Doch sieht man rechts, daß die beiden unteren Schleifenenden dicht aneinander gepreßt sind, wogegen ihre oberen Antagonisten weit voneinander abstehen, und zwar ist die Entfernung noch größer, als dies in der Figur zum Ausdruck kommt. Aller Voraussicht nach wird aus der unteren Gruppe ein Kern mit zwei, aus der oberen ein solcher mit drei Blindsäcken entstehen.

Zwei fertige Kerne, von denen der eine einen Fortsatz mehr hat als der andre, sind in Fig. 22 (Taf. IX) wiedergegeben. Betrachten wir zuerst den rechten Kern, so sind hier zwei Fortsätze vorhanden, ein sehr dicker, der drei Enden enthält, und ein ganz dünner mit nur einem Ende. Der linke Kern zeigt nur einen Fortsatz, in dem drei Enden unterscheidbar sind. Dieser Fortsatz entspricht also dem rechten dreiwertigen. Nahe an seiner Wurzel bemerkt man, der Kernmembran entlang verlaufend, das vierte Schleifenende, nach

3 Um festzustellen, ob die verschiedene Raschheit des Teilungsverlaufes auf diese Verhältnisse von Einfluß ist, habe ich *Ascaris*-Eier des gleichen Uterus bei sehr verschiedenen Temperaturen (15° und 38°) sich teilen lassen. Die Teilungsfiguren zeigten jedoch nicht die erwartete Verschiedenheit.

oben zu in das unanalysierbare Gerüstwerk übergehend. Wir sehen es diesen beiden Kernen noch ganz gut an, worin sie bei ihrer Bildung differierten. Während in der unteren Chromosomengruppe alle vier Enden nahe zusammenlagen, wie etwa in Fig. 18 (Taf. VIII), hat sich in der oberen Gruppe ein Ende von den übrigen frei gemacht, wie wir etwas ganz Ähnliches in der Fig. 9 angetroffen haben. Man braucht sich in dem linken Kern das vierte Ende nur an seiner Wurzel herausgebogen zu denken, um zu einem dem rechten Kern genau entsprechenden Typus zu gelangen.

Halten sich hier und überhaupt bei dem Wurm A die beobachteten Verschiedenheiten in Grenzen, welche zumeist erlauben, die Konfiguration des einen Kerns auf die des andern zurückzuführen, so ist dies bei einem andern Wurm aus dem gleichen Pferd – wir wollen ihn B nennen – häufig nicht der Fall. Aber man braucht nur die früheren Stadien zu berücksichtigen, um alsbald die Ursache für diese auffallende Erscheinung zu erkennen. In ganz ungewöhnlicher Weise nämlich zeigen sich in den Eiern dieses Wurms an den frei im Protoplasma liegenden Tochterchromosomen sehr ausgiebige Gestalts- und Lageveränderungen, welche, da sie in den beiden Gruppen nicht parallel gehen, die durch den Teilungsmechanismus bewirkte Symmetrie der beiden Chromosomengruppen stark beeinträchtigen, ja unter Umständen ganz verwischen. In Fig. 12 u. 13 (Taf. VIII) sind Beispiele hierfür gegeben. Mit Sicherheit darf man von der letzteren Figur sagen, daß aus den hier zu konstatieren den Gruppierungen Schwesterkerne hervorgehen würden, die kaum eine Ähnlichkeit hätten, und von denen sich, besonders wenn noch die so häufig eintretende Lageveränderung der ganzen Kerne hinzukommt (vgl. den nächsten Abschnitt), nicht angeben ließe, wie ihre Fortsätze auf einander zu beziehen sind.

Aus allem, was wir im vorstehenden über die Kernfortsätze erfahren haben, ergibt sich folgendes Resultat. Zahl und Anordnung der Fortsätze sind ausschließlich bedingt durch die Lage, welche die Schleifenenden der Tochterchromosomen zur Zeit der Kernbildung einnehmen. Diese Lage der Tochterchromosomen ist abhängig von zwei Umständen: erstens und vor allem von der Chromosomenstellung in der Äquatorialplatte des Eies, zweitens von Lage- und Gestaltsveränderungen, welche diese Elemente v o r d e r Kernbildung erfahren. In Fällen, wo fast ausschließlich das erste Moment eine Rolle spielt (Wurm A), sind die Verhältnisse sehr leicht zu durchschauen. Da der mitotische Prozeß zu einer symmetrischen Anordnung der Tochterschleifen führt, stimmen auch die aus ihnen entstehenden Kerne in Zahl und Lage ihrer Fortsätze spiegelbildlich miteinander überein. Die Variationen aber, die von einem Keim zum andern bestehen, entsprechen nicht nur im allgemeinen, sondern auch prozentisch den verschiedenen Schleifenstellungen, die in den Äquatorialplatten der Eier des gleichen Tieres zur Beobachtung kommen.

Ändern die Tochterschleifen vor der Kernbildung ihre Lage und Form, so können Kerne entstehen, die in der Ausbildung ihrer Fortsätze gar keine Ähnlichkeit mit einander haben (Wurm B).

Alle Tatsachen zusammen lassen keinen Zweifel, daß die Kernfortsätze Bildungen sind, denen nicht die geringste funktionelle Bedeutung zukommt. Ein Blastomerenkern ohne jede Aussackung entwickelt sich ebenso normal weiter wie einer, der drei oder vier besitzt.

III. Lageveränderungen der Blastomerenkerne.

Eine Erscheinung, die bei Untersuchung unsrer Frage den flüchtigen Beobachter irreführen kann, ist die, daß die beiden Kerne, die sich ihrer Entstehung nach symmetrisch gegenüberstehen sollten und in manchen Fällen diese Stellung auch wirklich beibehalten, in vielen Eiern ihre Lage ändern, so daß sie sowohl in der Achse der vorausgehenden Teilungsfigur als auch in jeder andern Richtung sich drehen können. So kann es kommen, daß z. B. die ursprünglich der Schwesterzelle zugekehrte Seite nun gerade entgegengesetzt gerichtet ist. Wenn ich diese Veränderungen als Drehungen des K e r n s i n n e r h a l b s e i n e r Z e l l e bezeichne, so ist dabei vorausgesetzt, daß die beiden Blastomeren ihrerseits diejenige gegenseitige Stellung bewahren, in der sie sich voneinander abgeschnürt haben. Es ist jedoch denkbar, daß die g a n z e n Z e l l e n sich gegen einander verschieben, und dies würde, auch bei fixierter Lage der Kerne, den gleichen Effekt haben, wie wenn sich die Kerne im Plasma drehen. Verschiedene Umstände, auf die ich hier nicht eingehe, scheinen mir für die erstgenannte Alternative: Kerndrehung innerhalb der Zelle, zu sprechen.

Die Neigung zu solchen Drehungen ist bei verschiedenen Würmern sehr verschieden. Sehr beträchtliche Drehungen hat zuerst Nussbaum (27) eingehend beschrieben; damit völlig übereinstimmende Beobachtungen hat neuerdings Zur Strassen (35) mitgeteilt. Auf diese beiden Autoren sei daher verwiesen. Auch in meinem neuen Material sind solche Drehungen, und zwar der verschiedensten Art und des verschiedensten Grades ungemein häufig. Als ein Beispiel mäßiger Drehung sei Fig. 21 (Taf. IX) angeführt, wo der rechte Kern die ursprüngliche Orientierung zur Berührungsfläche der beiden Zellen beibehalten hat, wogegen in der linken Zelle eine Drehung erfolgt ist, so daß die beiden Kernfortsätze, die gegen diejenigen des andern Kerns gerichtet sein sollten, etwas schief gegen den Beschauer gekehrt sind. Da in diesem Falle jeder Kern zwei zweiwertige Fortsätze besitzt, ist es nicht möglich zu sagen, welcher Fortsatz des einen Kerns einem bestimmten des andern entspricht. Zwar wird man geneigt sein, den unteren links mit dem unteren rechts als zusammengehörig zu betrachten, und ebenso die oberen. Allein es ist nicht auszuschließen, daß der eine Kern eine Achsendrehung um etwa 180° erfahren hat. Daß so starke Drehungen vorkommen können, lehrt Fig. 20 (Taf. IX). Auch hier wäre man gewiß eher geneigt, die beiden oberen Fortsätze miteinander zu homologisieren, und desgleichen die beiden unteren, wenn nicht ein zwischen zwei Fortsätzen ausgespannter Faden anzeigen würde, daß sie umgekehrt aufeinander zu beziehen sind. Einen Fall, wo der eine Kern sich so vollkommen umgedreht hat, daß die Kernfortsätze, die eigentlich nach dem Äquator gerichtet sein sollten, die entgegengesetzte Stellung einnehmen, gibt Fig. 23 (Taf. IX) wieder.

Die durch unkontrollierbare Kernverlagerungen bedingte Schwierigkeit, die ruhenden Blastomerenkerne richtig aufeinander zu beziehen, macht sich übrigens nicht bei allen Gruppierungstypen geltend. Beim Typus 5, der zu Schwesterkernen führt, die einen dreiwertigen und einen einwertigen Fortsatz besitzen, wie in der eben genannten Fig.23, sind die einander entsprechenden Aussackungen bei jeder beliebigen Verlagerung zu erkennen; und das gleiche gilt für die aus Typus 2 und 4 sich ableitenden Ruhekerne mit einem zweiwertigen und zwei einwertigen Fortsäzen. Da aus der Art, wie die Fortsätze aus der Hauptvacuole entspringen, stets die, „Polseite" des Kerns erkannt werden kann, braucht man die Kerne nur symmetrisch zu orientieren, um zu wissen, welcher einwertige Fortsatz des einen Kerns mit einem bestimmten einwertigen des andern Kerns korrespondiert.

IV. Die Chromosomenanordnung in den Blastomerenkernen bei der Vorbereitung zur nächsten Teilung.

Nachdem im ruhenden Kern jede Spur des Schleifenverlaufs geschwunden ist und nur jene Stellen, welche den Schleifenenden entsprechen, durch dichtere Häufung stärker färbbarer Substanz kenntlich sind, treten bei der Vorbereitung zur neuen Teilung die Chromosomen, sobald sie als kompakte Fäden verfolgbar sind, ungefähr wieder in der gleichen Anordnung hervor, welche die Tochterchromosomen in den jungen Kernen gezeigt hatten. Dies habe ich ja schon vor 21 Jahren eingehend dargestellt. In den Kernfortsätzen, falls solche vorhanden sind, bilden sich die Schleifenenden aus, und zwar ohne Zweifel genau so viele, als bei der Entstehung des Fortsatzes in einen jeden eingegangen waren. Aber auch die mittleren Bezirke der Schleifen bieten einen Verlauf dar, der an die Bilder vor der Kernrekonstruktion aufs lebhafteste erinnert.

Man vergleiche den jungen Kern in der oberen Blastomere der Fig. 15 (Taf. VIII) mit dem zur nächsten Teilung sich anschickenden Kern der Fig. 49 (Taf. XI). Die Schleifen im letzteren sind bedeutend länger, sie zeigen dementsprechend viel stärkere Knickungen; aber der Gesamtverlauf ist sehr ähnlich.

Die Fragen, die sich nun erheben, sind folgende:

4. ist die Gruppierung der neuen Mutterschleifen in den beiden Schwesterkernen die gleiche;
5. wenn dies bejaht werden kann, bietet diese Gruppierung die gleichen Typen dar, die wir oben für die Äquatorialplatte der Eier und damit auch für die in den Ruhekern übergehenden Tochtergruppen konstatiert haben;
6. wenn dies zutrifft, erscheinen diese Gruppierungstypen nach der Kernruhe im gleichen Prozentsatz wie vorher?

Die Antwort lautet in jeder Hinsicht bejahend. Es sei dies zunächst an der Hand der Fig. 1–7 (Taf. VII) erläutert. In jeder dieser Figuren zeigt a die Äquatorialplatte eines Eies; die sieben Platten repräsentieren die im Abschnitt I unterschiedenen Gruppierungstypen. Die Figuren b und c geben die Kerne zweier Schwesterblastomeren in Vorbereitung zur Teilung wieder. Zu jedem Typus von Äquatorialplatte sehen wir in den daneben gestellten Blastomerenkernen das entsprechende Prophasenstadium, in den beiden Kernen immer prinzipiell gleich. Daß die Übereinstimmung mit den Äquatorialplatten nicht überall auf den ersten Blick deutlich ist, rührt vor allem daher, daß bei der Äquatorialplatte alle Abschnitte der Schleife sich in einer Ebene befinden, wogegen bei den damit zu vergleichenden Blastomerenkernen die Schleifenenden abgebogen sind und bei polarer Ansicht, n der alle diese Kerne gezeichnet sind, in bedeutender Verkürzung erscheinen. Dies war ja auch schon bei den Tochtergruppen der Fall, ja diese ließen, wie ein Blick auf Fig. 14b lehrt, den Typus ihrer Äquatorialplatte wegen der engen Lagerung der beiden Schleifen sogar weniger deutlich her vortreten als die uns jetzt beschäftigenden Stadien.

Bei etwas genauerer Betrachtung sind hier unsre sieben Typen leicht wiederzuerkennen, und ebenso leicht überzeugt man sich von der Übereinstimmung der Schleifenanordnung in den beiden Schwesterkernen. Diese zwischen jedem Kernpaar bestehende Gruppierungsgleichheit tritt besonders dann äußerst frappant hervor, wenn man die sieben Kernpaare untereinander vergleicht und beachtet, welche verschiedenen Anblicke die Kerne verschiedener Keime darbieten können.

In einigen Fällen ist die Symmetrie der Schwesterkerne erstaunlich, so besonders in Fig. 5b und c; in andern zeigen sich leichte Differenzen. So sind bei Fig. 1 die beiden oberen Schleifenenden im Kern b einander erheblich näher als im Kern c; bei Fig. 3 laufen im Kern b die beiden Schleifen beiderseits zusammen, wogegen sie im Kern c oben divergieren. Diese kleinen Ungleichheiten sind jedoch nicht imstande, die grundsätzliche Übereinstimmung zu verwischen; sie sind nicht größer als die Abweichungen, die oben zwischen den beiden Tochtergruppen vor der Kernbildung zu konstatieren waren.

Das ist also genau das gleiche, was ich früher unter den schwierigeren Verhältnissen der Varietät *bivalens* hatte nachweisen können:

7. prinzipielle Identität der Schleifengruppierung in den zur Teilung schreitenden Schwesterkernen,
8. prinzipielle Übereinstimmung dieser Gruppierungen mit den in den Äquatorialplatten der Eier nachweisbaren Anordnungstypen.

Was aber damals nur an einigen besonders günstigen Objekten konstatierbar war, dies läßt sich an meinem neuen Material, man darf wohl sagen, beliebig oft feststellen. Ich habe eine nicht geringe Zahl von Kernpaaren genau durch Zeichnung analysiert und mich an vielen andern, die leicht zu durchschauen waren, ohne Zeichnung von der Art ihrer Schleifengruppierung überzeugt. Immer mit dem nämlichen Ergebnis. Fast könnte es überflüssig scheinen, dies noch durch weitere Abbildungen zu belegen; angesichts der Einwände von Fick mögen noch einige weitere mitgeteilt sein.

Ich beginne mit Fig. 28a (Taf. IX), welche zwei Schwesterblastomeren in situ darstellt. Betrachtet man die beiden Kerne, so sind die Bilder, die sie darbieten, recht verschieden, und oberflächliche Betrachtung könnte dazu führen, ihnen eine wesentlich verschiedene Schleifenanordnung zuzuschreiben. In b ist der Kern der linken Blastomere gezeichnet, nachdem das Objekt solange gedreht worden war, bis der Kern sich in derjenigen Ansicht darbot, welche der des rechten Kerns in a entspricht. Die Übereinstimmung läßt nun nichts mehr zu wünschen übrig. Ebenso verschiedenartig präsentieren sich die beiden Kerne in Fig. 25. Nach Drehung des Eies, der Art, daß die beiden Blastomeren übereinanderlagen, ergab der linke Kern ein Bild, das dem, welches der rechte in der Figur darbietet, ungemein ähnlich war. Da die in dieser Stellung angefertigte Zeichnung durch einen Zufall verlorenging, mag es dem Leser überlassen bleiben, sich aus der

gegebenen Ansicht die andre zu konstruieren[4].

Die Erscheinung, der wir hier begegnen, ist oben im Abschnitt III besprochen worden, es ist die Drehbarkeit der Blastomerenkerne. Nur sehr selten präsentieren sich bei einer und derselben Stellung des Objekts die bei den Blastomerenkerne so, wie es ihrer Symmetrie gemäß ist. Einer dieser seltenen Fälle ist in Fig. 24 (Taf. IX) abgebildet. Zwar haben sich auch hier beide Kerne gedreht, aber beide so symmetrisch, daß sie immer noch die einander entsprechenden Seiten dem Beschauer zuwenden und sich selbst ungefähr symmetrisch gegenüberstehen.

In fast allen übrigen von mir untersuchten Keimen war es, um die Kerne in der gleichen Orientierung wiedergeben zu können, notwendig, den einen bei dieser, den andern bei einer andern Stellung des Keimes zu zeichnen. Dies gilt für Fig. 1–8 (Taf. VII) und ebenso für Fig. 29–38 (Taf. X), weshalb in allen diesen Fällen nur die Kerne gezeichnet werden konnten.

Eine weitere Erläuterung zu diesen Bildern dürfte überflüssig sein; es sei nur noch bemerkt, daß die Kernpaare der Fig. 34–38 in Polarer, diejenigen der Fig. 29–33 in einer seitlichen Ansicht gezeichnet sind.

Wir kommen nun noch zu einem sehr wichtigen Punkt. Ich habe im Abschnitt I hervorgehoben, daß die sieben im Ei zu beobachtenden Typen von Äquatorialplatten bei dem Wurm A in sehr verschiedener Häufigkeit vorkommen. Genau das Gleiche zeigt sich jetzt für die entsprechenden Gruppierungen der Chromosomen in den zur Teilung schreitenden Blastomerenkernen. Typus 6 [Fig. 6, 8 (Taf. VII), 25 (Taf. IX), 33 (Taf. X), 48 (Taf. XI)] begegnet dem Beobachter bei Durchmusterung der Präparate hier wie dort auf Schritt und Tritt. Dann folgen, in der Häufigkeit wieder ganz gleichmäßig auf beiden Stadien, Typus 4 Fig. 4 (Taf. VII), 32, 34, 35 und 38 (Taf. X) und 5 (Fig. 5 (Taf VII), 24 (Taf. IX), 29, 37 (Taf. X)). Von Typus 1 habe ich in den Blastomeren außer dem in Fig. 1 (Taf. VII) dargestellten Fall nur noch einen gesehen, entsprechend der Seltenheit dieses Typus im Ei. Der im Ei gleichfalls seltene Typus 2 ist mir in den Blastomerenkernen dreimal begegnet (Fig. 2). Der im Ei nur einmal konstatierte Typus 3 ist auch in den Blastomeren nur einmal (Fig. 3) zur Beobachtung gelangt, auch hier nur in dem einen der beiden Kerne rein.

Mit einigen Worten haben wir schließlich der Kerne ohne Fortsätze oder mit nur einer einzigen sehr großen Aussackung zu gedenken. In den Prophasen solcher Kerne laufen, wie zu erwarten, alle vier Schleifenenden in der Ausbuchtung (Fig. 26, Taf. IX) oder, wo eine solche fehlt, wenigstens an dem einen Pol des längsellipsoiden Kerns zusammen (Fig. 27). Derartige Anordnungen sind in den Blastomerenkernen nicht selten, wogegen ich korrespondierende Äquatorialplatten (Typus 7) nur ganz vereinzelt gefunden habe. Wie aber schon im Abschnitt II, auseinander gesetzt worden ist, kann es kaum einem Zweifel unterliegen, daß die in Rede stehenden Kerne aus allen Typen von Äquatorialplatten sich ableiten können, dann nämlich, wenn die während der Metaphasen dicht um die Spindelachse zusammengedrängten Schleifenenden in dieser Position in den Ruhezustand übergehen (Fig. 18, Taf. VIII). So ist also diese Ausnahme nur eine scheinbare.

V. Diskussion der Beobachtungen.

Nachdem feststeht, daß die Kernfortsätze ihre Entstehung den Schleifenenden verdanken und daß sie dauernde, bis zur Kernauflösung sich an der gleichen Stelle erhaltende Bildungen sind, können wir zunächst den Satz aufstellen: an der Stelle, wo ein Schleifenende in den Ruhezustand übergegangen ist, da kommt auch wieder ein solches zum Vorschein. In Fällen, wo – bei der Varietät *univalens* – vier Fortsätze vorhanden sind, wird man, noch präziser sagen dürfen: was aus einem Schleifenende im Ruhekern entstanden ist, das wird auch wieder zu einem solchen; womit natürlich nicht gemeint sein kann, daß jedes Atom, das dem Ende früher zugehörte, nun wieder mit hineingelangen muß, und daß nicht auch vorher anderswo gelegene Teile durch Assimilation aufgenommen seien. Aber jedenfalls wäre es eine durch nichts motivierte Vorstellung, wenn man annehmen wollte, daß etwa durch Bewegung innerhalb des Ruhekerns nun gerade andre Teile der früheren Chromosomen sich zu einem neuen Ende zusammenfinden sollten, als die früher an ihm beteiligt waren. Und diese Vorstellung hätte um so weniger Berechtigung, als bei vielen *Ascaris*-Weibchen durch die ganze Kernruhe hindurch die Stellen der Schleifenenden durch stärkere und intensiver färbbare

4 Bei den Zeichnungen solcher Kernbilder wäre das Ideal, daß alle im gleichen optischen Schnitt gelegenen Schleifenabschnitte genau den gleichen Differenzen. So sind bei Fig. 1 die beiden oberen Schleifenenden im Ton erhalten, die obersten den dunkelsten, die untersten den hellsten. Die Tiefenausdehnung, mit der wir es hier zu tun haben, ist jedoch oft so groß, daß die verfügbare Skala bei weitem nicht ausreicht. Die verschiedene Tönung in der Zeichnung kann daher nur annähernd die relative Höhe verschiedener Schleifenabschnitte ausdrücken; und auch hiervon geht in der Lithographie noch manches verloren.

Gerüstbezirke kenntlich sind.

Bei dieser Frage sind auch die Kerne ohne Fortsätze von Wichtigkeit. Bei einem Kern mit vier Fortsätzen könnte man diese Aussackungen gerade als Stätten betrachten, welche ihrem Inhalt bei der Bildung der neuen Schleifen die Eigenschaft von „Enden" verleihen, gleichviel aus welchen Teilen der früheren Schleifen sich dieser Inhalt zusammensetzt. Wo keine Fortsätze vorhanden sind, würden dann diese Prädilektionsstellen fehlen, und man müßte, wenn hier überhaupt direkt freie Enden entstehen können, erwarten, daß sie an ganz beliebigen Stellen auftreten. Die Art, wie sie in diesen gerundeten Kernen tatsächlich zum Vorschein kommen: in beiden Kernen in gleicher Weise an dem einen Kernpol zusammengedrängt, also da, wo sie vor der Gerüstbildung zu finden waren, diese Tatsache läßt, im Zusammenhang mit den andern Befunden, keine Wahl als die, daß die neuen Enden aus demjenigen Material gebildet werden, aus dem die alten zusammengesetzt waren.

Lehren nun die Kerne mit einwertigen Fortsätzen, daß das darin enthaltene neue Ende genau einem bestimmten Ende der vorausgegangenen Tochtergruppen entspricht, so ist es das Nächstliegende, daß wenn aus einem zweiwertigen Fortsatz wieder zwei Schleifenenden herauskommen, auch jedes von diesen Enden mit einem bestimmten Ende der den Kern bildenden Chromosomen identisch ist.

Gehen wir nun auf die mittleren Teile der Chromosomen über, so scheinen mir die konstatierten Tatsachen unweigerlich zu dem Schluß zu führen: die mittleren Abschnitte verbinden stets die gleichen Enden, die vor der Rekonstruktion des Kerns verbunden waren. Diese Aussage erlauben ohne weiteres allerdings nicht sämtliche von uns unterschiedenen Gruppierungstypen, sondern nur vier von ihnen, nämlich

Bei zwei andern ließe sich nämlich leicht eine Umgruppierung der Enden in dem einen der beiden Schwesterkerne denken, welche das Bild von dem des andern Kerns, der die alte Anordnung beibehalten haben soll, nicht auffallend verschieden machen würde. Dies zeigt die folgende Figur:

Bei den Typen 2, 4, 3 und 6 ist eine solche unkontrollierbare Umgruppierung der Enden in dem einen Kern allein unmöglich; denn durch eine solche würde Typus 2 in Typus 4 übergeführt, Typus 3 in Typus 6 und umgekehrt. Hier also läßt sich etwas Entscheidendes für unser Problem gewinnen. Wenn

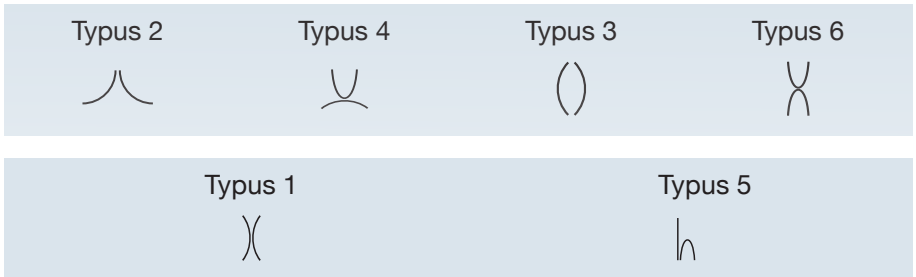

nämlich, wie ich es gefunden habe, ausnahmslos beide Kerne bei der Vorbereitung zur Teilung den gleichen Typus darbieten, also z. B. den Typus 4, obgleich nach der Beschaffenheit der Kernfortsätze ebensogut Typus 2 entstehen könnte, oder den Typus 6, obwohl die opponierten zweiwertigen Fortsätze, die diesem

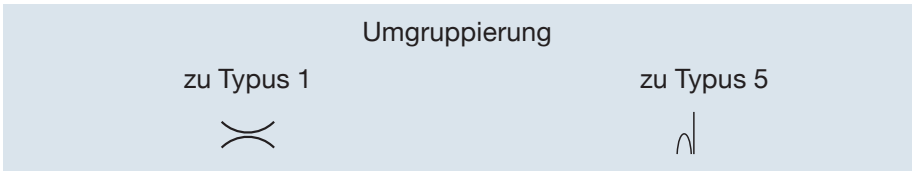

Typus zukommen, genau ebenso dem Typus 3 eigen sind, so kann diese stets konstatierte identische Gruppierung in den beiden Schwester kernen unmöglich Zufall sein; vielmehr wird sich kaum ein andrer Schluß ziehen lassen als der: es ist in diesen Kernen eine Einrichtung vorhanden, welche dafür sorgt, daß stets die nämlichen Enden verbunden werden, die vorher zusammengehört hatten.

Und dieser Schluß wird bekräftigt durch die weitere Tatsache, daß von den zwei nach der Anordnung der Kernfortsätze gleich möglichen Schleifenanordnungen diejenige, die vor der Kernbildung die häufigere war, es auch jetzt ist. Dies ist deshalb von Bedeutung, weil der Skeptiker einwenden könnte,es sei denkbar, daß die Tendenz zur Umgruppierung der Enden, wenn sie in der einen Blastomere bestebt, der andern in gleicher Weise zukäme, in welchem Fall die Umordnung natürlich gar nicht bemerkbar wäre. Die Feststellung der Häufigkeit der vertauschbaren Typen vermag diese Ausflucht zu beseitigen. Gerade die vier hier in

Betracht kommenden Gruppierungen eignen sich durch ihre so äußerst verschiedene Häufigkeit vorzüglich zur Prüfung dieser Frage. Typus 6 ist in der Äquatorialplatte des Eies weitaus der häufigste, der nach dem Aussehen des Ruhekerns mit ihm konkurrierende Typus 3 der seltenste. Und dementsprechend werden, wie oben schon erwähnt, in den Prophasen in großer Überzahl Schleifenstellungen nach Typus 6 getroffen, während mir eine solche nach Typus 3 nur einmal vorgekommen ist, auch sie nicht in voller Reinheit.

Ganz ebenso verhält es sich mit den beiden andern während der Kernruhe nicht unterscheidbaren Typen 2 und 4: Typus 4 ist unter den Äquatorialplatten des Eies recht häufig, Typus 2 sehr selten; und das gleiche Häufigkeitsverhältnis zwischen beiden Gruppierungen besteht auf unserm Stadium. Angesichts dieser Tatsachen muß die ja von vornherein schon sehr unwahrscheinliche Annahme, daß Umgruppierungen, wo sie vorkommen, stets in bei den Kernen in der nämlichen Weise sich vollziehen und daher nicht erkennbar seien, als unhaltbar zurückgewiesen werden.

Kehren wir nun noch einmal zu den beiden Typen 1 und 5 zurück, für welche oben gezeigt worden ist, daß auch bei einer nur in dem einen Kern stattfindenden Neugruppierung der Enden das Aussehen der Kerne sehr ähnlich bliebe, so ist jetzt noch zu bemerken, daß selbst für diese Typen in der Regel das Nichteintreten eines solchen Ereignisses erwiesen werden kann, nämlich aus der Symmetrie der beiden Kerne. Dies gilt speziell für den Typus 5. Wohl wäre hier auch nach der im einen Kern erfolgten Umgruppierung das Bild des Schleifenverlaufs wesentlich das gleiche; aber, wenn wir die beiden Kerne in gleicher Ansicht, beide z. B. vom Pol gesehen, nebeneinanderstellen, so mußten die beiden Bilder nun nicht mehr symmetrisch sein, wie bei Erhaltung des ursprünglichen Zusammenhangs, sondern kongruent. Man betrachte daraufhin die in Fig. 5 und 37 abgebildeten Schwesterkerne des Typus 5. Sie und alle sonst von mir beobachteten Paare zeigen Symmetrie ihres Schleifenverlaufs und nicht Kongruenz.

Auch bei Typus 1 wird in den verschiedenen Abständen der einzelnen Blindsäcke voneinander manchmal ein Merkmal gegeben sein, um die einander entsprechenden Fortsätze erkennen und damit die Frage, ob Umgruppierungen im einen Kern allein stattgefunden haben können, entscheiden zu lassen. So glaube ich, daß die Frage für unsre Fig. 1 (Taf. VII) auf Grund der ganzen Kernform verneint werden darf. Hier jedoch hört die Sicherheit auf.

Allein, wenn alle diejenigen Fälle, welche eine Entscheidung zulassen, die Gruppierung in bei den Schwesterkernen so zeigen, wie es der Annahme einer Identität der Schleifen vor und nach dem Ruhezustand gemäß ist, so wäre es sinnlos, nun gerade in den Fällen, die ihrer Natur nach nicht analysierbar sind, etwas andres vorauszusetzen. Und so halte ich den Satz, den ich vor 21 Jahren als höchst wahrscheinlich hinstellen konnte, heute für gesichert: es sind in den Prophasen der Blastomerenkerne stets die gleichen Schleifenenden verbunden, die vor der Kernbildung verbunden waren.

Nun bleibt noch die Frage übrig: werden diese Enden auch wieder durch die gleichen Teile verbunden, welche vorher den mittleren Abschnitt zwischen diesen beiden Enden gebildet hatten? Wobei nochmals, um jedes Mißverständnis zu vermeiden, betont sei, daß diese „Gleichheit" ebensowenig eine absolute sein soll, wie wenn wir einen Menschen von gestern auf heute noch als den "gleichen" betrachten. Sondern es soll damit nur gesagt sein, daß von den Teilen, welche die Kontinuität zwischen den Schleifen von Mitose zu Mitose vermitteln, immer diejenigen wieder in einem Chromosoma sich zusammenfinden, welche vorher in einem vereinigt waren, gleichgültig, ob bei dem Stoffwechsel, den sie inzwischen durchgemacht haben, auch nur ein Molekül noch das nämliche ist.

Wenn wir beachten, daß der Verlauf der aus dem Ruhezustand hervortretenden mittleren Schleifenabschnitte sowohl zwischen den beiden Schwesterkernen meist sehr ähnlich ist, als auch mit demjenigen vor der Kernbildung auffällig übereinstimmt, so scheint mir keine andre Annahme so einfach und plausibel zu sein als die, daß die Teile, welche von jedem Tochterchromosoma in den Ruhekern übergehen, sich ziemlich gleichmäßig über einen gewissen Bezirk ausdehnen, ohne ihren Zusammenhang aufzugeben und ohne mit den in gleicher Weise sich metamorphosierenden Bestandteilen des andern Chromosoms sich zu vermischen.

Für diese Hypothese spricht, wie mir scheint, auch noch ein andrer gewichtiger Grund. Wenn man sich die mittleren Schleifenbezirke in eine gleichartige Masse übergegangen denkt, in der die früher verbundenen Teilchen sich genau ebenso fremd gegenüberstehen wie denjenigen der andern Schleife, so dürfte es schwer sein, sich eine Vorstellung zu bilden, wie die durch solche Auflösung ihrer Verbindungstücke vollkommen voneinander isolierten Enden sich immer wieder in der gleichen Kombination zusammenfinden können. Soll man etwa eine Fernwirkung der früher verbundenen Enden aufeinander annehmen, der Art, daß sie aus jenem Magma heraus immer wieder ihre Verbindung erzwingen, und zwar nicht eine Verbin-

dung auf dem kürzesten Weg, sondern (vgl. Fig. 49 und 50) in einem charakteristischen, für verschiedene Keime verschiedenen, sehr komplizierten Verlauf von bestimmter Länge? Sollte diese Annahme natürlicher sein, als sich vorzustellen, daß der Kernbezirk, der aus einem mittleren Schleifenabschnitt entstanden ist, einen gewissen Zusammenhang in sich und mit den ihm zugehörigen Enden bewahrt, um in den Prophasen sich wieder zu einem entsprechenden Stück zu gestalten?

Die einzige im vorstehenden noch nicht berührte Möglichkeit, die konstatierten Tatsachen ohne die Individualitätshypothese zu erklären, scheint mir die zu sein, daß man jedem Ei und den von ihm abstammenden Zellen die Tendenz und Fähigkeit zuschreibt, die sich jeweils formierenden Chromosomen in eine ganz bestimmte Biegung und gegenseitige Stellung zu zwingen. Wenn also in der Äquatorialplatte des Eies z. B. diese Anordnung ⋂ vorhanden wäre und in den bei den zur Teilung schreitenden Blastomerenkernen wieder, so läge dies nicht daran, daß die Anordnung sich erhalten hat, sondern es wären außerhalb des Chromatins gelegene Faktoren, nach Fick könnte man vielleicht sagen: es wäre das in diesem bestimmten Keim geltende Exerzierreglement, welches die Chromatinteilchen beider Zellen zwingt, wieder in gleicher Weise sich aufzureihen und nebeneinander aufzustellen.

Wäre dies nun wirklich so, dann wäre einmal zu erwarten, daß die in den ersten Stadien der Embryonalentwicklung zu beobachtende Übereinstimmung sich auch weiterhin erhält, und zweitens müßte die Gleichheit der Anordnung besonders klar auf den einander entsprechenden Stadien hervortreten, also zwischen der Äquatorialplatte des Eies und den Äquatorialplatten der beiden primären Blastomeren.

Beide Voraussetzungen treffen nicht zu. Während nämlich in dem Material A bis zur Kernauflösung die Chromatinanordnung der Schwesterkerne, wie oben dargelegt, fast ausnahmslos sehr ähnlich ist, gilt dies für die aus diesen Kernen hervorgehenden Äquatorialplatten bei weitem nicht in gleichem Maß. Ich habe von einer großen Zahl von Keimen die beiden Äquatorialplatten des Zweizellenstadiums gezeichnet; vier solche Paare sind in Fig. 40–43 (Taf. X) wiedergegeben. Man erkennt wohl meistens eine gewisse Ähnlichkeit, man kann auch oft mit ziemlicher Bestimmtheit die einander entsprechenden Chromosomen, speziell in Fig. 42 und 43, bezeichnen.

Aber genau der gleiche Typus der Form und gegenseitigen Stellung ist, wie in diesen Figuren, so auch in der Mehrzahl der sonst von mir gezeichneten nicht mehr vorhanden. Die Chromosomen werden eben nach der Kernauflösung mehr oder weniger stark bewegt, bis sie in der neuen Äquatorialplatte zur Ruhe kommen.

Die gleiche Differenz geht natürlich auch auf die beiden Paare von Tochtergruppen über. Ein solches Bild zeigt Fig. 39 (Taf. X). Während in der unteren Zelle der Typus 6 besteht: zwei in sich zurücklaufende Schleifen, die Enden beider opponiert, sind in der oberen Zelle alle vier Enden auf der einen Seite zusammengedrängt (Typus 7). Denken wir uns aus diesen beiden Anordnungen Ruhekerne entstanden, so ist nach dem, was wir oben erfahren haben, zu erwarten, daß zwar jedes neue Kernpaar unter sich ungefähr symmetrisch ist, das eine Paar von dem andern dagegen erheblich verschieden. In der Tat ist auf dem Vierzellenstadium eine solche Verschiedenheit etwas sehr Gewöhnliches. Betrachtet man die zum Rhombus geordneten vier Zellen während der Kernruhe, so lassen sich sehr häufig nach der Form ihrer Kerne zwei Paare unterscheiden, deren jedes ohne Zweifel ein Paar Schwesterzellen repräsentiert. Zwei solche Keime sind in Fig. I u. II gezeichnet. Man sieht, daß die Kerne,wie wir es auch im Zweizellenstadium gefunden haben, zumeist aus ihrer symmetrischen Anfangsposition mehr oder weniger stark verlagert worden sind, so daß es in der Regel nicht möglich ist, ihre Zusammengehörigkeit aus der S t e l l u n g zu eruieren. Wohl

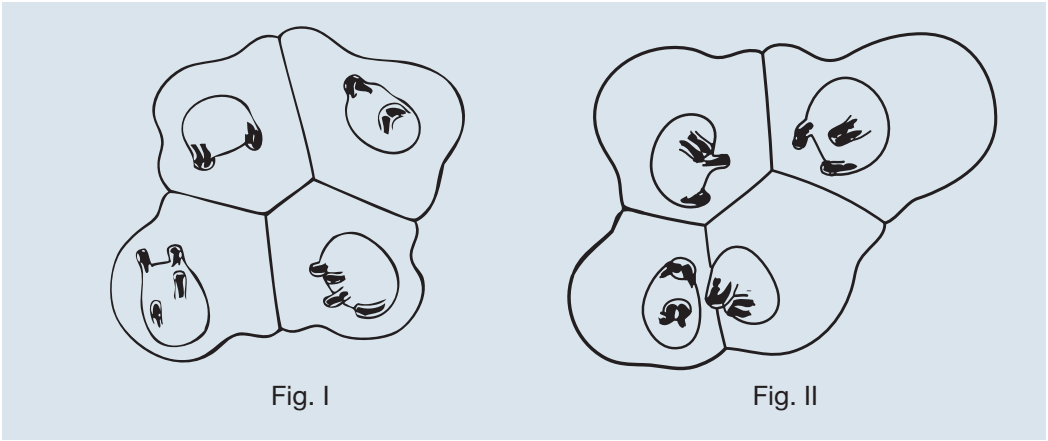

Fig. I Fig. II

aber aus den K e r n f o r t s ä t z e n . So zeigt in Fig. I das eine Paar je vier einwertige Fortsätze, das andre Paar zwei zweiwertige Fortsätze. In· Fig. II finden wir gleichfalls ein Kernpaar mit je zwei Fortsätzen, das andre Paar zeigt je drei Blindsäcke, von denen der eine deutlich zwei Enden er kennen läßt.

Wir gelangen demnach zu dem bemerkenswerten Ergebnis: von dem Stadium der Äquatorialplatte bis zur Auflösung der beiden von ihr abstammenden Tochterkerne er hält sich bei dem Wurm A fast ausnahmslos die gleiche Konstellation; von der Auflösung dieser Kerne an bis zur Bildung der neuen Äquatorialplatten wird sie häufig zerstört.

Und dazu kommt noch eine weitere wichtige Konstatierung. Ich habe oben von einem Wurm B berichtet, bei dem die Tochterchromosomen vor der Kernbildnng infolge erheblicher Bewegungen ihre Symmetrie mit denen der andern Seite mehr oder weniger verlieren können. Als ich die ersten Präparate dieses Wurms studierte, und zwar zunächst die Stadien, wo in den Kernen der beiden primären Blastomeren die Schleifen wieder verfolgt werden können, da war ich frappiert über das häufige Vorkommen von Schwesternkernen, deren Chromosomenanordnung sich nicht aufeinander beziehen ließ. Mein erster Gedanke war, daß hier wirklich die frühere Anordnung im ruhenden Kern verloren gegangen und eine neue aufgetreten sei. Allein das Studium der früheren Stadien klärte die Verhältnisse alsbald dahin auf, daß eben schon v o r d e r K e r n b i l d u n g die Schleifengruppierung der beiden Schwesterzellen häufig eine ebenso große Verschiedenheit er kennen läßt.

Halten wir diese Befunde mit den vorher besprochenen zusammen, so kommen wir zu dem wichtigen Resultat: Wo die Chromosomengruppierung verwandter Zellen different wird, da geschieht diese Veränderung auf denjenigen Stadien, in denen uns die Chromosomen als isolierte Körper in voller Klarheit vorliegen. Von der Bildung der Tochtergruppen bis zur Kernrekonstruktion und dann wieder von der Kernauflösung bis zur Bildung der neuen Äquatorialplatten, das sind die Zeiten, wo die Chromosomen von Schwesterzellen, sei es durch Eigenbewegung, sei es passiv bewegt, ihre Form und gegenseitige Stellung ändern. Sind sie aber einmal in den ruhenden Kern eingegangen, so kommen sie, dafür sprechen alle positiven Erfahrungen, auch in prinzipiell gleicher Weise wieder aus ihm heraus. Der Ruhezustand des Kerns zeigt sich also, ganz im Gegensatz zu dem, was man zunächst glauben möchte, als die in bezug auf die Chromosomenkonfiguration konservativste Phase. Ob dieser Satz freilich allgemein glültig ist, das ist eine andre Frage. Von einer jedem Keim inhärenten Eigenschaft, seine Chromosomen immer wieder in die nämliche Stellung zu bringen, kann angesichts dieser Befunde keine Rede sein. Und wenn wir alle Tatsachen überblicken, so zeigt sich nirgends auch nur der leiseste Anhaltspunkt, daß es ein a u ß e r h a l b des Chromatins gelegenes Moment sein könnte, das da, wo wir die in Vorbereitung zur Teilung begriffenen Schwesterkerne identisch finden, ihnen diese Identität aufprägt.

Wenn sonach alle bisher mitgeteilten Beobachtungen für die Vorstellung sprechen, daß sich die Chromosomenform im ruhenden Kern, für unsre Hilfsmittel unerkennbar, erhält, so habe ich jetzt noch über einige Beobachtungen zu berichten, welche diesem Satz zu widersprechen scheinen, wo nämlich kein Zweifel bestehen kann, daß sich die Schleifenanordnung in dem einen von zwei Schwesterkernen in einer ganz bestimmten Weise geändert hat. Ich habe diese Abnormität, wie man es nennen muß, unter vielen hundert Fällen fünfmal beobachtet, ausschließlich bei dem Wurm A. Ein Blick auf Fig. 45–47 (Taf. XI) lehrt sofort, um was es sich handelt . Während immer der eine Kern das uns bekannte typische Bild darbietet, zeigen sich im andern die zwei Schleifen ineinander verhängt. Dadurch sehen die beiden Kerne, auch bei symmetrischer Orientierung, auf den erst en Blick ziemlich verschieden aus. Aber genauere Vergleichung lehrt, daß sie in jedem Fall beide dem gleichen Typus angehören, Fig. 45 u. 47 dem Typus 6, Fig. 46 dem Typus 4. Die Verschiedenheit der Bilder rührt vor allem daher, daß die Chromosomen da, wo sie von einander unabhängig sind, infolge der Verkürzung ihrer mittleren Abschnitte sich voneinander entfernen, wozu die ineinander verhängten nicht imstande sind.

Nachdem ich den ersten Keim dieser Art gefunden hatte, achtete ich darauf, ob sich nicht Folgezustände auffinden ließen, die speziell für gewisse Probleme der Teilungsmechanik von Interesse wären. Es ist mir aber kein solcher zu Gesicht gekommen. Daß die verhängten Schleifen in dieser Lage in die Spindel eintreten, geht aus der Fig. 47 hervor. Wie sich aber nun die Trennung der Schwesterfäden vollzieht, diese interessante Frage muß ich unbeantwortet lassen. Es läßt sich kaum annehmen, daß eine geregelte Verteilung auf die Tochterzellen hier möglich ist. Wenn allerdings die Abnormität nur in derjenigen Blastomere auftreten würde, deren Chromosomen zur Diminution bestimmt sind , dann wäre sie vielleicht unschädlich; denn hier wird ja der mittlere Teil der Schleifen später in eine Anzahl kleiner Chromosomen zerlegt. Aber wie Fig. 46 zeigt, kommt die Verhängung auch in der an ihrer Kleinheit kenntlichen Stammzelle vor.

Wir kehren nach dieser Abschweifung zu unserm Problem zurück. Da ohne allen Zweifel die Kerne mit

verhängten Schleifen aus Tochterchromosomen entstanden sind, die nicht verhängt waren, so läßt sich hier wirklich behaupten, daß die neuen Schleifen mit den alten nicht streng (in dem bisher gebrauchten Sinne) identisch sein können, sondern daß eine Umgruppierung von Teilen stattgefunden haben muß. Die Frage ist nur, ob dieses Faktum die Individualitätshypothese umzustoßen vermag. Ich glaube nicht, daß wir zu dieser Folgerung genötigt sind.

Um dies zu begründen, möchte ich an die Schilderung erinnern, die ich 1888 (9, S. 28–38) für das *Ascaris*-Ei von dem Übergang der Eikernchromosomen in den Ruhezustand gegeben habe. Ich verglich damals diesen Vorgang mit der Pseudopodienbildung eines Rhizopoden. Auf allen Seiten erhebt sich die oberflächliche Schicht eines jeden Chromosoma zu Fortsätzen, die immer länger und zahlreicher werden, mit einander anastomosieren und so ein Schwammwerk bilden, in welches schließlich der ganze Chromatinkörper aufgegangen ist. Zunächst lassen sich die den beiden Chromosomen zugehörigen Teile des Reticulums noch auseinanderhalten. Später, nachdem sie in Berührung gekommen sind, gelingt dies nicht mehr.

Auf Grund dieses Befundes, der an ungemein klaren Präparaten gewonnen worden ist, ließe sich die Verhängung der neuen Mutterschleifen in folgender Weise erklären. Wenn die beiden in den Kern eingegangenen Tochterschleifen ihre zum Anastomosieren befähigten Pseudopodien bilden, so ist es möglich, daß Fortsätze des einen Chromosoms einen Bezirk des andern umfassen, wie etwa Pseudopodien einer Amoebe um einen Algenfaden herumfließen, und daß sie sich hinter ihm vereinigen. Die schematische Zeichnung der Fig. III mag dies anschaulich machen. Sie stellt ein Stück eines Kerngerüstes dar, in welchem die von dem einen Chromosoma stammenden Bälkchen dunkel, die des andern hell gehalten sind. Die starken ausgezogenen Linien markieren den ursprünglichen Verlauf der Tochterchromosomen, das, was Rabl primäre Kernfäden nennen würde. Von diesen aus haben sich die andern Bälkchen gebildet, die sich teils an solche des andern Chromosoms anlegen, teils untereinander anastomosieren. Durch eine solche Anastomose des dunklen Chromosoma ist der Hauptstamm der hellen umgriffen. Wenn nun bei der Zusammenziehung des Gerüsts in den Prophasen diese ursprüngliche Nebenbahn zur Hauptbahn wird, wie dies in der Zeichnung durch die punktierte Linie ausgedrückt worden ist, dann sind die bei den Chromosomen ineinander verhängt.

Daß die von einem Chromosoma ausgehenden Bälkchen mit einander anastomosieren und auf diese Weise Ringe bilden, denen die Fähigkeit zukommen muß, etwas zu umgreifen, läßt sich für diejenigen Schleifenenden, welche einzeln in einem Kernfortsatz liegen, mit aller Sicherheit feststellen. In Fig. 44 (Taf. XI) ist dies an dem oben gelegenen einwertigen Fortsatz ganz klar zu sehen. Und auch die zweite Annahme, daß eine solche sekundäre Bahn zur Hauptbahn werden kann, erscheint für die Schleifenenden durchaus nicht unbegründet. Denn wie schon oben ausgeführt worden ist, habe ich den Eindruck erhalten, daß die Enden der Tochterschleifen in den Gerüstzustand übergehen können, ohne daß vorher die von K. Bonnevie beschriebene Spiralstruktur aufgetreten ist. Vielmehr scheint es bei dem mir vorliegenden Material so zu sein, daß das in der Achse des Blindsacks liegende Schleifenende sich zuerst in einige gröbere Segmente gliedert, von denen dann die gegen die Membran strebenden anastomosierenden Fortsätze ihren Ursprung nehmen. Da nun die Enden der neuen Schleifen sehr häufig in deutlichen, meist dicht unter der Membran des Blindsacks verlaufenden Spiralen erscheinen, ist die Vorstellung sehr naheliegend, daß der neue Faden sich wenigstens zum Teil aus den sekundären Bälkchen aufbaut.

Für die mittleren Schleifenabschnitte läßt sich wenigstens soviel anführen, dass sie bei ihrem Wiedererscheinen viel stärker in unregelmäßgem Zickzack verlaufen, als ihn die Tochterschleifen, so lange sie verfolgbar waren, darboten (man vergl. Fig. 16 [Taf. VIII] mit Fig. 48, 49 und 50 [Taf. XI]). Auch hier ist es also keineswegs unwahrscheinlich, daß der neue Faden zum Teil aus Collateralen gebildet wird.

So lassen sich auch diese Abnormitäten mit der Individualitätshypothese zwanglos in Einklang bringen, und zwar, wie betont werden darf, auf Grund einer Vorstellung vom Bau des Ruhekerns, die lange vorher aus ganz andern Tatsachen abgeleitet worden war. Wollte man die Abnormität etwa so erklären, daß ein Umtausch der mittleren Abschnitte stattgefunden habe, wie es in nebenstehendem Schema (Fig. I Va) ausgedrückt ist, so wäre nicht einzusehen, warum, wenn dieses möglich ist, nicht auch und sogar viel häufiger solche Umgruppierungen vorkommen sollten, bei denen die Enden in andrer Weise kombiniert werden als vorher, wie das Schema der Fig. IVb es darstellt. Gerade die unbeirrbare Zähigkeit, mit der auch in den fünf von mir beobachteten abnormen Fällen die dem Kern bei seiner Entstehung eigene Anordnung der Schleifen festgehalten wird, so daß wir z.B. in den beiden Kernen der Fig. 46 sofort die einander entsprechenden Chromosomen erkennen, ist meines Erachtens ein gewichtiges Argument dafür, daß der aus jedem Chromosoma entstandene Gerüstbezirk in irgend einer Weise seine Einheit bewahrt.

Es sei als Abschluß dieser Erörterungen noch untersucht, welcher Art die Befunde an unsern Keimen sein

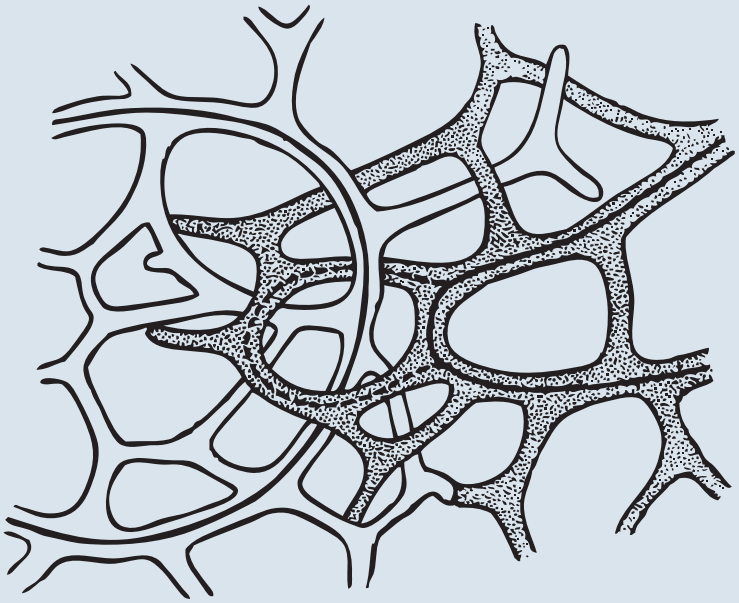

Fig. III

müßten, um ein Aufgeben der Individualitätshypothese nötig zu machen. Da mag zuerst gesagt sein, daß alle diejenigen Fälle, welche nichts weiter zeigen, als daß die beiden Schwesterkerne im Ruhezustand oder in den Prophasen voneinander verschieden sind, kein Argument gegen unsre Hypothese darstellen. Denn diese Hypothese fordert ja nicht, daß die Form der einzelnen Schleifen oder deren gegenseitige Gruppierung sich erhalten müsse. Wir haben oben für den Wurm B erfahren, daß hier bereits die beiden Chromosomenschwestergruppen vor der Kernbildung sehr verschieden sein können und dementsprechend dann die Ruhekerne. Es steht natürlich mit der Individualitätshypothese in bestem Einklang, wenn sich in diesem Material schließlich auch die Prophasenkerne ebenso erheblich voneinander unterscheiden. Von der Varietät *bivalens* liegen mir Eier vor, wo diese Unterschiede noch größer sind. Die Variabilität verschiedenen Eimaterials in dieser Beziehung ist erstaunlich. Der strengen Regelmäßigkeit, wie sie uns bei dem Wurm A begegnet ist, steht in den eben genannten Eiern von *bivalens* eine Regellosigkeit gegenüber, die, wenn man nur sie kennen würde, wohl nicht leicht zu der Annahme hätte führen können, daß jedes in den Kern eingegangene Chromosoma als solches wiedererscheint. Aber als rein negativ können diese Befunde unsrer an günstigen Fällen gewonnenen Auffassung nicht widersprechen. Und es sei noch bemerkt, daß selbst dann, wenn die Chromosomen in andrer Konfiguration wieder auftauchen wurden, als sie in den Kern eingegangen sind, wofür allerdings nach meinen Erfahrungen bei *Ascaris* gar kein Anhaltspunkt vorliegt, auch dieses keinen Widerspruch gegen unsre Hypothese darstellen würde. Denn es wäre wohl denkbar, daß sich die aus den einzelnen Schleifen hervorgegangenen Kernbezirke gegeneinander verschieben könnten, ohne ihre Einheit zu verlieren.

Ein mit der vorgetragenen Auffassung unvereinbarer Befund würde nur dann vorliegen, wenn sich positiv zeigen ließe, daß eines der neuen Mutterchromosomen Teile enthält, die vorher verschiedenen Chromosomen angehört hatten. Daß ein solcher Nachweis mit unsern jetzigen Mitteln, die eine Feststellung des

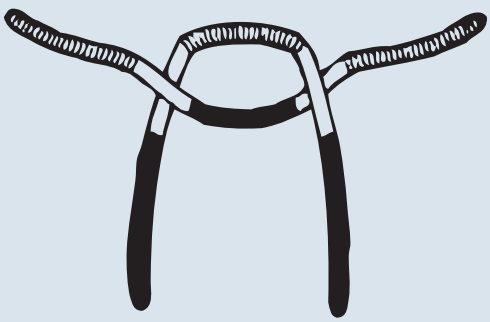

Fig. IVa

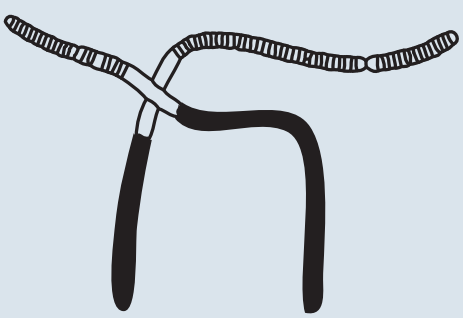

Fig. IVb

Schleifenverlaufs im Leben nicht zulassen, streng nicht geführt werden kann, ist nach dem Gesagten klar. Wir haben es hier eben mit einem jener so häufigen Fälle zu tun, wo die uns möglichen Beobachtungen nur in einem Sinn eine sichere Antwort erlauben. Immerhin sind Tatsachen denkbar, aus denen mit einiger Wahrscheinlichkeit auf eine Umgruppierung von Schleifenabschnitten geschlossen werden könnte. Wenn in einem Material von solcher Beständigkeit wie demjenigen unsers Wurmes A Schwesterkerne gefunden wurden, welche z. B. in klarster Symmetrie zwei einwertige und einen zweiwertigen Fortsatz besitzen, und wenn dann im einen Kern die Prophase den Gruppierungstypus 2, im andern den Typus 4 darbieten wurde, oder wenn von zwei ganz gleich gestalteten Schwesterkernen mit je zwei opponierten zweiwertigen Fortsätzen der eine den Typus 3, der andre den Typus 6 aufweisen würde, dann wäre unsre Auffassung gefährdet. Aber nichts dieser Art hat sich bis jetzt gezeigt.

VI. Literaturverzeichnis.

1. Artom, C. Über ein Verfahren, die beschalten Eier von *Ascaris meg.* mit jedem gewünschten Konservierungsmittel zu fixieren. Zeitschr. f. wiss. Mikrosk. Bd. 25. 1908.
2. Baltzer, F. Die Chromosomen von Strongylocentrotus lividus und Echinus microtuberculatus. Arch. f. Zellforschung. Bd. 2. 1909.
3. Beneden, E. van. Recherches sur la maturation de l'oeuf, la fécondation et la division cellulaire. Gand et Leipzig. 1883.
4. Beneden, E. van et A. Neyt. Nouvelles recherches sur la fécondation et la division mitosique chez l' *Ascaride megalocephale*. Bull. Acad. roy. de Belg. 1887.
5. Bonnevie, K. Chromosomenstudien. Arch. f. Zellforschung. Bd. I. 1908.
6. Boveri, Th. Über die Befruchtung der Eier von *Ascaris meg.* Sitz.–Ber. d. Ges. für Morph. u. Phys. in München. Bd. 3. 1887.
7. Boveri, Th. Zellenstudien. I. Jena. 1887.
8. Boveri, Th. Über Differenzierung der Zellkerne während der Furchung des Eies von *Ascaris meg.* Anatom. Anz. Bd. 2. 1887.
9. Boveri, Th. Zellenstudien. II. Jena. 1888.
10. Boveri, Th. Ein geschlechtlich erzeugter Organismus ohne mütterliche Eigenschaften. Sitz.–Ber. d. Ges. f. Morph. u. Physiol. München. Bd. 5. 1889.
11. Boveri, Th. Zellenstudien. III. Jena. 1890.
12. Boveri, Th. Über die Befruchtungs- und Entwicklungsfähigkeit kernloser Seeigeleier usw. Arch. f. Entw.–Mech. Bd. 2. 1895.
13. Boveri, Th. Die Entwicklung von *Ascaris meg.* mit besonderer Rücksichtauf die Kernverhältnisse. Festschr. für C. von Kupffer. Jena. 1899.
14. Boveri, Th. Über die Polarität des Seeigeleies. Verh. d. phys.-med. Ges. Würzburg. N. F. Bd. 34. 1901.
15. Boveri, Th. Über mehrpolige Mitosen als Mittel zur Analyse des Zellkerns. Verh. d. phys. - med. Ges. Würzburg. N. F. Bd. 35. 1902.
16. Boveri, Th. Ergebnisse über die Konstitution der chromatischen Substanz des Zellkerns. Jena. 1904.
17. Boveri, Th. Zellenstudien. V. Jena. 1905.
18. Boveri, Th. Zellenstudien. VI. Jena. 1907.
19. Boveri, Th. u. N. M. Stevens. Über die Entwicklung dispermer *Ascaris*eier. Zool. Anz. Bd. 27. 1904.
20. Child, C. M. Amitosis as a Factor in normal and regulatory Growth. Anat. Anz. Bd. 30. 1907.
21. Fick, R. Über die Eireifung bei Amphibien. Verh. d. Anatom. Ges. in Tübingen. Anat. Anz. Ergänzungsheft zu Bd. 16. 1899.
22. Fick, R. Betrachtungen über die Chromosomen, ihre Individualität, Reduktion u. Vererbung. Arch. für Anat. u. Phys. Anat. Abt. Suppl. 1905.
23. Fick, R. Vererbungsfragen, Reduktions- und Chromosomenhypothesen, Bastardregeln. Erg. d. Anat. u. Entw.–Gesch. Bd. 16. 1907.
24. Herla, V. Étude des variations de la mitose chez l' *Ascaride megalocephale*. Arch. de Biol. Tom. 13. 1893.
25. King, H. D. The Oogenesis of Bufo lentiginosus. Journ. of Morph. Bd. 19.1908.

26. Moenkhaus, W. J. The development of the Hybrids between Fundulus heteroclitus and Menidia notata with especial Reference to the Behavior of the maternal and paternal Chromatin. Americ. Journ. of Anat. Vol. 3. 1904.

27. Nussbaum, M. Über Kern- und Zellteilung. Arch. f. mikrosk. Anat. Bd. 59. 1902.

28. Nussbaum, M. Befruchtung und Vererbung. Anatom. Anz. Bd. 28. 1906.

29. Prowazek, S. Das Lecithin und seine biologische Bedeutung. Biol Centralbl. Bd. 28. 1908.

30. Rabl, C. Über Zellteilung. Morph. Jahrb. Bd. 10. 1885.

31. Rabl, C. Über "organbildende Substanzen" und ihre Bedeutung für die Vererbung. Leipzig. 1906.

32. Rückert, J. Zur Entwicklungs geschichte des Ovarialeies bei Selachiern. Anat. Anz. Bd. 7. 1892.

33. Stevens, N. M. On the Ovogenesis and Spermatogenesis of Sagitta bipunctata. Zool. Jahrb. Abt. f. Anat. u. Ont. Bd. 18. 1903.

34. Strassen, O, Zur. Über die Riesenbildung bei *Ascaris*eiern. Arch. f. Entwickl.-Mech. Bd. 7. 1898.

35. Strassen, O, Zur. Die Geschichte, der T-Riesen von *Ascaris meg.* Zoologica. Heft 40. Stuttgart. 1906.

36. Tellyesniczky, K. Von Die Entstehung der Chromosomen. Evolution oder Epigenese? Berlin, Wien. 1907.

37. Whitney, D. D. Artificial Removal of the green Bodies of Hydra viridis. Biol. Bull. Bd. 13. 1907.

38. Zoja, R. Sulla indipendenza della cromatina paterna e materna nel nucleo delle cellule embrionali. Anat. Anz. Bd. 11. 1895.

Tafelerklärung.

Alle Figuren beziehen sich auf *Ascaris megalocephala univalens*. Die Vergrößerung beträgt überall etwa 2000.

Tafel VII.

Fig. 1–8. In jeder von diesen Figuren zeigt a die Äquatorialplatte eines Eies in polarer Ansicht, b und c stellen die Schwesterkerne zweier ½-Blastomeren dar, gleichfalls in polarer Ansicht. Fig. 1–7 repräsentieren die sieben im Text (S. 184) unterschiedenen Gruppierungstypen; Fig. 8 gehört dem Typus 6 an.

Tafel VIII.

Fig. 9. Ei, in Teilung begriffen.

Fig. 10–14. Zweizellenstadium. Tochterchromosomen vor der Kernrekonstruktion. Fig. 14b zeigt die beiden Chromosomengruppen der Fig. 14a in der Richtung der Teilungsachse.

Fig. 15–19. Zweizellenstadium. Bildung der Kerne. In Fig. 19 sind nur die beiden Kerne gezeichnet.

Tafel IX.

Fig. 20–23. Zweizellenstadium. Ruhende Kerne.

Fig. 24–28. Zweizellenstadium. Kerne in Vorbereitung zur Teilung.

Fig. 28b zeigt den linken Kern der Fig. 28a in andrer Ansicht.

Tafel X.

Fig. 29–38. a und b zeigen Überall die beiden zusammengehörigen Schwesterkerne des Zweizellenstadiums. In Fig. 29–33 sind die Kerne in seitlicher, in Fig. 34–38 in polarer Ansicht gezeichnet.

Fig. 39. Übergang vom Zwei- zum Vierzellenstadium

Fig. 40–43. Äquatorialplatten des Zweizellenstadiums. a und b in jeder Figur gehören dem gleichen Keim an.

Tafel XI.

Fig. 44. Ruhender Kern einer ½–Blastomere.

Fig. 45–47. Zweizellenstadium. Die Kerne in Vorbereitung zur Teilung. Überall sind in der einen der beiden Blastomeren die Schleifen ineinander verhängt.

Fig. 48. Zweizellenstadium. Kerne in Vorbereitung zur Teilung.

Fig. 49. Kern einer ½–Blastomere in Vorbereitung zur Teilung.

Fig. 50. Desgleichen, aus einem andern Keim.

Fig. 51. Vierzellenstadium nach Erreichnng der Rautenform. P2 Stammzelle. EMSt Urzelle für Ento-Mesoderm und Stomodaeum A und B primäre Ektodermzellen. X Diminutionskörner.

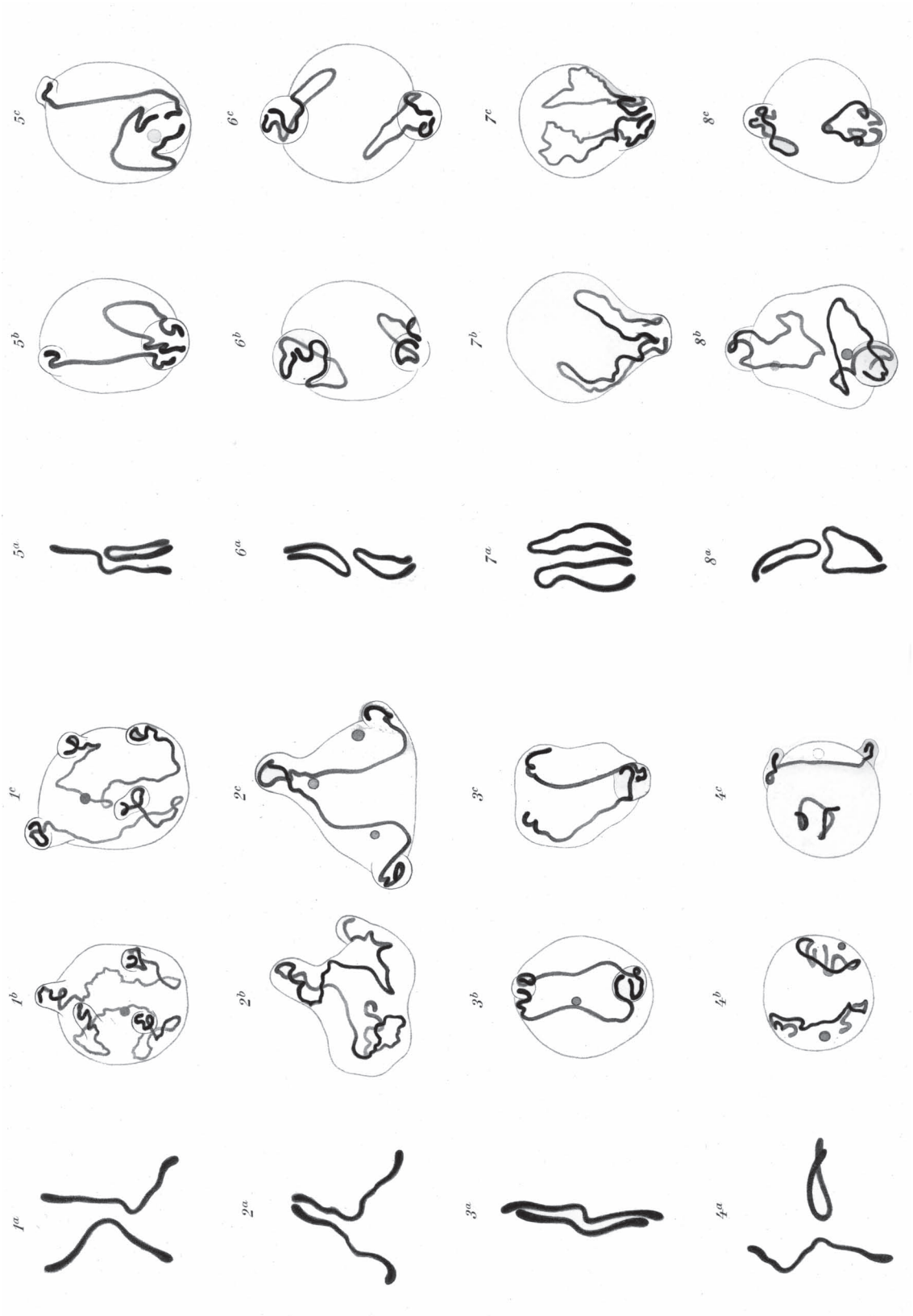

Fig. VII

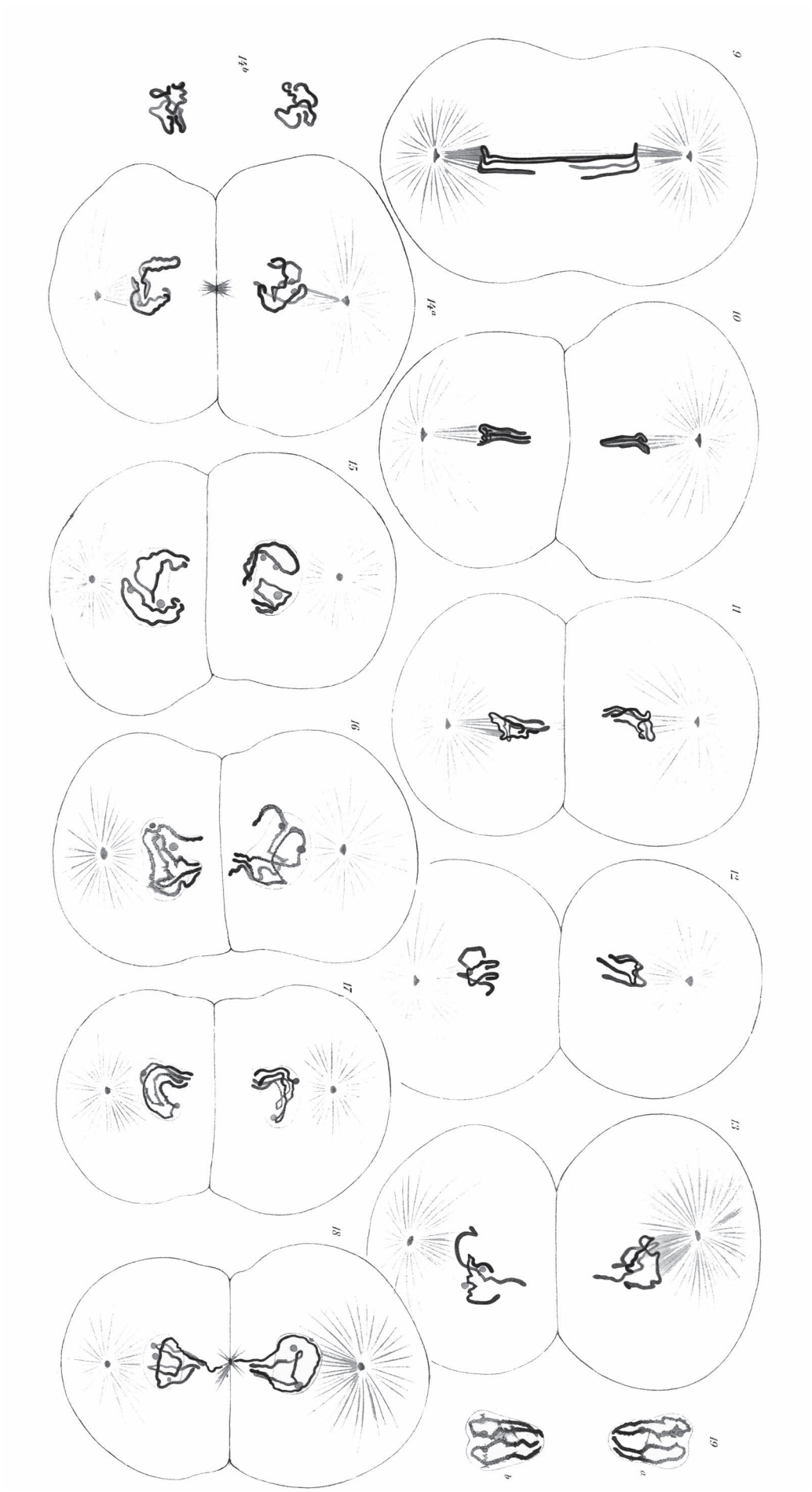

Fig. VIII

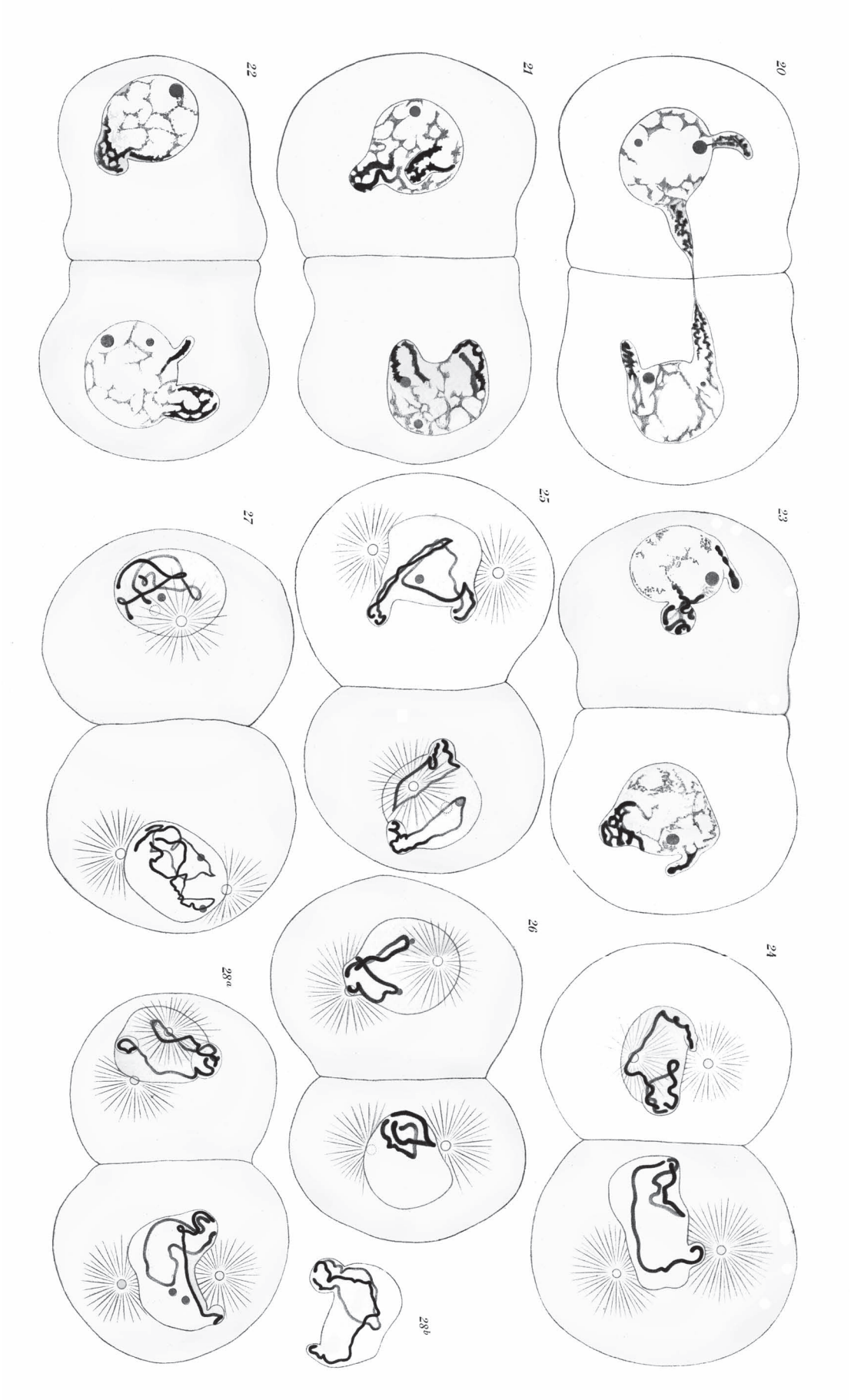

Fig. IX

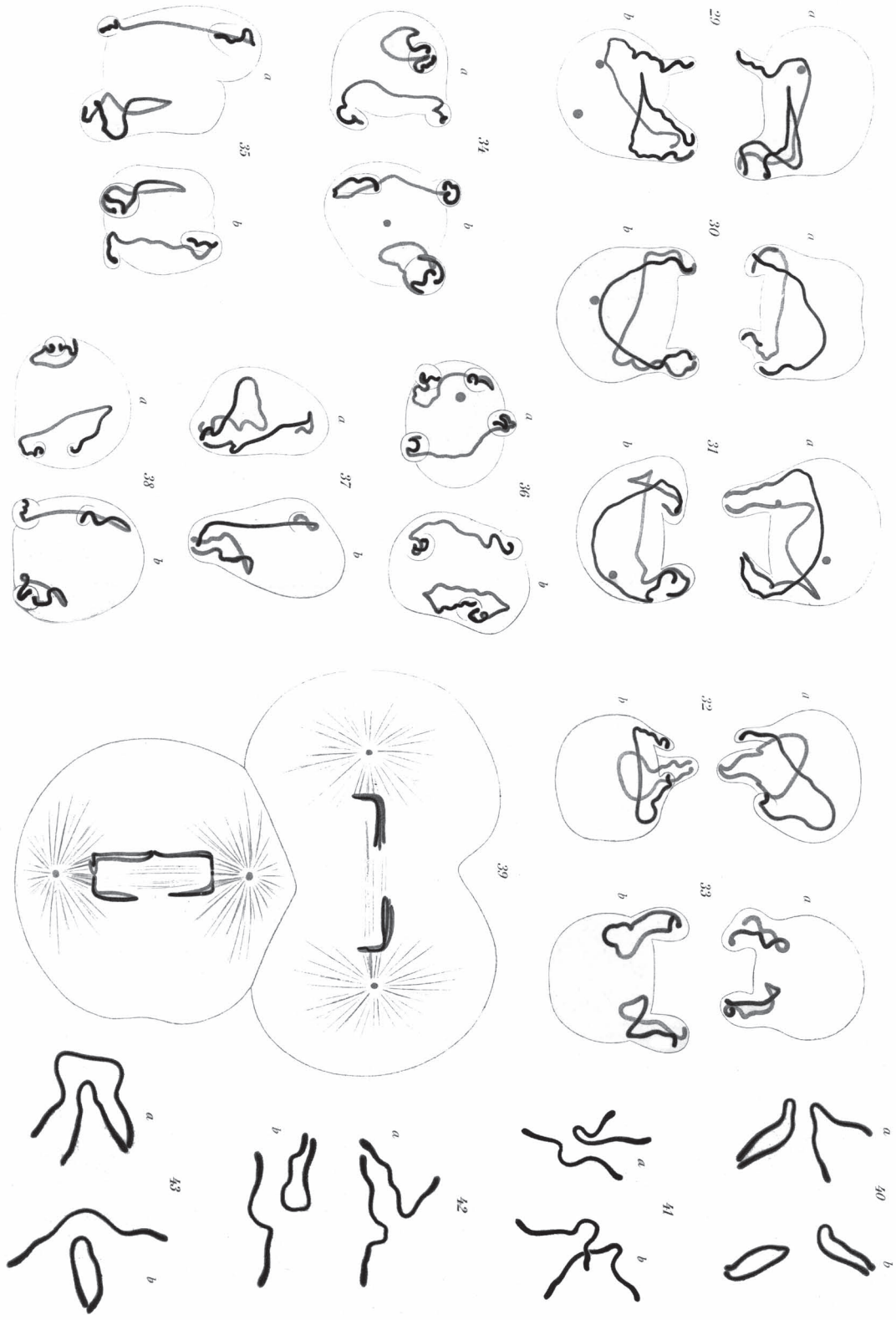

Fig. X

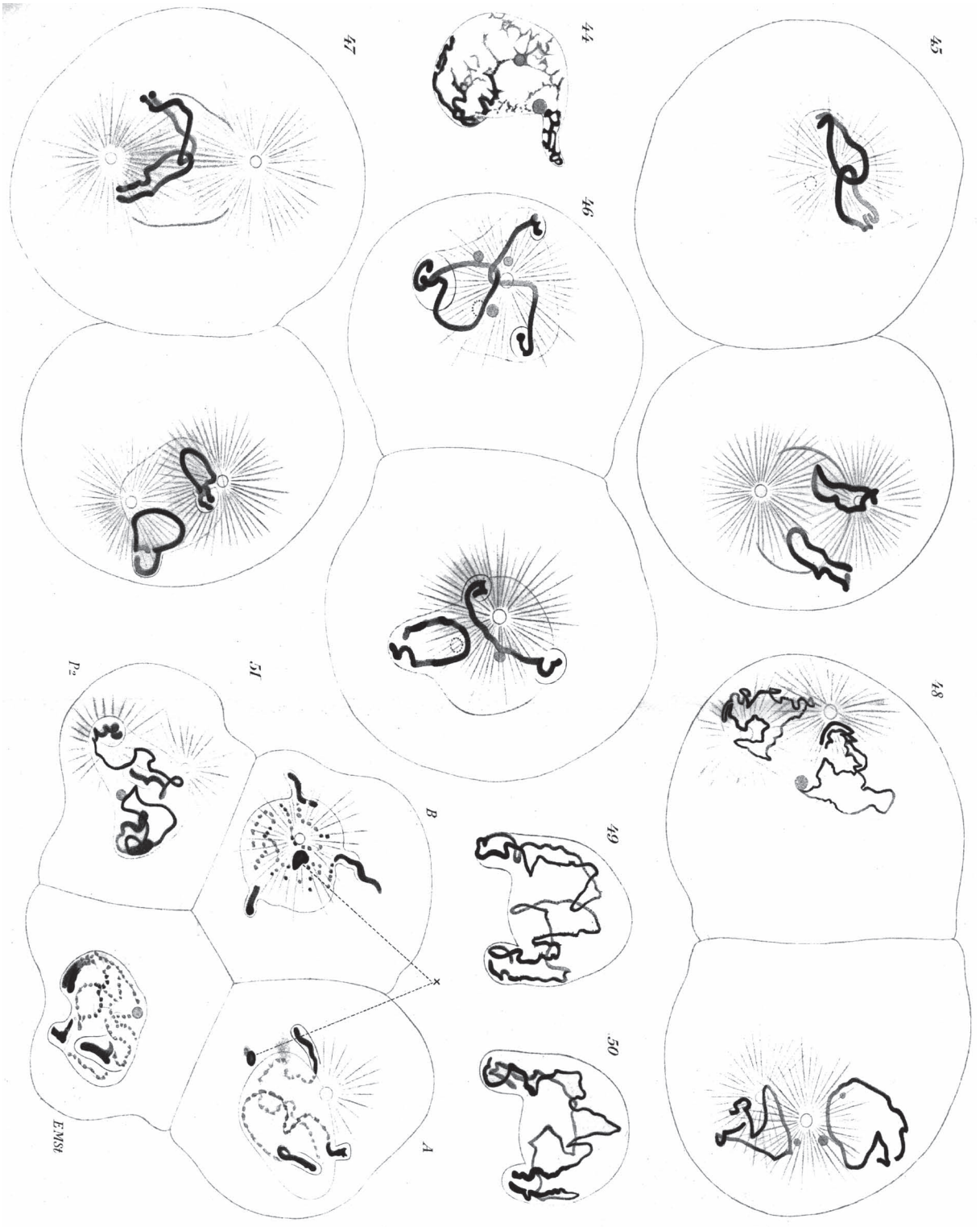

Fig. XI

7 Appendix I

7.1 Overview on fluorescent proteins:

Protein (Acronym)	Excitation Maximum (nm)	Emission Maximum (nm)	Molar Extinction Coefficient	Quantum Yield	in vivo Structure (* Weak Dimer)	Relative Bright-ness (% of EGFP)
GFP (wt)	395/475	509	21.000	77	Monomer*	48
Green Fluorescent Proteins						
EGFP	484	507	56.000	60	Monomer*	100
Emerald	487	509	57.500	68	Monomer*	116
Superfolder GFP	485	510	83.300	65	Monomer*	160
Azami Green	492	505	55.000	74	Monomer	121
mWasabi	493	509	70.000	80	Monomer	167
TagGFP	482	505	58.200	59	Monomer*	110
TurboGFP	482	502	70.000	53	Dimer	102
AcGFP	480	505	50.000	55	Monomer*	82
ZsGreen	493	505	43.000	91	Tetramer	117
T-Sapphire	399	511	44.000	60	Monomer*	79
Blue Fluorescent Proteins						
EBFP	383	445	29.000	31	Monomer*	27
EBFP2	383	448	32.000	56	Monomer*	53
Azurite	384	450	26.200	55	Monomer*	43
mTagBFP	399	456	52.000	63	Monomer	98
Cyan Fluorescent Proteins						
ECFP	439	476	32.500	40	Monomer*	39
mECFP	433	475	32.500	40	Monomer	39
Cerulean	433	475	43.000	62	Monomer*	79
CyPet	435	477	35.000	51	Monomer*	53
AmCyan1	458	489	44.000	24	Tetramer	31
Midori-Ishi Cyan	472	495	27.300	90	Dimer	73
TagCFP	458	480	37.000	57	Monomer	63
mTFP1 (Teal)	462	492	64.000	85	Monomer	162

Yellow Fluorescent Proteins						
EYFP	514	527	83.400	61	Monomer*	151
Topaz	514	527	94.500	60	Monomer*	169
Venus	515	528	92.200	57	Monomer*	156
mCitrine	516	529	77.000	76	Monomer	174
YPet	517	530	104.000	77	Monomer*	238
TagYFP	508	524	64.000	60	Monomer	118
PhiYFP	525	537	124.000	39	Monomer*	144
ZsYellow1	529	539	20.200	42	Tetramer	25
mBanana	540	553	6.000	7	Monomer	13
Orange Fluorescent Proteins						
Kusabira Orange	548	559	51.600	60	Monomer	92
Kusabira Orange2	551	565	63.800	62	Monomer	118
mOrange	548	562	71.000	69	Monomer	146
mOrange2	549	565	58.000	60	Monomer	104
Red Fluorescent Proteins						
dTomato	554	581	69.000	69	Dimer	142
dTomato-Tandem	554	581	138.000	69	Monomer	283
TagRFP	555	584	100.000	48	Monomer	142
TagRFP-T	555	584	81.000	41	Monomer	99
DsRed	558	583	75.000	79	Tetramer	176
DsRed2	563	582	43.800	55	Tetramer	72
DsRed-Express (T1)	555	584	38.000	51	Tetramer	58
DsRed-Monomer	556	586	35.000	10	Monomer	10
mTangerine	568	585	38.000	30	Monomer	34
mRuby	558	605	112.000	35	Monomer	117
mApple	568	592	75.000	49	Monomer	109
mStrawberry	574	596	90.000	29	Monomer	78
AsRed2	576	592	56.200	5	Tetramer	8
mRFP1	584	607	50.000	25	Monomer	37
JRed	584	610	44.000	20	Dimer	26
mCherry	587	610	72.000	22	Monomer	47
HcRed1	588	618	20.000	15	Dimer	1
mRaspberry	598	625	86.000	15	Monomer	38

dKeima-Tandem	440	620	28.800	24	Monomer	21
HcRed-Tandem	590	637	160.000	4	Monomer	19
mPlum	590	649	41.000	10	Monomer	12
AQ143	595	655	90.000	4	Tetramer	11

7.2 Properties of selected Optical Highlighters

Protein (Acronym)	Excitation Maximum (nm)	Emission Maximum (nm)	Molar Extinction Coefficient	Quantum Yield	in vivo Structure	Rel. Brightness (% of EGFP)
PA-GFP (G)	504	517	17.400	79	Monomer	41
PS-CFP (C)	402	468	34.000	16	Monomer	16
PS-CFP (G)	490	511	27.000	19	Monomer	15
PA-mRFP1 (R)	578	605	10.000	8	Monomer	3
CoralHue Kaede (G)	508	518	98.800	88	Tetramer	259
CoralHue Kaede (R)	572	580	60.400	33	Tetramer	59
wtKikGR (G)	507	517	53.700	70	Tetramer	112
wtKikGR (R)	583	593	35.100	65	Tetramer	68
mKikGR (G)	505	515	49.000	69	Monomer	101
mKikGR (R)	580	591	28.000	63	Monomer	53
dEosFP-Tandem (G)	506	516	84.000	66	Monomer	165
dEosFP-Tandem (R)	569	581	33.000	60	Monomer	59
mEos2FP (G)	506	519	56.000	84	Monomer	140
mEos2FP (R)	573	584	46.000	66	Monomer	90
Dendra2 (G)	490	507	45.000	50	Monomer	67
Dendra2 (R)	553	573	35.000	55	Monomer	57
CoralHue Dronpa (G)	503	518	95.000	85	Monomer	240
Kindling (KFP1)	580	600	59.000	7	Tetramer	12

taken from Nikon Microscopy U website

Ehrenwörtliche Versicherung

Hiermit bestätige ich, dass ich die vorliegende Dissertation selbständig und nur mit den angegebenen Materialien und Quellen durchgeführt habe.

München, den 1. Juli 2010

Hilmar Strickfaden

Erklärung über frühere Promotionsversuche

Hiermit bestätige ich, dass ich vor dieser Arbeit keine anderen Promotionsversuche unternommen habe. Dies ist meine erste Dissertation.

München, den 1. Juli 2010

Hilmar Strickfaden

Acknowledgements

I want to thank:

- **Thomas Cremer** for being a great mentor, for providing access to excellent state of the art light microscopic equipment and for bringing me into contact with a fascinating scientific field.
- **Peter Becker** for interesting conversations and doing the "Zweitkorrektur".
- **Marion Cremer**, who is an exceptionally talented proposal writer (spinning disc microscope) and the back-bone the group for 5 years of good cooperation. I especially want to thank her for proofreading the manuscript.
- **Heinrich Leonhardt** for his generosity to give me full access to his excellent lab resources, for always having an open ear and for good advice and funny conversations on the corridor.
- **Steffen Dietzel** for his generosity to give me full access to his greatly configured live-cell microscope.
- The cooperation partners of the ion microbeam project **Andreas Hauptner**, **Volker Hable**, **Christoph Greubel**, **Günther Dollinger**, **Anna Friedl**, **Doris Seiler**, **Guido Drexler**, **Iris Bauer**, and "**Siggi**".
- **Roland Kanaar** and the people in his lab (especially **Jeroen Essers**, **Berina Eppink** and **Cecile Beerens**) who gave me a warm welcome at the Erasmus Medical Center Rotterdam in summer 2006, for providing me with plasmid constructs that were crucial for this thesis and for teaching me new methods.
- **Daniel Sagan**, and **Friederike Eckhard-Schupp** who kindly provided me with the RPE1 cell line.
- **Manja Meggendorfer**, **Ruth Brack-Werner** and **Horst Wolff** for

the H2B mRFP construct.

★ **Martin Hess** for many interesting conversations about microscopy and 3D reconstructions.

★ **Heidi Jahn-Henninger** for excellent lab-maintenance.

★ **Carolin Bleese** for frequent, kind and competent help with Photoshop, Illustrator, InDesign and for many funny conversations.

★ students that I partially supervised **Christian H. Ottmann**, **Barbara Hübner**, **Simon Ernst**, **Belinda Mazurek** and **Wolf Holbein**.

★ **Andreas Bolzer**, **Roman Zinner** and **Michael Pulla** from Zeiss Microsystems for their always competent and generous help.

★ **Werner Schultheiß**, **Dietfried Molter**, from the IT-Group for their frequent help.

★ **Alexander Kaiser**, **Achim Klug** and **Michael J. Hendzel**, who helped me a lot during establishing the microinjection method in the Cremer-Lab.

★ **Werner Grundei** and **Bernhard Pöller** from the technical facility of the Biocenter for their kind and professional help.

★ **Christian Lanctôt**, **Heiner Albiez**, **Alessandro Brero** and **Peter J. Nielsen** for being my role models of good scientists.

★ **Andreas Zunhammer** and **Jens Nagel** for being great colleagues and friends, for the many common joint adventures and for the sacrifices to Bacchus. "*Ceterum censeo Carthaginem esse delendam*".

★ **Stanislav Fakan** and **Jacques Rouquette** for many good scientific conversations and for excellent Swiss chocolate.

★ **Ben**, **Alex**, **Daniel**, and **Manfred** (from security staff) for endless table football matches during many night sessions.

★ **Doris Illner** for the many nice candies and cakes she surprised me with during the past years and for being a good mom for our frogs *Kermit*, *Hops* and *Lurchi*.

★ **Monika Holik** and **Sabrina Schenk** from the animal facility for the many kind gifts to the frogs.

★ **Daniela Köhler** and **Claudia Dahlem** for kind and competent advice in all circumstances inside and outside of the lab and for organizing so many of the social events!

★ some members of the old Cremer group: **Katrin** (**Küpper, Teller, Pfleghaar**), **Michaela Neusser**, **Stefan Müller**, **Roy Hessing**, **Verena Vitt**, **Radka Symonova**, **Florian Grasser**, **Claudia Hepperger**, **Robert Mayer**, **Nina Ketterl**, **Isabel Liebhart**, **Corella Casas-Delucchi**, **Kourosh Zolghadr**, **Charlotte Hauser**.

★ and some members of the new Cremer Group: **Daniel Smeets**, **Yolanda Markaki**, **Birgit Groß**, **Martina Simon**, **Nadine Schrode**, **Gustavo Folle**, **Peffi & Teffi**.

★ **Chris Schiller**, **Jana Novak**, **Nadja Hoke** (feat. **Roxie**), **Rike Campen** (feat. **Momo**) **Oliver Mortusewicz**, **Danni Meilinger**, **Anja Gahl**, **Andrea Rottach**, **Lothar Schermelleh**, **Fabio Spada**, **Karin Fellinger**, **Katrin Schneider, Alexander Wolf** & **Stefanie Färberböck** and many more for being good neighbors in the Biocenter.

♥ Second–last but definitely not least I want to thank my family and friends. Special thanks go to my parents **Margot** and **Udo Strickfaden** who massively contributed to this work by generous emotional and financial support.

♥ And finally and especially I want to thank my dearest **Marina** for her incredible patience, her emotional warmth and her ability to brighten up my life.